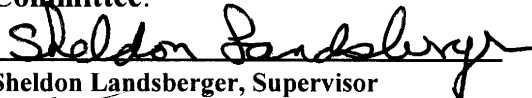


Copyright
by
M. Shamsuzzoha Basunia
2002

**The Dissertation Committee for M. Shamsuzzoha Basunia
certifies that this is the approved version
of the following dissertation:**

**CHARACTERIZATION OF FINNISH ARCTIC AEROSOLS
AND RECEPTOR MODELING**

Committee:

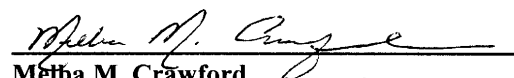

Sheldon Landsberger, Supervisor



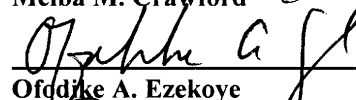
Steven R. Biegalski



William S. Charlton



Metba M. Crawford



Ofodike A. Ezekoye



Phillip K. Hopke

**CHARACTERIZATION OF FINNISH ARCTIC AEROSOLS AND
RECEPTOR MODELING**

by

M. Shamsuzzoha Basunia, M.S.E.

Dissertation

Presented to the Faculty of the Graduate School of
the University of Texas at Austin
in Partial Fulfillment
of the Requirements
for the Degree of

Doctor of Philosophy

The University of Texas at Austin

December 2002

**Dedicated to
my daughter Tasnima Naoshin,
nieces Farhana Akhter, Sumona Sharmin, and
wife Mahfuja Begum**

Acknowledgements

I would like to express my sincere thanks to my supervisor, Professor Sheldon Landsberger, for his guidance, support and encouragement throughout this work. His attention for required classes, experimental work, and for many other small issues is very well appreciated.

I also wish to express my sincere thanks to Professor Phillip K. Hopke, Clarkson University, for helping to formulate a research goal and valuable advice throughout this work. I would like to thank Paul Wishinski, Vermont Department of Environmental Conservation, for providing his expertise and the Residence Time Analysis plots for this work. I would also like to thank Dr. Ronald Henry, University of Southern California, for providing the Unmix computer code for this work.

Sincere thanks are also due to Professor Melba Crawford for her multivariate statistical class, which helped to follow the basics of the modeling part in this work. I would like to thank Dr. William S. Charlton for his help and support during this work. I wish to thank Dr. Steven R. Biegelski for his valuable discussion in some specific issues in this research.

I would like to thank Sean O’Kelly, Associate Director, Michael Krause, Reactor manager, Larry Welch, Md. Golam Faruk, Kevin Witt, and all NETL staff and members for providing me 700 hours of reactor time. I wish to thank Dr. Donna O’Kelly for giving a high priority in reactor scheduling and for helping me in various instances during the experimental work. I also wish to thank my friends, Dr. David Dodoo-Amoo and Sukesh Aghara, for helping me at countless instances during this work.

I wish to remember and thank all my teachers, colleagues, and family members, whose teachings and philosophy were very helpful to finish up this work. Especially, I remember my elder brother Abul Kalam Azad and uncle late Amir Uddin Ahmed, whose inspiration for education kept me focused over the years.

I would like to thank IARC/CIFAR for supporting the project work.

Finally, I would like to thank my wife, Mahfuja Begum, for her support, patience, and love throughout the period of this work.

December 6, 2002

CHARACTERIZATION OF FINNISH ARCTIC AEROSOLS AND RECEPTOR MODELING

Publication No. -----

M. Shamsuzzoha Basunia, Ph.D.

The University of Texas at Austin, 2002

Supervisor: Sheldon Landsberger

Lower atmospheric aerosols have been characterized for the period of 1964-1978 in the European sub Arctic region at Kevo, northern Finland. A total of 685 weekly samples were analyzed for Ag, Al, As, Br, Ca, Cl, Co, Cu, I, In, K, Mn, Na, Sb, Si, Sn, Ti, V, W, and Zn using neutron activation analysis. Study of time series concentration levels, box plots of the monthly subsets, and the descriptive statistics of seasonal datasets showed that seasonal weather had less influence in the lower atmospheric elemental concentration levels at Kevo. Two very distinct silver concentration level periods, high and low, were observed in the Kevo atmosphere during 1964-1970 and 1971-1978. A comparison of anthropogenic elemental concentration levels in the Kevo lower atmosphere were found in the same range or 2-8 fold higher than reported literature data of Russian and Canadian Arctic during winter and spring seasons. Elements like In, Cu, Zn, As, Sb, Sn, and Ag were highly enriched in the Kevo lower atmosphere. Principal component factor analysis showed a strong smelting factor consisting of copper, zinc, indium, and tin. This factor was found to be more important in the principal component factor analysis (PCFA) in winter dataset than that of summer. A crustal factor was easily recognized in the winter PCFA results, but crustal components were mixed up with industrial components in the summer results. Sea source components appeared in a single factor in the summer PCFA results but were found in pairs into several factors in winter results. Antimony was mostly found in a single factor. The Unmix model was used to identify sources and source composition in the Kevo atmosphere. Residence time

analysis was used for identifying the source location of all elements using an air parcel back trajectory ensemble. The impact of this research is three fold. First, it's contribution to the ongoing Arctic research. Second, the modeling experience obtained from this very large dataset could be used for future research and monitoring. Third, the development of new NAA methodologies for determining important industrial marker elements, like silver and cobalt, and the development of a new scheme for cost-effective determination of medium lived isotopes.

TABLE OF CONTENTS

List of Tables and Figures.....	xi, xiii
1. INTRODUCTION.....	1
1.1 Literature Review	6
1.2 Literature Review Summary.....	12
1.3 Objectives	13
2. NEUTRON ACTIVATION ANALYSIS	15
2.1 NAA Working Equations	15
2.1.1 Neutron Nuclei Reactions	16
2.1.2 Reaction Rates	17
2.1.3 Calculation of Concentrations by NAA	18
2.2 Gamma Ray Spectrometry.....	19
2.3 Irradiation and Counting Facilities	22
3. EXPERIMENTAL.....	24
3.1 Sampling	24
3.1.1 Sample Collection	24
3.1.2 Particle Size Distribution.....	27
3.2 Analysis	28
3.2.1 Sample and Standard Preparation.....	28
3.2.2 Irradiation and Counting.....	31
3.2.3 Spectrum Analysis	33
3.2.4 Blank Correction	34
3.3 Quality Control and Results.....	36
3.4 New Approaches of NAA Routine Use	37
3.4.1 Irradiation and Counting.....	37
3.4.2 Silver and Cobalt determination.....	39

4. RECEPTOR MODELING.....	41
4.1 Introduction.....	41
4.2 Principal Component Factor Analysis	44
4.3 Unmix	48
4.4 Residence Time Analysis	50
5. RESULTS AND DISCUSSION	54
5.1 Descriptive Statistics and Results	55
5.1.1 Distribution Characteristics.....	55
5.1.2 Elemental Ambient Concentration Levels	58
5.1.3 Elemental Ratios.....	74
5.1.4 Enrichment Factors.....	85
5.2 Receptor Model Results.....	88
5.2.1 Principal Component Factor Analysis	88
5.2.2 Unmix	98
5.3 Residence Time Analysis Results.....	102
5.3.1 Explanation of silver anomaly.....	103
5.3.2 RTA results for all elements	108
6. IMPACT OF THIS RESEARCH	160
7. CONCLUSIONS AND RECOMMENDATIONS.....	165
7.1 Conclusions	165
7.2 Recommendations	167
APPENDIX	169
REFERENCES	181
VITA.....	189

List of Tables

Table 2.1: Irradiation facilities of the TRIGA MARK II research reactor	23
Table 3.1: Location, distance and industrial activities near to Kevo	27
Table 3.2: Elements, nuclear reactions and nuclear data	32
Table 3.3: NAA scheme for sample irradiation, decay, and counting on the same filter; Reactor power 500 kW	32
Table 3.4: Filter blank statistics from 5 filters for subtraction from measured quantity ..	36
Table 3.5: Elemental concentration determined by NAA in SRM	37
Table 5.1: Sample number, period of sampling, and notes of unusual samples	55
Table 5.2: Elemental arithmetic mean, median, mode, skewness, and kurtosis	56
Table 5.3: Kolmogorov-Smirnov (K-S) statistics D and significance level for the fitted variables	57
Table 5.4: Geometric mean (GM), geometric standard deviation (GSTD), range, detection limit (DL), and percent of data below DL for each element	59
Table 5.5: A comparison mean concentrations (ng/m^3) of this work with other Arctic data	61
Table 5.6: A comparison of mean concentrations (ng/m^3) of this work with other Arctic data.....	62
Table 5.7: Silver concentration levels of x-ray film exposed to blank filters	64
Table 5.8: Geometric mean (GM), geometric standard deviation (GSTD) in summer, autumn, winter, and spring seasons at Kevo for the period of 1964-1978	81
Table 5.9: Elemental ratio matrix for 1964-1978 period of GMs for anthropogenic, crustal and marine source elements (ratio = row title/column title)	82
Table 5.10: Summer elemental ratio matrix of GMs for anthropogenic, crustal and marine source elements (ratio = row title/column title)	83
Table 5.11: Winter elemental ratio matrix of GMs for anthropogenic, crustal and marine source elements (ratio = row title/column title).....	84
Table 5.12: Elemental global average, estimated local average, and EF median values..	87
Table 5.13: Factors, communalities, eigenvalues, and variance for full dataset (681 samples)	93
Table 5.14: Factors, communalities, eigenvalues, and variance for summer dataset (277 samples)	94
Table 5.15: Factors, communalities, eigenvalues, and variance for winter dataset (404 samples)	95

Table 5.16: Factors, communalities, eigenvalues, and variance for winter dataset without sample 10 and 29	96
Table 5.17: Elements and samples related to highest concentration levels	97
Table 5.18: Unmix results for source number, composition, and contribution	101
Table 5.19: Uncertainty and source composition/ 2σ ratios for all sources	101
Table 5.20 Highest concentration levels of silver related to bromine, iodine, and sodium	108
Table A.1: Irradiation and counting data of standards and SRM for thermal irradiation	169
Table A.2: Irradiation and counting data of standards and SRM for epithermal irradiation	170
Table A.3: HYSPLIT output for an air parcel back trajectory for a 120-hour period	180

List of Figures

Figure 1.1 A Map of the Arctic region	5
Figure 1.2 Northern Finland, northern Norway, part of Kola Peninsula	5
Figure 2.1 Block diagram of the normal mode HPGe gamma ray spectrometry	21
Figure 2.2 Schematic of Compton suppressed counting system.....	22
Figure 2.3: An internal view of the pneumatic laboratory.....	23
Figure 3.1: Map of Finland showing the sampling sites of the Finnish Meteorological Institute	25
Figure 3.2: Schematic diagram of the aerosol sampling arrangement in Kevo	26
Figure 3.3: Steps of aerosol filter preparation for a pneumatic irradiation.....	30
Figure 3.4 Relative neutron flux variation during individual sample irradiation	33
Figure 3.5: A comparison of 58.6 keV gamma ray sensitivity from the ^{58m} Co isotope in different irradiation and counting modes.....	40
Figure 5.1: Histogram plots for a) chlorine 64-73 b) chlorine 74-78 c) sodium and d) indium data	68
Figure 5.2 a) Gridded domain used in RTA, b) Part of the domain showing 10 km grid squares used for RTA	102
Figure 5.3: Time series plots of silver, aluminum, arsenic, and bromine	112
Figure 5.4: Time series plots of calcium, chlorine, cobalt, and copper	113
Figure 5.5: Time series plots of iodine, indium, potassium, and manganese	114
Figure 5.6: Time series plots of sodium, antimony, silicon, and tin.....	115
Figure 5.7: Time series plots for titanium, vanadium, and zinc	116
Figure 5.8: Box plots of monthly data for silver, aluminum, arsenic, and bromine	117
Figure 5.9: Box plots of monthly data for calcium, chlorine, cobalt, and copper	118
Figure 5.10: Box plots of monthly data for iodine, indium, potassium, and manganese	119
Figure 5.11: Box plots of monthly data for sodium, antimony, silicon, and tin.....	120
Figure 5.12: Box plots of monthly data for titanium, vanadium, and zinc	121
Figure 5.13: Time series plots of non crustal Mn/non crustal V, excess bromine and Br/I	122
Figure 5.14: Time series plots of Na/I, Cl/I, and Cl/Na.....	123
Figure 5.15: Scatter plots of Al vs. Si, As vs. Co, As vs. Cu, and As vs. In.....	124
Figure 5.16: Scatter plots of As vs. Sb, As vs. Sn, As vs. Zn, and In vs. Sb	125

Figure 5.17: Scatter plots of Mn vs. V, Cu vs. Zn, Al vs. Sb, and Mn_x vs. V_x	126
Figure 5.18: Enrichment Factor using a) global and b) local crustal average values	127
Figure 5.19: Scree plot for the full dataset.....	128
Figure 5.20: Scree plot for the summer dataset	128
Figure 5.21: Scree plot for the winter dataset	129
Figure 5.22: Factor score plots for factor 1, factor 2, and factor 3 of full dataset	130
Figure 5.23: Factor score plots for factor 4, factor 5, and factor 6 of full dataset	131
Figure 5.24: Factor score plots for factor 1, factor 2, and factor 3 of summer dataset ...	132
Figure 5.25: Factor score plots for factor 4, factor 5, and factor 6 of summer dataset ...	133
Figure 5.26: Factor score plots for factor 1, factor 2, and factor 3 of winter dataset	134
Figure 5.27: Factor score plots for factor 4, factor 5, and factor 6 of winter dataset	135
Figure 5.28: Factor score plots for factor 7 of winter dataset.....	136
Figure 5.29: Unmix main interactive window run under MATLAB environment	137
Figure 5.30: An air parcel back trajectory a) path in reference to earth's surface b) vertical height from ground	138
Figure 5.31: Silver RTA Incremental Probability Percent (IPP) plots, Smoothing Factor (SF) 441	139
Figure 5.32: Multielemental line plots for Ag, Cu, In, Sn, and Zn.....	140
Figure 5.33: Back trajectory plots for the first six highest silver samples.....	141
Figure 5.34: Silver RTA IPP plots, a) & b) SF 81, and c) & d) SF 25 (scales are relative)	142
Figure 5.35: Arsenic RTA incremental probability plots, SF 81	143
Figure 5.36: Cobalt RTA incremental probability plots, SF 81	144
Figure 5.37: Copper RTA incremental probability plots; a) & b) SF 81, c) SF 441	145
Figure 5.38: Indium RTA incremental probability plots, SF 81	146
Figure 5.39: Antimony RTA incremental probability plots, SF 81	147
Figure 5.40: Tin RTA incremental probability plots; a) & b) SF 81, c) SF 441	148
Figure 5.41: Zinc RTA incremental probability plots, SF 81	149
Figure 5.42: Manganese RTA incremental probability plots, SF 81	150
Figure 5.43: Vanadium RTA incremental probability plots, SF 81	151
Figure 5.44: Aluminum RTA incremental probability plots, SF 81	152
Figure 5.45: Silicon RTA incremental probability plots, SF 81	153

Figure 5.46: Calcium RTA incremental probability plots, SF 81	154
Figure 5.47: Titanium RTA incremental probability plots, SF 81	155
Figure 5.48: Sodium RTA incremental probability plots, SF 81	156
Figure 5.49: Chlorine RTA incremental probability plots, SF 81	157
Figure 5.50: Bromine RTA incremental probability plots, SF 81	158
Figure 5.51: Iodine RTA incremental probability plots, SF 81	159
Figure A.1: A spectrum of pneumatic thermal irradiation Compton mode count	171
Figure A.2: A spectrum of pneumatic thermal irradiation normal mode count	171
Figure A.3: A spectrum of pneumatic epithermal irradiation normal mode count.....	172
Figure A.4: A spectrum of pneumatic epithermal irradiation Compton mode count	172
Figure A.5: A spectrum of pneumatic epithermal irradiation Compton mode count with a 17 h decay time	173
Figure A.6: A spectrum of pneumatic epithermal irradiation normal mode count with a 17 h decay time	173
Figure A.7: A spectrum of one-minute epithermal irradiation and normal mode count	174
Figure A.8: Illustration of a trajectory residence time calculation	177

1. Introduction

Arctic air pollutants originate from various sources in Europe, Russia, far east Asia and North America. Subsequently atmospheric transportation of natural and anthropogenic emissions from lower and mid latitudes causes the Arctic haze phenomenon during the winter months in the high Arctic. Northern Finland, inside the 66°32' N latitude including northern Norway and northwest Russia is known as the European sub Arctic. This part of the sub Arctic region has received distinct attention in environmental research in the past decades mainly because of the huge industrial activities from the beginning of last century. Some of the world's largest emitters of heavy metals and sulfur dioxide are located in the Kola Peninsula, northwest Russia. A wide variety of industrial activities, like ferrous and non-ferrous smelters, peat fired power plants and naval bases for about 150 nuclear powered vessels have operated in this region for more than 60 years. Heavy metal emission is much higher for the non-ferrous mining, smelting, roasting, processing of nickel, copper, and aluminum to the atmospheric environment than any ferrous industry. The industrial locations at Norilsk (Siberia) and Kola Peninsula are the two prominent industrial spots in Russian Arctic. After World War II the need of minerals and natural resources expedited the extraction rapidly until 1992 under the socialist development policy. The Kola Peninsula in the Russian Arctic is also one of the most heavily militarized areas in the world and contains the world's largest concentration of nuclear weapons [Luzin *et al.*, 1994].

Arctos is Greek for bear, and the Arctic region derives its name from the stellar constellation of Ursa Major, the Great Bear. Climatically, the Arctic is often defined as the area north of the 10° C July isotherm, i.e. north of the line or region, which has a mean July temperature of 10°C and shown in Figure 1.1. The Arctic is characterized by a

harsh climate with extreme variations in light and temperature, short summers, extensive snow and ice cover in winter and large areas of permafrost. In northern Finland, the sun shines without setting from mid May to the end of July, and remains below the horizon from late November to mid January. The ground covers with snow in October and remains covered on average until mid of May.

Countries like Canada, Denmark (Greenland), Iceland, Norway, Sweden, Finland, Russia, and USA (Alaska) have a direct link by land to the Arctic region. As well, Russia encircles a vast arc of the Arctic Circle. A coordinated air sampling network of North American and European agencies, which started in 1977 produced the database of the concentrations of surface aerosol in Greenland (Heidam, 1984, 1981), Norwegian Arctic (Heintzenberg *et al.*, 1981; Joranger and Ottar, 1984; Pacyna *et al.*, 1984), north Canada (Barrie and Hoff, 1985) and northern Alaska (Lowenthal and Rahn, 1985). Beginning in 1991 the Central Kola Expedition (CKE) and the Geological Surveys of Finland (GTK) and Geological Survey of Norway (NGU) collaborated in multi compartmental and multielement studies of the impacts of the smelting and associated industries in the European Sub Arctic region and an extensive database was produced (Chekushin *et al.*, 1998, Jaffe *et al.* 1995, Kelly *et al.*, 1995, Reimann *et al.*, 1996). In 1991, The Arctic Monitoring and Assessment Program (AMAP) was established with responsibilities to monitor the levels and effects of anthropogenic pollutants in all compartments of the Arctic environment as a result of the Arctic Environmental Protection Strategy (AEPS) adopted by the governments of the eight Arctic rim countries.

Human activities both inside and outside the Arctic influence the physical, chemical and biological nature of Arctic ecosystems. It was not until mid 1970's when the Arctic haze research took it's full course of attention after an air pollution observatory report in 1956 over the Alaskan Arctic during the Ptarmigan weather reconnaissance flights [Mitchell, 1957]. In the following years, subsequent studies showed that Arctic haze layers consists of aerosols and gases, most of them having pollution-derived components from anthropogenic activities. However at times natural components like desert dust particles dominated [Rahn *et al.*, 1981; Raatz and Shaw, 1984]. It has been

proposed that a portion of the visibility-reducing haze in the Arctic may be composed of precipitating ice crystals [Curry, 1988]. The atmosphere contains relatively small amounts of contaminants compared with the total load in polar soil, sediments, and water. However, the rapid movement of air makes it an important pathway for delivering contaminants to the Arctic. Any chemically stable, wind-borne material will follow winds and weather patterns into and within the Arctic region. Over the last three decades Arctic haze has drawn the attention of many environmental scientists to study the nature and sources of these pollutants of this remote pristine region. Among these studies Arctic haze characterization, lower tropospheric chemistry, pollutants sources and pathways, trend analysis of Arctic pollution, determination of aerosol residence time, effects of pollutants, application of newly developed statistical receptor modeling etc., are the prime focuses [Baskaran and Shaw, 2001; Vinogradova, 2000; Polissar *et al.*, 1999; Sirois *et al.*, 1999; Hopke *et al.*, 1995; Ayotte *et al.*, 1995; Hopke *et al.*, 1993; McConnell *et al.*, 1992; Maenhaut *et al.*, 1989; Barrie *et al.*, 1988].

In the last two decades Arctic aerosol research provided some interesting phenomena like ozone destruction and initiated interest in the study the atmospheric chemistry of that region. At polar sunrise, sunlight-induced changes in the composition showed a bromine-ozone anti correlation, which indicated a possible link in the destruction of ozone by the catalytic reactions of BrOx radicals [Barrie *et al.* 1988]. In recent studies it was found that bromine was about 45 times stronger than chlorine as a catalyst for ozone destruction [Daniel *et al.*, 1999]. However, halogen chemistry occurring through suspended sea-salt aerosols could not fully explain the observed ozone depletion in the Arctic and indicated a possibility of snowpack halogen recycling to explain the observed depletion [Michalowski *et al.*, 2000]. Thus the interest of halogens, i.e. chlorine, bromine, and iodine, always remains at the forefront of the Arctic aerosol characterization.

Signatures of heavy metals and chemical species in the atmospheric aerosol can show the historical record of human activities and other phenomena of the sampling site and surrounding areas. A signature of manganese to vanadium ratio primarily showed

that the source region of Arctic haze pollutants came from thousands of kilometers away because of complex atmospheric transportation patterns [Rhan, 1981a]. In earlier days, it was almost impossible to think of anthropogenic pollutants like black carbon commonly known as soot, sulfur dioxide, nitrogen oxide etc. the main components of the Arctic haze, arrived at the pristine high Arctic sites from lower or mid latitude continental countries, located thousands of miles away from the observed sites. However, Rahn *et al.* (1984) was able to demonstrate that these pollutant species were carried out from the Eurasian sources by using the regional non-crustal Mn/V tracer ratio. In the later years, substantial research resolved better source locations by using seven tracer elements (As, Sb, Se, Zn, In, non-crustal Mn, non-crustal V) and source receptor modeling techniques [Lowenthal *et al.* 1985, Landsberger *et al.*, 1992, Hopke *et al.*, 1995, Xie *et al.*, 1999].

Although there are many episodic studies available at different locations of the circumpolar Arctic [Barrie *et al.*, 1981; Joranger and Otter, 1984; Cahill and Eldred, 1984; Heidam *et al.*, 1993; Djupstrom *et al.*, 1993] , there are a few data sets available on systematic long-term aerosol collection and analysis [Bodhaine and Dutton, 1993; Polissar *et al.*, 1999; Vinogradova, 2000].

Long-term studies at different locations in the Arctic are very important for two reasons. Firstly, it will help to understand the changes and the trends of the Arctic pollution status and secondly, estimation of long-term pollutant characteristics throughout the circumpolar Arctic region will bring a much better regional fingerprint of the trace constituents. A long-term (1980-1995) systematic aerosol sampling and



Figure 1.1 A Map of the Arctic region



Figure 1.2 Northern Finland, northern Norway, part of Kola Peninsula

chemical characterization at Alert (82.5°N, 62.3°W) in Canadian Arctic is reported in detail by several authors [Sirois *et al.*, 1999, Landsberger *et al.*, 1997; Xie *et al.*, 1999]. Other long-term (1986-1995) aerosol characteristics databases at three locations in the

eastern Arctic at Franz Jozef Land (81.1°N, 56.3°W), Severnaya Zemlya (79.5°N, 95.4°E), and Wrangel Island (71.0°N, 178.5°W), of Russian Arctic are available as well. However, these databases are only for the months of April and July in each year (Vingradova, 2000).

A historical batch of long-term (Oct. 1964 - Feb. 1978) air particulate sample archived in Finland is analyzed for trace elements using neutron activation analysis (NAA). Samples were collected in Kevo (69.7°N, 27.0°E), northern Finland, by the Finnish Meteorological Institute as part of the airborne radioactivity study to monitor former Soviet Union nuclear testing. Figure 1.2 shows the location of Kevo in northern Finland and parts of northern Norway and Kola Peninsula. A weeklong aerosol sampling of total suspended particles was done on Whatman 42 filter paper during the whole sampling period from 1964-1978. Analysis, results, some statistical modeling on the dataset are presented in this work, which reveals a time record of the aerosol composition dating back to a time before there were interest and concern for particulate contamination in the European sub Arctic. The study also links the present and past research findings to reveal the similarities and differences of this region to other sites in Arctic.

1.1 Literature Review

Luzin *et al.* (1994) reported geography, history and resources of the Russian Kola Peninsula. The Kola Peninsula in northwest Russia is one of the most important economic regions in the circumpolar North. The region contains valuable natural resources, including a wide variety of mineral and fish resources, and is proximate to the large gas fields of the Barents Sea. A large population, industrial complexes, and military infrastructure are also characteristic of the region. The Kola Peninsula developed rapidly during the Soviet period (1917 – 1992) under the principles of socialist development policy. That policy favored extensive resource extraction and industrialization and resulted in increased northern settlement, much of it involuntary. Soviet development policy prompted the opening of new mines and the construction of smelters and refining facilities, while Soviet military policy necessitated the establishment of large military basing operations. Resource development and processing

had led to severe environmental damage in the region and beyond. The paper also reported that Noril'sk ore has been processed in the Kola region since 1964. Noril'sk is an isolated city in Siberia and has no road or rail links to central Russia.

Rees *et al.* (1994) assembled information from a variety of sources and presented a coherent picture of the background to current extent of industrial pollution in Kola Peninsula. The peninsula lies in the Arcto-Atlantic sector of the moderate climate zone, so the regional climate conditions are determined by atmospheric process over the Atlantic Ocean. The prevailing winds are north to northeast in summer, and south to southwest in winter. The average wind speed in the central part of the peninsula exceeds 18 km h^{-1} , and storms occur an average 80 days a year. The three main industrial activities of the area are fisheries (mainly located at Murmansk), mineral mining, and non-ferrous metallurgy. Among these, non-ferrous metal plants are the foremost contributor to the air pollution. Copper and nickel ores are found at Monchegorsk and, further north, at Nikel and Pechenga. Until 1973 production of copper and nickel at Monchegorsk was quite small and based on local reserves. Since then, metal production of copper and nickel at Monchegorsk was increased five fold, using mostly ores much higher in sulfur content transported from Pechenga and Noril'sk (Siberia).

Reimann *et al.* (1997) reported the regional atmospheric deposition patterns of Ag, Bi, Cd, Hg, Mo, Sb and Tl in a $188,000 \text{ km}^2$ area of the European Arctic (NW Russia, N Finland and N Norway) using the biomonitoring moss technique. The Russian nickel mining and smelting industry (Nikel and Zapoljarnij (Pechenganike) and Monchegorsk (Severonikel) in the eastern part of the survey area represented two of the largest point sources for SO_2 and metal emissions on a world wide basis. In contrast, parts of northern Finland and northern Norway represent still some of the most pristine areas in Europe. Maps for most elements clearly showed elevated element concentrations near the industrial sites and delineated the extent of contamination. Pollution followed the main wind and topographical directions in the area (N-S). The gradients of deposition were rather steep. Background levels of all the elements were reached only within 150-200 km from the industrial plants. The higher silver concentrations in moss

around Monchegorsk smelter in comparison to that of the Nickel and Zapoljarnij smelters indicated that Noril'sk ore processed in Monchegorsk since 1972, had an elevated silver concentration. An expected resemblance of arsenic and antimony distribution was not found in the investigated area. Antimony displayed a very special signature that differed from all other reported elements.

The Environmental Geochemical Atlas of the central Barents region by Reimann *et al.* (1998) is a compiled version of the CKE, GTK and NGU collaborated project for natural and anthropogenic elements in moss, humus, B-horizon, and C-horizon over the 188,000 km² area of northern Norway, northern Finland, and northwest Kola Peninsula. The atlas reported 47 elemental concentration maps of the project area for all the above-mentioned compartments. An additional five elements (Au, Cs, Sn, Ta, Tb) some radionuclides, polycyclic aromatic hydrocarbons, pH etc. are reported without maps.

Virkkula *et al.* (1999) reported an 18-month set of concentration data of various elements in fine and coarse particles. The Finish Meteorological Institute collected the samples at Sevettijärvi (69°35'N, 28°50'E) during 1992-1994. The concentrations in aerosols arriving from the Norwegian Sea and the Arctic Ocean were very close to the values observed at more remote Arctic sites. However, in air from the Kola Peninsula, approximately one third of the samples, concentrations of some elements were ~2 orders of magnitude above the background concentrations. The elements most clearly transported in the pollution plume identified as Cd, Ni, Cu, V, Pb, As, Fe, and Co. The ratio of the chemical mass to the gravimetric mass of the aerosol samples was 80% both for the fine and coarse particle filters, regardless of the source area. Comparison of the aerosol concentrations with the concentrations of elements in snow showed that the deposition was proportional to the aerosol exposure. The contribution of Kola Peninsula to the deposition is high, ~80% for Ni, Cu, and Co and somewhat lower for other anthropogenic elements.

Maenhaut *et al.* (1989) reported 42 elemental concentrations in ninety-eight samples collected from Ny Ålesund (78°55'N, 11°57'E), Spitsbergen, and Vardø, Norway (70°23'N, 31°10'E) in the late winter of 1983, 1984 and 1986, and in the summer of 1984.

The winter atmospheric concentrations and aerosol compositions were similar at the two sites. In summer, atmospheric concentrations were significantly lower than in winter, particularly at Ny Ålesund and for the metallic pollutants. Elements such as V, Zn, As and Sb exhibited 20-50 times lower levels than in winter.

Regional variation of snowpack chemistry in the vicinity of Nikel and Zapoljarnij, Russia, northern Finland and Norway reported by Reimann *et al.* (1996). Meltwater and filter residues analyzed separately and differentiated for water soluble and particulate emissions. For a majority of the elements particles governed the total deposition chemistry. Four different sources of elemental input were identified as industrial emission, sea spray, geogenic dust, and anthropogenic dust. The study found that various elements spread differently from the emission source and this was explained as possibly due to differences in volatility of the elements or a varying particle size spectrum. A steep deposition gradient towards the west and a dominant distribution towards N-NE, which was the prevailing wind direction, of heavy metals were reported.

Kelly *et al.* (1995) had studied the size distribution of aerosol containing metals and reported that arsenic and lead occurred predominantly in the fine particles, while copper and nickel occurred both in fine and coarse particles. Finding the mean ratios of total mass Cu/Pb and Cu/As in the air, snowpack Cu enhancement was estimated relative to Pb and As, which clearly indicated that the Mochegorsk Pb and As emissions were transported longer distances than Cu and Ni prior to atmospheric removal.

Steinnes *et al.* (1992) used moss as a biomonitor for surveying multielement atmospheric deposition in Norway. Twenty-six elemental data from a nationwide survey illustrated the feasibility of the technique for multi-element studies of airborne trace elements from local point sources, transboundary air pollution, and natural cycling process. Contributions from non-atmospheric sources such as wind blown soil dust and leaching from vascular plants were identified and discussed. Long-range atmospheric transport strongly dominated the deposition of several pollutant trace elements in Norway. The paper reported the nationwide distribution of all elements. The highest cobalt concentrations were reported in the south and in the far northeast of Norway. The

strong correlation of cobalt with nickel in the northeast region indicated the source were from huge Cu-Ni smelters in the Kola Peninsula and a far smaller similar smelter in Kristiansand (58°12' N, 8°06' E), Norway. Otherwise the behavior of cobalt was that of crustal component, with high correlations with Fe, Sc, and Al.

Vinogradova *et al.* (1995) published elemental concentration levels of Central Russian Arctic archipelago, North Earth, for one spring month in 1985, 1986, and 1988. Enrichment factor (EF) analysis showed one to three orders of magnitude higher values for anthropogenic elements, like Mn, Ni, Cu, Zn, As, Mo, Ag, Cd, Sb, Au, Pb, etc. Air mass trajectories attributed the higher concentration from eastern Siberia, Norilsk, Kola Peninsula, Urals, etc. Vinogradova (2000) also estimated average contributions of six anthropogenic elements As, Ni, Pb, V, Zn, and Cd arising from industrial regions to the Russian Arctic in spring and summer for a ten-year period (1986-1995). The 5-day forward and backward trajectories showed that air mass transport to three observation points took approximately 20-40% of pollutants out of the Arctic in spring, however, in summer, more than 90% of pollutants transported into the Russian Arctic deposit within 5 days onto the surface inside the Arctic region.

Sirois *et al.* (1999) reported eighteen constituents of the analysis of Alert, Canada, aerosols, which included important anthropogenic and crustal elements, major ions and methane sulphonic acid. These constituents were associated with ten distinct aerosol factors (components). These were PHOTO-S (i.e., anthropogenic sulphur from oxidation of SO₂ in the Arctic), ANTHRO-S, MIXED PHOTO-S/SEA-SALT, MSA (i.e., biogenic sulphur), SEA SALT, SMELTER, SOIL, NITRATE, BROMINE, and IODINE. The ninth and tenth factors, bromine and iodine, were solely loaded by particulate form with a barely significant contribution of aluminum. Bromine peaked once in the year in March-April after polar sunrise, while iodine peaked twice, once at polar sunrise and once in September-October. The later peak of iodine was attributed as a biogenic component at Alert.

National Oceanic and Atmospheric Administration (NOAA) at Barrow, Alaska [Bodhaine and Dutton, 1993] reported a decreasing trend of the Arctic haze from a long-

term observation at Barrow, Alaska. These observations were on particle light scattering efficiency at four wavelengths, condensation nuclei counts, and aerosol optical depth. There were no reported data on particle compositions. The surface aerosol scattering measurements and total column aerosol optical depth measurements showed a maximum in 1982 and then a decreasing trend until 1992. The decreasing trend was statistically significant and the paper suggested that the decrease in Arctic haze at Barrow, as observed in the aerosol light scattering and optical depth records, was due to a decrease of anthropogenic emissions in Europe and the former Soviet Union. Barrie [1993] also observed a measurable but smaller decrease of sulphate aerosol in the Canadian baseline station at Alert over the same period of time.

Barrie *et al.* [1988] reported increasing evidence of sunlight-induced changes in the composition of the lower Arctic atmosphere (0-2km) during polar sunrise. These changes were important regarding the tropospheric cycles of ozone, bromine, sulfur oxides, nitrogen oxides and possibly iodine. A possible link to ozone destruction and catalytic reactions of BrO_x radicals was presumed in that paper.

Oltmans *et al.* [1989] reported the filterable bromine measurements and a concurrent destruction of O₃ in the high Arctic during the spring return. Multiyear observations showed that the pattern had an annual feature of O₃ concentration near the surface at Barrow, Alaska, and other Arctic locations. Aircraft measurements showed low O₃ amounts and high filterable bromine concentrations beneath the surface temperature inversion over ice throughout the Arctic in the spring. A wintertime build-up of the gaseous organic compound bromoform and a rapid depletion of bromoform in the spring were speculated as a link between the episodic O₃ depletion events and the accompanying rise in filterable bromine.

Landsberger *et al.* [1992, 1997] presented the seasonal fluctuations of antimony, arsenic, indium, manganese and vanadium in the airborne particulate matter from 1982-1987 at Alert in the Canadian high Arctic. Calculations of enrichment factors showed that arsenic and antimony were very enriched in the wintertime aerosol. While wintertime ratios of non-crustal manganese/non-crustal vanadium were in agreement with

previously published work, summertime ratios often resulted in negative values. Principal Source Contribution Factor Analyses were performed for arsenic, indium and manganese and showed regional signatures, which characterized as coming from distinct European and Asian areas.

Xie *et al.* [1999] used a new approach called Multilinear Engine (ME), based upon positive matrix factorization, for Arctic aerosol source identification. The paper presented the measured concentrations of 24 constituents into both 2-way and 3-way modeling and each factor representing a likely particle source. The two 3-way factors were (i) bromine characterized by a maximum in the spring around March and April; and (ii) biogenic sulfur that includes sulfate and methanesulfonate with maxima in May and August. The acidic sulfate, bromine, and iodine factors had a common maximum around March /April, just after polar sunrise, suggesting the influence of increased photochemistry at that time of year. The strength of the year-to-year biogenic sulfur factor showed a moderate correlation ($r^2 = 0.5$) with the yearly average northern hemisphere temperature anomaly suggesting a relationship of temperature with biogenic sulfur production.

Daniel *et al.* (1999) studied the relative effectiveness of bromine compared to chlorine for destroying stratospheric ozone. Calculation of relative effectiveness, usually referred to as α , with a two-dimensional radiative/chemical/dynamical model suggested that bromine was 45 times more effective than chlorine for global ozone destruction.

1.2 Literature Review Summary

This research is the only oldest long-range atmospheric trace elemental record to the present available data of European sub Arctic region. The above literature review showed that extensive episodic aerosol characterization and research were conducted at many sub Arctic locations around the North Pole, basically to explain the Arctic haze phenomenon observed in the high latitude. While sulfur bearing chemical species, black carbon, and NO_x are the main components and contributing mass to the Arctic haze, trace elements analyzed were used to identify and study the origin, source location of the Arctic haze and northern atmospheric chemistry.

Many authors, while using the regional aerosol signatures to identify the source location of the Arctic haze phenomenon based upon a few seasonal samples, cautioned and stressed the importance of routine observations, as the relative importance of European and Soviet sources might vary year to year. The results of this research will find a year to year and summer to winter variation for a 14-year continuous period. In explaining the origin and location of the Arctic haze phenomenon a term ‘regional signature’ is often used but the questions remain to answer is how many regions one might consider and where to draw the lines to distinguish one region from another. Comparison of this work with previous episodic data might be able to address some of these questions.

This research contributes the aerosol study of northwestern European Arctic in three ways. First, it will provide a long, continuous, and oldest time series elemental air concentration database for the Finish Lapland. Second, this research investigates the entire path of many trace metals using the residence time analysis, which is basically based upon back trajectories of air parcels from the sampling location. Third, aerosol filter analysis by epithermal neutron activation analysis helps to report some of the very crucial elements like silver, indium, and tin in this Finnish Lapland.

1.3 Objectives

The primary goals of this work are to develop a substantial trace elemental composition and air concentration levels on airborne particulate matter in northern Finland. The specific objectives of this research are the following:

- Determination of natural and anthropogenic trace elements concentration levels like aluminum, antimony, arsenic, bromine, calcium, cobalt, chlorine, copper, iodine, indium, silicon, manganese, potassium, silver, sodium, titanium, tin, tungsten, vanadium, zinc, etc.
- Enrichment Factor Analysis and elemental correlation.
- Time series analysis of all the elements to determine the trends and cyclical variations.

- Identification of source types and locations by principal component factor analysis (PCFA) and resonance time analysis (RTA) and
- Comparison of the results from northern Finland with other long-term records of Arctic aerosol behavior for similarities and differences in their temporal variations.

2. Neutron Activation Analysis

Neutron activation analysis (NAA) is a very suitable non-destructive multi-element determination technique in a simple or complex sample matrix. It is capable of determining about 30 elements including many environmentally crucial ones like aluminum, arsenic, antimony, bromine, copper, chromium, indium, manganese, nickel, selenium, silver, vanadium, zinc, etc. NAA is also capable of determining major elements such as sodium, chlorine and potassium, as well as many rare earth elements. The determination of the elemental concentrations is based on the measurement of induced radioactivity. The radioactive decay of many radioisotopes emits a characteristic gamma-ray energy spectrum. The characteristic gamma rays considered as fingerprints of the corresponding radionuclides and used for identifying and measuring the elemental concentration in the sample. Some of the important features of this methods are the following: 1) elemental response is independent of chemical or physical form of element in the sample, 2) liquid, solid or powder form of samples can be analyzed almost with equal convenience, 3) non-destructive, only in special cases pre or post chemical separation is needed, and 3) a wide range of detection capability of the elements from ng/g to percentage.

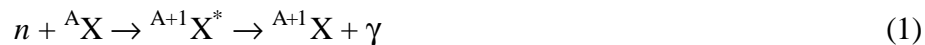
2.1 NAA Working Equations

Hevesy and Levi discovered the neutron activation analysis method in 1936 just four years after the neutron discovery. It has been widely used in the last three/four decades for its salient features. With the development of high-resolution semiconductor detectors in the 60's and availability of computers make it a popular analytical method. Sometimes the method is categorized depending upon the added chemical steps for

analysis. For example, if there is some pre-irradiation chemical separation involved then it is called as chemical neutron activation analysis (CNAA). For post irradiation chemical separation it is termed as radiochemical neutron activation analysis (RNAA). Sometimes the method is also termed based upon the type of neutron used during sample irradiation. For example, irradiation of samples by thermal neutron is called as thermal NAA (TNAA) or instrumental neutron activation analysis (INAA) or simply NAA, while the use of epithermal neutron for sample irradiation is commonly referred as epithermal NAA (ENAA) and similarly fast NAA (FNAA) for using the fast neutron during sample irradiation.

2.1.1 Neutron Nuclei Reactions

A variety of reactions may occur when a neutron collides with a nucleus. The reaction cross sections are a function of neutron energy and vary with different nucleus. The most common reactions are elastic scattering (n,n), inelastic scattering (n,n'), radioactive capture (n, γ), charged particle emission, i.e. (n,p) or (n, α), knockout (n,2n), and fission (n,f). For NAA radioactive capture is the most dominant and preferred reaction for it's high reaction cross-section and suitable emission spectrum. The target nucleus ${}^A\text{X}$ absorbs a neutron 'n' and forms a compound nucleus ${}^{A+1}\text{X}^*$ in an excited state. The compound nucleus de-excites by a prompt gamma-ray emission, so the process is called radiative capture, by notation



The resultant radionuclide then decays to the ground state following beta and gamma emissions. The detection and counting of these gamma rays is the key technique of neutron activation analysis. Usually in NAA work, the gamma photons of radioactive samples are counted using high purity germanium (HPGe) detector in combination with a multi-channel analyzer (MCA) and other spectroscopy grade amplifiers and electronic modules. The gamma peak energies in the spectrum identify the radioisotopes, and hence, the target nuclei X^A . The intensities of the peaks are used to determine the elemental concentration in the samples. If the product of the neutron nuclear reaction is stable, then NAA cannot be used to determine the concentration of the target element.

2.1.2 Reaction Rates

The rate of neutron interactions R_i of type i is obtained by integrating the product of the interaction cross-section $\sigma_i(E)$, the neutron flux $\phi(E)$, and the number of target nuclei N over the energy range of the incident neutrons.

$$R_i = N \int_0^{\infty} \sigma_i(E) \phi(E) dE \quad (2)$$

Concentrating on only radioactive capture reactions, the reaction rate is generally broken into three terms, which depend on the energy range (thermal, epithermal, and fast) of the incident neutrons,

$$R = R_{th} + R_{epi} + R_{fast} \quad (3)$$

Many nuclides, especially those with low atomic number, have neutron capture cross sections are proportional to $1/v$ for neutron energies below 0.5 eV, where v is the speed of the neutron. Generally the thermal cross section σ_{th} corresponding to the thermal neutron energy (~ 0.025 eV) is used to determine the thermal flux ϕ_{th} .

$$R_{th} = N \int_{th} \sigma(E) \phi(E) dE = N \sigma_{th} \Phi_{th} \quad (4)$$

Resonance peaks dominate the neutron capture cross sections in the epithermal energy range between 0.5 eV and 0.5 MeV. The epithermal neutron flux ϕ_{epi} in a water moderated reactor like the TRIGA follows a $1/E$ distribution. Since the epithermal capture cross section σ_{epi} varies rapidly, the radioactive capture integral I_o is used to refer to the cross section. The epithermal reaction rate can be calculated by

$$\begin{aligned} R_{epi} &= N \int_{epi} \sigma(E) \phi(E) dE \\ &= N \int_{epi} \sigma(E) \Phi_{epi} \frac{dE}{E} \\ &= N \Phi_{epi} \int_{epi} \sigma(E) \frac{dE}{E} \\ &= N \Phi_{epi} I_o \end{aligned} \quad (5)$$

where the epithermal Φ_{epi} is in units of $n.cm^{-2}s^{-1}$. The fast reaction rate R_{fast} is negligible because the capture cross-section at high energies is very small. The radioactive capture reaction rate can then be written as:

$$R = Ns_{th}\Phi_{th} + NI_o\Phi_{epi} \quad (6)$$

In thermal irradiations both terms in equation 6 are important. Compilations of thermal neutron capture cross sections and resonance integrals are available in several references and in computer databases.

2.1.3 Calculation of Concentrations by NAA

The expressions for reaction rates developed in the preceding section can be used to calculate the concentration of an element in an unknown sample knowing the concentration of the same element in a reference standard. The reaction rate for a specific target can be written:

$$R = Ns_{th}\Phi_{th} + NI_o\Phi_{th} = Ns_{act}\Phi \quad (7)$$

where, $s_{act}\Phi$ is the product of the activation cross-section and the neutron flux integrated over an appropriate energy range. The rate of change in the number of radioactive nuclei N^* is given by equation 8 where λ is the radioactive decay constant,

$$\frac{dN^*}{dt} = s_{act}\Phi N - \lambda N^* \quad (8)$$

Integrating Eq.8 to obtain $N^*=N^*(t)$ yields:

$$N_t^* = \frac{s_{act}\Phi N}{\lambda} (1 - e^{-\lambda t}) \quad (9)$$

In practice, a sample is irradiated for a time t_i , allowed to cool for a decay time t_d , and counted for a time t_c . These three time variables are important parameters to optimize the analytical sensitivity of any radionuclide of interest. The number of radioactive nuclei after irradiation time t_i and decay time t_d is:

$$N_{t_d}^* = \frac{s_{act}\Phi N}{\lambda} (1 - e^{-\lambda t_i}) e^{-\lambda t_d} \quad (10)$$

The measured counts depend on the intensity I_γ of the emitted γ -ray and on the efficiency ϵ_γ of the detector at that energy. Counting of radioactive sample for a time t_c after a decay time t_d is then

$$S = \epsilon_g I_g \int_0^{t_c} N_{t_d} I e^{-\lambda t} dt \quad (11)$$

which finally yields:

$$S = \frac{S_{act} \Phi N}{I} (1 - e^{-\lambda t_i}) e^{-\lambda t_d} (1 - e^{-\lambda t_c}) I_g \epsilon_g \quad (12)$$

For short NAA, standards and samples are irradiated separately often with different irradiation, decay, and counting times. However, they are counted at identical geometric configuration with the same detector. Then in the ratio of unknown (sample) to known (standard) for any radioactive element, many common terms are drop out and the ratio simply becomes:

$$\frac{S_u^*}{S_k^*} = \frac{N_u f_u (1 - e^{-\lambda t_{iu}}) e^{-\lambda t_{du}} (1 - e^{-\lambda t_{cu}})}{N_k f_k (1 - e^{-\lambda t_{ik}}) e^{-\lambda t_{dk}} (1 - e^{-\lambda t_{ck}})} \quad (13)$$

The number of target nuclei N is a product of concentration C and mass M and equation (13) can be rewritten solving for the concentration of the unknown sample as:

$$C_u = C_k \frac{M_k N_u^* f_u (1 - e^{-\lambda t_{iu}}) e^{-\lambda t_{du}} (1 - e^{-\lambda t_{cu}})}{M_u N_k^* f_k (1 - e^{-\lambda t_{ik}}) e^{-\lambda t_{dk}} (1 - e^{-\lambda t_{ck}})} \quad (14)$$

where the subscript u and k denote unknown sample and known standard, respectively. If the sample and standards are irradiated at different times, then flux monitors are employed to account for any variations in the neutron fluency.

2.2 Gamma Ray Spectrometry

Photons interact with matter mainly by three processes, namely photoelectric effect, Compton effect, and pair production. Any type of these interactions is energy and material dependent. Pair production is reserved for energetic photons ($E_\gamma > 1.022\text{MeV}$). In the photoelectric process the gamma ray completely transfers its energy to the target atoms (inner electrons). The photoelectron is ejected and usually deposits

its energy within the crystal. This effect is prominent for lower energy photons. For typical photon energies the most important interaction with germanium is the Compton effect. In this process partial energy is transferred to the target electron and incident photon, which are scattered with lower energies.

The photon energy loss is related to the scattering angle, θ , as:

$$E_{g'} = \frac{E_g}{1 + (1 - \cos \theta) \frac{E_g}{mc^2}}$$

where $E_{g'}$ and E_g are the scattered and incident photon energies, respectively, and m is the mass of electron. In Compton scattering a maximum energy transfer occurs when $\theta = 180^\circ$, and the photon energy is reduced to

$$E_{g' \min} = \frac{E_g}{1 + \frac{2E_g}{mc^2}}$$

Interaction at $\theta = 0^\circ$ does not reduce the photon energy. The consequence of Compton effect is the inability of the target to completely eliminate the identical photons. The photoelectrons deposit their energy within the crystal but the scattered photons are free to interact with other electrons by the photoelectric or Compton effect process. Relating to the detection system, Compton scattering produces many low energy signals (from the photoelectrons) with the possibility of escaping the crystal depositing only its partial energy. The low energy signals create an augmented background continuum, which increases the detection limit of medium energy photons.

The block diagram of a normal HPGe gamma-ray spectrometry and a Compton suppression spectroscopy are shown in Figure 2.1 and Figure 2.2. The detrimental effects of Compton scattering can be alleviated dramatically by the use of an anti-coincidence suppression system (Petra *et al.* 1990). The system blocks the signal when a gamma-gamma coincidence occurs in the germanium and surrounding NaI detector. In opposite case, it is passed through the gated amplifier and stored in the MCA. The HPGe detector is surrounded by a NaI(Tl) detector shell and when a photon escapes the HPGe detector

depositing a fraction of its energy, then it is likely to be captured by the NaI(Tl) shell. If the two events occur within the appropriate time (100 ns) the system rejects the signal. High activities produce random signals from radioactive decay within the window of 100 ns and results in random coincidence rejection of detector signal. Generally, samples with <10% dead time work well.

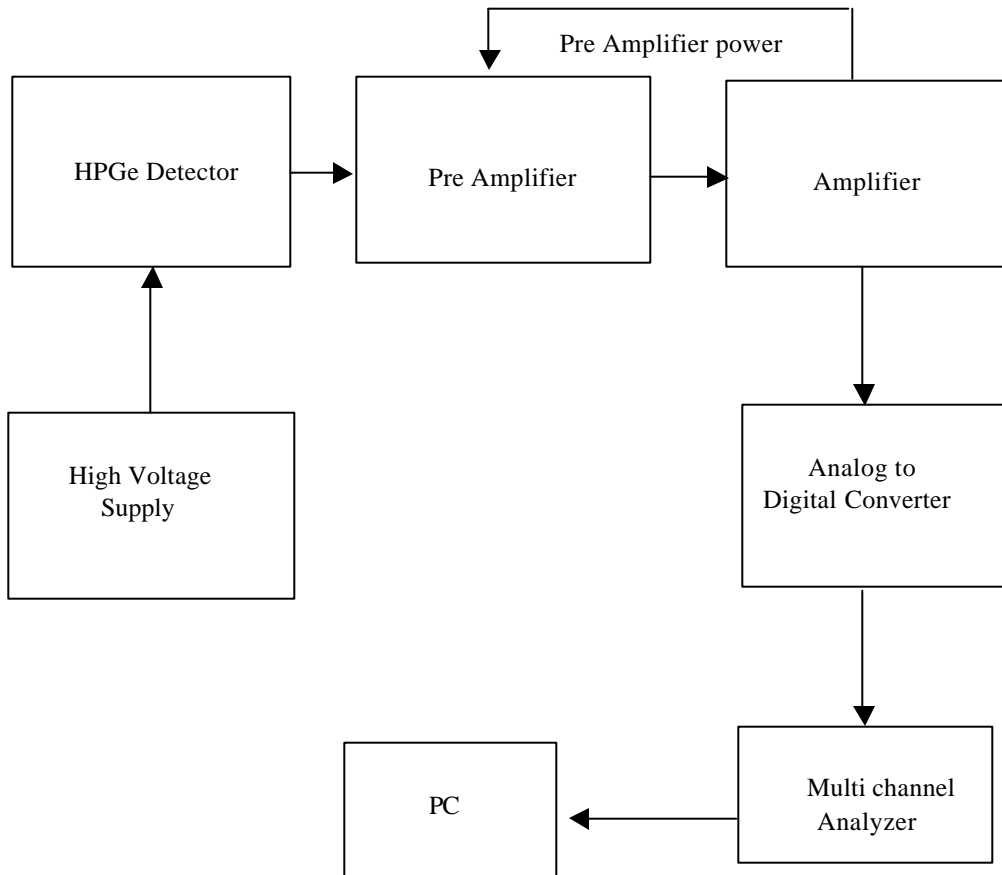


Figure 2.1 Block diagram of the normal mode HPGe gamma ray spectrometry

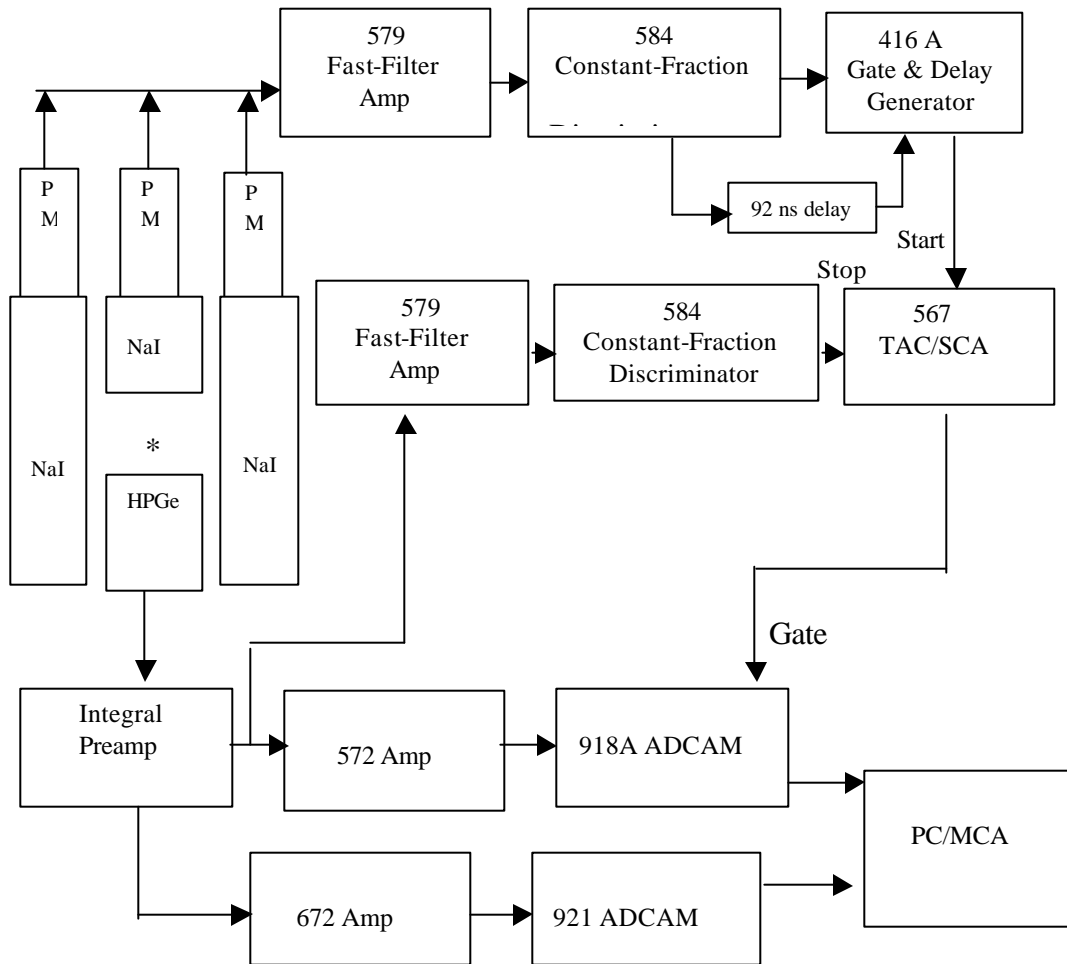


Figure 2.2 Schematic of Compton suppressed counting system

2.3 Irradiation and Counting Facilities

In this work, samples were irradiation in a TRIGA MARK II research reactor at Nuclear Engineering Teaching Laboratory, University of Texas at Austin. A pneumatic facility (rabbit) laboratory for sending samples back and forth to the reactor core is adjacent to the reactor hall. A rabbit terminal is available inside the fume hood with different time settings with a maximum of a ten-minute irradiation. A Compton suppressed system with the HPGe detector equipped with electronic modules is available inside the pneumatic laboratory to allow the counting of samples simultaneously in normal mode and with Compton suppressed mode. The counting system also has an auto

sample changer unit to aid medium or long counting for determining other than short lived isotopes. An internal view of the laboratory is shown in Figure 2.3.



Figure 2.3: An internal view of the pneumatic laboratory

Four irradiation facilities are available in the reactor, and two of them are presented in Table 2.1. In this work only Pneumatic System (PS) and Cadmium Lined Pneumatic System (CLPS) were used for irradiations.

Table 2.1: Irradiation facilities of the TRIGA MARK II research reactor

Facility	Cadmium Ratio	Thermal flux ($\text{n cm}^2 \text{sec}^{-1}$)	Epithermal flux ($\text{n cm}^2 \text{sec}^{-1}$)
Pneumatic System (PS)**	5	2.8×10^{12}	1.3×10^{11}
Cadmium Lined Pneumatic System (CLPS)*	1		1.1×10^{11}

** Reference to 950 kW, *Reference to 500 kW

The PS and CLPS irradiations are operated from the pneumatic laboratory as one sample at a time.

3. Experimental

3.1 Sampling

3.1.1 Sample Collection

The Finnish Meteorological Institute started aerosol particulate sampling at several locations in Finland from 1959. The primary interest was to monitor potential airborne radioactivity due to the Soviet nuclear tests. After disposing the samples for a few years the institute began archiving the aerosol filters. So, for several locations, aerosol samples are available dating back to as far as 1963. The locations of sampling stations are shown in Figure 3.1. The four northernmost sampling sites namely Rovaniemi Airport (66°34' N, 25°50' E), Sodankylä Observatory (67°22' N, 26°39' E), Ivalo Airport (68°36' N, 27°25' E), and Kevo Observatory (69°45' N, 27°02' E, 98 m above the sea level) fall inside the common geographical Arctic Circle.

In this work, aerosol samples at Kevo Observatory, collected during the period of late October 1964 to February 1978, were analyzed for chemical characterization. A schematic diagram of the sampling arrangement is presented in Figure 3.2. The sampling unit had two filters, each equipped with a Geiger Muller (GM) counter for radioactivity counting. In a weeklong sampling period, four hours alternating airflow was maintained through each of the filters and the aerosol radioactivity was counted in the same alternating fashion on the off line filter. For reducing the background counts each GM tube including filter unit was lead shielded. A 3-way valve controlled the airflow to either of the filters. The air inlet was 7 meters high above the ground. The air suction motor was inside a room, so there was no contamination from the motor generated copper to the filter. Atmospheric aerosols were collected on Whatman 42 paper filters. The sampling unit was not equipped with size selective inlets and therefore total suspended

particles (TSP) were collected on the filter. Rectangular filters with a dimension of 12 cm × 14 cm were used for aerosol collection and resulted an aerosol exposed area of about 11 cm × 12 cm. An airflow rate through filters on average was about 113 L/min. The aerosol sampling procedure generated two filters per week and a total of 1370 samples for a period of 685 weeks.

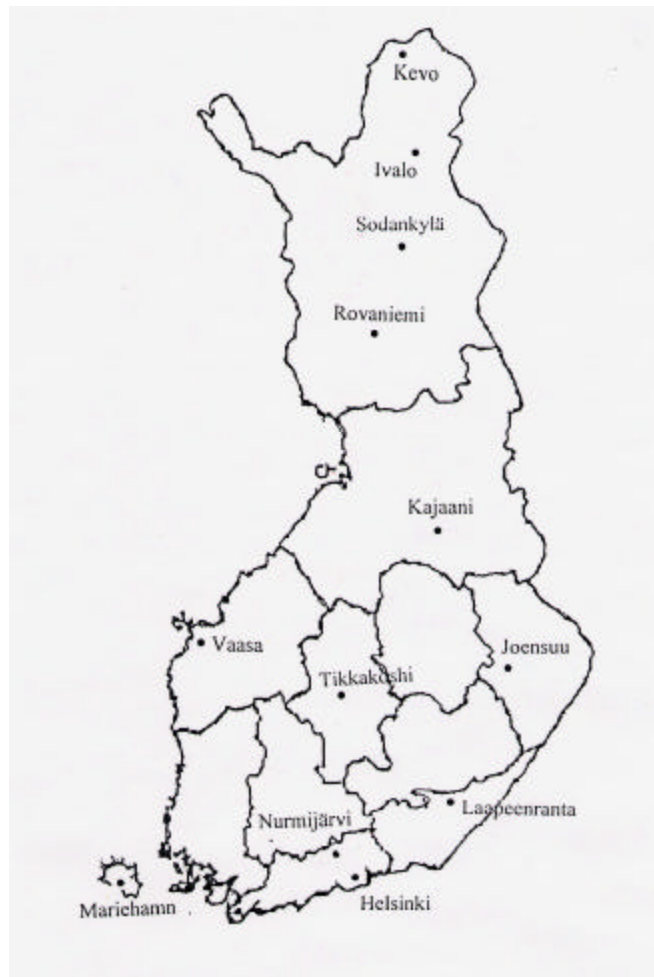


Figure 3.1: Map of Finland showing the sampling sites of the Finnish Meteorological Institute

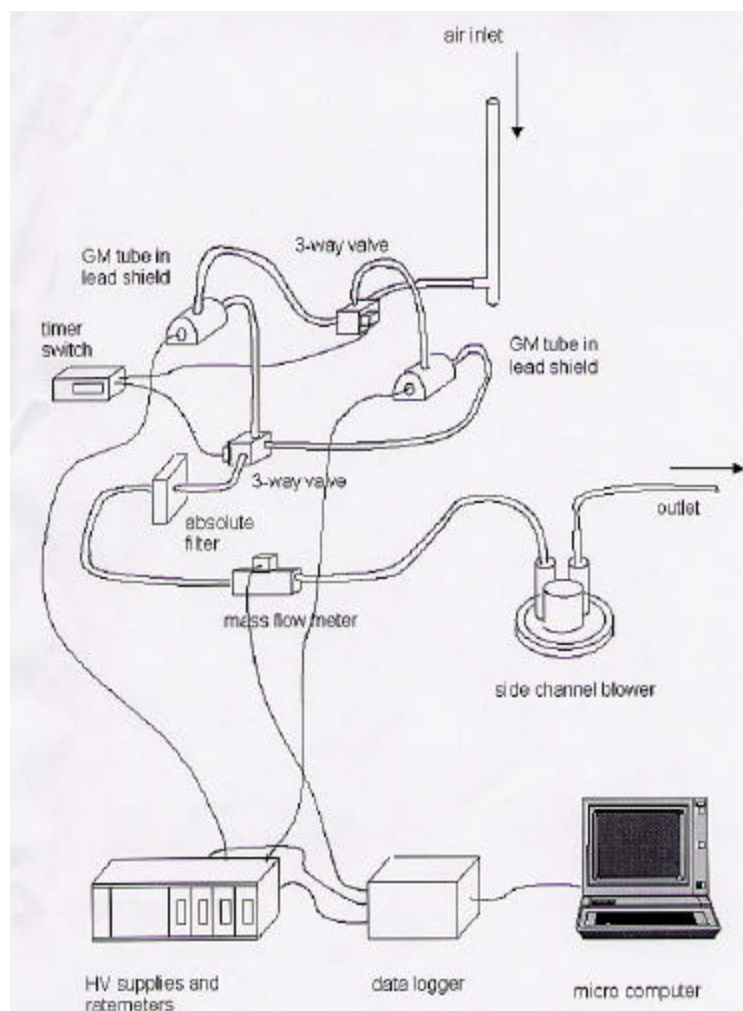


Figure 3.2: Schematic diagram of the aerosol sampling arrangement in Kevo

As it can be recognized from the earlier description, Kevo in northern Finland is surrounded by various industrial activities. A description of industrial activities and an approximate distance from the sampling location are presented in Table 3.1. The industrial location in Norilsk (69.2° N, 88.1° E), northern Siberia, Russia, which is about 6400 km away from Kevo. The Kola Peninsula extends from 66° to 69° N latitude and from 28° to 41° E longitude. However, most of the industrial cities in the Kola are in the western side of the Peninsula, i.e. close to the northeastern border of Finland.

Table 3.1: Location, distance and industrial activities near to Kevo

Sampling location at Finland (a)	Industrial locations (b)	Approximate Distance from (a) to (b) in km	Type of Industry
Kevo (69°45'N, 27°03'E)	Kirkenes, Norway (69°41'N, 30°02'E)	115	Iron ore mine and mill
	Nikel (69°25'N, 30°15'E)	134	Nickel smelter
	Zapoljarnij (69°30'N, 30°43'E)	145	Nickel ore roasting
	Murmansk (69°02'N, 33°15'E)	256	Large harbour town with related industries, base of about 150 nuclear powered vessels
	Kovdor (67°35'N, 30°40'E)	282	Iron ore mine and mill
	Monchegorsk (67°51'N, 32°48'E)	313	Nickel, copper and cobalt smelters
	Olenegorsk (68°08'N, 33°30'E)	314	Iron ore mining and mill
	Apatity (67°40'N, 32°47'E)	327	Thermal power station, processing of apatite ore
	Kandalaksha (67°13'N, 32°13'E)	352	Aluminum smelter, nuclear power station
	Rovaniemi		Peat fired power plant
	Kirovsk (67°36'N, 34°E)	370	Apatite open pit mine
	Norilsk (69.2°N, 88.1°E)	6400	Copper, nickel, etc. mining

3.1.2 Particle Size Distribution

Emissions released to the atmosphere through natural, industrial and automotive activities can widely differing particle sizes ranging from submicron diameters (e.g. cigarette smoke) to sea salt spray (tens of microns). Gaseous releases may condense onto particles or attach to secondary particles, while particles may deposit or become airborne. Typically, smaller or fine particles (less than 2.5 µm) travel much further distances in the atmosphere as compared to larger or coarse particles (> 2.5 µm). Industrial activities

such as coal burning and smelters can release fine particles due to the high combustion and volatility of many trace elements. Elemental size distribution of airborne particles can give a good insight to source identification. Samples collected in this study were not collected with any size cut-off. Although some important information can be lost without a size selective cut-off, a lot of valuable data is still available.

3.2 Analysis

3.2.1 Sample and Standard Preparation

For NAA about 1/4th of each filter was analyzed to determine the atmospheric elemental concentration. To obtain a mean weekly atmospheric concentration, two 1/4th filters were combined and then placed inside a pneumatic carrier vial. Combined filters occupied a volume of about 3 ml inside the pneumatic vial. Another 2/5th dram vial was placed on top of the filter inside the pneumatic vial, containing about 500 mg of sulfur powder. Sulfur powder was used as a neutron flux monitor to normalize the neutron flux for individual sample irradiation. Usually in NAA aerosol filters are irradiated several times to determine concentration levels of elements having different half-lives. So, careful handling during filter preparation for irradiation and transfer to non-irradiated vial after irradiation is of utmost importance for preserving the particles on the filter. A sequential process of sample preparation for a pneumatic irradiation is shown in Figure 3.3.

All calibration solutions were prepared using mono standard solutions from the National Institute of Standards and Technology (NIST) or from laboratory chemicals. Most NIST mono standard solutions were about 10,000 $\mu\text{g/g}$ in concentration. Depending upon the elemental sensitivity for NAA, either the original solutions of concentration level of 10,000 $\mu\text{g/g}$ or diluted solutions of concentration levels between 5-200 $\mu\text{g/g}$ were used as a primary standard. Primary standards for aluminum, calcium, copper, silicon, and titanium were used directly without dilution, while antimony, arsenic, cobalt, indium, manganese, potassium, vanadium, silver, tin, tungsten, and zinc were diluted to a convenient sensitive level for irradiation and counting. Bromine, chlorine, iodine, and sodium standard solutions were prepared from dried potassium bromide,

potassium iodide, and sodium chloride salts. All standards were prepared maintaining an equal volume and geometry with that of the aerosol filters inside the irradiation vial. As all the primary standards were liquid so either these were prepared for irradiation in a heat seal vial or used after absorbing onto a blank filter inside the vial. For quality control purpose, NIST Standard Reference Material (SRM) Coals 1632a, 1632b, and 1632c, Citrus Leaves 1572, and San Joaquin Soil 2709 were also analyzed. In subtracting elemental filter blanks from the measured data new Whatman 42 filters were used, since no field blanks were taken during the sampling period.

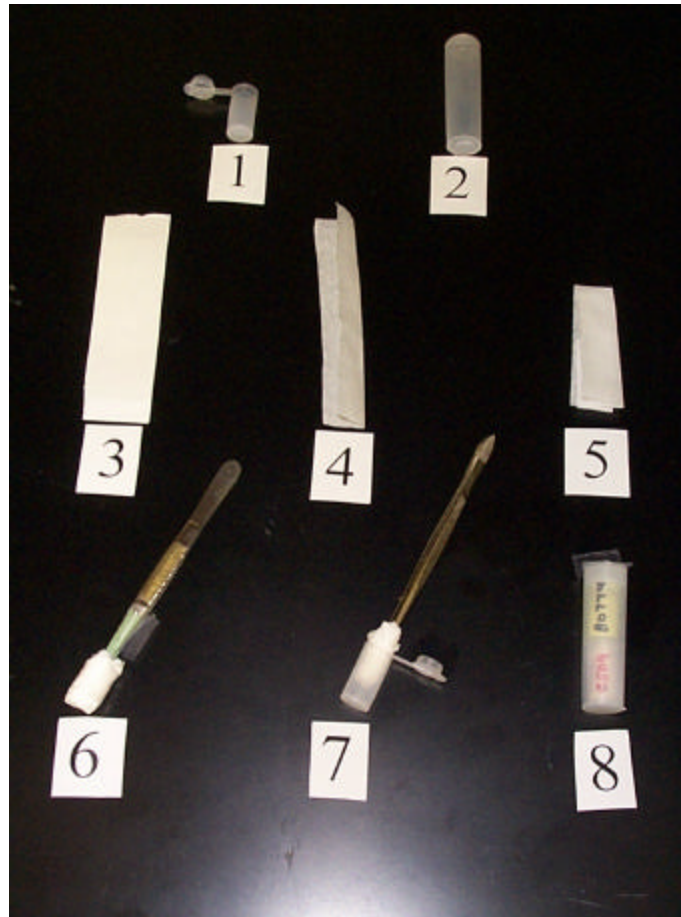


Figure 3.3: Steps of aerosol filter preparation for a pneumatic irradiation

Description of Figure 3.3:

- 1) 2/5th dram vial used for sulfur and filter (height 2.2 cm, diameter 1.2 cm)
- 2) A pneumatic (PNT) vial (height 5.5 cm, diameter 1.5 cm)
- 3) A fraction of an aerosol filter (~ 3.5 cm × 12 cm)
- 4) & 5) Folding of a filter, keeping the particulate matter in the inner side
- 6) Twisted to a cylindrical form using a tweezers
- 7) Placing of aerosol filter inside a 2/5th vial
- 8) A PNT vial loaded with a filter vial at the bottom and sulfur powder on the top

3.2.2 Irradiation and Counting

The I_γ/σ_{th} ratio for all the elements of interest were investigated to determine the best sensitivity for thermal or epithermal irradiation. Elements which have an I_γ/σ_{th} ratio more than unity, are favorable to be determined by epithermal NAA. Some of the nuclear properties of the measured elements are presented in Table 3.2. Three separate irradiations were conducted on each filter at the TRIGA MARK II research reactor facility followed by a count using HPGe gamma spectrometry system. Many radioisotopes emit more than one characteristic gamma ray, so a careful choice for suitable gamma rays, free from any interference, was used for elemental determination. These are shown in Table 3.2. A scheme for irradiation type, duration, decay and counting times, counting facility and elements determined is presented in Table 3.3.

Table 3.2: Elements, nuclear reactions and nuclear data

Element	Nuclear Reaction	I_g/S_g^0 *	Gamma Energy (keV)	Half-life
V	$^{51}\text{V}(n,\gamma)^{52}\text{V}$	0.55	1434.2	3.75 m
Na	$^{23}\text{Na}(n,\gamma)^{24}\text{Na}$	0.59	1368.6	15.02 h
Ti	$^{50}\text{Ti}(n,\gamma)^{51}\text{Ti}$	0.66	320.1	5.75 m
Cl	$^{37}\text{Cl}(n,\gamma)^{38}\text{Cl}$	0.69	1642.4	37.2 m
Al	$^{27}\text{Al}(n,\gamma)^{28}\text{Al}$	0.74	1778.7	2.24 m
Ca	$^{48}\text{Ca}(n,\gamma)^{49}\text{Ca}$	0.82	3084.4	8.72 m
K	$^{41}\text{K}(n,\gamma)^{42}\text{K}$	0.97	1524.6	12.36 h
Cu	$^{65}\text{Cu}(n,\gamma)^{66}\text{Cu}$	1.01	1039.2	5.10 m
Mn	$^{55}\text{Mn}(n,\gamma)^{56}\text{Mn}$	1.05	1810.7	2.58 h
Co	$^{59}\text{Co}(n,\gamma)^{60\text{m}}\text{Co}$	1.91	58.6	10.5 m
W	$^{186}\text{W}(n,\gamma)^{187}\text{W}$	12.80	685	23.9 h
As	$^{75}\text{As}(n,\gamma)^{76}\text{As}$	13.56	559.1	1.1 d
Ag	$^{109}\text{Ag}(n,\gamma)^{110}\text{Ag}$	15.38	657.7	24.6 s
In	$^{115}\text{In}(n,\gamma)^{116\text{m}}\text{In}$	16.33	416.9	54.15 m
Br	$^{81}\text{Br}(n,\gamma)^{82}\text{Br}$	18.52	776.5	1.47 d
I	$^{127}\text{I}(n,\gamma)^{128}\text{I}$	23.71	442.9	25 m
Sb	$^{121}\text{Sb}(n,\gamma)^{122}\text{Sb}$	33.90	563.9	2.7 d
Zn	$^{68}\text{Zn}(n,\gamma)^{69\text{m}}\text{Zn}$	43.06	438.6	13.76 h
Sn	$^{124}\text{Sn}(n,\gamma)^{125\text{m}}\text{Sn}$	61.54	332.1	9.52 m
Si	$^{29}\text{Si}(n,p)^{29}\text{Al}$	-	1273	6.5 m

* I_γ = radiative capture resonance integral, S_g^0 = Neutron radiative capture cross-section measured at 2200 m/sec (Data from Mughabghab *et al.* 1981)

Table 3.3: NAA scheme for sample irradiation, decay, and counting on the same filter; Reactor power 500 kW

Irradiation type	Irradiation facility	Irradiation time	Decay time	Counting time	Element determined	Counting mode
Thermal short	Pneumatic	2 m	~ 7 m	10 m	Al, Ca, Cl, Mn, Na	Normal
					Cu, Ti, V	Compton
Epithermal short	Pneumatic	1 m	~24 s	100 s	Ag	Normal
Epithermal short	Pneumatic	10 m	10 m	15 m	In	Normal
					I, Co, Si, Sn	Compton
			5-15 h	1 h	Br	Normal
			As, K, Sb, Zn, W	Compton		

Due to the very short half-life of ^{110}Ag , samples were manually counted without transferring the filter from an irradiated vial. However, for all other irradiations samples were always transferred to a non-irradiated vial and counted both in the normal and Compton mode. For epithermal short irradiations a maximum of sixteen samples were irradiated per day. Immediately following the short count, samples were loaded into an auto sample changer in sequence of irradiation and counted for an hour.

The use of sulfur powder for neutron flux normalization adjusted for the neutron flux fluctuations as can be seen in Figure 3.4.

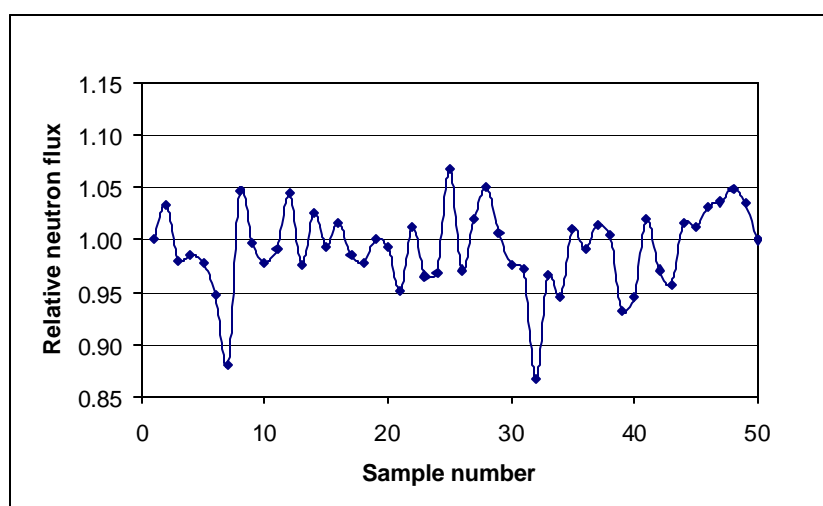


Figure 3.4 Relative neutron flux variation during individual sample irradiation

3.2.3 Spectrum Analysis

Quantitative elemental determination in the aerosol filters was done following a comparative method as shown in equation 14. The neutron activation data analysis code NADA93 [Landsberger *et al.*, 1994] was used to analyze all spectra for elemental concentration. An input file required for this analysis is a text report of selected energies generated from each gamma ray spectrum. These files were readily produced from the ORTEC MCA gamma spectrum display mode. All report filenames with other parameters like irradiation time, decay time, and flux factor were gathered in a batch file for the NADA93 run. An output file of NADA93 contains all elemental concentration is

conveniently imported to an Excell sheet and all desired calculations for blank correction and conversion to atmospheric concentrations were conveniently performed afterward.

3.2.4 Blank Correction

During the sampling period of 1964-1978 no field blanks were taken, since it was not necessary for the aerosol radioactivity-monitoring project. However, in determining elemental and chemical species in aerosol collected on filters, it is very important to investigate and subtract the field blank contribution from the measured concentration. In this work, five new filter blanks from the same batch of Whatman 42 were analyzed for all the reported elements. Blank elemental statistics are calculated as the following and presented in Table 3.4.

A) Concentration of blank above the analytical detection limit

If more than 50% elemental concentrations are above the analytical detection limit, then the mean and the standard deviation of the elemental concentration was calculated based on the concentrations of these blank filters. The elemental concentrations in the blank filter greater than the mean plus two-standard deviation are deleted. Then the mean and standard deviation of the elemental concentrations are recalculated. So, then a delectable limit 'A' for the filter is:

$$A = B + 3 \sigma_b$$

B --- the mean of the elemental concentration of the blank filters.

σ_b --- standard deviation of the elemental concentration of the blank filter

Finally, the air concentrations are calculated as the following:

If $X_{\text{sample}} > A$

Then $C = 264 (X_{\text{sample}} - B)/V$

Else $C < 264 \times 3 \sigma_b/V$

The total exposed area 264 cm^2 was multiplied to elemental mass/ cm^2 of the filter.

B) Concentration of the blank below the detection limit

If more than 50% elemental concentrations are below the analytical detection limit in the blank filters, the mean and standard deviation of the elemental concentrations were calculated based on the analytical detection limit of those blank filters. In this case, the filter detection limit is calculated as:

$$A = 3 B$$

and a value for subtraction from the measured data is obtained as:

$$D = (2/3) B$$

These procedures of determining the detection limit and blank correction were adopted from classical treatment of detection limits (Currie, 1968) and the procedure followed at Atmospheric Environmental Service, Ontario, Canada. Again, the atmospheric concentrations were calculated as:

$$\text{If } X_{\text{sample}} > A$$

$$\text{Then } C = 264 (X_{\text{sample}} - D)/V$$

$$\text{Else } C < 264 D / V$$

Table 3.4: Filter blank statistics from 5 filters for subtraction from measured quantity

	Average	Stdev	A=B+3 s	A=3B	D=(2/3)B	3 s
	$\mu\text{g}/\text{cm}^2$	$\mu\text{g}/\text{cm}^2$	$\mu\text{g}/\text{cm}^2$	$\mu\text{g}/\text{cm}^2$	$\mu\text{g}/\text{cm}^2$	$\mu\text{g}/\text{cm}^2$
<i>Ag</i> *	1.89E-04	1.62E-05		5.7E-04	1.3E-04	4.86E-05
Al	1.17E-02	1.6E-03	1.65E-02			4.81E-03
As	2.32E-05	2.72E-06		7.0E-05	1.5E-05	8.16E-06
Br	1.92E-03	8.96E-05	2.19E-03			2.69E-04
Ca	3.54E-01	5.5E-02	5.18E-01			1.64E-01
Cl	6.84E-01	1.3E-02	7.22E-01			3.79E-02
<i>Co</i>	3.60E-05	3.79E-06		1.08E-04	2.40E-05	1.14E-05
<i>Cu</i>	2.26E-03	4.2E-04		6.8E-03	1.5E-03	1.27E-03
I	1.34E-04	1.18E-05	1.70E-04			3.53E-05
<i>In</i>	5.49E-07	1.88E-08		1.65E-06	3.7E-07	5.65E-08
K	1.05E-02	3.41E-03	2.07E-02			1.02E-02
<i>Mn</i>	4.36E-04	8.0E-05		1.3E-03	2.9E-04	2.39E-04
Na	1.28E-01	5.4E-03	1.45E-01			1.63E-02
<i>Sb</i>	1.88E-05	1.42E-06		5.6E-05	1.3E-05	4.27E-06
<i>Si</i>	8.45E-02	4.29E-03		0.2535	5.6E-02	1.29E-02
Sn	6.93E-04	7.37E-05	9.14E-04			2.21E-04
<i>Ti</i>	4.59E-03	7.9E-04		1.4E-02	3.1E-03	2.38E-03
V	1.43E-05	1.6E-05	6.14E-05			4.71E-05
W	1.71E-04	1.29E-04	5.58E-04			3.87E-04
Zn	6.29E-03	3.92E-03	1.81E-02			1.18E-02

* *Italic* elements fall to the group b) as of section 3.2.4, while other elements to group a) in this work

3.3 Quality Control and Results

For stringent quality control purposes Standard Reference Materials (SRM) were analyzed. The quality control results are presented in Table 3.5. Optimized parameters for standard and SRM irradiation are presented in Appendix A. Only for Ag, irradiated SRM's were counted at higher counting position and later normalized for the sample counting position. Silver was counted in normal mode, so coincidence factor is not applicable for a different counting position. As can be seen from Table 3.5, the results are in excellent agreement with certified reference and consensus values.

Table 3.5: Elemental concentration determined by NAA in SRM

Elements	This work ppm	Certified value ppm	SRM
			Canadian CRM
Ag	25.1 ± 2.6	24.2 ± 2.0	Gold Ore CH2
Al	8680 ± 88	8550 ± 190	NIST 1632 b
As	10.0 ± 1.0	9.3 ± 1.0	NIST 1632 a
Br	18.1 ± 1.8	18.7 ± 0.4*	NIST 1632c
Ca	1998 ± 81	2040 ± 60	NIST 1632 b
Cl	1041 ± 104	1139 ± 41	NIST 1632c
Co	12.2 ± 0.6	13.4 ± 0.7*	NIST 2709
Cu	19.5 ± 6.0	16.5 ± 1.0	NIST 1632 a
I	1.86 ± 0.19	1.84 ± 0.03	NIST 1572
In	0.038 ± 0.004	0.036 ± 0.004*	NIST 1632 a
K	709 ± 76	748 ± 28	NIST 1632 b
Mn	11.8 ± 1.2	12.4 ± 1.0	NIST 1632 b
Na	500 ± 50	515 ± 11	NIST 1632 b
Sb	7.8 ± 0.8	7.9 ± 0.6	NIST 2709
Si	27.93 ± 0.84 %	29.66 ± 0.23 %	NIST 2709
Ti	1651 ± 46	1630 ± 130*	NIST 1632 a
V	42 ± 4	44 ± 3	NIST 1632 a
W	2.1 ± 0.2	2**	NIST 2709
Zn	27.8 ± 6.4	28 ± 2	NIST 1632 a

* Consensus value [Germanl *et al.*, 1980] **Reference value

3.4 New Approaches of NAA Routine Use

3.4.1 Irradiation and Counting

Nuclear analytical techniques like neutron activation analysis (NAA), X-ray fluorescence (XRF), particle induced x-ray emission (PIXE) are routinely used in many laboratories for trace element determination in aerosols and other samples. Employment of epithermal NAA was reported to be very useful for determining indium, which is a crucial trace element for receptor modeling (Landsberger *et al.* 1992a). Other important tracer elements such as arsenic, antimony, tin, and tungsten are the precursors of many industrial activities and can be determined more conveniently with epithermal NAA and Compton suppressed counting [Landsberger *et al.*, 1997]

In spite of many unique advantages of NAA, this method always faces the competition with other nuclear techniques, i.e. PIXE, XRF as well as with non-nuclear technique, such as inductively coupled plasma mass spectroscopy (ICP-MS). Sometimes a time factor for completing any analysis might appear as a restriction to use of NAA methodology, since, any successive irradiations on the same sample for determining the short, medium, and long-lived isotopes require a time period for decaying the induced activity. Almost always, when the quantity of available samples is small or very precious, a single sample is subjected to several irradiation and counting procedures, i.e. thermal short, epithermal short, epithermal medium, and thermal long. After each irradiation samples need to decay for a minimum required time before using it for the next irradiation. Usually after thermal short irradiation, a one week decay time is enough, however, after a short ten-minute epithermal irradiation three weeks decay time is required before employing medium irradiation for determining the medium lived isotopes ($t_{1/2} = \sim 20\text{-}40\text{ h}$) in the sample. Sample handling procedures, i.e. packaging, loading, unloading etc., for a medium epithermal run are different than that of a short irradiation procedure using a pneumatic facility. Sometimes repeated irradiations make a filter very brittle and consequently it is very challenging to handle the filters. Furthermore, for medium-lived isotope determinations, a one-day decay after a medium epithermal irradiation does not result in a better detection limit in comparison to a ten-minute epithermal irradiation followed by a 3-15 hour decay time due to a ^{24}Na .

For all these reasons, a different procedure of irradiation and counting was employed in this work. In this approach, a ten-minute epithermal irradiation was used to determine both the short and medium-lived radionuclides, as presented in Table 3.3. The process totally bypasses the additional procedures for a separate epithermal medium run for all the samples. For a better sensitivity, a maximum of 16 samples were irradiated per day. The first count, for a 15-minute duration, was done following each irradiation and the second count started for all samples immediately after the first count of the last sample. For the second count, all samples were loaded into an auto sample changer in sequence of irradiation and counted in both the normal and Compton modes. In

determining short and medium-lived radioisotopes in aerosol filters, the ten-minute epithermal irradiation followed by two different decay and counting times was found to be very effective in this work, especially when the project had as much as 700 samples.

3.4.2 Silver and Cobalt determination

In NAA, a long irradiation is a common choice for determining silver and cobalt in the sample. The radioactive products ^{110m}Ag and ^{60}Co of half-lives 249.77 days and 5.27 years, respectively, are used for measuring these concentrations. A silver isotope ^{110}Ag ($T_{1/2} = 25$ sec.) of a $15.38 I_g/S_g^0$ ratio, as presented in Table 3.2, clearly indicates its suitability to be determined by epithermal NAA. However, the short-lived reaction product needs a quick handling for to be measured before decaying out. A one-minute epithermal irradiation followed by ~ 25 second decay time and 100 second counting time was followed for determining silver. Only one elemental concentration was determined using this epithermal irradiation, the scheme allowed to process as many as 100 samples in a five-hour long run in a day.

For cobalt determination, ^{58m}Co is a suitable isotope to be measured by a short irradiation with its 10.5 minutes half-life. However, the main difficulty arises due to its low energy gamma peak of 58.6 keV, which lies in a high background region of the spectrum, where bremsstrahlung peaks and Compton scattered gamma energies randomly accumulate and result in a higher detection limit. The usual p-type HPGe detector, which is surrounded by aluminum for vacuum purpose, is detrimental for this soft gamma ray due to an aluminum attenuation factor. A recently installed X-type HPGe detector (Canberra, Detector Model: GR 3519, Serial # 10996138) in the pneumatic laboratory, which has a beryllium window, allows an easy access of this soft gamma ray to interact with the germanium crystal. So, all the advantages of detector type, epithermal neutron irradiation, and Compton suppressed counting, aided to determine this element to a much lower concentration level in the aerosol filters. A comparison of the 58.6 keV peak and adjacent base line for different irradiation and counting modes is shown in Figure 3.5.

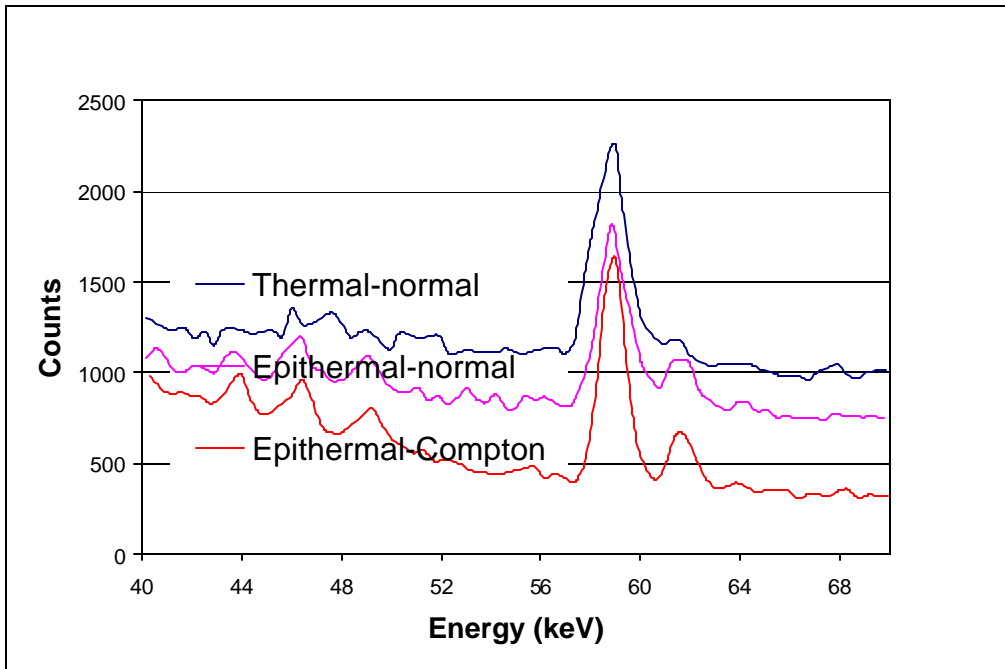


Figure 3.5: A comparison of 58.6 keV gamma ray sensitivity from the ^{58m}Co isotope in different irradiation and counting modes

4. Receptor Modeling

4.1 Introduction

Mathematical and statistical methods are very useful for interpreting, and predicting multivariate sets of environmental or chemical data. Analytical techniques used in many studies and research, equipped with modern computers and instruments often produce a plethora of data. Some of the prime objectives using a multivariate technique are data reduction or simplification, sorting or grouping, investigation of the dependence among variables, prediction, etc. [Johnson *et al.*, 1998].

In aerosol research, the application of such methods is very important to be able to understand a local or regional response of airborne pollutants or species since most of the monitoring techniques often end up with a large database with many samples that are analyzed for many constituent species [Hopke, 1983]. There are two types of mathematical models used to estimate the contributions of a single source or multiple sources in the ambient air; dispersion model and receptor model. Dispersion models attempt to simulate the behavior of plumes emitted to the atmosphere from ground level or stack height sources and predict the ambient concentration. On the other hand, receptor models use the aerosol constituent signals at the receptor site to identify sources and their contribution to the receptor site.

All receptor models are based on the principal of mass conservation. Among various approaches, Chemical Mass Balance (CMB) and multivariate receptor models, such as principal components analysis (PCA) and target transformation factor analysis (TTFA) receptor models were successfully applied in the past to both particulate and gaseous species of the ambient air (Hopke, 1991).

In CMB method, aerosol samples collected at a receptor site are analyzed for constituent species that are characteristic of the sources. A mass balance equation can be written to account for all m chemical species in the n samples as contributions from p independent sources

$$x_{ij} = \sum_{k=1}^p f_{ik} \cdot g_{kj} \quad (4.1)$$

where x_{ij} is the i^{th} elemental concentration measured in the j^{th} sample, f_{ik} is the gravimetric concentration (ng mg^{-1}) of the i^{th} element in material from the k^{th} source, and g_{kj} is the airborne mass concentration (mg m^{-3}) of material from the k^{th} source contributing to the j^{th} sample. If the sources that contribute to the samples can be identified and their composition patterns measured, then equation (4.1) can be solved for the source contributions to each sample. However, in many situations, the sources are either unknown or the compositions of the local particulate emissions have not been measured. Furthermore, the source profiles may have changed since they were last measured.

When sources are unknown or the profiles are not reasonably available, a multivariate analysis method, principal components factor analysis (PCFA), can be used for identifying the common sources around the receptor location. A receptor model mainly seeks to estimate three sets of unknowns, i.e. number of sources, source compositions, and source contribution (mass apportionment). A PCA factor model can be used for identifying the number of sources and source compositions in an airshed. However, additional computation is necessary to apportion the total aerosol mass to the individual sources. Thurston *et al.* (1985) reported a quantitative source apportionment technique, called absolute PCA (APCA), and applied it for five fine mass particle source classes and six coarse particle source classes in metropolitan Boston, MA. Target Transformation Factor Analysis (TTFA) is another approach of mass apportionment as reported by Hopke (1988), Chang *et al.* (1988), Alpert *et al.* (1981, 1980). For ambient air quality monitoring and control, qualitative and quantitative information about sources and their contribution are very important. The US Environmental Protection Agency (EPA) has adopted and used these models beginning in 1986 as part of the air quality

measurement strategies in the USA. Hopke (1991) and Henry (1997) presented excellent reviews of the historical background, earlier developments, and use of receptor models as a tool to solve the ambient air pollution problems.

In the literature, the PCA factor model is also called Principal Component Factor Analysis (PCFA), Factor Analysis (FA), and Convenient Factor Analysis (CFA). In a tutorial of PCFA, Hopke (1983) presented a detailed discussion with explicit examples on four types of errors that can be identified using PCFA. These were called as individual data point errors, bias errors, random variable errors and errors due to improper use of factor analysis. However, one of the major problems of using PCFA for the physical or chemical application is the scaling of the variables. PCFA scales the whole columns and/or rows of the data variables assuming an equal error for all observations, but in quantitative sciences (physics, chemistry, geophysics, etc.,) each observation is associated with error estimates [Paatero and Tapper, 1993]. Thus, Paatero *et al.* (1993) presented an optimal scaling procedure and solved the PCFA as a least squares fit problems. Henry (1987) showed that the PCFA receptor models were ill posed, since many implied constraints in the model, such as, reproduction of the original data by the model, non-negative source compositions, elemental mass fraction less or equal to unity, etc. could lead an infinite number of solutions. Thus, Paatero *et al.* (1993) and Henry *et al.* (1999, 1994) proposed two new approaches for receptor models.

Paatero (1997) called his new factor analytic technique as Positive Matrix Factorization (PMF), which uses a least squares fit to the matrix on properly weighted data points with non-negative constraints on the scores and loadings. A number of applications of PMF have been reported in the literature with its salient features, success, and comparison with other receptor models [Anttila *et al.*, 1995; Polissar *et al.*, 1999; Xie *et al.*, (1999), Wanna *et al.*, (2000), Poirot *et al.*, 2001; Qin *et al.*, (2002)].

Henry incorporated a graphical ratio analysis for composition estimations (GRACE)/source apportionment by factors with explicit restriction (SAFER) (Henry *et al.*, 1994) and an statistical algorithm called NUMFACT for determining the number of factors (Park *et al.*, 2000) including basic principals of PCA in a MATLAB based

computer code called Unmix. Kim *et al.* (2000), and Poirot *et al.* (2001) used this model to PM₁₀ and PM_{2.5} air particulate data of Los Angeles and northern Vermont, respectively. Miller *et al.* (2002) applied and compared all these four receptor models, i.e. CMB, PCA, PMF, and Unmix, for source apportionment of exposures to volatile organic compounds.

In this work, principal component factor analysis and Unmix receptor models were used for determining number of sources and source composition on the elemental composition data of total suspended particulate matter collected in northern Finland during 1964-1978. A possible source location identifying technique called Residence Time Analysis (RTA) is also employed in this work and described at the end of this chapter.

4.2 Principal Component Factor Analysis

Geometrically, if samples are considered as points in a multi-dimensional coordinate system, whose coordinates are the measured variables of the sample, then a principal component analysis would try to describe the maximum variance of the system with a reduced number of uncorrelated components called principal components. Algebraically, principal components are particular linear combinations of the measured variables. Geometrically, these linear combinations represent the selection of a new coordinate system obtained by rotating the original system of coordinate axis. Principal component analysis (PCA) is one of the methods for solving the factor model, which is described in the following paragraphs.

Factor analysis model assumes that the variables are linearly dependent upon a few unobservable random variables F_1, F_2, \dots, F_p , called common factors. In atmospheric study factors represent the sources in an airshed or receptor location. The factor model can be written as

$$X = GF + E \quad (4.2)$$

where X is an $n \times m$ matrix of the m measured chemical species in n samples. G is an $n \times p$ matrix of source contribution to the samples (time variation). F is a $p \times m$ matrix of

source compositions (source profiles). E is defined as an $n \times m$ residual matrix, the difference between the measured X and the approximation of GF .

Traditionally, a PCA solution of the factor model proceeds through eigenvalues-eigenvector decomposition of the covariance or correlation matrix of X . Usually a correlation matrix is preferred when the magnitudes of the variables are very different. A correlation matrix R of X can be computed using following equations:

$$\mathbf{Z}_j = \begin{bmatrix} \frac{(x_{j1} - \bar{x}_1)}{\sqrt{s_{11}}} \\ \frac{(x_{j2} - \bar{x}_2)}{\sqrt{s_{22}}} \\ \vdots \\ \frac{(x_{jp} - \bar{x}_p)}{\sqrt{s_{pp}}} \end{bmatrix}, \quad j = 1, 2, \dots, n \quad (4.3)$$

where s_{jj} are the expected variance of the variables and a spectral decomposition is followed on a correlation matrix R , which can be obtained as

$$\mathbf{R} = \mathbf{Z}_j \mathbf{Z}'_j \quad (4.4)$$

As can be seen from equation (4.3), individual components of X are centered by the column mean and divided by the standard deviation of the column. Construction of covariance matrix S of X also centers individual components of X matrix. In some branches, (psychology and biology) centering of individual components is natural and there is no loss of information. However, in quantitative science (physics or chemistry) centering the variables often leads to a loss of the implicit information [Paatero *et al.*, 1993; Malinoswski, 1991]. Scaling the whole column by a common standard deviation assumes an equal error to all data points, which is not true in physics and chemistry [Pattero *et al.*, 1993], since measured data points are associated to uncertainties as well. Pattero *et al.* (1993) also showed that minimum variance could not be achieved in PCA with conventional scaling procedure. So, the results of the principal component factor

analysis (PCFA) for physics or chemistry data should be interpreted with caution when used for quantitative applications.

Once a correlation matrix is considered, it is then diagonalized by an eigenvalues-eigenvector as follows:

$$U^{-1}RU = L \quad (4.5)$$

where L is a diagonal matrix whose diagonal elements are eigenvalues, λ . The corresponding eigenvectors are the column vectors of matrix U . The eigenvectors are also called the principal components of the data matrix X . These eigenvectors or principal components also represent G of the factor model. The number of factors or principal components for a factor model solution is always equal to the number of variables, but a factor model is useful when the factors are less than the number of variables in the model.

A decision to retaining the number of factors in the model for a physically meaningful solution is very crucial. A few decision aiding methods for selecting the number of factors in the model are adopted in the commercially available software, such as eigenvalues more than one, cumulative variances of 90%, scree plot, etc. However, a detailed knowledge of the system under study and experience of using the model are very important for a physically meaningful solution.

Once a solution is achieved by spectral decomposition of a covariance or correlation matrix of the dataset, then the next important step is to identify factors for physically meaningful explanation. Often factor rotation is a very common practice at this point to interpret the principal component factors as the physically intuitive sources. There are many types of rotational criteria available for this purpose and each of them involves a different mathematical principle, yielding a different solution. The ultimate goal of factor rotation is to extract meaningful factors that have the simplest factor structure. All rotations attempt to locate a set of axes so that as many points as possible lie close to the final factor axes, with only a small number of points remaining between the rotated axes [Malinowski, 1991]. These rotational methods can be classified into two groups, called *orthogonal rotations* and *oblique rotations*. *Orthogonal rotations* preserve

the angular dependence between the original set of eigenvectors that emerge from FA. Quartimax and varimax rotations belong to this group. *Oblique rotations* do not preserve the angles between the eigenvectors. Oblimax, quartimin, biquartimin, covarimin, binormamin, maxplane, and promax rotations are belongs to the second group. In PCFA, a varimax rotation is the most popular and widely used technique.

An orthogonal rotation technique finds a rotation matrix \mathbf{T} to satisfy $\mathbf{T}\mathbf{T}' = \mathbf{T}'\mathbf{T} = \mathbf{I}$, which is then used to obtain a new rotated factor loading matrix \mathbf{L}^* as

$$\mathbf{L}^* = \mathbf{L}\mathbf{T}.$$

All factor loadings obtained from the initial loadings by an orthogonal transformation have the same ability to reproduce the covariance or correlation matrix [Johnson *et al.*, 1998]. A varimax procedure selects the orthogonal transformation \mathbf{T} that makes

$$V = \frac{1}{p} \sum_{j=1}^m \left[\sum_{i=1}^p l_{ij}^{*4} - \left(\sum_{i=1}^p l_{ij}^{*2} \right)^2 / p \right]$$

as large as possible [Kaiser, 1958].

4.3 Unmix

Unmix is a computer code classified as an advanced atmospheric receptor model. It uses source apportionment by factors with explicit restrictions (SAFER) and a statistical algorithm called NUMFACT for determining the number of factors to be considered in a receptor model [Henry *et al.*, 1990, Park *et al.* 2000]. The SAFER model is a multivariate receptor model, which uses the PCA approach and predicts the number of sources and their compositions. The special feature of the SAFER model is that these predictions are consistent not only with the observed correlations of the variables but also with any explicit physical constraints that can be expressed as linear combinations of the measured variables [Henry *et al.* 1994]. In determining the physical constraints to use in SAFER, the graphical ratio analysis for composition estimation (GRACE) technique is used. The GRACE uses scatter plots of the measured variables to find the minimum and maximum edges in a mixture problem and is presented by Henry *et al.* (1994). The method requires some data points in the variables with one source missing or low contribution. These data points help to find the slopes of the lower and upper edges of the main body of data in a scatter plot to serve as the physical constraint for a particular source.

The NUMFACT statistics developed by Park *et al.* (2000) is incorporated in the Unmix to determine the number of factors in the receptor model. Basically, the method recommends the number of factors in the model by a cut off value of NUMFACT statistics. Park *et al.* (2000) and Henry *et al.* (1997) presented the development of NUMFACT as the following.

Let \mathbf{X} denote the $n \times p$ data matrix (n observations and p variables), and \mathbf{R} is the sample correlation matrix of \mathbf{X} . The eigenvectors of sample correlation matrix are denoted by b_1, b_2, \dots, b_p and the corresponding eigenvalues are l_1, l_2, \dots, l_p . A bootstrap sample matrix denoted by \mathbf{X}^* , drawn independently from \mathbf{X} with replacement, and $b_1^*, b_2^*, \dots, b_p^*$ denote the eigenvectors of the bootstrap correlation matrix \mathbf{R}^* . Finally, let N denote the number of independent bootstrapped resamples. In particular,

X_j^* denotes the j th bootstrapped sample and $b_{1j}^*, b_{2j}^*, \dots, b_{pj}^*$ denotes the eigenvectors of sample correlation matrix of X_j^* .

The NUMFACT algorithm proceeds through resampling the data matrix and calculates the average squared length of the projected i th eigenvector of the resampled data onto the space spanned by the first i original eigenvectors. The basic idea behind NUMFACT is that if there are q factors in the data, then the first q eigenvectors of the resampled data will have a large projection on the space spanned by the original eigenvectors. The eigenvectors associated with measurement error are dominated by errors and the directions of these eigenvectors are random and so their projections are also random.

The NUMFACT statistics depend upon the ratios of the average squared projections of the resampled eigenvectors on the spaces spanned by the original eigenvectors, which can also be viewed as the regression sum of squares and the error sum of the squares. The i th ratio is defined as W_i , where

$$W_i = \frac{\text{avg} \|P(b_i^* : \text{span}\{b_1, \dots, b_i\})\|^2}{\text{avg} \|P(b_{i+1}^* : \text{span}\{b_{i+1}, \dots, b_p\})\|^2} = \frac{\sum_{j=1}^N b_{ij}^{*t} (b_1 b_1^t + b_2 b_2^t + \dots + b_i b_i^t) b_{ij}^*}{\sum_{j=1}^N b_{ij}^{*t} (b_{i+1} b_{i+1}^t + \dots + b_p b_p^t) b_{ij}^*} \quad (4.8)$$

$i = 1, 2, \dots, p-1$ and $W_p = 0$.

The i th NUMFACT statistic is denoted by $\text{sn}(i)$, where

$$\text{sn}(i) = \frac{\text{signal}(i)}{\text{noise}} = \frac{\frac{l_i \sqrt{W_i}}{1 + W_i}}{\left(\sum_{k=1}^{p-1} \frac{l_k}{1 + \sqrt{W_k}} \right) / (p-1)} \quad (4.9)$$

$i = 1, 2, \dots, p-1$ and $\text{sn}(p) = 0$.

The NUMFACT statistic increases with W . In addition, they are bigger for statistics corresponding to relatively big eigenvalues. The denominator in equation (4.9) represents the average noise in all the eigenvalues, discounting the last. The numerator

and the denominator of $sn(i)$ are obtained by assuming that $\sqrt{W_i} = \text{signal}(i)/\text{noise}(i)$ and $l_i = \text{signal}(i) + \text{noise}(i)$, and solving for $\text{signal}(i)$ and $\text{noise}(i)$, respectively. If there are q factors in the data, $b_1^*, b_2^*, \dots, b_q^*$ are expected to have a large projection on the space spanned by the original eigenvectors, so W_1, W_2, \dots, W_q and $sn(1), sn(2), \dots, sn(q)$ are also expected to be large. But, for the remaining $p-q$ eigenvectors of the resampled data, $b_{q+1}^*, b_{q+2}^*, \dots, b_p^*$, which are dominated by errors, the projection on the space spanned by the original eigenvectors is expected to be small, and so are $W_{q+1}, W_{q+2}, \dots, W_{p-1}$ and $sn(q+1), sn(q+2), \dots, sn(p-1)$. The estimated number of factor q is thus related to some cut off value. Based upon the asymptotic results for the above statistics contained in Park *et al.* (2000), Henry *et al.* (1999) choose 2 as the cutoff value.

4.4 Residence Time Analysis

Receptor models as discussed above are usually used to identify sources, their composition, and to infer the mass contribution to a receptor site. However, these models do not provide information on the locations of the sources contributing to a receptor. In the early 80's Ashbaugh (1983, 1985) first developed and applied the basic analytical technique to identify the source locations by using ensemble air parcel back trajectories. Later a number of investigators used that approach by varying the procedures to seek the potential source region of the air pollutants [Malm *et al.* 1986; Poirot *et al.*; 1986, Zeng *et al.*, 1989; Hopke *et al.*; 1993, Poirot *et al.*, 2001]. Some of these air parcel back trajectory metrics are known as Residence Time Analysis, Potential Source Contribution Function, Quantitative Bias Trajectory Analysis, and Residence Time Weighted Concentrations.

Meteorological data for an air parcel history, called back trajectory, for a period of time from the sampling location can be obtained using several methods. Usually, a back trajectory is computed for a maximum 5 days, because air mass histories more than that period are associated with large uncertainties. At present, an air parcel back trajectories can be computed by downloading or online using the HYSPLIT_4 model [Draxler *et al.* 1998] from National Oceanic and Atmospheric Administration (NOAA).

HYSPLIT_4 stands for the Hybrid Single-Particle Lagrangian Integrated Trajectory version 4. The model calculation method is a hybrid between Eulerian and Lagrangian approaches. Eulerian and Lagrangian models are the two broad categories of the atmospheric dispersion modeling. The output of the HYSPLIT_4 provides both a graphical image and a text file containing endpoints of hourly latitude, longitude, height, etc. of an air parcel. The use of these endpoints to develop a probability metric on a gridded array of cells is the key technique to locate the likely emission sources of air pollution.

In this work, residence time analysis (RTA) as developed by Poirot and Wishinski (1986, 2001) is used to locate the sources of ambient elemental concentrations in Kevo for the time period of 1964-1978. Initially, Ashbaugh (1983) termed this technique as RTA, which proceeds by forming a gridded array over and around the sampling location. The residence time of an air parcel for a cell can be determined from the endpoints falling into that grid cell using the air parcel endpoints. The total residence time for a cell is the total number of endpoints falling into that cell for a given number of back trajectories. A likely source location is the grids, which have higher endpoint probability values. These grids can be inspected visually by plotting the computed probabilities of gridded array superimposed on a regional map around the sampling location. A geometrical problem of this method is that the probability of randomly passing air parcels over the grid squares closure to the termination point, i.e. sampling site, is higher than that of the grid squares far from the termination point.

Poirot and Wishinski (1986) modified initial RTA approach by introducing computations of the residence time, for instance in hours, of an air parcel for a particular grid square by assuming a constant speed during the time interval between segment endpoints. This approach can weight the grid cells appropriately because of the slow or fast moving air parcels, but it is a computationally intensive technique. It also adds a geometric adjustment factor to lessening the probability that any particular trajectory will pass over a grid square progressively further and further from the terminus point by considering an annular ring at different distances from the trajectory terminus point. In a

recent publication, Poirot *et al.* (2001) used a new approach called incremental probability to reduce the geometrical biasing for the grid squares closer to the trajectory termination point. This metric first calculates a total residence time probability for each grid square considering all air parcel back trajectories of the sampling period. Then a second residence time probability is calculated using the back trajectories, which are related to the high concentration subset sampling days, called the high-value probability. Afterward, a difference from the high-value probability to total residence time probability represents the difference probability or incremental probability. As it is clear that the incremental probabilities of the grid cells signify the potential source location for the high concentration days of the pollutants. Finally, a plot can be created for these incremental probabilities of the gridded array to aid a visual display of the source region by using a smoothing factor and a multiplying factor to boost the small probability quotients.

The incremental probability can be calculated for a grid square (i,j) by the following equation

$$TR_{IP} \% = (TR_{p(i,j)}^h - TR_{p(i,j)}) \times 100 \quad (1)$$

where $TR_{(i,j)}$ = The total residence time for all the trajectories over grid square (i,j)

$TR_{(i,j)}^h$ = The total residence time for all the trajectories related to high subset samples over grid square (i,j)

and can be calculated by equations

$$TR_{p(i,j)} = \left(\frac{TR_{(i,j)}}{\sum_{i=1}^l \sum_{j=1}^m TR_{(i,j)}} \right) \quad (1)$$

and

$$TR_{p(i,j)}^h = \left(\frac{TR_{(i,j)}^h}{\sum_{i=1}^l \sum_{j=1}^m TR_{(i,j)}^h} \right) \quad (2)$$

The development of these equations is presented in Appendix section 4.

Further discussions of a gridded array considered over and around northern Finland, back trajectory computation, and other related parameters used in RTA for this work with figures are presented in results and discussion chapter.

5. Results and Discussion

Surface level atmospheric concentrations of twenty elements were determined for the period of 20th October 1964 - 3rd March 1978 at Kevo, northern Finland, by NAA. Six hundred and eighty five weekly samples covered a full thirteen-year period, 1965 – 1977, and partial years in 1964 and 1978. Although the period consists of about six hundred and ninety-three weeks, but there were 8 weekly missing periods resulting 685 air filters. Among these, the recorded air volumes of four samples were suspicious, so eventually all analysis and reported results are based on 681 samples. Six weekly concentrations were determined using only one filter, because the other part were missing or donated for other analysis earlier by the Finish Meteorological Institute. All missing and unusual sample records are presented in Table 5.1.

The elemental database was analyzed to describe various aspects of this historical dataset and used in factor analysis for determining possible source numbers and their compositions, and in RTA for locating the potential source regions around Kevo. The dataset is analyzed as a single set for the whole period and regrouped into four seasonal subsets. Descriptive and seasonal results are presented in section 5.1, receptor model results in section 5.2, and RTA results in section 5.3. In all sections a comparison of present results with other Arctic data are presented and discussed.

Table 5.1: Sample number, period of sampling, and notes of unusual samples

Sample #	Sampling period	Sampling duration (day)	Notes
156	11/20/67 - 11/27/67		no filter
383	4/17/72 - 4/27/72		no filter
109	12/26/66 - 1/2/67		only one filter
147	9/18/67 - 9/25/67		only one filter
153	10/30/67 - 11/6/67		only one filter
155	11/13/67 - 11/20/67		only one filter
472	12/31/73 - 1/7/74		only one filter
495	6/10/74 - 6/17/74		only one filter
14	1/18/65 - 1/28/65	10	Sampling > a week
29	5/4/65 - 5/17/65	13	Sampling > a week
45	8/30/65 - 9/21/65	22	Sampling > a week
56	11/29/65 - 12/20/65	21	Sampling > a week
64	2/7/66 - 2/21/66	14	Sampling > a week
85	7/11/66 - 7/21/66	10	Sampling > a week
247	8/18/69 - 8/28/69	10	Sampling > a week
296	8/17/70 - 8/27/70	10	Sampling > a week
5	11/16/64 - 11/23/64		Suspicious air volume
283	4/27/70 - 5/29/70		Suspicious air volume
284	5/29/70 - 6/1/70		Suspicious air volume
635	- 2/16/77		Suspicious air volume

5.1 Descriptive Statistics and Results

5.1.1 Distribution Characteristics

Investigation of the distribution characteristics of the atmospheric elemental concentration levels is very important to understand the nature of any variable before using them in any receptor modeling [Cheng *et al.*, 1991]. There are several measures to investigate the distribution pattern of a variable. These include calculating the mean, standard deviation, geometric mean, geometric standard deviation, median, mode, skewness, and kurtosis. Definitions of these parameters are given in Appendix I section 3. For a symmetric Gaussian distribution, the values of the arithmetic mean, median, and mode are all same. If the arithmetic mean \geq median $>$ mode, then the upper tail of the distribution extends toward larger values (i.e. positively skewed). If the order is reversed, then it is negatively skewed. These three numbers are called the location parameters of a distribution because these are used to describe the central location of a probability distribution. Skewness is a measure of asymmetry from a normal distribution and

kurtosis is an indicator of a steep shape at the center of the distribution that has heavy tail in comparison to that of a normal distribution.

Arithmetic mean, median, mode, skewness, and kurtosis of the measured elements were determined using SPSS statistical package (Version 10) and presented in Table 5.2 in increasing order of skewness. Skewness and kurtosis are dimension less parameters, and the unit of all location parameters is ng/m³. As it can be seen from Table 5.2 that all elemental distributions are positively skewed. The highest and lowest skewness values are found for Sn and Cl, respectively. A positive value of kurtosis indicates a heavier steep shape at the distribution center and a longer tail in comparison to that of a normal distribution.

Table 5.2: Elemental arithmetic mean, median, mode, skewness, and kurtosis

Elements	Mean ng/m ³	Median ng/m ³	Mode ng/m ³	Skewness	Kurtosis
Cl	116.84	90.31	4.26	2.19	8.69
Si	292.46	197.16	99.45 ^a	3.07	15.92
Mn	1.62	1.16	0.78	3.40	19.41
V	0.81	0.42	0.07	3.47	16.30
Co	0.08	0.06	0.04 ^a	3.48	20.29
As	1.08	0.64	0.27	3.78	22.86
I	0.93	0.82	0.63	3.81	24.68
K	83.46	72.22	49.36 ^a	4.03	27.96
In	0.004	0.003	0.002	4.04	28.59
Ca	56.09	33.50	11.74 ^a	5.67	46.48
Cu	14.95	12.20	11.59	6.32	73.09
Na	281.40	247.66	174.49 ^a	6.86	77.47
TI	7.19	5.96	1.38 ^a	7.44	95.37
Zn	22.31	17.77	12.48 ^a	8.31	107.55
Al	42.93	32.62	20.83 ^a	8.34	104.47
Sb	0.29	0.19	0.11	9.39	126.66
Br	3.13	2.17	2.03 ^a	12.99	184.24
Ag	1.04	0.12	0.02	15.99	283.19
W	0.02	0.01	0.01 ^a	17.54	372.66
Sn	3.70	2.39	1.67 ^a	17.90	391.61

^a multiple modes exist. The lowest value is presented

The incremental order of skewness and kurtosis is found almost sequential for all measured variables except V and Al. The observed skewness and kurtosis of this work are about 2-3 times and 9-10 times higher respectively, than those reported by Cheng *et*

al. (1991) in Alert, Canadian Arctic for the same variables. This exercise shows that the frequency of extreme high concentration levels at Kevo is higher than that at Alert, Canada. This is reasonable since Kevo is very close to industrial locations.

A continuous long-term aerosol compositional database, rarely available, is highly suitable to test the hypothesis for a commonly conceived log normal distribution. All elemental concentrations were log transformed and tested for a normal distribution using Kolmogorov-Smirnov (K-S) goodness-of-fit test using SPSS. The results are presented in Table 5.3.

Table 5.3: Kolmogorov-Smirnov (K-S) statistics D and significance level for the fitted variables

Element	K-S static D	Asymp. Sig. (2-tail)
Ag	0.168	0.000
Al	0.048	0.085
As	0.031	0.555
Br	0.082	0.000
Ca	0.136	0.000
Cl	0.104	0.000
Co	0.057	0.024
Cu	0.049	0.090
I	0.062	0.012
In	0.018	0.968
K	0.055	0.037
Mn	0.043	0.169
Na	0.028	0.654
Sb	0.027	0.659
Si	0.082	0.000
Sn	0.045	0.139
Ti	0.056	0.029
V	0.025	0.788
W	0.224	0.000
Zn	0.061	0.015

An asymptotic significance level (2-tail), also called ‘p’ value, directly helps to conclude whether the variable statistically significant for a normal distribution or not instead of looking to a table of the related statistics. An asymptotic significance value more than 0.05 states that the variable statistically significant to follow a normal distribution. So, the asymptotic values in Table 5.3 for K-S goodness-of-the-fit show that a normal distribution is only significant for Al, As, Cu, In, Mn, Na, Sb, Sn, and V at $\alpha = 0.05$ level.

A two-tailed critical value D_a for $n > 100$ can be computed by equation

$$D_a = \sqrt{-In\left(\frac{1}{2}\alpha\right)} / \sqrt{2n} \text{ [Rohlf and Sokal, 1981]. So, for } n = 681, \text{ a } D_{0.05} \text{ is found to be}$$

0.052. Since the variables were tested on log- transformed data, so these elements follow a log normal distribution. As can be seen from Table 5.3, except Ag, Ca, Cl, and W all other elemental two tailed significance levels are very close to the critical value of 0.052. This exercise shows that aerosol data mostly and very closely follows the log normal distribution.

Cheng *et al.* (1991) reported the distribution characteristics of aerosol chemical database at Alert, Canadian Arctic using K-S statistics. Among various elements and chemical species, distribution characteristics of seven elements determined by NAA were reported. Among those I, Mn, V, Al, and Cl were statistically significant for a log normal distribution at Alert, Canada.

5.1.2 Elemental Ambient Concentration Levels

For a log normal distribution, geometrical mean, geometrical standard deviations are more representative than the arithmetic mean and standard deviation of a variable. Assuming an approximate log normal distribution for all the measured variables, geometrical mean (GM), geometrical standard deviation (GSTD) are calculated and presented in Table 5.4, including a range of detection limits, and percent of data below the detection limit (BDL) for each of the variables. For calculating the GM and GSTD, all BDL data points were replaced by half of the detection limit (DL) as suggested by Cohen and Ryan (1989). Time series plots are presented in order to elemental alphabetic symbols in Figures 5.3 - 5.7. A monthly-sorted data, useful to check the monthly trend of an element, are presented as box plots in Figures 5.8 - 5.12. A box plot provides a simple graphical summary of the data. A horizontal line inside the box reads the 50th percentile value of the data (median) and the lower and upper horizontal lines of the box represent the 25th and 75th percentiles. The 10th and 90th percentiles are represented by the lower and upper *Whiskers* outside the box and connected by lines called *Whisker line* with the 25th and 75th percentiles. All data points outside the *Whiskers* are called outliers.

Table 5.4: Geometric mean (GM), geometric standard deviation (GSTD), range, detection limit (DL), and percent of data below DL for each element

	GM	GSTD	Range	Detection limit		BDL (%)
				from	to	
Ag	0.11	4.91	0.01-190	0.03	0.63	41
Al	34.43	1.81	9.5-779	0.4	14.7	0
As	0.61	3.03	0.02-14	0.01	0.20	0
Br	2.07	2.05	0.2-144	0.06	1.39	0
Ca	37.50	2.32	8.3-814	11.3	182.7	50
Cl	73.07	3.22	0.13-935	2.0	22.9	4
Co	0.06	2.37	0.004-0.7	0.004	0.28	14
Cu	12.73	1.70	2.9-182	0.5	8.0	0
I	0.85	1.49	0.32-5.77	0.002	0.06	0
In	0.003	2.090	0.00-0.04	0.0002	0.004	0
K	74.58	1.57	21-576	3.3	59.3	0
Mn	1.22	2.05	0.2-16	0.1	1.3	0
Na	249.47	1.59	67-2841	1.9	22.0	0
Sb	0.19	2.37	0.02-7.8	0.01	0.2	0
Si	220.53	2.04	48-2713	18	329	1
Sn	2.47	2.19	0.13-194	0.1	3.1	1
Ti	5.44	2.09	0.6-121.4	1	23	22
V	0.43	3.00	0.03-10.7	0.01	0.13	0
W	0.02	1.83	0.01-1.5	0.01	0.22	96
Zn	18.48	1.75	2.7-358	2	37	2

*681 samples, BDL data are replace by half of the BDL values for the above calculations

Literature data of elemental concentration levels at different Arctic locations are tabulated in Table 5.5 and Table 5.6 for some anthropogenic and other elements including the corresponding GM, GSTD, arithmetic average, and standard deviations of this work for comparison. The tabulated data from Virkkula *et al.* (1999) were reported on a two-day aerosol collection during the periods of Dec 27, 1992 – Dec 1, 1993 and Oct 27, 1993 – July 5, 1994 at Sevetijärvi, northern Finland. A virtual impactor (VI) collected aerosol particles of aerodynamic diameter $D < 2.5 \mu\text{m}$ and $2.5\mu\text{m} < D < 15\mu\text{m}$. Polissar *et al.* (1998) presented the geometric mean from weeklong samples covering the period of 1981-1991 at Alert, Canadian Arctic for comparison with Alaska data. Mean concentration levels of Alert data also presented in Table 5.5 and Table 5.6 taken from Landsberger *et al.* (1990). The arithmetic mean and standard deviation of 12 daily samples at Alert in March 1985 were reported. Vinogradova and Polissar (1995) reported

one spring month data for the years in 1985, 1986, and 1988 at North Earth Archipelago, Russian Arctic. The aerosol collection time varied from 1-7 days. At three Russian Arctic locations, Vinogradova (2000) reported the average data for the two months, April and July, of the year over a ten-year period. Table 5.5 also contains two Norwegian Arctic data reported by Maenhaut *et al.* (1989) at Ny Ålesund, Vardø in 1983, 1984, and 1986. The aerosol collection schedule for that campaign was three filters per week as 2-2-3 days. An overall discussion on time series, box plots, and a comparison of present data with other Arctic sites are discussed element by element in the following.

Ag - Ambient silver concentration levels were reported in many episodic studies in European sub Arctic and Russian Arctic regions. This long-term study reveals a quite interesting observation of this element at Kevo. As can be seen from Figure 5.3a, silver concentrations are representing two very different trends before and after 1971. While the earlier period maintains on average an 1 ng/m^3 with a few huge spikes of about $\sim 100 \text{ ng/m}^3$ concentration levels, the later part maintains an average concentration level of about 0.1 ng/m^3 with no value higher than 1 ng/m^3 . Virkkula *et al.* (1999) reported average silver concentration at Sevetijärvi, 60 km east from Kevo, of 0.09 ng/m^3 and 0.13 ng/m^3 for fine and coarse particles, respectively. Most of the silver concentrations were above the detection limit for period 1964-1971 and had only 13% below detection limit (BDL) data points. However, the later period, 1972-1978, had 73% BDL data points for silver concentration level at Kevo. Silver is rare in nature. The copper and nickel ore processing facilities at the Kola Peninsula is the most probable sources of this element at Kevo. Determining the concentration levels of moss in the central Barents region, Reimann *et al.* (1997) suggested that Norilsk ore processed at Monchegorsk smelters must have had relatively high silver contents, whereas the local Pechenga ore, mainly processed at Zapoljarnij and Nikel smelters close to the Norwegian border, was comparatively low in silver.

Table 5.5: A comparison mean concentrations (ng/m³) of this work with other Arctic data

		Ag	As	Co	Cu	In	Mn	Sb	V	Zn
This work	Ave	1.0± 9.4	1.1 ± 1.4	0.08 ± 0.07	15 ± 11	0.004 ± 0.003	1.6 ± 1.5	0.3 ± 0.5	0.81± 1.14	22 ± 21
	GM	0.11±4.91	0.6 ± 3.0	0.06 ± 2.37	12.7±1.7	0.003±2.090	1.22±2.05	0.19±2.37	0.43±3.00	18.48±1.75
SV ¹	Fine, Ave	0.09 ± 0.05	0.12 ± 0.10	0.11 ± 0.14	1.8 ± 2.8	0.0036±0.0031	0.63 ± 0.67	0.056±0.075	2.0 ± 2.9	3.4 ± 3.3
	Coarse, Ave	0.13	0.047 ± 0.051	0.098 ± 0.150	1.3 ± 2.2	0.0006±0.0002	0.38 ± 0.41	0.021±0.016	0.10 ± 0.16	0.41± 0.37
Alert ²	GM	-	0.13 ± 4.86	-	-	-	0.69 ± 2.76	-	0.21± 3.45	2.25 ± 2.93
Alert ³	Ave		0.349±0.187	0.032±0.044	-	0.001±0.004	0.778±0.640	0.060±0.001	0.295±0.163	8.5±12.1
NEA ⁴	1985	0.12 ± 0.07	1.8 ± 0.3	0.12 ± 0.11	5.5 ± 1.8		2.5 ± 1.9	0.16 ± 0.11	0.73 ± 0.49	3.2 ± 1.0
	1986	0.16 ± 0.26	-	-	2.1 ± 1.8	-	1.7 ± 1.2	-	0.79 ± 0.48	13.6±16.1
	1988	4.0 ± 10.0	-	0.036 ± 0.077	-	-	0.11± 0.08	0.22 ± 0.43	-	0.63±0.52
FJL ⁵	Apr, 86-95,Ave	-	0.26	-	-	-	-	-	0.85	1.9
FJL ⁵	Jul, 86-95, Ave	-	0.007	-	-	-	-	-	0.021	0.056
SZ ⁵	Apr, 86-95,Ave	-	0.19	-	-	-	-	-	0.46	1.1
	Jul, 86-95,Ave	-	0.019	-	-	-	-	-	0.02	0.04
WI ⁵	Spr, 86-95, Ave	-	0.8	-	-	-	-	-	0.86	11
Ny ⁶	83,84,86w, M	0.52	<0.018	0.009	<0.9	0.0016	0.77	<0.04	0.54	3.9
	1984s, M	0.01	<0.018	<0.004	<0.3	<0.0012	0.07	<0.004	0.022	<0.15
Vardø ⁶	83, 84w, M	0.016	0.97	0.032	1.09	0.0023	0.97	0.12	1.68	6.1
	1984 s, M	<0.010	0.099	0.0069	0.2	<0.0027	0.12	0.012	0.26	1.28

This work at Kevo (69.75°N, 27.02°E), northern Finland; Ave = Arithmetic mean, GM = Geometric mean

¹Virkkula *et al.* (1999), SV = Severtijärvi, northern Finland (69.35°N, 28.50°E)

²Polisser *et al.* (1998), Alert, Canadian Arctic (82.5°N, 62.3°W)

³Landsberger *et al.* (1990), Alert, Canadian Arctic

⁴Vinogradova and Polissar (1995), NEA= North Earth Archipelago (79.5°N, 95.4°E), Russian Arctic

⁵Vinogradova (2000), FJL=Franz Jozef Land (81.1°N, 56.3°W), SZ= Severnaya Zemlya (79.5°N, 95.4°E), Wrangel Island (71.0°N, 178.5°W), Russian Arctic; Spr = Spring

⁶ Maenhaut *et al.* (1989), Ny = Ny Ålesund (78.9°N, 11.9°E), Vardø (70.4°N, 31.1°E), Norway; w = Winter, s = Summer; M = median

Table 5.6: A comparison of mean concentrations (ng/m³) of this work with other Arctic data

		Al	Br	Ca	Cl	I	K	Na	Si	Ti	W
This work	Ave	42.9±47.0	3.1±8.6	56.1±72.2	116±104	0.93±0.49	83.5±49.4	281.4±187.9	292.5±270.0	7.197.34	0.02±0.06
	GM	34.4±1.8	2.07±2.05	37.5±2.3	73.1±3.2	0.85±1.49	74.6±1.6	249.5±1.6	220.5±2.0	5.4±2.1	0.02±1.83
SV ¹	Fine, Ave	9.7 ± 9.8	2.3 ± 1.0	11 ± 6	85 ± 173	0.66 ± 0.27	23 ± 18	141 ± 111	28 ± 23	0.86 ± 0.46	0.054 ± 0.041
	Coarse, Ave	12 ± 13	1.3 ± 1.1	17 ± 12	307 ± 389	0.088 ± 0.069	11 ± 9	184 ± 212	32 ± 30	1.1 ± 0.86	0.030 ± 0.027
Alert ²	GM	58.4±3.0	1.5±5.0	70.6±2.9	51.3±5.3	-	7.3±3.9	71.1±4.1	192.0±3.4	5.2±3.9	-
Alert ³	Ave	38.6±27.9	18.5±10.5	62.6±69.1	406.5±225.5	1.00±0.28	23.1±16.4	234.5±142.8	-	10.4±23.3	-

This work at Kevo (69.75°N, 27.02°E), northern Finland; Ave = Arithmetic mean, GM = Geometric mean

¹Virkkula *et al.* (1999), SV = Sevettijärvi, northern Finland (69.35°N, 28.50°E)

²Polisser *et al.* (1998), Alert, Canadian Arctic (82.5°N, 62.3°W)

³Landsberger *et al.* (1990), Alert, Canadian Arctic

One might assume that the Norilsk ore processed at Kola Peninsula is a probable reason for high silver concentrations during 1964-1971 period for the Kevo ambient atmosphere. Luzin *et al.* (1994) reported that Norilsk ore has been processed in the Kola region since 1964. Norilsk is an isolated city in Siberia and had no road or rail links to central Russia. Rather than constructing a 2000 km railway, the state decided to ship Norilsk ore to the Kola region for processing. Riemann *et al.* (1998) reported the beginning of this ore processing at Monchegorsk in 1971-1972. However, the beginning of Norilsk ore processing at Monchegorsk, Kola Peninsula, does not support this assumption since no report mentions any stoppage of Norilsk ore processing at Kola region after 1971, when the observed air concentration is lower after 1971. So, it is imperative to search for other explanations for these high/low silver concentration periods observed at Kevo.

The Finish Meteorological Institute collected these samples for monitoring the air borne radioactivity in the atmosphere. In addition to online GM counting of the aerosol filters during sampling hours, the air filters collected before January 1967 were also subjected to autoradiography in the early 90s' at the Finnish Meteorological Institute in Finland. The main purpose of autoradiography was to find any remaining radioactive particles in the aerosol filters from the Soviet nuclear tests. The experiment was performed by placing filters in direct contact to Agfa Curix Blue HC-S Plus x-ray film and leaving for a 2-3 days period in a dark room. So, there was a speculation of any possible silver contamination of those filters from the x-ray film chemical components. This idea was supported to some extent due to the high bromine and iodine concentration levels occurred simultaneously with silver high concentration levels. Silver, bromine and iodine are elemental components of an x-ray film. However, a main shortfall of this idea was the observed high occurrences of silver, bromine, and iodine concentration levels after January 1967; those are easily visible in 1969 from Figure 5.3a. Nonetheless, an experiment was replicated for determining any possible contamination from x-ray film on blank Whatmann-42 filters.

Specific Agfa Curix Blue HC-S Plus x-ray films of early 90s' quality were collected from AGFA Company. Autoradiography experiments were conducted following the same procedure on blank Whatmann-42 filter as done by FMI on original filters. Later all exposed filters were analyzed by NAA for silver concentration and the results are presented in Table 5.7. All silver concentration levels in these filters except S1 were found at BDL. Using a total filter area of 260 cm² and a total air volume of 1200 m³, which were typical for the original filters, a 0.3 ng/cm² would result an average air concentration of 0.07 ng/m³. This is higher than the minimum observed silver concentration of 0.03 ng/m³ (Table 5.4), but definitely far below than many observed high occurrences of ~ 120-190 ng/m³ during 1964-1971 period. So, it can be concluded that the high occurrences of silver concentration at the Kevo ambient atmosphere were not caused from the contact of filters with x-ray films during autoradiography.

Table 5.7: Silver concentration levels of x-ray film exposed to blank filters

Sample ID*	Exposure Description	Concentration ng/cm ²	Uncertainty ng/cm ²	Detection limit ng/cm ²
S1	3 days exposure	0.286	0.057	0.148
S2	3 days exposure	0.0	0.0	0.133
S3	2 days 2 sides	0.094	0.039	0.122
S4	2 days 2 sides	0.0	0.0	0.148
B1	3 days exposure	0.0	0.0	0.140
B2	3 days exposure	0.121	0.044	0.134
B3	2 days 2 sides	0.0	0.0	0.121
B4	2 days 2 sides	0.0	0.0	0.119
Filter Blank 1	No exposure	0	0	0.208
Filter Blank 2	No exposure	0	0	0.177
Filter Blank 3	No exposure	0	0	0.183

* B1 - B4 - aluminum sheet-filter-aluminum sheet – weight

S1, S2 - aluminum sheet- filter-film-aluminum sheet – weight

S3, S4 - aluminum sheet-film-filter-film-aluminum sheet-weight

Al - Aluminum concentration time series presented in Figure 5.3b shows a weak yearly cyclic variation with a higher trend in winter and lower in summer months. This trend is also visible in Figure 5.8b box plot of sorted monthly data for the studied period. There were several high concentration levels of Al, ranging from 300 ng/m³ to 800 ng/m³,

that occurred in 1965, 1966, 1967, and 1974. These sporadic high concentration levels could be related due an aluminum smelter operating at Kandalasha, Kola Peninsula. Overall a persistent influence of the aluminum smelter, which is about 352 km southeast from Kevo [Table 3.1], is not observed at Kevo. A geometric mean (GM) of 34 ng/m³ aluminum in the ambient atmosphere is quite natural. Table 5.5 shows that the GM is lower than the Alert data, while an average value for aluminum of this work is higher than that is reported by Virkkula *et al.* (1999) at Sevettijärvi, northern Finland in early 90s'.

As - Arsenic is an important industrial trace element. A time series plot of the arsenic concentration levels is shown in Figure 5.3c. A cyclic variation is visible with higher concentration levels in the winter and lower in the summer. The median levels of the box plot show a stronger cyclic trend than that of aluminum trend in Figure 5.8c. An average concentration level of 1.1 ng/m³ over the 1964-1978 period shows that it is about an order of magnitude higher than all reported concentration in the Arctic region and of the same order of magnitude with the data from North Earth Archipelago (NEA), Russian high Arctic [Vinogradova and Polissar, 1995].

Br - Bromine is essentially a well-known sea component in the ambient atmosphere. Kevo is about 150 km far in the south from the Barents Sea. The sampling location is also exposed to Arctic Ocean and northern Atlantic Ocean. A soft yearly cyclic variation is visible in a time series plot as shown in Figure 5.3d and from box plot of monthly data in Figure 5.8d. A curious point in studying bromine concentration behavior was it's simultaneous occurrences of high concentration levels in 1965, 1966, and 1969 with the silver concentration levels. This is discussed in detailed in Ag section. These occurrences are also matched quite well with iodine as can be seen in Figure 5.5a. While a simultaneous occurrence of high level bromine and iodine is acceptable as both elements originate from the sea spray, their co-occurrence with purely industrial component like silver needs a different explanation. The average bromine concentration of this work is in good agreement with the Sevettijärvi's, northern Finland, data as shown in Table 5.5, which indicates that probably bromine was not lost much during the long

achieved period from filters. The GM of this location also agrees well with that of Alert's value. A box plot of bromine in Figure 5.8d shows a soft seasonal trend with higher level in March-April and a lower level in August months of the year.

Ca – Calcium is a major crustal element and weathering is the main source of this element in the ambient concentration. In NAA, the detection and measurement of this element with a 3084.4 keV gamma energy often leads to a high detection limit because of the low HPGe detector efficiency at that energy region. An analytical detection limit was found in the range of 11 - 182 ng/m³ for this element and 50% concentration levels of this work were found at BDL. A time series plot in Figure 5.4a shows this BDL effect with a flat level in the plot. A few samples in 1964 have higher calcium concentration and from 1975 onward the concentration level shoot up to an average level of about 90 ng/m³. A GM value of calcium is almost half than the Alert data and an average value of this work is higher than that reported by Virkkula *et al.* (1999). Calcium Box plot, presented in Figure 5.9a, shows no trend, probably because of a large fraction of BDL data points.

Cl – Chlorine is a sea source component in the ambient atmosphere. Time series and monthly box plots for this element are presented in Figure 5.4b and Figure 5.9b. An average value of 116 ng/m³ of this work is found lower than both Alert's total suspended aerosol and Sevetijärvi's coarse particle values, respectively as shown in Table 5.6. Kerminen *et al.* (1998) reported a chloride substitution mechanism in sea-salt particles by inorganic and organic anions in the northern Finland. The reported mechanism is 100% effective for sub micron particle size and decreases gradually for large particles. The collected aerosol of this work was total suspended particles, but still a small fraction of total chlorine might be lost due to the aforementioned process. The time series plot does not show any cyclic variation of this elemental concentration levels and shows a flat level beginning in 1974.

Initially, the use of a chlorine blank value of 0.72 µg/cm² determined from new blank filters resulted about 35% chlorine data below the detection limit (BDL). This is very unusual for an aerosol-sampling location like Kevo, which is very close to the sea and also a vast periphery exposed closely to Barents Sea and Norwegian Sea.

A blank value in the aerosol filters can change from batch to batch, especially, in a 14-year long sampling period the possibility is high. It is interesting to note that the use of a $0.72 \mu\text{g}/\text{cm}^2$ filter detection limit value resulted about 13% and 78% BDL values for 1964-1973 and 1974-1978 periods, respectively. This observation probably indicates a possible chlorine blank value change in the Whatmann 42 filters after 1973. An attempt was made to determine the elemental blank concentration levels in the original filter by using sample-aerosol-filter edges. However, the determined chlorine value was about 23% higher than the new filter blank value. Actually, the edges of the original filters were not very clean, since some aerosol particles were always attached to it. Finally a different technique is used to approximate a representative chlorine filter detection limit to subtract from the NAA measured total chlorine.

Considering a log normal distribution for the chlorine data, histogram plots were used to find out a tail in the low side histogram bins. It is assumed that tailing bins of the histogram are representing approximate values near the filter detection limit and used for approximating a filter blank value. Histogram plots of NAA determined chlorine data ($\mu\text{g}/\text{cm}^2$) are presented in Figure 5.1a and Figure 5.1b for 1964-1973 and 1974-1978 periods. Chlorine data were divided into two periods because of the observed BDL differences mentioned above. Two histogram plots of sodium and indium are also presented in Figure 5.1c and Figure 5.1d. Indium and sodium are found to be following a log normal distribution as described in section 5.1.1. These two plots show the histogram plot pattern for a variable following a log normal distribution. So, comparing with standard histogram plots for indium and sodium, a tail in the low side of the chlorine histogram plots was created considering more bin numbers. For the 1964-1973 chlorine data, the tail can be seen easily, however, for 1974-1978 data, the second bin in the low side was always inconsistent. Probably the later dataset was deviated from a log normal distribution. As can be seen from Figure 5.1a and Figure 5.1b, lowest frequencies occurred in the range of $0.405\text{-}0.504 \mu\text{g}/\text{cm}^2$ and $0.246\text{-}0.314 \mu\text{g}/\text{cm}^2$ about 8 and 12 times, respectively for the two different periods.

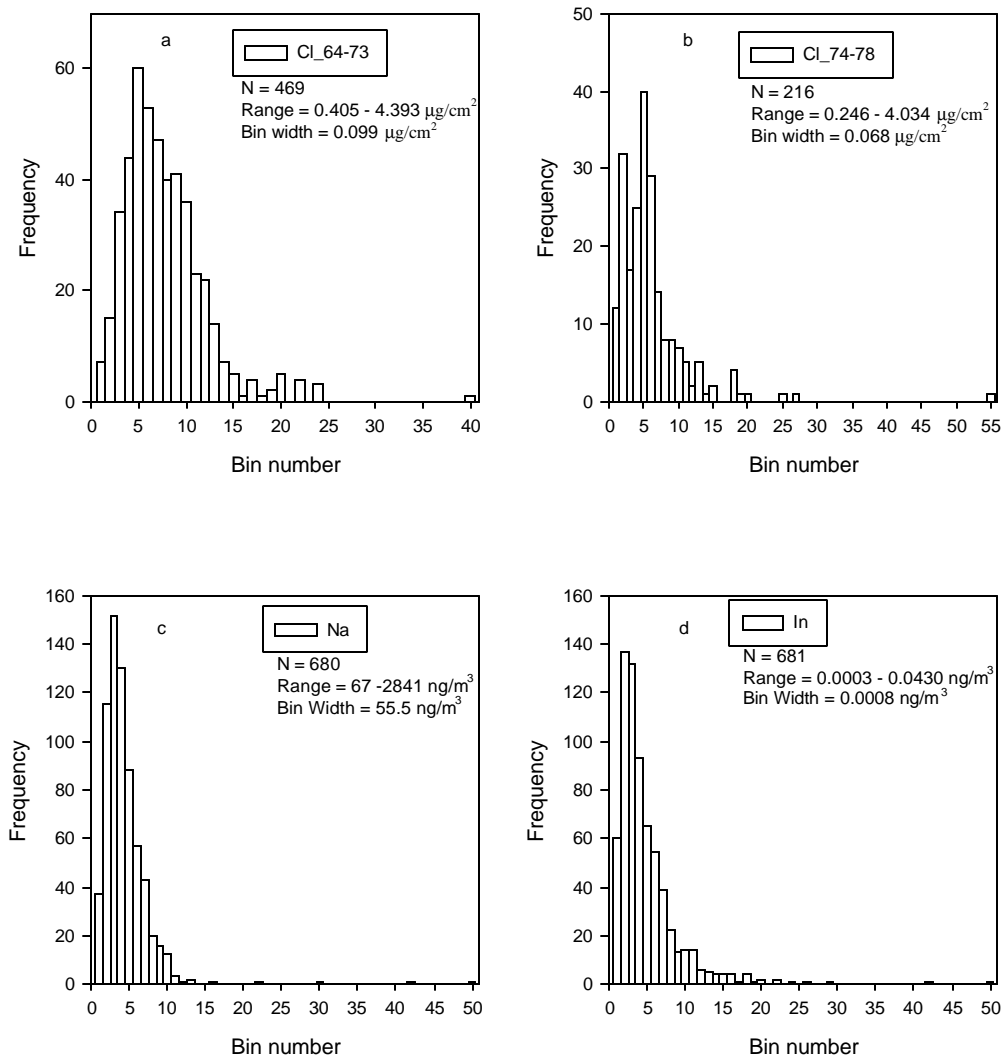


Figure 5.1: Histogram plots for a) chlorine 64-73 b) chlorine 74-78 c) sodium and d) indium data

If the upper values of the first bins of $0.504 \mu\text{g}/\text{cm}^2$ and $0.314 \mu\text{g}/\text{cm}^2$ are considered to be approximate filter detection limits for the two different periods, then these values would be about 30% and 56% lower than the new filter blank DL value of $0.72 \mu\text{g}/\text{cm}^2$ and about 6-10 times higher than the highest NAA analytical detection limits ($0.05 \mu\text{g}/\text{cm}^2$) for chlorine determination. It may be mentioned here that this approximated filter DL value resulted about 4% BDL data points for chlorine, which is

much less than previously obtained 35% BDL. This result was considered as a new filter blank value.

Co – Cobalt is a trace element in the earth crust. It is one of the major heavy metals emitted from the smelters at Kola Peninsula. Official figures for emission of cobalt metal in 1994 were 5.2 tons from Nikel, 5.4 tons from Zapoljarnij and 81.5 tons from Monchegorsk. A time series plot of cobalt in Figure 5.4c shows a frequent fluctuation during the studied period. The median values in box plot as shown in Figure 5.9c shows no monthly trend. Probably this is because the crustal and industrial components of cobalt are producing a mixed concentration level in the Kevo ambient atmosphere. A GM and average concentration levels of this element are almost of the same order of magnitude with all other literature data over the Arctic region as tabulated in Table 5.5. About 14% data points were found at BDL in this work for the studied period at Kevo.

Cu – Copper is a major heavy metal emitted from the smelters of Kola Peninsula. In 1994, the official emission figures for Cu metal were 82 tons from Nikel, 81 tons from Zapoljarnij and 934 tons from Monchegorsk. A time series plot of copper presented in Figure 5.4d and a box plot in Figure 5.9d show no significant yearly or monthly cyclic variations. Possibly, this indicates that the influence of copper and nickel smelters at Kevo is almost uniform, so seasonal atmospheric changes in this part of the region does not make much difference in copper ambient air concentration at Kevo. This fact could also be applicable for cobalt as well, because cobalt also shows the same concentration behavior in the Kevo ambient atmosphere. A GM value of copper concentration level at Kevo is about 3 to 5 times higher than other Arctic literature data as presented in Table 5.5. Interestingly, early 90s' data at Sevetijärvi, which is closer than Kevo to Nikel and Zapoljarnij's smelters, are about 5 times lower than the average of present work.

I – Iodine time series plot in Figure 5.5a shows a broad cyclic variations higher in the earlier part and lower in the later part of the year. A number of high iodine concentration levels occurred in 1965, 1969, 1971, 1974 and 1978. Some of these high concentration levels coincided with silver and bromine values as already mentioned

earlier. A box plot of iodine in Figure 5.10a shows a nice monthly trend of median values, which peaks in April-May and is maintained at a lower level in September-October period of the year.

In – Indium has the lowest atmospheric concentration level among all the determined components in this work. This element is rarely reported in the literature. However, it is a very strong and an important industrial marker [Landsberger *et al.* 1992a]. A GM value in this work was found to be 0.003 ng/m³ at Kevo. A time series plot presented in Figure 5.5b can be characterized with frequent concentration level fluctuation, which is almost similar as cobalt and copper. A few very high concentration values occurred in 1969, 1970, 1971, and 1977 of this element. A box plot in Figure 5.10b shows a nice monthly trend with the highest median values occurred in March and the lowest in August. Literature data for indium concentrations at Ny Ålesund, Spitsbergen; Vardø, Norway; and Severtijärvi, northern Finland are very consistent with the data of this work as tabulated in Table 5.5.

K – Potassium is a known wood burning trace element in the lower troposphere. A time series plot of potassium for the period of 1964-1978 in Figure 5.5c shows frequent fluctuations at a number of times of the year. Some high values occurred simultaneously with iodine high levels as can be seen in 1965, 1969, and 1974. A box plot in Figure 5.10c shows no visible trend for the months of a year.

Mn – Manganese is emitted at the trace level from coal burning power plants. The GM and GSTD for of this work were found to be 1.22 ng/m³ and 2.05 ng/m³ at Kevo as shown in Table 5.4. This value is statistically similar with that of the Alert and Severtijärvi data as presented in Table 5.5. However, the mean value is higher than the mean values of Ny Ålesund, Spitsbergen and Vardø, Norway. A time series plot in Figure 5.5d shows a nice cyclic variation over the years. The cyclic trend is higher in the winter months and lower in the July-August period. A similar trend can be seen from a monthly box plot presented in Figure 5.10d.

Na – Sodium mainly occurs in the ambient atmosphere from the sea spray. A time series plot of sodium is shown in Figure 5.6a. No distinct feature is visible from this

figure, however, two very high concentration levels of about 2800 ng/m³ and 1700 ng/m³ occurred in 1969 and 1974. No monthly trend is visible from the median values of a box plot as shown in Figure 5.11a.

Sb – Antimony is a trace element in the earth's crust. It is a minor element emitted from industrial activities at Kola, but no official emission figures are available for the nickel smelters at the Kola Peninsula. Time series behavior of Sb presented in Figure 5.6b is not very similar to any other industrial components like arsenic, cobalt, copper, or zinc. Box plot for Sb presented in Figure 5.11b shows no strong monthly trend. Two high concentration levels occurred in the July month. A GM value of 0.19 ng/m³ is similar to an average value of 0.12 ng/m³ at Vardø and two reported values at North Earth Archipelago of 0.16 ng/m³ and 0.22 ng/m³. However, an average value 0.3 ng/m³ is about 4 times higher than a total concentration from fine and coarse particles of values 0.05 ng/m³ and 0.02 ng/m³, respectively at Sevettijärvi as presented in Table 5.5.

Si – Silicon is a major crustal element. Often it is chosen as a reference element for an enrichment factor analysis. It is considered as a pure crustal element like aluminum in the atmosphere and mainly occurs in the ambient air from weathering. However, a time series behavior of this element presented in Figure 5.6c shows other sources of this element in the ambient air at Kevo during the period of 1967-1969 in addition to crustal erosion. While a few silicon high values occurred in 1965, 1966, and 1969 matching well in a time sequence with aluminum concentration levels, a distinct elevated hump is clearly visible in the time series during the period of 1967-1969. The Environmental Geochemical Atlas of the Barents Region [Reimann *et al.*, 1998] reports a higher enrichment of silicon compared to aluminum in moss around Nikel and Zapoljarnij area suggested that the silicon emission from those industrial locations were higher.

Sn – Tin is being reported for the first time for an Arctic location in this work. The reason being that this element needs to be determined with an epithermal neutron irradiation and with a Compton suppression system. A GM and GSTD of this work are found to be as 2.47 and 2.19 ng/m³ respectively for the studied period at Kevo. A time

series plot in Figure 5.6d shows no unique feature of this element concentration level at Kevo. All data points of tin were found above the NAA detection limit, which had a DL range of 0.1-3.1 ng/m³. The median values of a box plot shows no monthly trend of ambient concentration of this element at Kevo as can be seen from Figure 5.11d.

Ti – Titanium is a minor element in the Earth crust and sometimes it is called the geogenic source indicator in atmospheric chemistry. Interestingly, in this work, a time series behavior of this element is found to be very different. An expected similarity in time sequence with aluminum is absent as can be seen from Figure 5.3a and Figure 5.7a. However, a weak time sequence occurrence can be seen for the period of 1969-1971 with that of the silicon concentration time series as shown in Figure 5.6c. Monthly median values in the box plot, is presented in Figure 5.12a, show no monthly trend for this element. About 22% data points were found at BDL for this element in the present work for the studied period at Kevo.

V – Vanadium emitted to the ambient atmosphere mainly from oil and coal combustion. It is a trace element in the earth's crust. Vanadium emissions from industrial activities at Kola Peninsula were reported as V₂O₅ in 1994: 91 tons for Murmansk, 60 tons for Monchegorsk, 44 tons for Kirovsk, 21 tons for Zapoljarnij, 20 tons for Kovdor, 19 tons for Kandalaksha, 13 tons for Nikel and 0.4 tons each for Apatity and Olenegorsk [Reimann *et al.*, 1998]. A time series plot of vanadium concentration levels at Kevo shows the best cyclic yearly variation as can be seen in Figure 5.7b. Similarly, a box plot in Figure 5.12b shows a nice trend of a monthly variation with the highest median values occurred in January-March and the lowest during June-September periods of a year. A GM for vanadium in this work is found to be 0.43 ng/m³. The GM or average value of this element is statistically in the same range with other Arctic locations as shown in Table 5.5.

W – Tungsten is a trace element emitted into the atmosphere from industrial activities. Like tin, determination of tungsten at low levels needs an epithermal irradiation followed by a Compton suppressed counting. Tungsten has integral to thermal radiative cross section ratio of 12.8 for ¹⁸⁶W(n,γ)¹⁸⁷W nuclear reaction, as presented in

Table 3.2, is favorable to occur through epithermal irradiation. However, only a 10-minute epithermal irradiation of the filters resulted in a less induced radioactivity due to a 23.9 hours half-life of the ^{187}W radioisotope. This eventually produced a very weak signal at 685 keV gamma energy of the gamma spectrum. An NAA detection limit for this element was found to be in the range of 0.01-0.22 ng/m³. About 96% concentration levels of tungsten of this work were found at BDL. So, no time series or box plots are presented for this element.

Zn – Zinc is a trace component in the earth's crust. It is not known to be a component in the ores smelted in the Kola Peninsula [Reimann et al, 1998]. The combustion of coal could be one source of anthropogenic zinc at Kevo. Traffic emits zinc via the wear of tires and some of the minerals occurring in alkaline intrusions can contain elevated Zn concentrations. Zinc is an essential element and plants can contain zinc levels. A GM value of 18.48 ng/m³ at Kevo is about 9 times higher than the Alert GM value for the period of 1981-1991 as shown in Table 5.5. Also the average value of this work is about 5 times higher than early 90's average value at Sevetijärvi, northern Finland. The GM or average value for zinc is higher for all other Arctic locations as can be seen in Table 5.5. A time series plot in Figure 5.7c shows that high zinc concentration levels are almost consistent in time sequence with that of the copper time series presented in Figure 5.4d. Two high values occurred in 1964 and 1977 are easily visible. A box plot of sorted monthly data of zinc in Figure 5.12c shows no monthly trend.

General comments:

The time series plots for all the measured elements presented in Figures 5.3 -5.7 revealed some features, which could only be explained looking through the historical fact of industrial activities at the Barents region of European sub Arctic. Most of the elements do not show a strong seasonal variation, which was clearly observed in Canadian Arctic, except for vanadium and manganese concentrations at Kevo, northern Finland. Probably this implies that Kevo is sitting in the same industrial airshed of Kola Peninsula, Norway, and Finland. Official figures show that a considerable amount of vanadium was emitted from the Kola Peninsula smelters in 1994, but as being from residual combustion sources

and predominantly attached to finer particles, this element can travel further. So, it is suspected that vanadium was essentially transported from the European countries and contributed to the ambient vanadium concentrations at Kevo. Manganese could have a number of sources, e.g. coal burning, residual oil combustion etc., and it is also capable of traveling long distances because of attachment with finer particles. So, similarly as vanadium, it may be transported from other European countries and also contributed to the Kevo ambient concentrations. As being a long transported component, a sharper visible seasonal trend can be seen only for these two elements at Kevo from both its time series and box plots as shown in Figure 5.5d, Figure 5.7b, Figure 5.10d, and Figure 5.12b.

Overall the box plots, presented in Figures 5.8 - 5.12, did not show any strong winter or summer trend. Outliers were present almost in all monthly datasets.

5.1.3 Elemental Ratios

The use of elemental ratios in developing local, regional, and continental signatures is ever growing since successful use of noncrustal Mn/noncrustal V (Mn_x/V_x) ratio, first proposed by Rahn [1981a], in explaining feasible source region of Arctic aerosol. Later Rahn and Lowenthal (1984) proposed a seven-element tracer system consisting of As, Sb, Se, Zn, In, Mn_x , and V_x for identification of distant pollution aerosol. For being an effective tracer, especially to identify them after traveling a long distance, several requirements should be met by elements. For example, the elements should be pollution-derived, sampled and measured accurately, emitted stably and homogeneously in each region, present on particles small enough to be transported long distances, and each signature should remain recognizable during transportation.

With a growing number of aerosol database at different locations around the globe, other approaches of trace elemental signatures include crustal, industrial, and marine sources. To achieve this objective one needs a large number of spatial datasets from different locations around the globe. Often a scaling of such datasets is done with a specific element. For example, in the seven-element tracer system scaling was done in unit of ambient selenium concentration level, as selenium being a unique industrial

precursor. Often a database could consist of missing such a particular element for many reasons. In this work, selenium was not determined, so a different approach of scaling or elemental ratio is presented to facilitate reading of elemental ratios in any pairs for a group of elements, such as anthropogenic, crustal, and marine.

The database was sorted for seasonal subsets in northern Finland considering June-August as summer, September - November as autumn, December - March as winter, and April and May as spring. Seasonal geometric mean (GM), geometric standard deviation (GSTD), and a winter/summer ratio are presented in Table 5.8 in an increasing order of winter/summer ratio of the measured elements. Several observations can be made from the winter/summer ratios of the measured elements. Vanadium, arsenic, indium, and antimony are topping the winter/summer ratio in Table 5.8 with ratios 3.96, 2.93, and 1.72 for both the indium and antimony respectively. On the low side of the Table 5.8, chlorine, silicon, silver show less than unity values with an approximate unity ratio value for iodine. Other industrial components like copper, zinc, tin, cobalt, manganese, etc. show a winter/summer ratio ranging from 1.05 – 1.63. These ratios clearly show that ambient elemental concentration levels of these elements are not affected much by the seasonal climate at Kevo in northern Finland. A winter/summer ratio for a ten-year period measurement at Alert for arsenic was reported to be 22 by Landsberger *et al.* (1997).

The highest winter/summer ratio 3.96 of vanadium concentration at Kevo implies that it was transported from other European parts to the sampling location and probably also due to a higher residence time of this element in the winter atmosphere because of its attachment with fine aerosol particles. A manganese winter/summer ratio of 1.63 probably implies that manganese in the Kevo aerosols have slightly different existence mechanism than the vanadium. For example, an examination of fine ($D < 2.5 \mu\text{m}$) to coarse ($2.5 \mu\text{m} < D < 15 \mu\text{m}$) particle ratios for vanadium and manganese median concentration levels are found to be of 16 and 1.36 respectively at Sevetijärvi, about 60 km east from Kevo, northern Finland [Virkkula *et al.*, 1999]. So, even if vanadium and manganese occurs at the same proportion in different seasons at Kevo, then a difference

of the aerosol residence time in the ambient atmosphere could make a difference of these two elemental concentration levels in winter and summer months of the year. A similar explanation could be assumed for explaining the observed difference for winter/summer ratios of arsenic with other industrial precursor elements. From the similar work of Virkkula *et al.* (1999) at Sevetijärvi, fine to coarse particle concentrations were calculated from median arsenic, antimony, cobalt, copper, indium concentration values and found to be 2.64, 2.66 (average value ratio), 1.08, 1.5, and 6 (average value ratio), respectively. These values show that fine to coarse particle concentration ratios for antimony is similar to that of arsenic and about 6 times higher for indium. This observation probably indicates that antimony and indium contribution in the Kevo atmosphere during summer and winter months are occurring differently than that of arsenic. At the low ratio side in Table 5.8, chlorine winter/summer ratio of 0.68 indicates a lower value in the winter months than that of in the summer months. If it is assumed that in summer months, a more movable air mass should bring more chlorine rich aerosols from marine sources, then this idea could be rejected examining winter/summer ratios of other marine component elements, like, sodium, bromine, and iodine. All marine elements in the later group show an equal or higher winter concentration than that of summer. So, for chlorine other possible explanation could be the replacement of chloride ions in the aerosol particles by inorganic species [Kerminen *et al.*, 1998]. During winter months, with a stagnant air mass and relatively enriched inorganic species than that of during summer months, the possibility of a chloride replacement mechanism is more favorable than summer time. This probably caused an unusual winter/summer ratio number for chlorine. Another interesting observation of winter/summer ratio is for silver. It shows a less than unity ratio of 0.84, unlike other industrial component ratios of unity or more than unity. As it is described in section 5.1.2 that a time series plot of silver showed two distinct concentration levels, high and low, during 1964-1971 and 1971-1978, respectively. Even for the high silver period, winter and summer GM values were calculated to be 0.26 ng/m³ and 0.34 ng/m³ respectively (not shown in Table 5.8), leads to a winter/summer ratio of 0.76. These observations indicate that most of the high

silver concentration levels of $\sim 100 \text{ ng/m}^3$ occurred mostly in other than winter months, which means a possible reason of those high concentration weeks could be explained by the meteorological data in addition to industrial activities. This is discussed further in section 5.3.1.

Elemental ratios computed from geometric mean (GM) are presented in Tables 5.9-5.11 in a square matrix form in groups of anthropogenic, crustal, and marine source elements. Table 5.9 presents elemental ratios computed for the whole period, and Table 5.10 and Table 5.11 present the summer and winter ratios at Kevo atmosphere, respectively. In each of these tables noncrustal manganese and noncrustal vanadium ratios are also shown. Any ratio can be read as:

$$\text{Elemental Ratio} = R_{ij} = \frac{i}{j}$$

where $i = \text{row title}$ and $j = \text{column title}$, for example, a ratio of noncrustal Mn/noncrustal V can be found in ‘Anthrop’ section in Table 5.9 as $R_{Mn_x, V_x} = \frac{Mn_x}{V_x} = 2.21$, where Mn_x is the row title and V_x is the column title. It is obvious that elemental ratio presentation in a square matrix form basically gives a mirror reflection of the inverse of one triangular part above or below the diagonal elements to the other, i.e. $R_{V_x, Mn_x} = \frac{V_x}{Mn_x} = 0.45$ would represent a reciprocal ratio of Mn_x/V_x . A noncrustal manganese or noncrustal vanadium was calculated as

$$X_{aer, noncrustal} = X_{aer, total} - \left[\frac{X}{Al} \right]_{ref} Al_{aer}$$

where X represents either Mn or V, and a $(X/Al)_{ref}$ value was used from global crustal mean [Mason, 1966].

The Tables 5.9-5.11 represent a broad band of elemental ratios of total suspended particles (TSP) in any pair at Kevo. While anthropogenic elemental ratios are useful for a long distance signature, a crustal elemental ratio could be useful to distinguish local/regional geogenic signatures since these elements occur in the ambient atmosphere

mainly from erosion of the earth's crust. A few of these ratios can be checked with reported elemental ratios. For example, Mn/V ratios for whole, summer, and winter periods are found to be 2.85, 4.54, and 1.87, respectively and 2.21, 3.76, and 1.45 for Mn_x/V_x for the studied period at Kevo. A Mn_x/V_x ratio is always about 17%-22% lower than the total Mn/V ratio. It is already reported that European region is enriched in Mn [Rahn, 1981a], i.e. a Mn/V ratio is higher than unity, however, it can be seen from this work that the magnitude of winter ratio is not much stronger than in summer. A time series plot of Mn_x/V_x is presented in Figure 5.13a. As can be seen that the plot is kind of divided into two parts, the period 1964-1971 shows higher ratios in every year during the June-August months, but the 1972-1978 period shows almost a consistent base ratio level except in 1976.

A Cl/Na ratio 0.29 of this work is about 6 fold lower than sea level ratio of 1.79, computed from the average ocean concentration [Bowen, 1979]. This probably indicates that a small fraction of chlorine occurred in finer particles is lost as a mechanism of inorganic species with marine source particles at Kevo atmosphere or during the long storage period as already mentioned earlier. A time series plot of Cl/Na presented in Figure 5.14c shows a soft seasonal trend during the study period and an average ratio level probably applicable only for the period of mid 1967-1973. It is not clear why other years are less than one. A Cl/I ratio time series plot presented in Figure 5.14b. A consistent ratio pattern for Cl/I can be seen for most of the year except 1974, 1976 and 1977. These years had a low Cl concentration level throughout the year. This plot indicates that the contribution of these two elements at Kevo atmosphere is more symmetric than Cl/Na, since a ratio level is more stable in the time series plot for Cl/I than that of Cl/Na. A time series plot of Na/I ratio presented in Figure 5.14a shows a cyclic variation, high in the winter and autumn months, and low in the summer months. Ratios of Na/I for the whole, summer, and winter periods are found to be 294, 240, and 319 respectively.

A Br/Na ratio of 0.0083, similar in summer and winter periods, can be found from Table 5.9. This ratio was computed from geometric means of these two elements. The

use of arithmetic mean leads to a ratio equal to 0.011, which is about twice than the oceanic mean level ratio of 0.006. The oceanic ratio is used to calculate the excess bromine in the Kevo atmosphere as

$$Br_{excess} = Br_{aer} - \left[\frac{Br}{Na} \right]_{ocean} Na_{aer}$$

Landsberger *et al.* (1990) reported a phenomenon of excess bromine at Alert. During the polar sunrise at Alert, an ozone destruction photochemical mechanism produces filterable bromine in the atmosphere. A suitable way to observe this phenomenon is the calculation and examination of excess bromine concentration levels in the atmosphere in a time series plot. An excess bromine time series plot is presented in Figure 5.13b. No visible pattern can be found at Kevo during late winter or spring of excess bromine, although a few sporadic high values occurred in 1965, 1969, and in 1975. So, it can be concluded that no excess bromine phenomenon is present at Kevo.

Ratios of Si/Al are found to be 6.41, 8.30, and 5.19 for the whole, summer, and winter periods. The earth crust ratio for Si/Al is about 3.4, which can be obtained from global average values reported by Mason (1966). This ratio is about half of the Kevo aerosol ratio. As it is already mentioned in section 5.1.2 that there might be activities at Kola Peninsula resulted a higher ambient silicon concentration levels at Kevo.

Kelley *et al.* (1995) reported the size distribution of aerosols containing metal at Monchegorsk region, Kola Peninsula. It showed that lead and arsenic occurred predominantly in the fine particles (< 1 µm) and copper and nickel occurred both in fine (< 1 µm) and coarse particles. Samples were collected between July 21 and August 6 in 1993. A mean Cu/As ratio of 16 was reported in Monchegorsk region for total suspended particles [Kelly *et al.*, 1995]. Ratios for Cu/As in this work are found to be 21, 35, and 12.4 for the 1964-1978, summer and winter periods, respectively, calculated from geometric means. Clearly, the reported Cu/As ratio 16 of Monchegorsk is less than half from the summer ratio 35 of this work. However, arithmetic mean or geometric mean ratios are not comparable. For example, considering arithmetic mean for a summer ratio of this work gives a 25.5 value (not presented in any table) of Cu/As ratio, but still this

ratio is about 50% higher than the Kelly *et al.* (1995). This clearly indicates a higher copper concentration at the Kevo atmosphere during the study period. It would be interesting to note that consideration of arithmetic mean and geometric mean plays an important role for elemental ratios, and it is necessary to consider a uniform methodology for calculation of elemental ratios. For example, it is already shown in case of Br/Na ratio that an arithmetic average of these elements produced a higher ratio for Br/Na, however, in case of Cu/As the opposite is being shown, i.e. consideration of arithmetic mean produced a lower ratio value than that calculated from geometric mean values of these elements. All of these happened because of the distribution pattern of the measured elements. As it already shown the section 5.1.1 that all the measured elements of this work are positively skewed, however, the degree of skewness is not proportionately related to arithmetic mean of a measured variable.

Scattered plots of As vs. Co, Cu, In, Sb, Sn, and Zn are presented in Figure 5.15bcd and Figure 5.16abc. Aluminum vs. Si and Sb scatter plots are presented in Figure 5.15a and Figure 5.17c. Indium vs. antimony and copper vs. zinc scatter plots are presented in Figure 5.16d Figure 5.17 b respectively. A total Mn vs. V and noncrustal Mn (Mn_x) vs. noncrustal V (V_x) scatter plots are presented in Figure 5.17a and 5.17d respectively. None of these plots reveal any unique relation between a pair of elemental concentration levels at Kevo. Almost in all plots the points are distributed uniformly and emerged as if a wide beam originating from the coordinate origin. These plots reveal that Kevo is sitting in an industrial airshed. If pollution components would travel from distant sources then atmospheric mixing and seasonal influence probably would have shown some unique relation in these plots as it was observed in case of a arsenic vs. antimony scatter plot at Alert [Landsberger *et al.*, 1997].

Table 5.8: Geometric mean (GM), geometric standard deviation (GSTD) in summer, autumn, winter, and spring seasons at Kevo for the period of 1964-1978

	Summer		Autumn		Winter		Spring		Win/Sum
	GM	GSTD	GM	GSTD	GM	GSTD	GM	GSTD	Ratio
Cl	81.47	2.48	116.93	2.59	55.84	3.74	42.86	2.18	0.68
Si	256.94	1.94	185.63	2.14	205.76	1.99	259.04	1.98	0.80
Ag	0.12	5.09	0.11	4.53	0.10	4.40	0.14	6.38	0.84
I	0.85	1.43	0.69	1.28	0.87	1.59	1.09	1.39	1.02
Cu	12.71	1.68	11.84	1.79	13.33	1.66	12.93	1.69	1.05
K	74.61	1.65	65.20	1.54	79.58	1.55	79.62	1.43	1.07
Ti	5.32	2.12	4.84	2.00	5.85	2.14	5.80	2.05	1.10
Ca	36.28	2.24	36.13	2.37	40.13	2.36	36.23	2.27	1.11
W	0.02	1.64	0.01	1.54	0.02	2.01	0.02	2.06	1.21
Zn	17.01	1.61	16.84	1.86	21.07	1.69	18.43	1.87	1.24
Al	30.95	1.66	25.45	1.57	39.68	1.88	47.83	1.76	1.28
Sn	2.24	2.26	2.05	2.12	2.94	2.04	2.66	2.28	1.31
Co	0.05	2.15	0.05	2.43	0.06	2.48	0.07	2.23	1.33
Na	204.97	1.54	237.19	1.48	276.96	1.59	296.37	1.66	1.35
Br	1.75	2.05	1.65	1.82	2.39	1.98	2.82	2.19	1.37
Mn	1.02	1.95	0.90	1.90	1.67	2.10	1.33	1.77	1.63
Sb	0.15	2.65	0.15	2.35	0.26	2.01	0.22	2.18	1.72
In	0.002	2.10	0.002	2.00	0.004	1.98	0.003	1.90	1.72
As	0.37	2.83	0.44	2.76	1.07	2.69	0.71	2.78	2.93
V	0.23	2.26	0.30	2.58	0.89	3.00	0.45	2.13	3.96

Table 5.9: Elemental ratio matrix for 1964-1978 period of GMs for anthropogenic, crustal and marine source elements (ratio = row title/column title)

<i>Anthrop</i>										
	Ag	As	Co	Cu	In	Sb	Sn	Zn	Mn_x*	V_x
Ag	1	0.1860	2.06	0.0090	38	0.5934	0.0462	0.0062	0.1525	0.3373
As	5.38	1	11.1	0.0482	205	3.19	0.2482	0.0332	0.8199	1.81
Co	0.4845	0.0901	1	0.0043	18.4	0.2875	0.0224	0.0030	0.0739	0.1634
Cu	112	21	230	1	4250	66	5.15	0.6889	17.0	38
In	0.0263	0.0049	0.0542	0.0002	1	0.0156	0.0012	0.0002	0.0040	0.0089
Sb	1.69	0.3134	3.48	0.0151	64	1	0.0778	0.0104	0.2570	0.5683
Sn	22	4.03	45	0.1941	825	12.9	1	0.1337	3.30	7.31
Zn	162	30	334	1.45	6169	96	7.48	1	25	55
Mn_x	6.56	1.22	13.5	0.0587	250	3.89	0.3027	0.0405	1	2.21
V_x	2.97	0.5514	6.12	0.0266	113	1.76	0.1368	0.0183	0.4521	1
<i>Crustal</i>										
	Al	Ca	Co	K	Mn	Si	Ti	V		
Al	1	0.9182	623	0.4617	28	0.1561	6.33	80		
Ca	1.09	1	679	0.5028	31	0.1700	6.89	87		
Co	0.0016	0.0015	1	0.0007	0.0451	0.0003	0.0102	0.1284		
K	2.17	1.99	1350	1	61	0.3382	13.7	173		
Mn	0.0356	0.0327	22	0.0164	1	0.0056	0.2250	2.85		
Si	6.41	5.88	3991	2.96	180	1	41	513		
Ti	0.1581	0.1451	98	0.0730	4.44	0.0247	1	12.6		
V	0.0125	0.0115	7.79	0.0058	0.3514	0.0020	0.0791	1		
<i>Marine</i>										
	Br	Cl	I	Na						
Br	1	0.0283	2.43	0.0083						
Cl	35.4	1	86	0.2929						
I	0.4109	0.0116	1	0.0034						
Na	121	3.4	294	1						

* x = non crustal

GM = Geometric mean

Table 5.10: Summer elemental ratio matrix of GMs for anthropogenic, crustal and marine source elements (ratio = row title/column title)

<i>Anthrop</i>										
	Ag	As	Co	Cu	In	Sb	Sn	Zn	Mn_x*	V_x
Ag	1	0.3338	2.60	0.0096	51	0.8078	0.0544	0.0072	0.2050	0.7702
As	3.00	1	7.80	0.0288	152	2.42	0.1631	0.0215	0.6140	2.31
Co	0.3842	0.1283	1	0.0037	19.5	0.3104	0.0209	0.0028	0.0788	0.2959
Cu	104	35	271	1.00	5284	84	5.67	0.7468	21	80
In	0.0197	0.0066	0.0513	0.0002	1	0.0159	0.0011	0.0001	0.0040	0.0152
Sb	1.24	0.4133	3.22	0.01	63	1	0.0674	0.0089	0.2537	0.9533
Sn	18.4	6.13	48	0.1763	932	14.8	1	0.1317	3.76	14.1
Zn	139	47	363	1.34	7075	113	7.59	1	29	107
Mn_x	4.88	1.63	12.7	0.0468	247	3.94	0.2656	0.0350	1	3.76
V_x	1.30	0.4335	3.38	0.0125	66	1.05	0.0707	0.0093	0.2662	1
<i>Crustal</i>										
	Al	Ca	Co	K	Mn	Si	Ti	V		
Al	1	0.8531	660	0.4149	30	0.1205	5.82	137		
Ca	1.17	1	774	0.4863	35.41	0.1412	6.82	161		
Co	0.0015	0.0013	1	0.0006	0.0457	0.0002	0.0088	0.2076		
K	2.41	2.06	1592	1	73	0.2904	14.03	330		
Mn	0.0331	0.0282	22	0.0137	1	0.0040	0.1927	4.54		
Si	8.30	7.08	5482	3.44	251	1	48	1138		
Ti	0.1718	0.1466	113	0.0713	5.19	0.0207	1	24		
V	0.0073	0.0062	4.82	0.0030	0.2203	0.0009	0.0425	1		
<i>Marine</i>										
	Br	Cl	I	Na						
Br	1	0.0214	2.05	0.0085						
Cl	46	1	95	0.3975						
I	0.4888	0.0105	1	0.0042						
Na	117	2.52	240	1						

* x = non crustal

GM = Geometric mean

Table 5.11: Winter elemental ratio matrix of GMs for anthropogenic, crustal and marine source elements (ratio = row title/column title)

<i>Anthrop</i>										
	Ag	As	Co	Cu	In	Sb	Sn	Zn	Mn_x*	V_x
Ag	1	0.0957	1.64	0.0077	25	0.3956	0.0349	0.0049	0.0900	0.1304
As	10.5	1	17.2	0.0803	259	4.14	0.3645	0.0508	0.9403	1.36
Co	0.6082	0.0582	1	0.0047	15.1	0.2406	0.0212	0.0030	0.0547	0.0793
Cu	130	12.4	214	1	3224	51	4.54	0.6327	11.7	17.0
In	0.0403	0.0039	0.0663	0.0003	1	0.0160	0.0014	0.0002	0.0036	0.0053
Sb	2.53	0.2418	4.16	0.0194	63	1	0.0881	0.0123	0.2274	0.3295
Sn	29	2.74	47	0.2204	711	11.3	1	0.1395	2.58	3.74
Zn	206	19.7	338	1.58	5096	81	7.17	1	18.50	27
Mn_x	11.1	1.06	18.3	0.0854	275	4.40	0.3876	0.0541	1	1.45
V_x	7.67	0.7339	12.6	0.0590	190	3.03	0.2675	0.0373	0.6900	1
<i>Crustal</i>										
	Al	Ca	Co	K	Mn	Si	Ti	V		
Al	1	0.9887	636	0.4986	24	0.1928	6.79	44		
Ca	1.01	1	644	0.5043	24	0.1950	6.86	45		
Co	0.0016	0.0016	1	0.0008	0.0373	0.0003	0.0107	0.0698		
K	2.01	1.98	1277	1	48	0.3868	13.6	89		
Mn	0.0422	0.0417	27	0.0210	1	0.0081	0.2862	1.87		
Si	5.19	5.13	3301	2.59	123	1	35	230		
Ti	0.1473	0.1457	94	0.0735	3.49	0.0284	1	6.55		
V	0.0225	0.0222	14.3	0.0112	0.5336	0.0043	0.1527	1		
<i>Marine</i>										
	Br	Cl	I	Na						
Br	1	0.0428	2.75	0.0086						
Cl	23.38	1	64.4	0.2016						
I	0.3631	0.0155	1	0.0031						
Na	116	5	319	1						

* x = non crustal

GM = Geometric mean

5.1.4 Enrichment Factors

One calculation that can roughly estimate a pollution level intensity in the ambient atmosphere above the natural level is called enrichment factor (EF) and can be calculated as

$$EF = \frac{(M/R)_{aerosol}}{(M/R)_{crustal}}$$

where M is the element of concern, R represents a reference element, *aerosol* refers to elemental ratio in the atmosphere, and *crustal* refers to the elemental global ratio in the earth crust.

To qualify for a good reference element in EF calculation, the element should purely be available in the ambient atmosphere from crustal source. Any anthropogenic emission of reference element would misrepresent the EF results. Rahn (1976) reported aluminum, iron, scandium, and silicon could be considered as reference elements primarily of being from pure crustal source. Both aluminum and silicon ambient concentration levels are determined at Kevo for the 1964-1978 period in this work. But by examining time series behavior and elemental ratios, etc. aluminum is considered as a reference element for EF calculation, because it is shown that there was elevated level of silicon concentration in the earlier part of the studied period probably caused from additional activities in addition to natural erosion. The global average values for all elements were taken from Mason (1966). There was a rare opportunity to consider local crustal average values for some elements because of a recently published the Environmental Geochemical Atlas of the Central Barents Region [Reimann *et al.*, 1998]. Local crustal elemental averages around Kevo were estimated from the B-horizon elemental concentration level of the Geochemical Atlas. B-horizon is a layer of soil profile and about more than 15 cm deep from earth's surface. Two EF plots for the measure elements are presented as a box plot in Figure 5.18a and Figure 5.18b, calculated from global and estimated local crustal averages respectively. Elemental global average, estimated local average, median values of calculated EF for both global and local references are presented in an increasing order of EF median values (global) in Table

5.12. Elements with enrichment factor close to unity are considered to be as non-enriched, an EF value more than unity can be considered as moderately enriched and more than 12 can be identified as enriched level.

As can be seen from median levels inside the box presented in Figure 5.18a that some industrial elements, like indium, copper, zinc, arsenic, antimony, tin, and silver are enriched in the range of 100-4000 times, considering median values, than the natural levels at Kevo ambient atmosphere. Vinogradova and Polissar (1995) reported some EF values at North Earth Archipelago (NEA), Russian high Arctic, for mid 80's, using aluminum and scandium as a reference elements and global averages from Mason (1966). For comparison approximate values were read from reported Figures and presented in Table 5.12. A comparison shows that arsenic, antimony, and silver EF values of this work are almost similar to that of at NEA, however the copper and zinc EF values of present work is about four and two fold higher than that of at NEA. This comparison shows two striking features. First, trace elemental concentration levels other than the main smelting industry, i.e. copper or nickel smelters, probably have a consistent enrichment factor in the Russian Arctic. Second, since Kevo is much closer to copper smelting industries than NEA, a higher EF median value for copper is reasonably understandable. A comparison of EF values at Alert reported by Landsberger *et al.* (1990) during mid 80's showed that indium and arsenic EF values are about similar to Kevo EF values. The EF values of antimony and zinc in this work are found to be about three and two times higher than that of at Alert, Canada.

A comparison of EF median values can be examined for EF calculations made from global and estimated local elemental average concentration levels. For a few elements, like cobalt, vanadium, and antimony it worked reasonably well, but for other elements local elemental average give lower median EF values. There could be small errors in the estimation procedure, since the Geochemical Atlas figures were read from block color code values around Kevo in northern Finland. However, both plots are very useful, because the first one facilitates the comparison with other reported EF values and the later EF values are more representative for the consideration of local soil references.

Table 5.12: Elemental global average, estimated local average, and EF median values

	Global crustal average µg/g	Estimated local crustal average µg/g	Median EF (from global)	Median EF (from local)	~EF values at NEA ¹ (ap)	~EF values at Alert ² (ap)
Cl*	19350000		0.09	**		
Al	81300	22211	1	1		
Na*	10770000	19200	1	**		
Br*	67300		1.30	**	2000	18
Si	277200	308571	1.53	0.38		
Ca	36300	21960	2.26	1.02	3	
Ti	4400	3917	2.77	0.85	1	
Mn	950	668	2.91	1.13	7	
Co	25	6.07	5.26	5.91	3	
K	25900	14429	6.98	3.42		
V	135	49	7.08	5.30	11	
In	0.10		72	**		50
Cu	55	15	573	587	150	
I*	60		615	**		
Zn	70	30	626	399	300	300
As	1.80	2.49	845	167	1000	600
Sb	0.20	0.04	2180	2860	2000	700
Sn	2		2930	**		
Ag	0.07	0.0268	3872	2759	3000	

* Ocean average (µg/l), ** not available from Raimann *et al.* (1998)

EF = Enrichment Factor

ap = approximately

¹Vinogradova and Polissar (1995), NEA= North Earth Archipelago (79.5°N, 95.4°E), Russian Arctic

²Landsberger *et al.* (1990), Alert, Canadian Arctic

5.2 Receptor Model Results

5.2.1 Principal Component Factor Analysis

Principal component factor analysis (PCFA) was used to find the factors or sources and their compositions for the Kevo lower atmospheric aerosols. The database was analyzed for full, summer, and winter periods separately. Samples collected during June-October and November-May were included in the summer and winter subsets, respectively. The PCFA results are presented in Table 5.13 and Table 5.14 for full and summer datasets. Winter dataset results are presented in Table 5.15 and Table 5.16 with 404 samples and 402 samples, respectively. Communalities and eigenvalues associated with each of the variables and factors are also presented in the tables including the total variance explained by all the considered factors. A communality value shows the fraction of variance explained for a variable. An eigenvalue can be used to calculate the fraction of total variance explained by each of the factors and also indicates the importance of a factor in the model. Scree plots are presented in Figures 5.19-5.21. Several sets of figures are presented for sample number vs. factor scores in Figures 5.22-5.23, Figures 5.24-5.25, and Figures 5.26-5.28 for full, summer, and winter factors, respectively. A factor score plot helps to find out how each sample contributes to a factor and usually is used as a diagnosis tool for an unusual contribution. The first and second highest elemental concentration levels, occurred for each element, are presented in Table 5.17 including the sample number in the database.

In the PCFA model no variable with more than 30% below detection limit (BDL) data points was used. Variables like titanium, cobalt, chlorine, silicon, and tin with BDL data points of 22%, 14%, 4%, 1%, and 1%, respectively are included by replacing all BDL data points by random numbers in the range of zero to BDL. PCFA was done on the correlation matrix, because the indium concentration level on average varies from 38-6000 times in comparison to other elemental concentration levels. A varimax rotation was done on all PCFA solutions. All factor loadings less than 0.3 or negative were deleted from the varimax rotated PCFA results.

As can be seen from the scree plots presented in Figures 5.19-5.21, an elbow pattern is not very clear in these plots. So, factor numbers for a PCFA model were determined from several trials and from the knowledge of elemental sources, sampling location. Six factors were considered for full and summer periods. Winter database was examined with seven and eight factors.

The PCFA results for the full period presented in Table 5.14 were examined with factor score plots presented in Figure 5.22 and Figure 5.23. The first factor in Table 5.13 appears to be a mixed source of anthropogenic and crustal elements. In this factor arsenic, indium, and cobalt are industrial components, however, aluminum is a crustal element. Manganese and vanadium have both the crustal and anthropogenic sources. Iodine and potassium in the Factor 1 are not clearly explainable. Actually, potassium is known as a wood-burning component in the atmosphere, but without having any other same source component in the database, it is attached with other source groups. A lower communality value of 0.67 shows that only 67% potassium variance is explained by the factor model, in other words, this indicates that potassium is not strongly represented by any specific factor in the model. Factor 2 represents a pure industrial source consisting of copper, indium, tin, and zinc. A factor score plot is presented in Figure 5.22b shows that sample number 636 highly contributed to this factor. So, to check any possible error in this particular sample, PCFA was repeated without sample number 636 and it reproduced the same composition elements Cu, In, Sn, and Zn in factor 2. So, this experiment showed that Factor 2 was not influenced by only one sample. Actually, this sample simultaneously represented the highest concentration levels of copper, indium, tin, and zinc in the database as can be seen in Table 5.17. Factor 3 represents a sea source consisting of sodium, bromine, iodine, and a weak loading (0.365) of chlorine. A communality of 0.61 for chlorine in Table 5.13 shows that only 61% variance of this variable is explained by the factor model and it is not strongly coupled with any particular factor. Instead it appeared into several factors with low loading values. Factor 4 in Table 5.13 represents a crustal source of composition elements silicon, titanium, aluminum, and manganese. Potassium, iodine, and chlorine are also present in factor 4,

but these are not representative components of a crustal source. Factor 5 is a unique factor with antimony as the only element. Factor score plot of factor 5 is presented in Figure 5.23b and it shows that a number of samples highly contributed to this unique factor. So, factor 5 in Table 5.13 reasonably represents the element antimony as a unique factor. One would always expect a resemblance of antimony with other industrial precursor elements, especially with arsenic. Reimann *et al.* (1997,1998) reported on an antimony anomaly in Kola Peninsula and a number of high values were also observed on moss in the Norwegian coast north from Kevo. The Geochemical Atlas of the central Barents region also shows the highest B-horizon antimony concentration level near Sodankylä (Figure 3.1) in Finland south from Kevo. So, clearly the natural source origin dominated the industrial antimony contribution in the Kola atmosphere, specifically on high concentration days and produced a unique factor of antimony in the PCFA model. Factor 6 consists of cobalt and potassium is not clearly attributable to any source. Elimination of this factor highly disturbs the sea source compositions in factor 3, so this factor was retained in the model.

Factor analysis results for the summer dataset are presented in Table 5.14. As can be seen from this table, all crustal and industrial components are mixed up and are represented by factors 1, 3, 4, and 5. This indicates that summer air mass movement produced a soup of crustal and industrial components at the Kevo atmosphere at such a level that factor analysis could not distinguish these two sources independently. Sea source components Br, Cl, Na and I are represented by factor 2, which was more important in PCFA factor than that of a winter factor. This was an expected result for a location like Kevo in the sub Arctic region. Since it was anticipated that the regional climate and freezing condition should show a stronger sea component in the summer than in the winter. The presence of cobalt in the summer sea factor 2 can be considered as noise. Factor 6 represents again represents a unique factor of antimony, the reason already explained earlier. All summer factor score plots were examined for unusual contributions from any sample. High contributions from samples 94, 88, and 32 can be seen in Figures 5.24a, 5.24b, and 5.25c. All of these samples were examined and found

to be real event during the sampling week, since those were associated with multiple elemental high concentration levels.

The PCFA results for winter data are presented in Table 5.15. Factor 5 contains the titanium only and factor 6 contains a high loading for bromine. Score plots for these factors are presented in Figures 5.27a and 5.27b. Sample number 10 in factor 5 and sample number 29 contributed the most. These samples correspond to the numbers 11 and 49, respectively, in the full database. Examination of these samples showed that titanium concentration level in sample 11 was unusually high among all the samples and sample 49 contained the 4th highest value for bromine in the database. Without these two samples the PCFA was repeated on the winter dataset and the results are presented in Table 5.16 with eight factors. It may be mentioned here that in the repeated attempt of winter dataset a seven-factor solution appeared with a high negative chlorine loading (-0.765) in the 2nd factor mixed with industrial components. A six-factor solution was also intuitively not reasonable, so finally an eight-factor solution was considered and the results are presented in Table 5.16. As can be seen, Table 5.16 presents a much better factor composition than Table 5.15 for the previous winter PCFA results, especially since titanium is grouped with the soil source components in factor 3. Sea components bromine, chlorine, iodine, and sodium appeared in a number of pairs in factor 4, 5, and 6. In factor 4, the strong presence of sodium was moderately related to potassium and iodine. In factor 5, bromine paired weakly with iodine and moderately with titanium. However, presence of titanium in factor 5 with bromine and iodine is not reasonable. Strong loading of chlorine in factor 6 weakly coupled with sodium in this factor. A close time series observation of sodium to chlorine does not show a good correlation in the winter months at Kevo aerosol concentration. Probably in the winter months a frozen northern ocean and sea and accumulated atmospheric reactive pollutants, stagnant air mass, etc., may have caused a different distribution pattern of bromine, chlorine, iodine and sodium in the Kevo atmosphere. Crustal components like, aluminum, manganese, silicon, and titanium have high loading in factor 3 and a weak loading of potassium. A strong industrial component composed of copper, indium, tin, and zinc appeared in the

2nd factor in winter. This industrial factor also was in the 2nd factor for full dataset and in the 4th factor for a summer PCFA results. This means in winter months, these industrial components dominated the atmospheric concentration levels more than summer time. Factor 1 represents strong industrial and anthropogenic components like arsenic, indium, vanadium, manganese, and cobalt. However, the presence of aluminum and iodine in this group need some explanation. There is an aluminum smelter at Kandalaksha, Kola Peninsula, about 350 km southeast from Kevo. However, time series observation, and many other statistical data presented in earlier sections did not support aluminum contribution to the Kevo airshed. According to Reimann *et al.* (1998) winds from the south and southwest dominate the Kola Peninsula during winter. During summer the wind directions are predominantly from east to west. So, the wind direction does not support the aluminum aerosol transportation from the Kandalaksha aluminum smelter in the direction of Kevo. As can be seen from Table 5.16, most of the aluminum loading (0.72) appeared in factor 3, a crustal source. Probably a favorable meteorological condition produced a mixed signal with industrial component in the industrial source factor 1 in Table 5.16. The presence of iodine with a loading value 0.537 in factor 1 is not clearly explainable.

General Comments

PCFA results presented in Tables 5.13 - 5.16 show a number of striking features in the Kevo lower atmosphere. First, crustal and industrial components were mixed up in summer and were not recognized individually by PCFA factors. Second, the sea component is much stronger in summer than in winter. Third, antimony is represented by a unique factor. Fourth, in winter sea source components did not show a unique behavior. However, in summer, all the sea source components like sodium, iodine, bromine, and chlorine were found in a single factor. Fifth, an industrial source factor consisting of copper, indium, tin, and zinc was found more important in PCFA factor in winter than that of the summer dataset factor.

In PCFA, elemental presence from the same source group is very essential for an acceptable explanation of factor composition. For example, as it is shown above, without having any other elemental source signature from the wood or vegetation- burning source, it was difficult to explain the presence of potassium in some factors. Similarly, a non-representative blank chlorine value, used earlier, resulted in 35% data points below the detection limit. Thus, it was not included in the PCFA model. Even if included, it did not show clearly visible a chlorine to sodium correlation in the PCFA results as a sea source factor. This prompted to find an alternate representative chlorine blank value, which is presented in section 5.1.2. The inclusion of revised chlorine data in the PCFA model not only showed the anticipated sea source behavior in a factor, but also improved the PCFA results. This exercise clearly showed the important of a correct elemental blank value to determine trace elements in the aerosol filters for using them in a receptor model like PCFA.

Table 5.13: Factors, communalities, eigenvalues, and variance for full dataset (681 samples)

	Factor 1	Factor 2	Factor 3	Factor 4	Factor 5	Factor 6	Communality
Al	0.605			0.563			0.72
As	0.775						0.71
Br			0.881				0.78
Cl			0.365	0.391			0.61
Co	0.499					0.536	0.65
Cu		0.862					0.84
I	0.441		0.644	0.34			0.74
In	0.666	0.564					0.79
K	0.327			0.463		0.433	0.67
Mn	0.817			0.397			0.84
Na			0.85				0.80
Sb					0.964		0.97
Si				0.816			0.72
Sn		0.915					0.88
Ti				0.677			0.72
V	0.874						0.78
Zn		0.855					0.86
Eigenvalue	5.611	2.472	2.042	1.228	0.96	0.771	
Total variance explained by six factors = 78%							

Table 5.14: Factors, communalities, eigenvalues, and variance for summer dataset (277 samples)

	Factor 1	Factor 2	Factor 3	Factor 4	Factor 5	Factor 6	Communality
Al			0.734				0.71
As					0.722		0.66
Br		0.918					0.85
Cl	0.549	0.482					0.78
Co		0.372	0.349		0.585		0.69
Cu	0.662			0.403			0.63
I	0.367	0.758					0.78
In			0.351	0.847			0.84
K	0.711						0.62
Mn			0.844				0.76
Na		0.912					0.86
Sb						0.925	0.90
Si	0.777						0.69
Sn				0.866			0.82
Ti	0.523						0.75
V			0.851				0.81
Zn	0.634			0.303	0.432		0.68
Eigenvalue	5.272	2.406	1.875	1.324	1.065	0.887	
Total variance explained by six factors = 76%							

Table 5.15: Factors, communalities, eigenvalues, and variance for winter dataset (404 samples)

	Factor 1	Factor 2	Factor 3	Factor 4	Factor 5	Factor 6	Factor 7	Communality
Al	0.537			0.639				0.78
As	0.786							0.76
Br						0.961		0.95
Cl			0.545					0.68
Co	0.382						0.789	0.84
Cu		0.889						0.87
I	0.638		0.368			0.342		0.76
In	0.646	0.577						0.79
K	0.547		0.511					0.83
Mn	0.78			0.403				0.87
Na			0.893					0.83
Sb	0.635		0.424					0.73
Si				0.914				0.89
Sn		0.93						0.90
Ti					0.883			0.87
V	0.82							0.77
Zn		0.902						0.91
Eigenvalue	5.952	2.504	1.824	1.213	1.071	0.766	0.695	
Total variance explained by seven factors = 82.5%								

Table 5.16: Factors, communalities, eigenvalues, and variance for winter dataset without sample 10 and 29

	Factor 1	Factor 2	Factor 3	Factor 4	Factor 5	Factor 6	Factor 7	Factor 8	Communality
Al	0.431		0.724						0.81
As	0.787						0.305	0.317	0.84
Br					0.912				0.86
Cl						0.912			0.94
Co	0.301						0.889		0.96
Cu		0.9							0.90
I	0.537			0.533	0.361				0.81
In	0.746	0.529							0.89
K	0.388		0.364	0.638					0.86
Mn	0.765		0.502						0.91
Na				0.838		0.342			0.88
Sb								0.921	0.95
Si			0.885						0.86
Sn		0.93							0.89
Ti			0.602		0.576				0.75
V	0.833								0.82
Zn		0.899							0.92
Eigenvalue	6.069	2.504	1.888	1.227	1.122	0.778	0.639	0.614	
Total variance explained by seven factors = 87.3%									

Table 5.17: Elements and samples related to highest concentration levels

	1st highest sample #	2nd highest sample #	Sample # RTMHE*	Related element
Ag	233	35	6	Ca, Co, Cu, Zn
Al	221	26	26	Al, Mn
As	323	219	35	Ag, Br
Br	233	232	221	Al, Mn, Sn
Ca	6	1	232	Br, Na
Cl	529	367	233	Ag, Br, I, Na
Co	476	6	239	K, Si
Cu	636	6	323	As, In
I	481	233	481	I, K
In	636	323	636	Cu, In, Sn, Zn
K	239	481		
Mn	221	26		
Na	232	233		
Sb	86	576		
Si	221	239		
Sn	636	285		
Ti	11	225		
V	683	632		
Zn	636	6		

*RTMHE = related to multiple elements of high concentration; compiled from column 2 and 3

5.2.2 Unmix

Unmix is a computer code classified as an advanced receptor model and discussed in section 4.3. An Unmix output directly provides the source number, source composition, contribution to the receptor site, and an error estimate of the source compositions. A decision for factor number in the model is taken by a signal/noise statistics and another parameter called r^2 . The recommended values equal to or more than 2 and 0.8, respectively, were followed. An Unmix manual, available with Unmix code, provides a detailed running procedures and use of window commands of the code conveniently. An Unmix main command widow is presented in Figure 5.29.

Unmix results for all samples are presented in Table 5.18. The error estimates of the source contribution are presented in Table 5.19. As it is discussed in section 4.3, the incorporation of explicit physical constraints like SAFER and factor determination statistics NUMFACT into Unmix makes it a conservative model. As can be seen from Table 5.18, only six elements out of seventeen could be used for a four-source solution in the Unmix model in order to obtain a statistically significant solution. Statistical parameters are shown at the bottom of the Table 5.18. An r^2 value 0.84 is explained by four factors, signal/noise ratio of the 4th source is 2.82 and a strength value is 4.09 (recommended > 3). All these parameter values show that the solution is statistically significant. An r^2 value 0.84 implies that at least 84% variance of each of the variables was explained by four sources. A filter parameter equal to 0.15 states that if the sum of the negative values for any species in a source composition is greater than 15 percent of its mean, the source composition is rejected and not displayed by Unmix. So, a zero value for this parameter would result only in a positive source composition in all factors and if a negative value occurred in the solution then the solution would be rejected. For example, in Table 5.19 source #1 provides a negative composition for vanadium (-0.04). If a filter parameter equal to '0' would be set, then Unmix would not find a feasible solution for this situation. Many times in a correct solution small negative values appears in the source composition induced by errors in the data.

As can be seen from Table 5.18 that source #1 represents the highest silicon concentration level of 227.45 ng/m³ among the four sources. So, this source represents a soil source. Several attempts to add other known soil components like aluminum and titanium in the model were in vain for statistical reasons. It was speculated that probably it was because strong correlations (> 0.8) of silicon to aluminum or silicon to titanium was not found in a PCFA model as presented in the previous section. The use of winter dataset in Unmix did not allow a simultaneous inclusion of both the silicon and aluminum. The winter dataset gave PCFA loading values of 0.724 and 0.885 in factor 3 presented in Table 5.16. This clearly indicates that a good correlation may not be the only criteria to include a variable in Unmix model for a statistically significant solution. The sum of apportioned silicon concentration into four factors (227.45 + 29.84 + 20.68 + 16.87 = 294.84 ng/m³) represents the mean concentration of silicon concentration level in Table 5.18. In a similar way, if total aerosol mass would be included in the model as a variable, then it would be apportioned in the same way as a variable and would give the apportioned mass to each source. However, for this database no aerosol total mass was recorded during sampling period at Kevo, so a total mass apportionment to sources was not possible in this work. Source #2 in Table 5.18 shows the highest contribution of sodium (205.37 ng/m³) among four sources and indicates a sea source. But again, no chlorine, bromine, or iodine variables were statistically supported by the code to be included in the model such as source #1. Copper and zinc is the highest contributor to Source #3 and so it represents a smelting source. Tin or indium was statistically not allowed to be included in Unmix model, although in PCFA showed a specific strong factor for copper, zinc, tin, and indium. Source #4 is the highest for manganese and vanadium and clearly representing an anthropogenic source resulted from coal and fuel combustions.

Unmix also produced the uncertainty associated with each source composition. One sigma uncertainties and ratios of source composition to two-sigma uncertainty value are presented in Table 5.19. The uncertainty levels associated with each source are quite acceptable, since one-sigma values are well below than the source composition levels.

For example in source #1 silicon shows a one-sigma uncertainty value of 17.57 ng/m³, a much lower than the composition value of 227.45 ng/m³. However, for source #4 one-sigma values for manganese and vanadium are more than 50% of the composition levels.

General comments

The literature review indicates that Unmix has always a less tendency or ability to use the trace elemental aerosol data in the model. An application of Unmix model on the 1988-1995 fine particle database of Vermont aerosol reported by Poirot *et al.* (2001) showed that only 5 out of 11 trace elements having 70% data points above the detection limit were used in the model. Unmix manual presented an example considering a real air particulate database obtained from Environmental Protection Agency (EPA). The example also included only trace elements like Al, Si, K, Ca, Mn, Fe, and Br for a statistically significant solution and rejected the inclusion of trace elements like Ti, Cu, Zn, As, Sr, and Pb.

One of the major reasons of using an advanced receptor model like Unmix was mass apportionment to sources as discussed in Receptor Model Chapter 4. Actually, in comparison to sulfur bearing compounds and black carbon total mass, trace elements always bear a small fraction of the total aerosol mass. So, at many times ignorance of such a low mass trace elements does not influence the mass apportionment to the sources significantly. However, certainly trace elemental behavior is lost in the system.

Unmix model assumes a constant source composition through out the sampling period in an airshed. This assumption most probably is not valid for this database, since an ore smelting emission inventories most likely changed during a 14-year sampling period. Second, Unmix is highly sensitive to outliers, so in the manual it is recommended, if possible, to search for a solution eliminating the outliers from the database. However, from the earlier discussion as presented in section 5.1, it has been shown that there are too many outliers present in this database. In section 5.2.1 it is also shown that many outliers represent real events. So, elimination of so many outliers was not reasonable.

Probably for all the above reasons, Unmix was only able to include six variables of this database out of seventeen for a statistically significant solution.

Table 5.18: Unmix results for source number, composition, and contribution

	Source #1 comp. & cont.* (ng/m ³)	Source #2 comp. & cont. (ng/m ³)	Source #3 comp. & cont. (ng/m ³)	Source #4 comp. & cont. (ng/m ³)
Cu	3.18	3.30	7.43	0.80
Mn	0.38	0.12	0.18	0.91
Na	35.76	205.37	27.99	13.96
Si	227.45	29.84	20.68	16.87
V	-0.04	0.04	0.03	0.79
Zn	3.95	1.82	13.49	3.48

*comp. & cont. = composition and contribution

Filter Parameter: 0.15

Weighting Parameters: 0.15 1

6 Variables, 681 Cases, 4 Factors,

Minimum R² = 0.84; Minimum Signal/Noise = 2.82; Strength = 4.09

Table 5.19: Uncertainty and source composition/2s ratios for all sources

Source #1	Uncertainty			Source #2	Uncertainty		
	Composition (ng/m ³)	σ (ng/m ³)	Comp/2 σ		Composition (ng/m ³)	σ (ng/m ³)	Comp/2 σ
Cu	3.18	0.49	3.24	3.30	0.67	2.46	
Mn	0.38	0.18	1.03	0.12	0.15	0.41	
Na	35.76	8.53	2.10	205.37	20.39	5.04	
Si	227.45	17.57	6.47	29.84	9.29	1.61	
V	-0.04	0.15	-0.14	0.04	0.12	0.15	
Zn	3.95	0.90	2.20	1.82	0.72	1.26	

Source #3	Uncertainty			Source #4	Uncertainty		
	Composition (ng/m ³)	σ (ng/m ³)	Comp/2 σ		Composition (ng/m ³)	σ (ng/m ³)	Comp/2 σ
Cu	7.43	0.80	4.63	0.80	0.58	0.69	
Mn	0.18	0.19	0.49	0.91	0.49	0.93	
Na	27.99	13.11	1.07	13.96	12.81	0.54	
Si	20.68	9.27	1.12	16.87	11.82	0.71	
V	0.03	0.16	0.09	0.79	0.43	0.92	
Zn	13.49	1.27	5.32	3.48	1.99	0.87	

5.3 Residence Time Analysis Results

A gridded domain of 500×500 squares was considered in this work for residence time analysis (RTA). The RTA domain is shown in Figure 5.2. A side of a single grid square was 10 kilometer long. The red dot in Figure 5.2a shows the sampling location Kevo, northern Finland and Figure 5.2b shows an expanded part of the domain around the sampling location. The gridded domain covered most of Europe, almost half of Russia, most of Greenland (Denmark) and a part of the Arctic region including the North Pole.

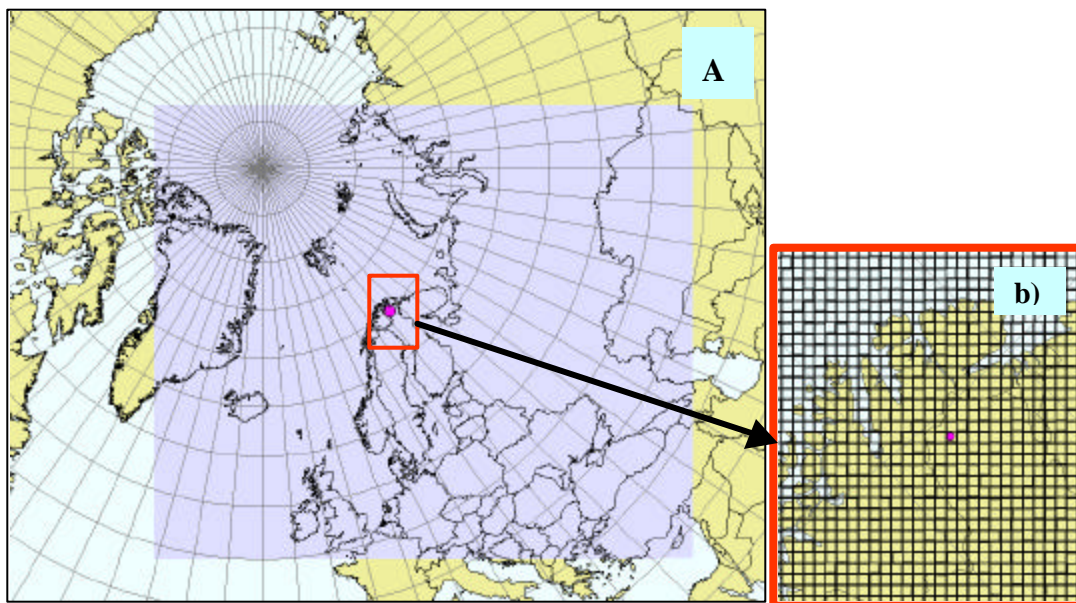


Figure 5.2 a) Gridded domain used in RTA, b) Part of the domain showing 10 km grid squares used for RTA

Poirot *et al.* (1986, 2001) used a domain consisting of 80×80 km grid cells in their earlier work. In this work, 10×10 km grid cells were used for the RTA domain over and around Kevo. One of the main advantages of choosing smaller grid cells was that incremental probability records of these smaller cells could be added to produce RTA plots for grid squares of any larger size. This technique is termed as **smoothing factor** (SF) in this work. For example, a SF 25 means incremental probabilities of 5×5 grid cells is averaged up and resulted RTA plot would emerge from the incremental

probabilities of 50×50 km cells over the RTA domain. Similarly, a SF 81 means redefined cell size of 90×90 km and 441 means 210×210 km cells in the RTA domain. Basically, initial consideration of a smaller grid cell like 10×10 km in the RTA domain enables the user to reproduce RTA plots for any desired cell for a detailed study. The basics of the RTA metric are discussed in section 4.4.

In this work, two back trajectories were computed per day at 6 hrs and 18 hrs UTC and at a 500-meter height using the HYSPLIT_4 model. Like GMT (Greenwich Mean Time), UTC stands for Coordinated Universal Time in *French*. Each back trajectory history was a 5-day (120-hour) long backward starting from a given time and within a height of 500 meters above the ground level. So, for a weeklong sampling period, 14 back trajectories represent the total air mass history coming to the sampling site related to a particular sample. A total of 9,608 back trajectories were computed for the whole sampling period, 1964-1978, and used in RTA. A single back trajectory image of HYSPLIT_4 is shown in Figure 5.30. The total residence time probability for each of the cell was calculated using all trajectories for a given period, and the high-value residence time probabilities for each of the variables was calculated using back trajectories related to the highest 3.5% concentration samples for 1964-1970 and 1971-1978 periods. However, for some seasonal RTA plots, 7% of the highest concentration samples related to back trajectories were used. Incremental probabilities for each of the grid cells of the domain were calculated by subtracting the total residence time probabilities from the high-value residence time probabilities for each of the variables. Usually, these incremental probability values are very small, so a common multiplication factor was used for boosting those values for plotting. The color code scales shown with RTA plots represent the absolute incremental probabilities in percent.

5.3.1 Explanation of silver anomaly

Two very distinct silver concentration level periods, high and low, were observed in the Kevo lower atmosphere. These occurred during 1964-1970 and 1971-1978, respectively. Originally it was speculated that contamination of silver, bromine, and iodine came from x-ray films during autoradiography of aerosol filters as discussed in

section 5.1.2. Both the historical fact and replicated autoradiography experiments on blank filters supported that x-ray films did not contaminate aerosol filters. So, an acceptable explanation is needed for the unusual high silver concentration levels observed in the Kevo atmosphere for the period of 1964-1970. Such a high silver concentration level in the aerosol has never been reported in the literature for any place.

Since 1921, various ore bodies were discovered in Kola Peninsula. In 1932, at Nikel a nickel smelter was built for smelting local ore bodies. In 1938, a larger nickel smelter was built at Mochegorsk. In 1965, a roasting plant at Zapoljarnij was built after discovering a good quality ore body nearby in 1956 [Reimann *et al.*, 1998]. An approximate distance of these locations from Kevo is presented in Table 3.1. Since 1938, at Monchegorsk good quality nickel ores supplied from local and Pechenga area, near Zapoljarnij, were smelted. However, good quality ores at Monchegorsk were quickly exhausted and very good quality ore bodies, rich with nickel, cobalt, silver, gold, and platinum, were discovered at Norilsk in northern Siberia. However, the lack of mass transportation system from Norilsk to major Russian cities and the Siberian extreme weather condition prohibited any attempt for developing a complete smelting facility at Norilsk. So, in 1964 it was decided to bring newly discovered good quality ore to Kola Peninsula for smelting [Horensma, 1991]. Reimann *et al.* (1998) reported that since 1971-1972 Norilsk ore has been smelted at Mochegorsk smelter and the highest moss silver concentration levels around Monchegorsk area showed that it occurred due to smelting of silver rich ores supplied from Norilsk. No report specifically mentioned the smelting locations of Norilsk ore for the period of 1964-1970 at Kola Peninsula, i.e. Nikel, Zapoljarnij, and Monchegorsk. Horensma (1991) reported some historical facts related to establishing a challenging northern sea route for Norilsk ore transportation to Kola Peninsula. Initially the transportation was seasonal. In 1969, ships from Norilsk reached Kola Peninsula as late as November. Later the shipping season had been lengthened from five to ten months and resulted from 600,000 tons in 1970 to 1 million tons in 1977.

Probably more historical records could show clearly whether the Norilsk ores were smelted at Nickel/Zapoljarnij or not. However, if it is assumed that during the 1964-1970 period transported ores were smelted or roasted at Nickel or Zapoljarnij, then high silver concentration levels observed at Kevo during the period 1964-1970 probably is explainable. As it is discussed earlier, a less fluctuating seasonal concentration levels showed that the Kevo lower atmosphere was directly influenced by industrial activities, as if Kevo area is under the same industrial airshed of Kola Peninsula. However, the influence of Nickel's and Zapoljarnij's smelters, which are within 150 km, is more in the Kevo atmosphere than the Monchegorsk's smelters, which is about 313 km away from Kevo. Since it has been observed that an aluminum smelter at Kandalaksha, 352 km southeast from Kevo, did not influence the natural ambient aluminum concentration level at Kevo, it could be assumed that Monchegorsk smelting activities also had less influence in the Kevo atmospheric aerosols. This would support that higher silver concentration at Kevo during the period of 1964-1970 occurred probably due to the Norilsk ore smelted or roasted at Nickel or Zapoljarnij. The RTA probability plots presented in Figure 5.31a and Figure 5.31b for the period of 1964-1970 and 1971-1978, respectively, show supportive patterns for this assumption. The later plot covers the Monchegorsk area very well and supports the literature report that high silver Norilsk ore has been processed at the Monchegorsk smelter since 1971-1972. But in Figure 5.31a the 2nd highest RTA probable area in the upper right corner slightly covered Nickel and Zapoljarnij and highest probable area covered lower Finland. These plots were generated using a smoothing factor of 441, discussed in the second paragraph of this section. Could there be any possible source from lower Finland? In Finland, open-pit chromite mining began at Kemi in 1966 and ferrochrome production in 1967 for nickel production to make stainless steel at nearby Tornio. Tornio is located near Sodankylä (Figure 3.1). However, any assumption of high silver contribution from any Finland mining could be rejected because in many instances the highest silver concentration level simultaneously occurred with the highest bromine, iodine, and sodium concentration levels. The first ten highest silver concentration levels are presented in Table 5.20 with sampling periods

corresponding to the highest occurrences for bromine, iodine, and sodium. As can be seen from Table 5.20 for first four highest silver concentration levels, bromine, iodine and sodium are also linked with their highest levels. These sea components were checked for the first 20 highest values. This observation indicates that in some favorable meteorological conditions the industrial component silver transported with sea source components bromine, iodine, and sodium simultaneously to the receptor site. So, an immediate question arises in mind, should silver not be accompanied by other high smelting components at the receptor site? For a closer look, a few samples vs. silver concentration is presented in Figure 5.32, including copper, indium, tin, and zinc. As can be seen from Figure 5.32 that most of the highest silver concentrations are correlated well to the other smelting component elements, although the signal strength of those elements are not that strong as that of silver.

Air mass back trajectory paths for the six highest silver samples, as presented in Table 5.20, are presented in Figure 5.33 labeled by sample number and arranged in decreasing concentration order. It can be easily seen that the first four highest sample trajectory air masses related to sample # 233, #35, #232 and #49 followed the path more over Barents Sea, Norwegian Sea, and the Gulf of Bothnia than sample #87 and #230. In Table 5.20, it can be seen that the former four samples also represent some of the highest sea source components like bromine, iodine, and sodium but not for samples 87 and 230. Also most of the trajectories of the presented samples in Figure 5.33 show a pattern of flow over Kola Peninsula and then to the Kevo receptor center. Four “zoom in” RTA plots for smoothing factors 81 and 25 are presented in Figure 5.34 for the periods of 1964-1970 and 1971-1978. The RTA plots presented in Figures 5.34a and 5.34c clearly show that incremental probabilities of Nickel and Zapoljarnij area are higher than Monchegorsk area for the high silver period. A map of these locations can be seen from Figure 1.2. As can be seen from Figures 5.34b and 5.35d that the incremental probabilities totally missed the Mochegorsk area, although it was known as the location of Norilsk ore smelting for the period of 1971-1978. The main reason for missing that location was the selection of high subsets to generate the RTA plots. RTA plots

presented in Figure 5.31 considered the highest subset consists of the 12 highest silver concentration weeks. However, in Figure 5.34 the subset consists of the 6 highest weeks. For the period of 1964-1970 this subset was very distinct, about two order higher, than the rest of the data, but for 1971-1978 period, the subset was very similar to rest of the data and so the RTA resolution was poor for such a subset.

Based on all the aforementioned historical facts, observations, and explanations, it can be concluded that the high silver concentration period observed in the Kevo atmosphere during 1964-1971, occurred due to smelting of silver rich Norilsk ores at Nikel and Zapoljarnij smelters. The reason for a few extremely high silver concentrations probably occurred due to repeated air parcel transportation over the Kola region in those particular weeks. Estimating the sample air mass history with only 14 back trajectories is probably statistically good enough for this large batch of samples, but certainly a 14 back trajectory ensemble represents a small fraction of the total air mass history for a week period. The observed low silver concentration period in the Kevo atmosphere for the 1971-1978 period, and high moss silver concentration around Monchegorsk area reported by Reimann *et al.* (1998) showed that silver did not travel a long distance through atmosphere from the emission sources.

Table 5.20 Highest concentration levels of silver related to bromine, iodine, and sodium

Silver highest	Bromine highest	Iodine highest	Sodium highest	Sample #	Sampling start-end	Ag ng/m ³
1 st	1 st	2 nd	2 nd	233	5/12/69 - 5/19/69	190.73
2 nd	3 rd	4 th		35	6/23/65 - 6/28/65	118.43
3 rd	2 nd	6 th	1 st	232	5/5/69 - 5/12/69	77.61
4 th	4 th	18 th		49	11/16/64 - 11/23/64	60.05
5 th	7 th			87	10/11/65 - 10/18/65	25.86
6 th	8 th			230	7/25/66 - 8/1/66	16.61
7 th			10 th	6	4/21/69 - 4/28/69	7.76
8 th				15	11/23/64 - 11/28/64	4.43
9 th				78	1/28/65 - 2/1/65	4.42
10 th				13	5/23/66 - 5/30/66	3.81

5.3.2 RTA results for all elements

RTA incremental probability plots are presented in sequence of anthropogenic, crustal, and sea source. Anthropogenic elements are presented in Figures 5.35 - 5.43, crustal elements like aluminum, silicon, calcium, and titanium RTA plots are presented in Figures 5.44 - 5.47 and the sea source components sodium, chlorine, bromine, and iodine are presented in Figures 5.48 - 5.51.

RTA plots were generated and examined for whole, seasonal, and two subdivided periods. A number of smoothing factors were tested to identify the source locations. However, most of the presented plots are for two periods, i.e. 1964-1970 and 1971-1978.

RTA probability plots for arsenic, cobalt, indium, and zinc presented in Figure 5.35, Figure 5.36, Figure 5.38 and Figure 5.41, respectively, show almost similar patterns. As can be seen from arsenic and cobalt plots, the most probable source region extends beyond Kola Peninsula in the later period and show the highest incremental probability area at Arkhangelsk city in northwest Russia. However, high probable emission area in the zinc plot is bounded mostly within the Kola Peninsula. The earlier period for these elements shows a sparse pattern for the emission sources and probably indicates a less active and well-mixed pollutants in the atmosphere. It is interesting to point out that Kola Peninsula is a known place for copper smelters and in the PCFA result a strong factor was found consisting of copper, indium, zinc, and tin. But an RTA plot

with smoothing factor 81 did not identify the copper emission region as strongly as the zinc and indium emission region, as can be seen from Figure 5.37a and Figure 5.37b. It could be due to the choice of only 3.5% (12 weeks) high subset samples for calculation of high-probability residence time. It is found that the decreasing concentration level for copper is not very steep in the data set, i.e. the 12th concentration level of the high subset sample is followed by many samples with a very close concentration levels. This probably means, the 12 high weeks, used for incremental probability calculation, are not very strongly represented by a high subset for this variable. A winter plot for copper, presented in Figure 5.37c, clearly shows the source region for copper at Kola Peninsula. Incremental probability RTA plots for tin are presented in Figure 5.40. Tin is a known smelting component from Kola Peninsula smelters in the atmosphere and bonded strongly in a PCFA factor with copper, zinc, and indium. But RTA did not locate the emission sources like zinc and indium. Several attempts with different smoothing factors did not give a strong source location for tin. Probably the reason again as of copper, i.e. tin appeared in the region so uniformly and its decreasing concentration level in the database is smoothly changed that probably a 3.5% subset could not find a distinct difference to produce a strong source location for tin. A winter plot for the whole period of tin, is shown in Figure 5.40c, shows the high incremental probable area for source region extends to Kola Peninsula and in the upper mid Finland. RTA antimony plots are presented in Figure 5.39. The third highest color code of incremental probability 0.003% indicated the emission sources for this element are partly from Kola Peninsula and northern Norway for the earlier period as can be seen from Figure 5.39a. The later period in Figure 5.39b shows areas in mid Finland and some coastal area with a incremental probability of about 0.002%.

The RTA plots for manganese and vanadium are presented in Figure 5.42 and Figure 5.43. Among all the RTA plots, these two plots show very distinct source locations for these two elements. The probable source region includes most of the northern European countries including Moscow, Russia, as can be seen from Figure 5.42a and Figure 5.43a. The later period RTA plots, 1971-1978, added the Kola region with

the former source region for manganese and vanadium. This probably indicates that a strong smelting activity started after 1971 at Kola Peninsula with an established stable northern route to transport Norilsk ores to Kola Peninsula. Vanadium emissions from industrial activities at Kola Peninsula were reported as V_2O_5 in 1994: 91 tons for Murmansk, 60 tons for Monchegorsk, 44 tons for Kirovsk, 21 tons for Zapoljarnij, 20 tons for Kovdor, 19 tons for Kandalaksha, 13 tons for Nikel and 0.4 tons each for Apatity and Ole negorsk [Reimann *et al.*, 1998].

Crustal elements aluminum, silicon, calcium, and titanium RTA plots, presented in Figures 5.44 - 5.47, show a reasonable source area from south Finland, Sweden, Norway, north western Russia, etc. The RTA plots for the later period show a higher incremental probability region in the Kola Peninsula for aluminum and calcium. The silicon plot for 1964-1971 shows a higher incremental probability region adjacent to Nikel/Zapoljarnij area at Kola Peninsula. This could be the location for large silicon emissions during 1967-1969 in the Kevo atmosphere, as it was seen in silicon time series in Figure 5.6.

Sea source components are very well identified for their source locations by RTA incremental probability plots presented in Figures 5.48 - 5.51. Sodium and chlorine originated from all over the vast sea regions around Kevo. However, for bromine and iodine the source region is localized more to the Barents Sea.

From all the above RTA results and discussions, it is found that, a single smoothing factor is not always equally effective to identify a source region for all the elements. For example, a smoothing factor of 441 worked well for seasonal RTA plots but not for the whole period. Smoothing factors 441, and 81 worked well for two subdivided periods, but not for all cases. It is also seemed that RTA incremental probability plots are sensitive on selection of high-value subset samples, i.e. if the subset concentration values are not very high from the adjacent samples in the dataset then it does not strongly produce a source location.

One should be cautious about attributing too much accuracy to the patterns in the RTA plot. For some elements it worked very well, especially when the cutoff value is

very distinct for a subset to consider. For many elements it was not easy to select an appropriate subset from the dataset, since the concentration level varied very smoothly. The use of only 14 trajectories for a weeklong could also cause a less resolution to identify source locations for some elements.

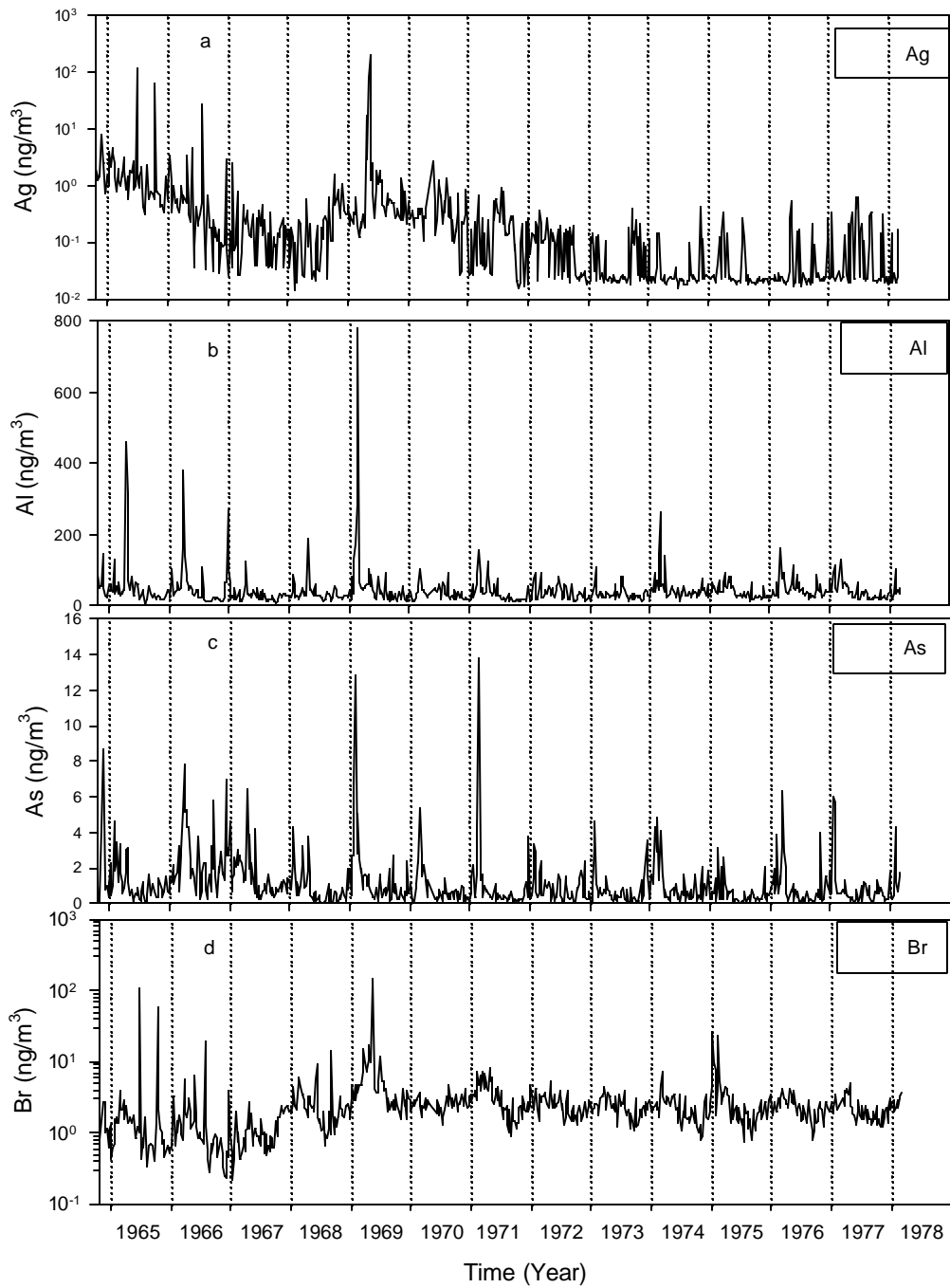


Figure 5.3: Time series plots of silver, aluminum, arsenic, and bromine

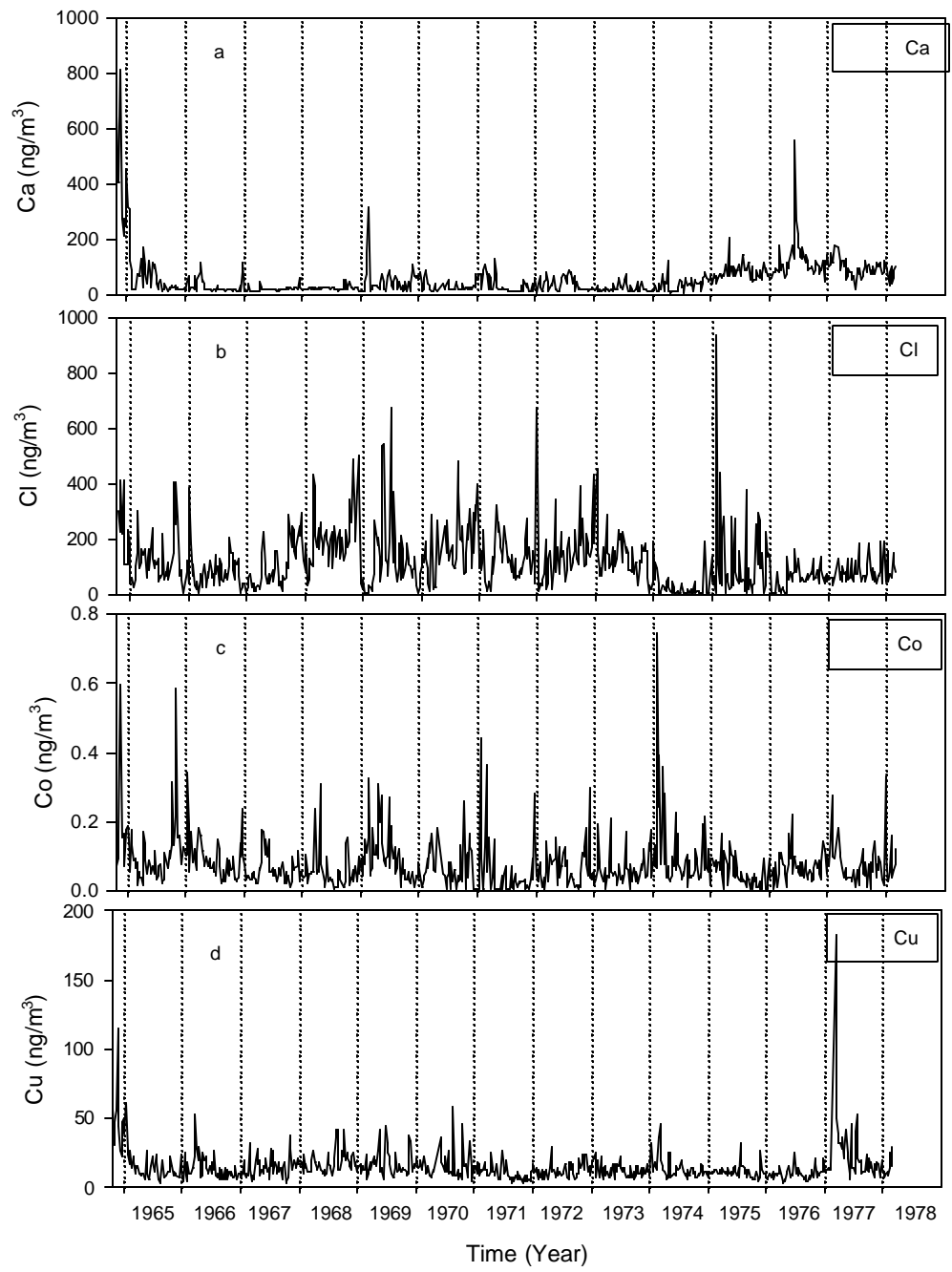


Figure 5.4: Time series plots of calcium, chlorine, cobalt, and copper

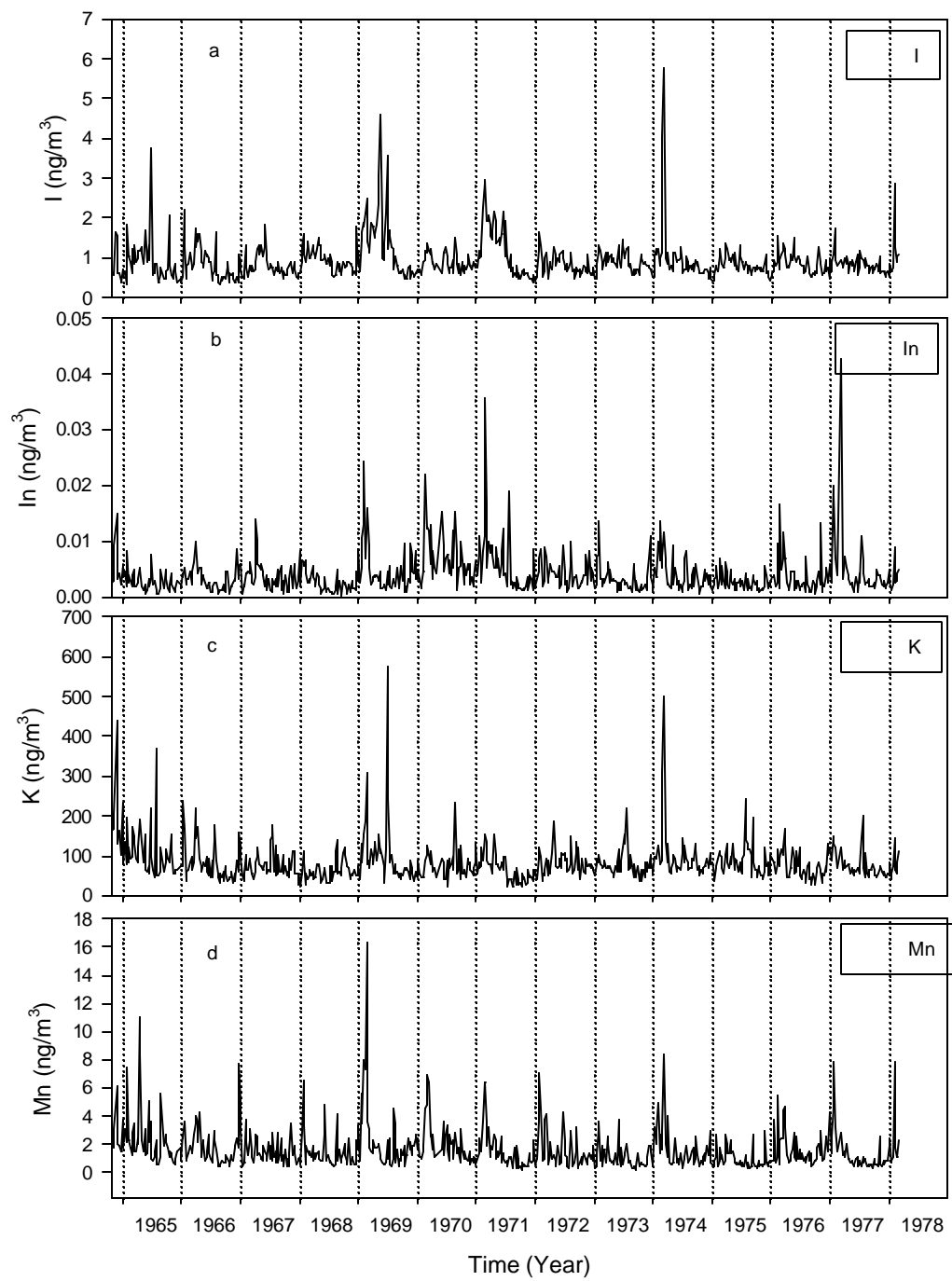


Figure 5.5: Time series plots of iodine, indium, potassium, and manganese

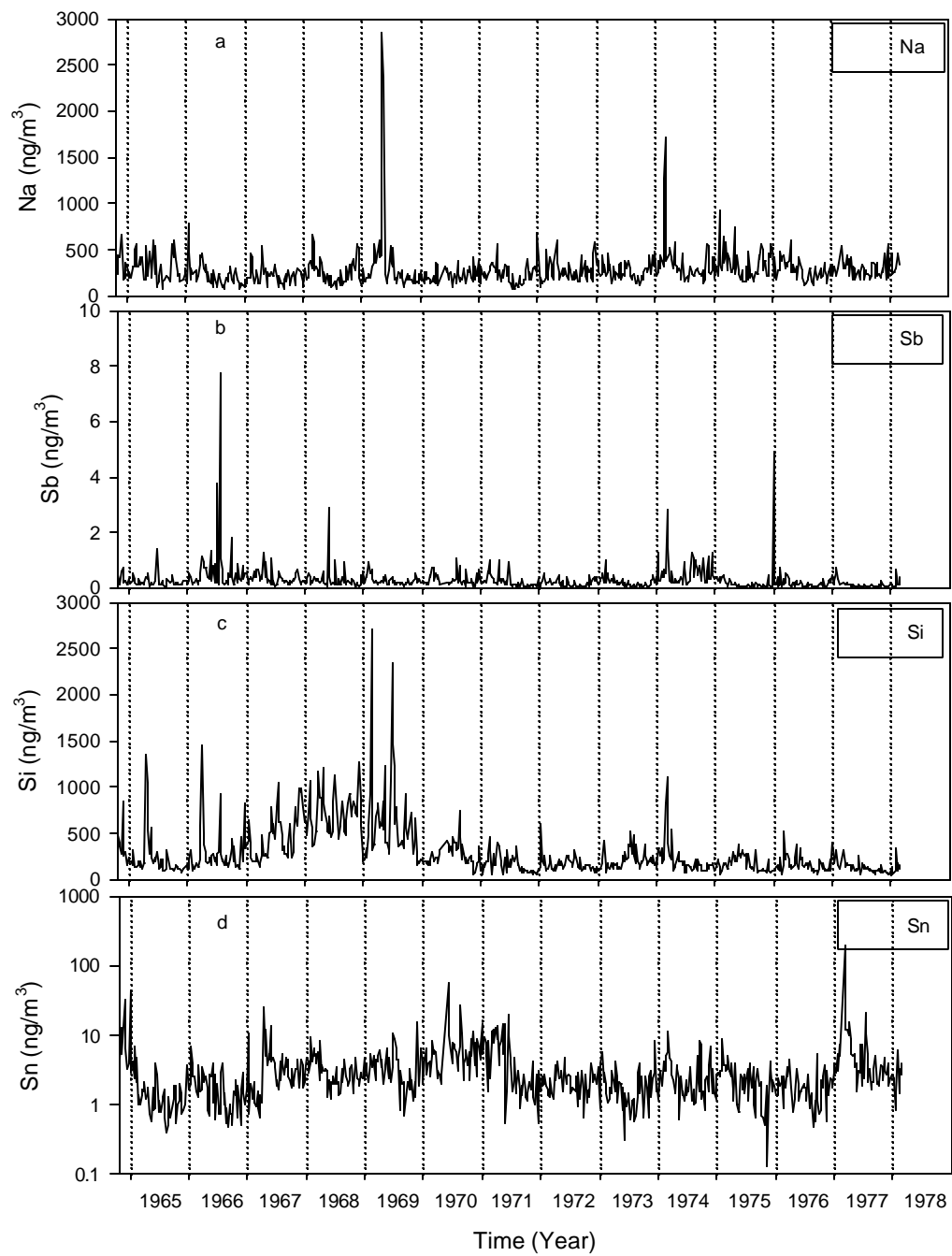


Figure 5.6: Time series plots of sodium, antimony, silicon, and tin

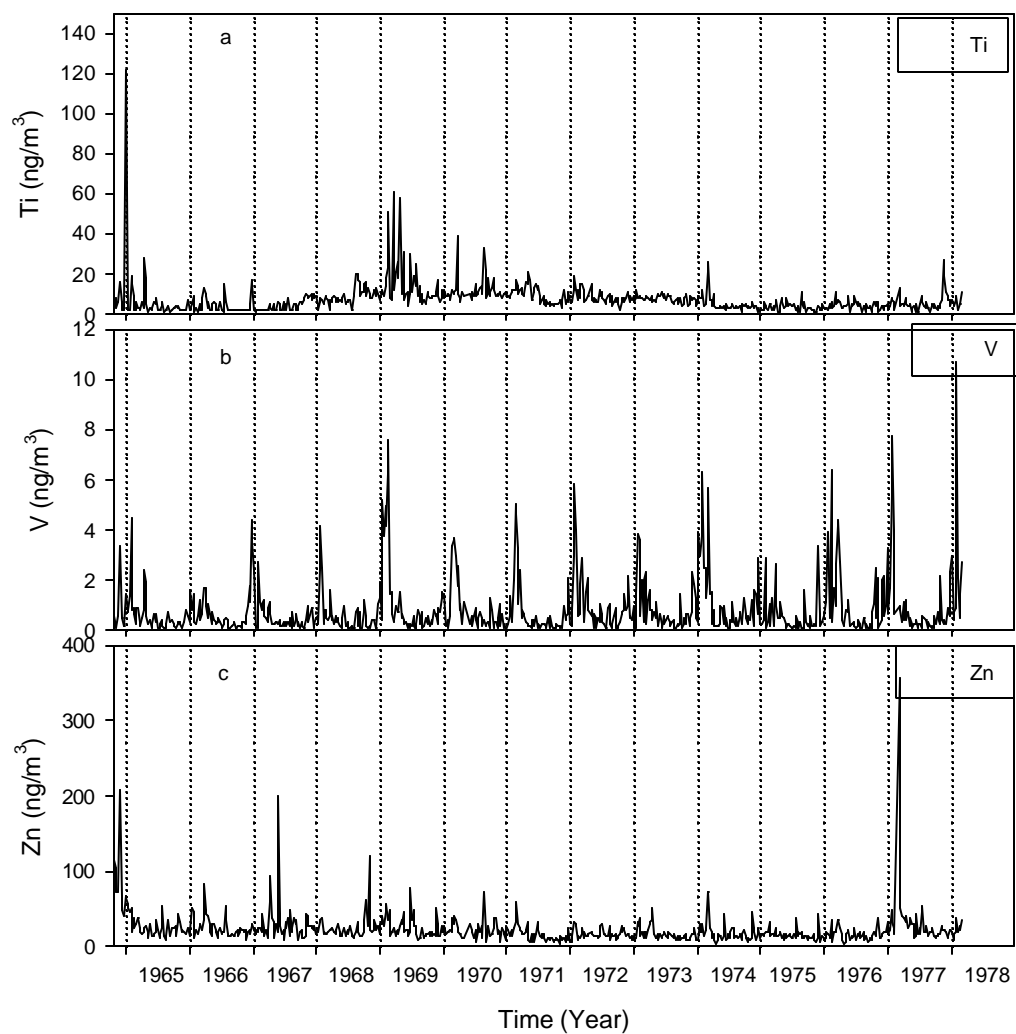


Figure 5.7: Time series plots for titanium, vanadium, and zinc

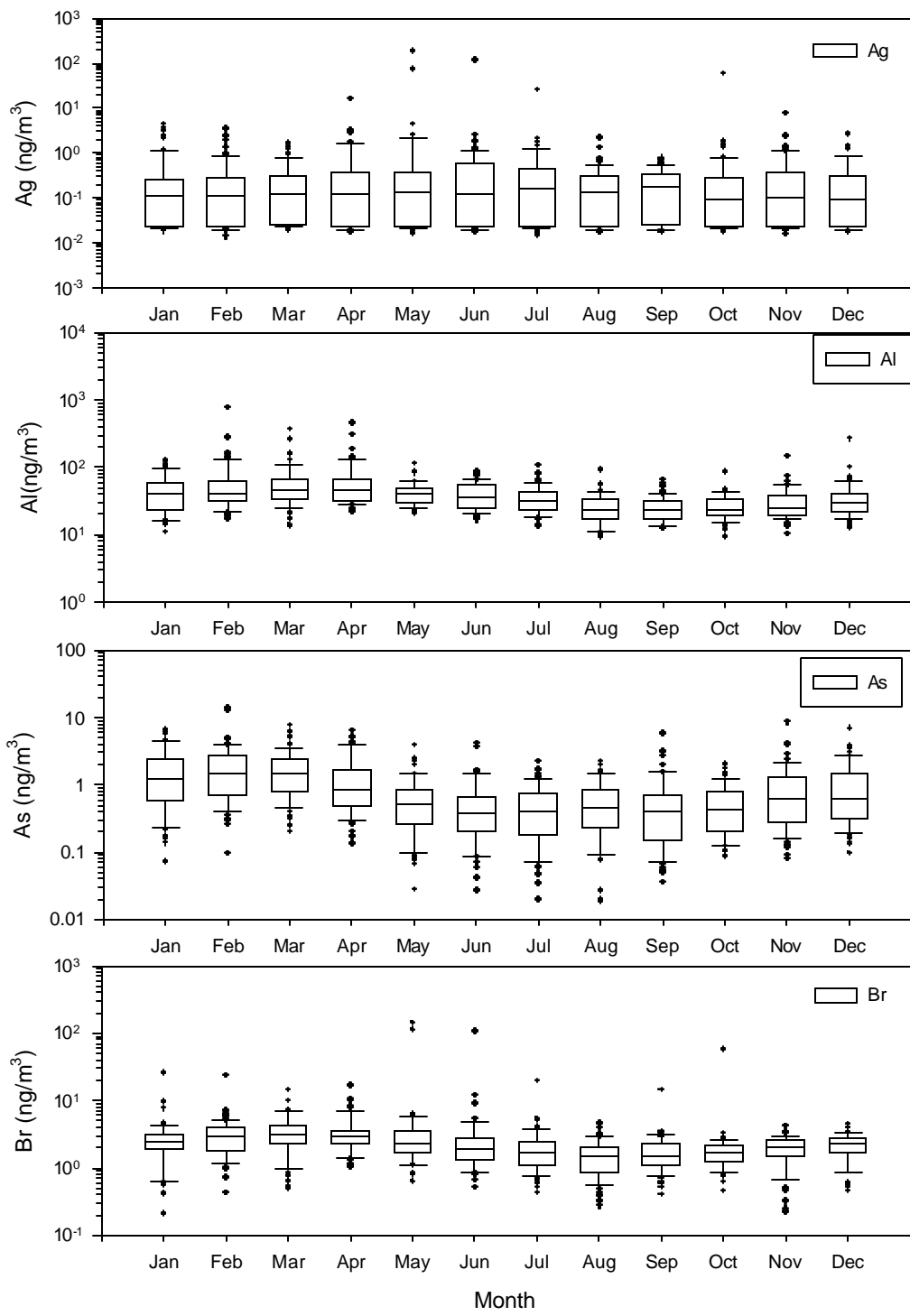


Figure 5.8: Box plots of monthly data for silver, aluminum, arsenic, and bromine

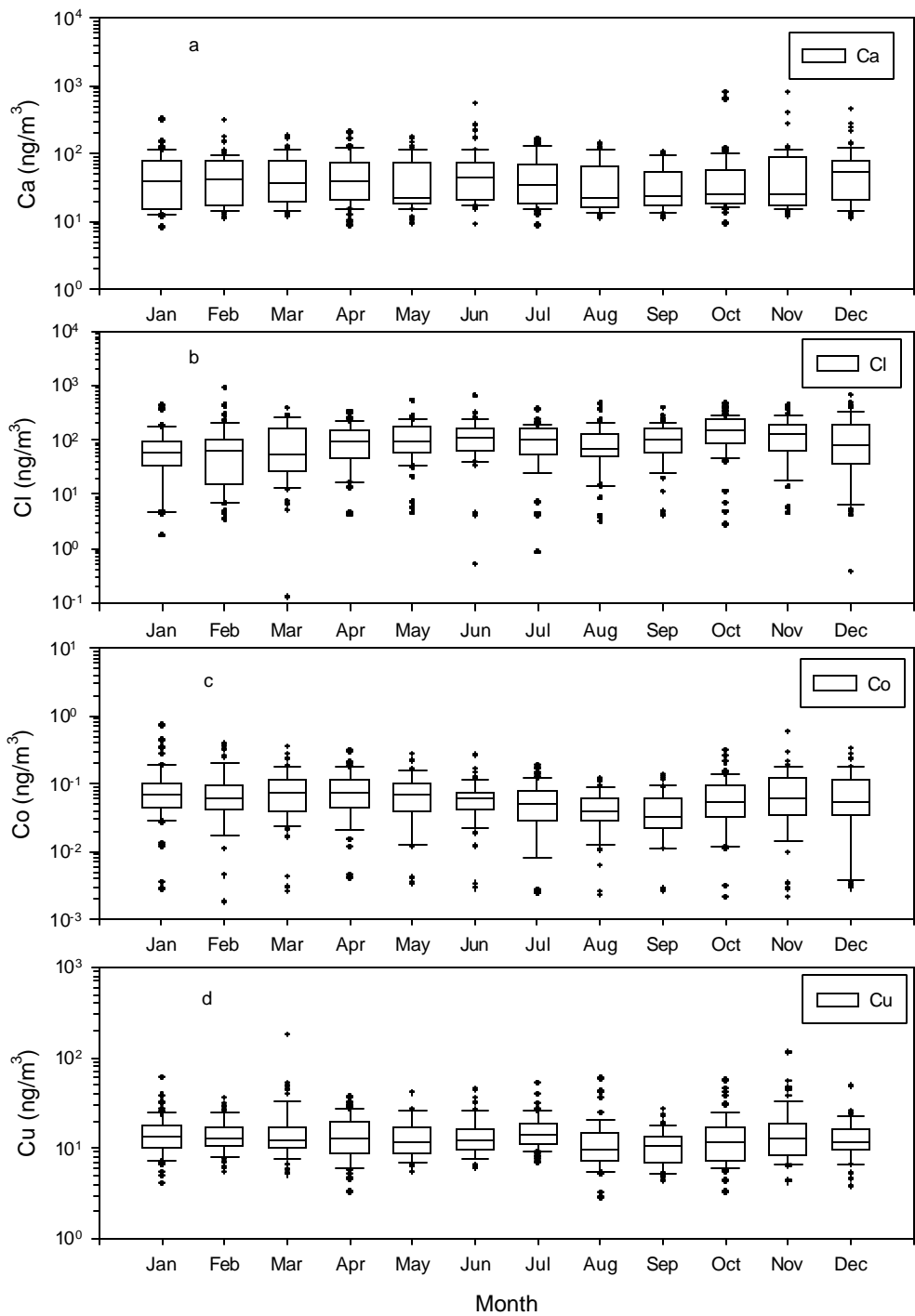


Figure 5.9: Box plots of monthly data for calcium, chlorine, cobalt, and copper

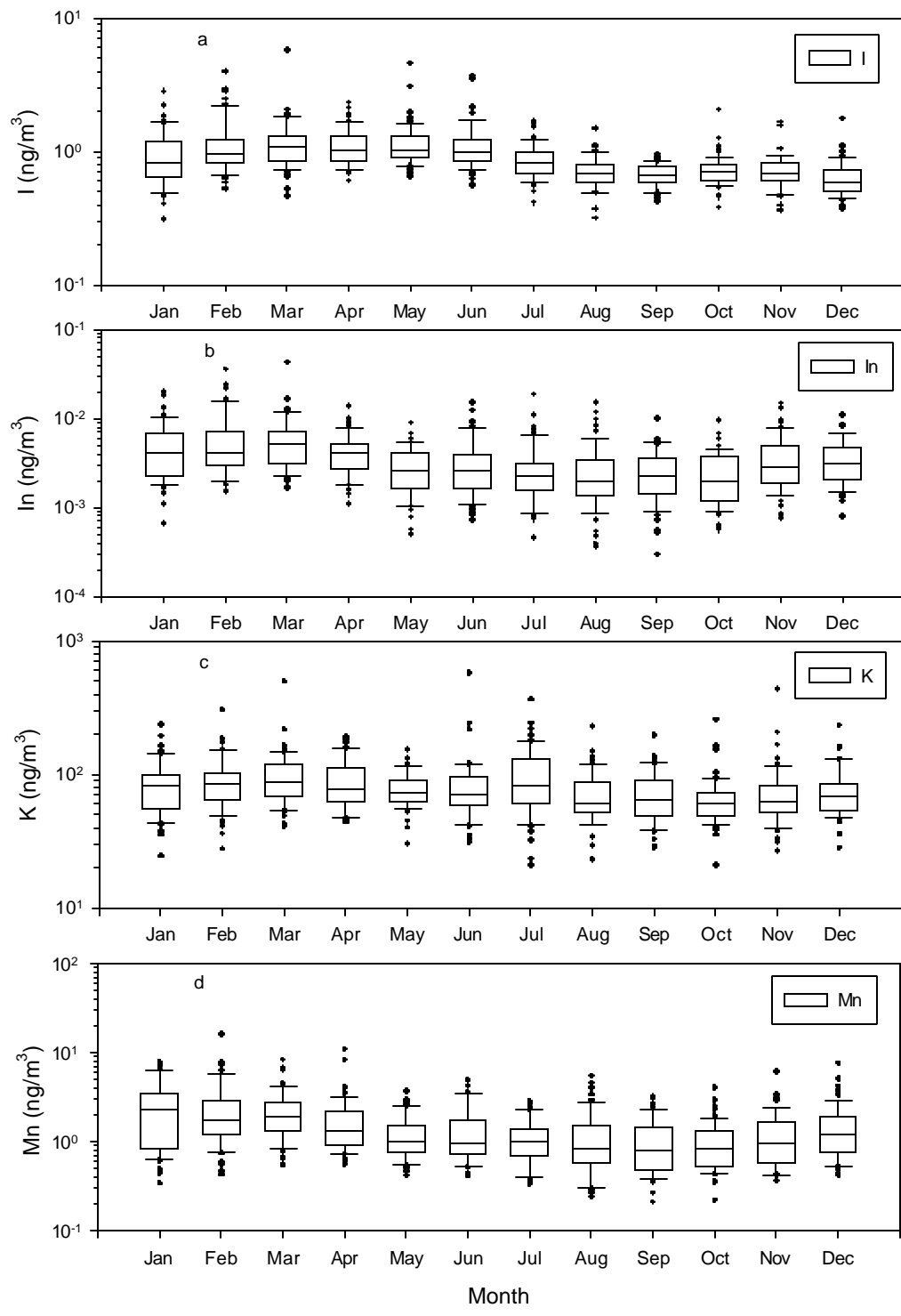


Figure 5.10: Box plots of monthly data for iodine, indium, potassium, and manganese

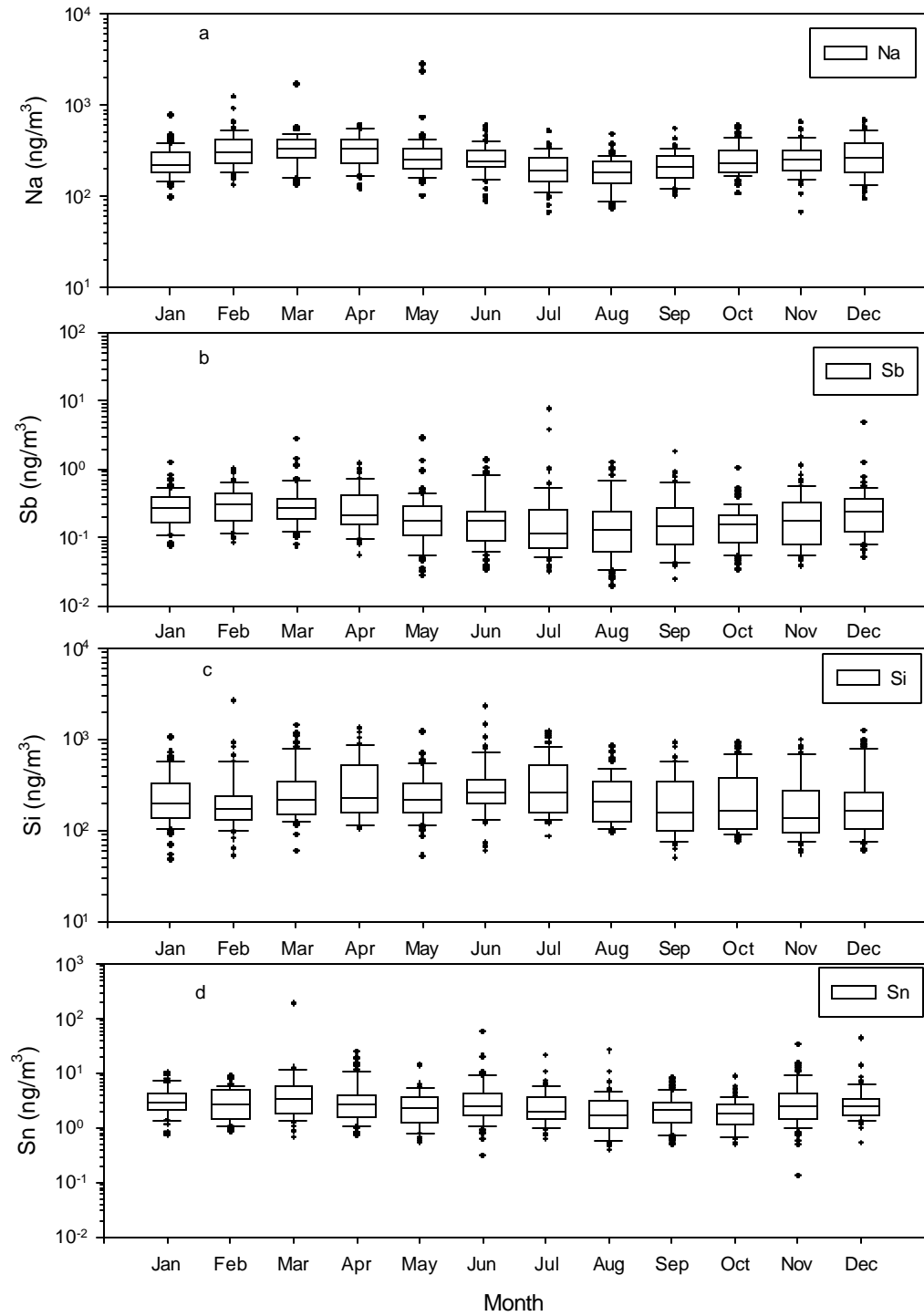


Figure 5.11: Box plots of monthly data for sodium, antimony, silicon, and tin

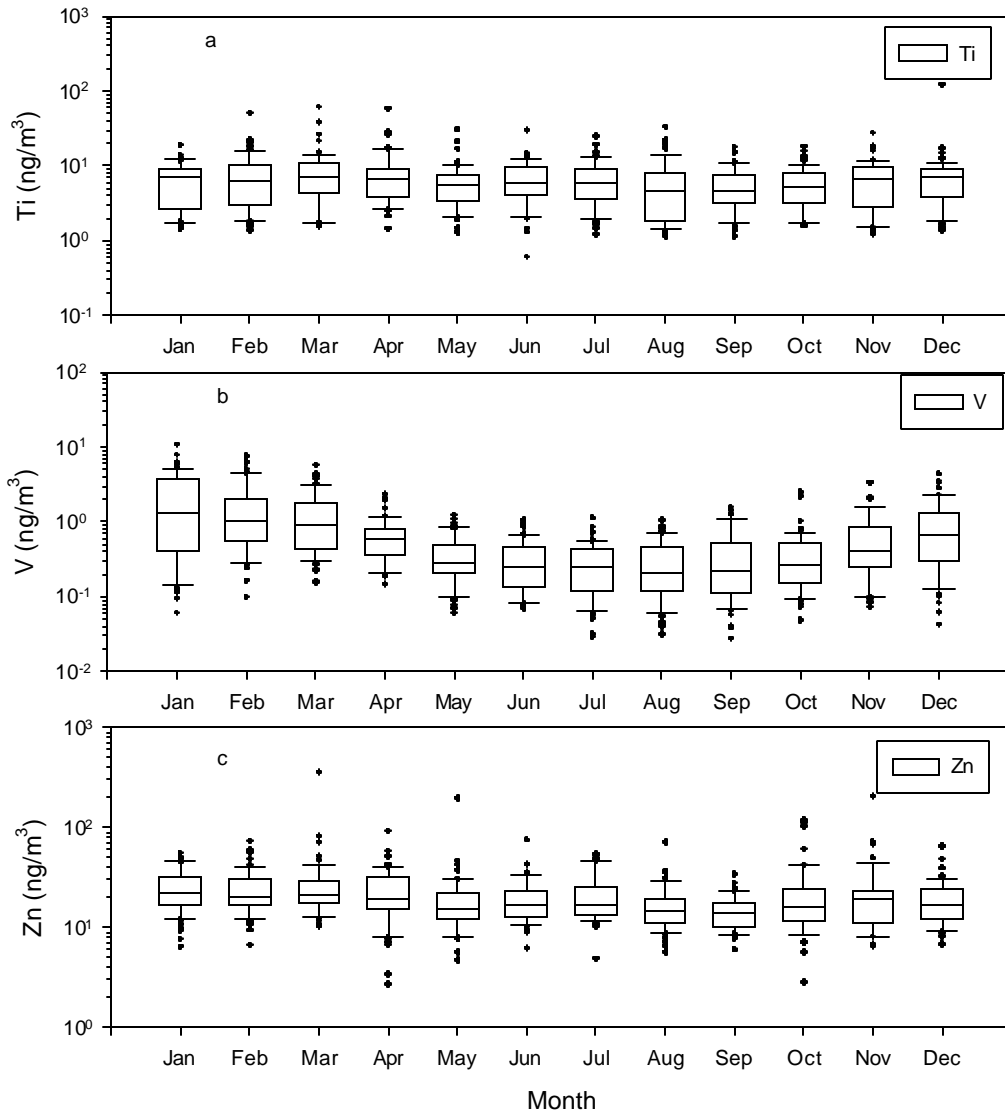


Figure 5.12: Box plots of monthly data for titanium, vanadium, and zinc

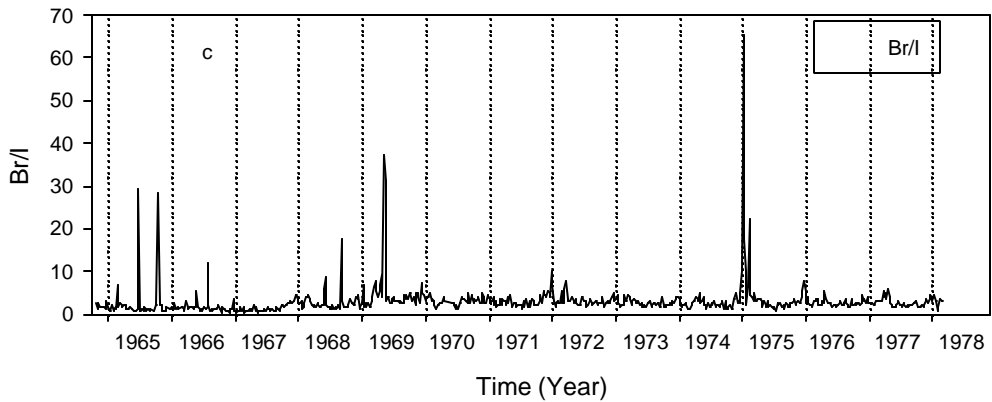
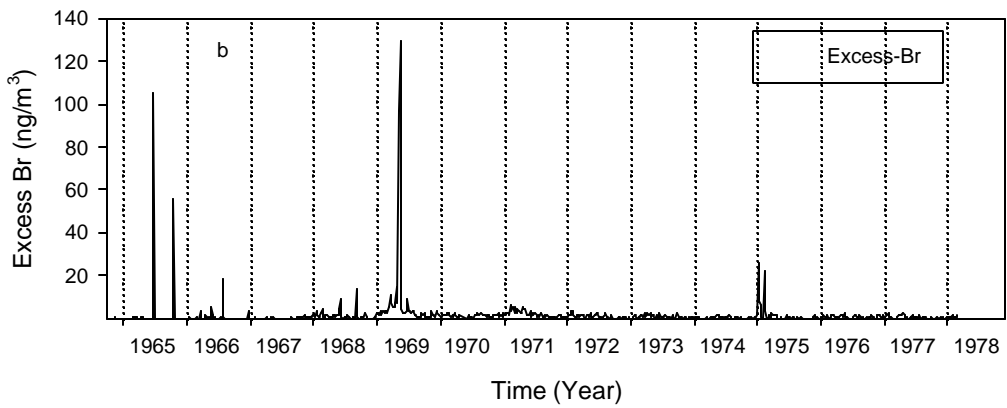
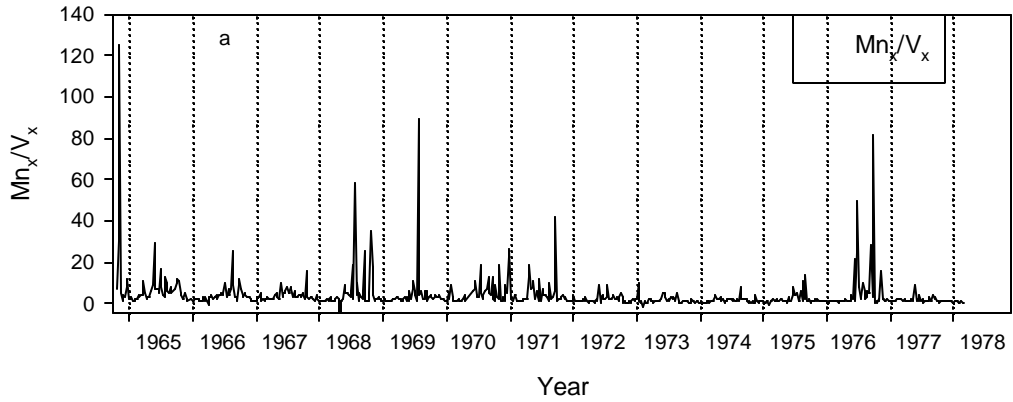


Figure 5.13: Time series plots of non crustal Mn/non crustal V, excess bromine and Br/I

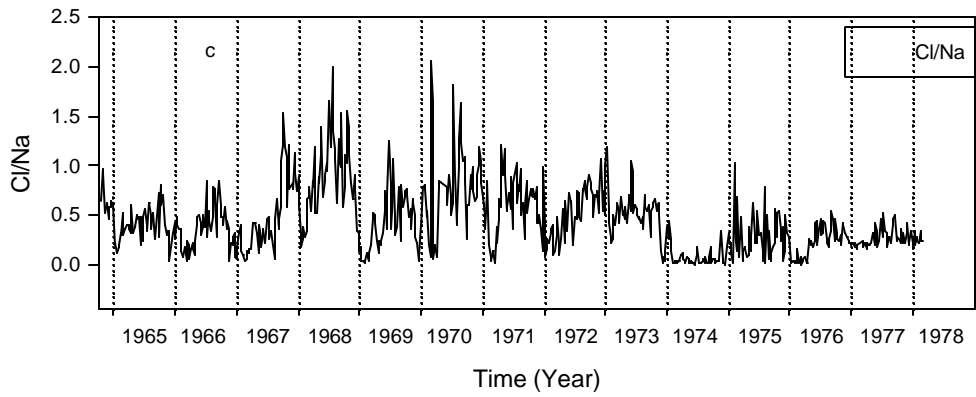
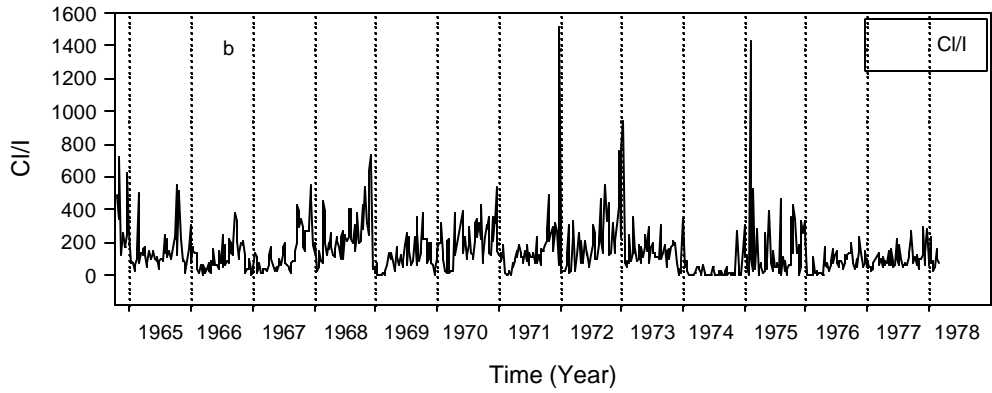
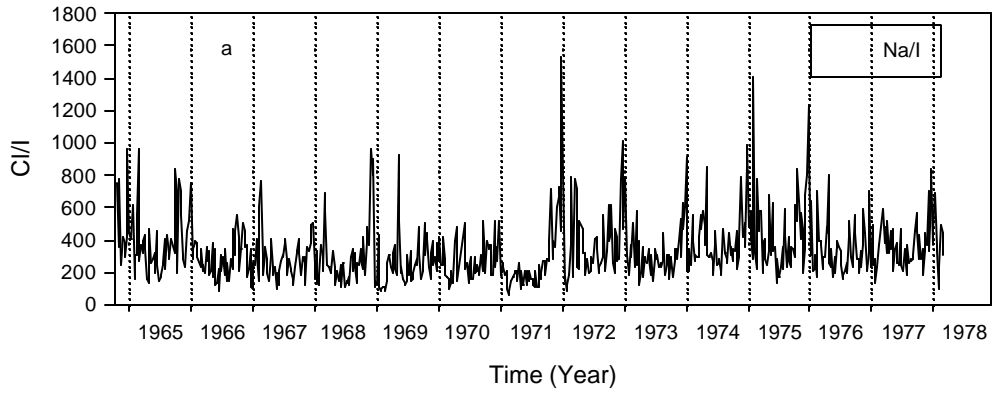


Figure 5.14: Time series plots of Na/I, Cl/I, and Cl/Na

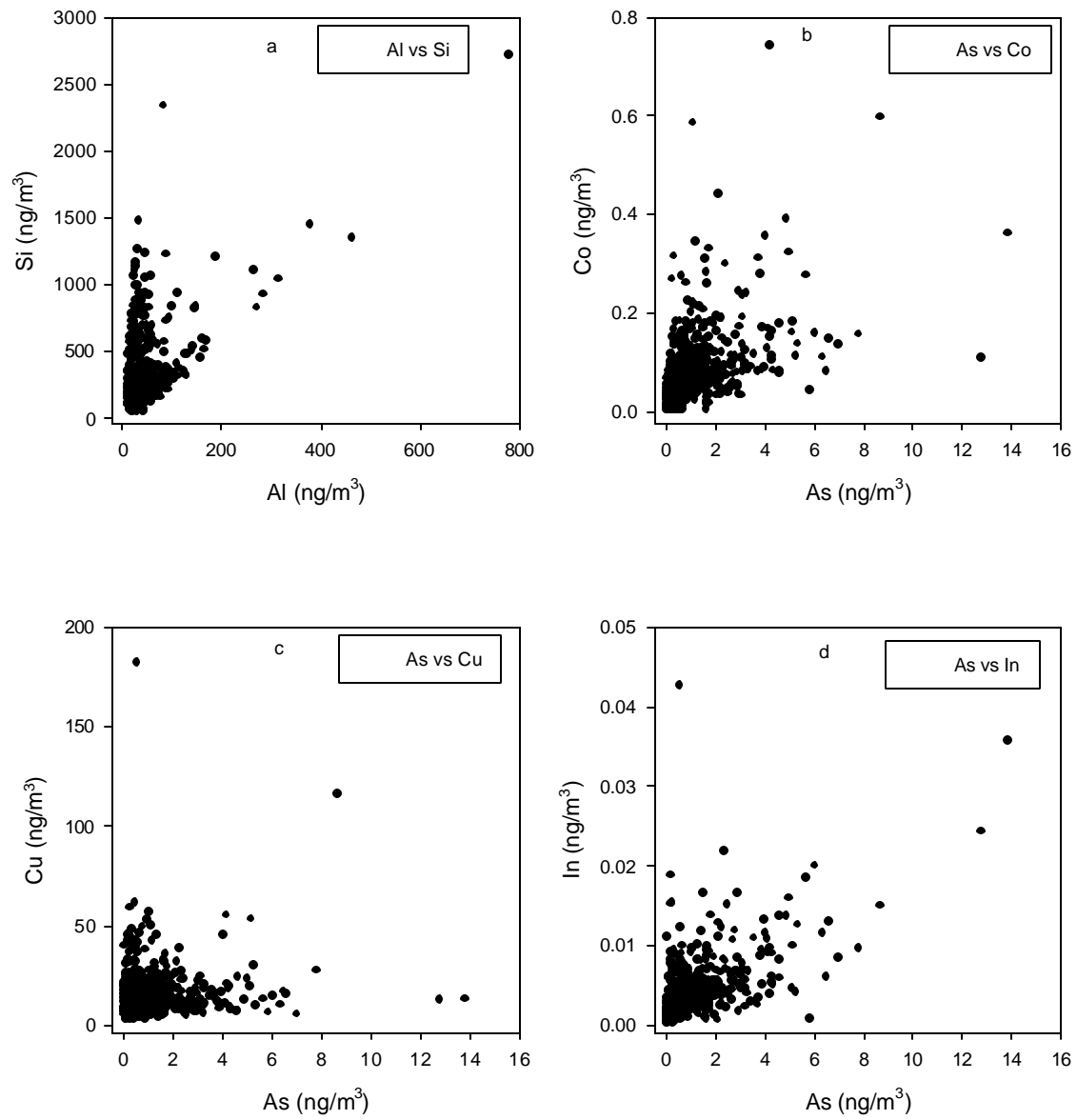


Figure 5.15: Scatter plots of Al vs. Si, As vs. Co, As vs. Cu, and As vs. In

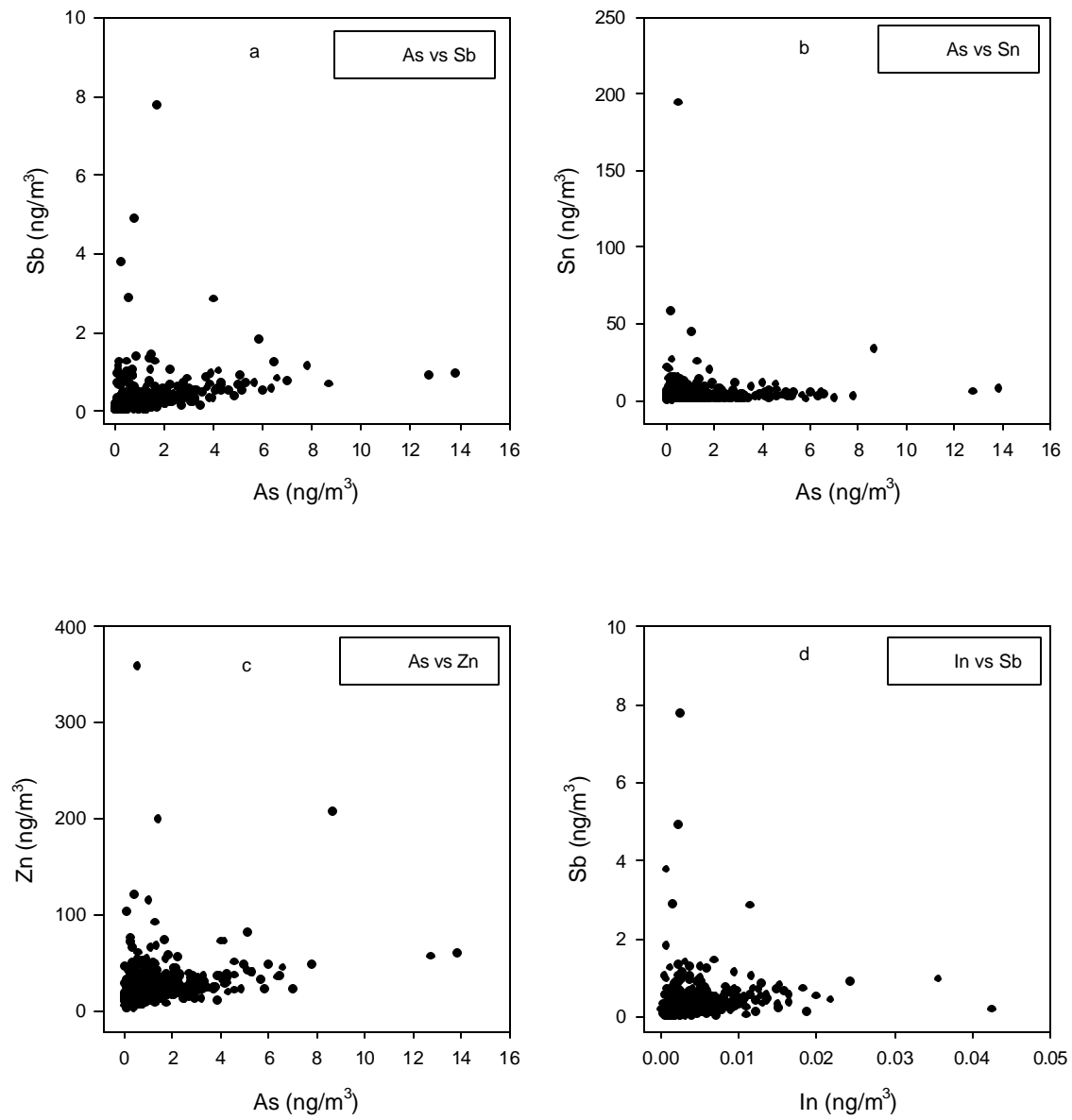


Figure 5.16: Scatter plots of As vs. Sb, As vs. Sn, As vs. Zn, and In vs. Sb

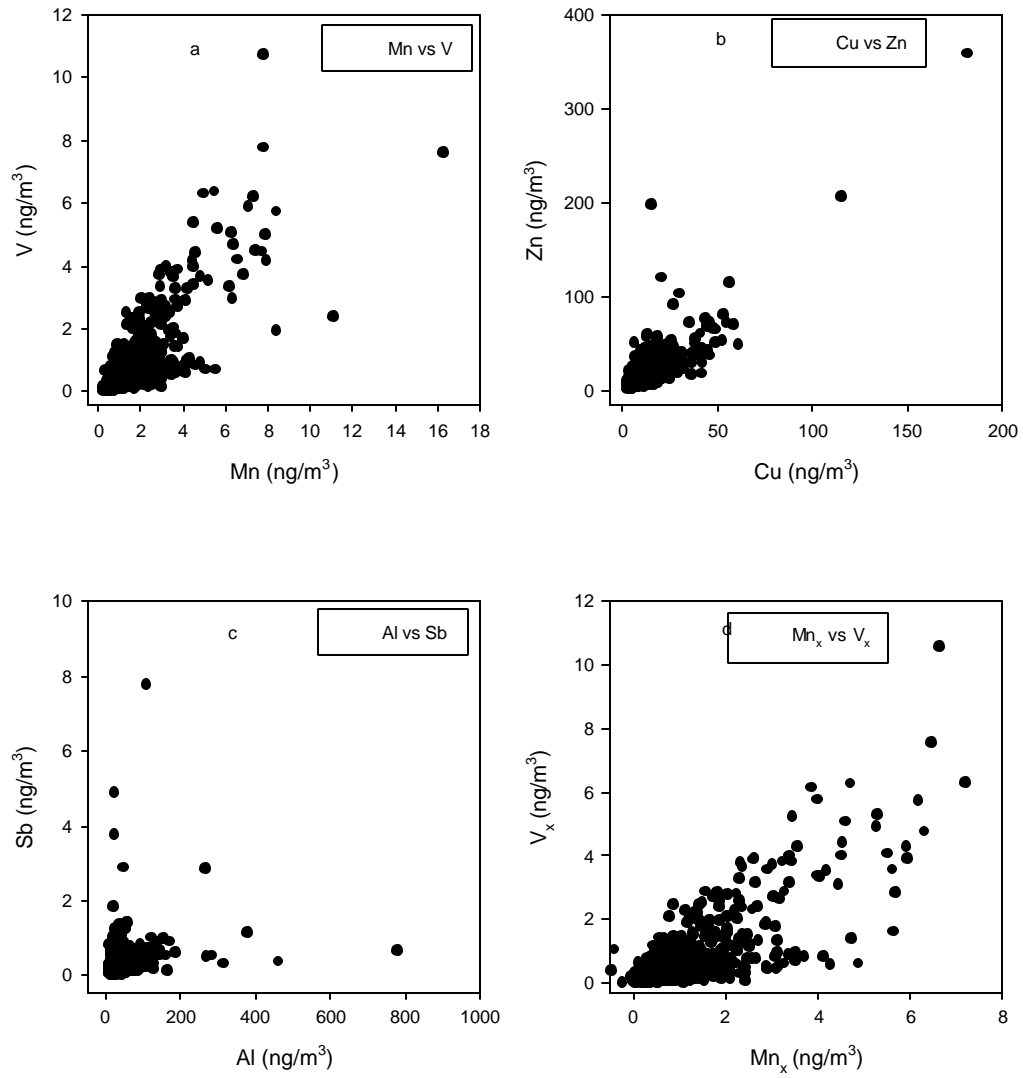


Figure 5.17: Scatter plots of Mn vs. V, Cu vs. Zn, Al vs. Sb, and Mn_x vs. V_x

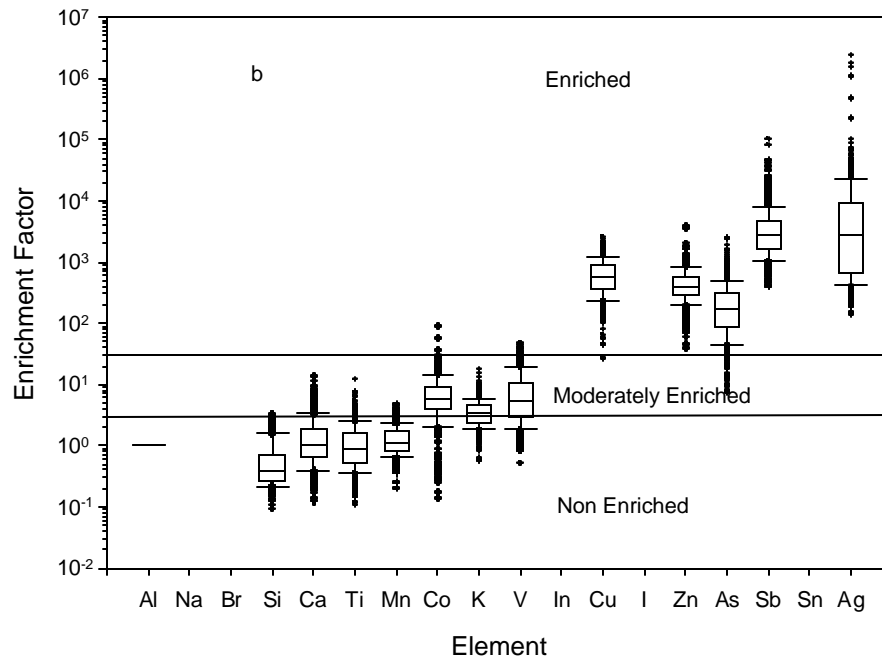
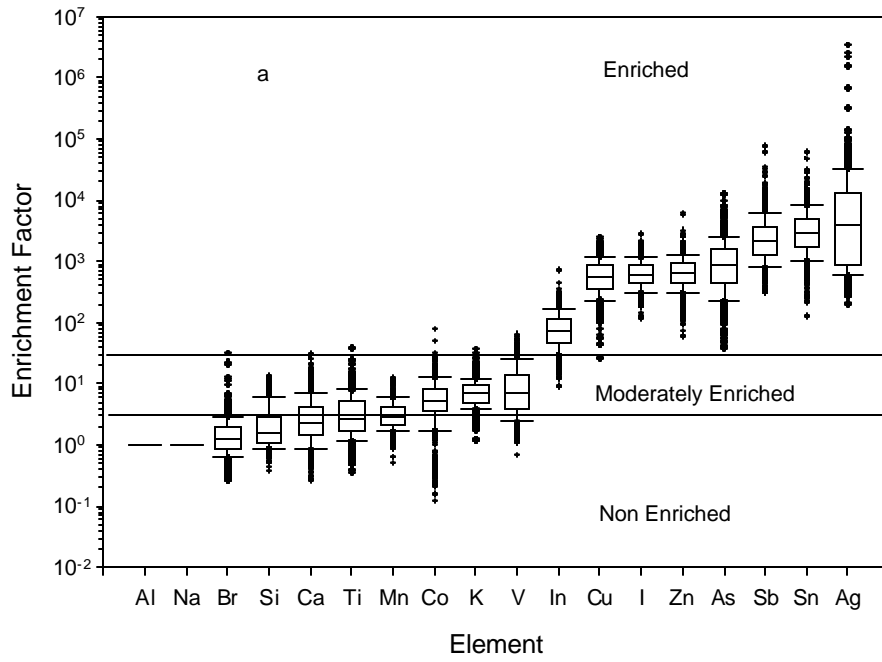


Figure 5.18: Enrichment Factor using a) global and b) local crustal average values

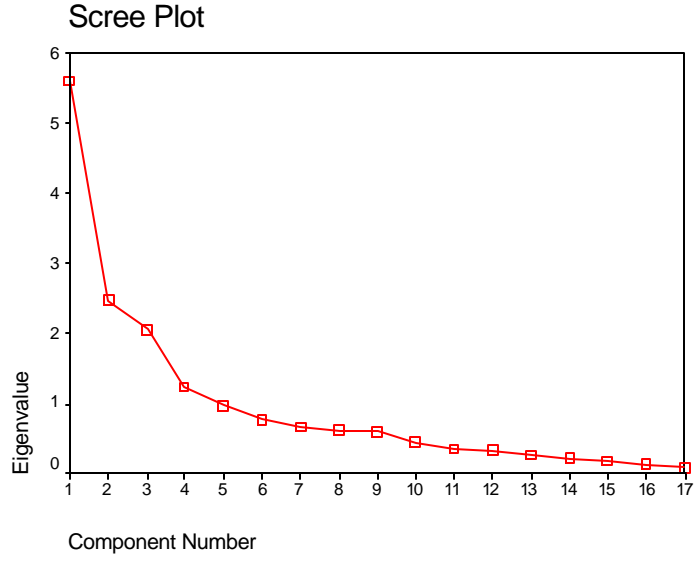


Figure 5.19: Scree plot for the full dataset

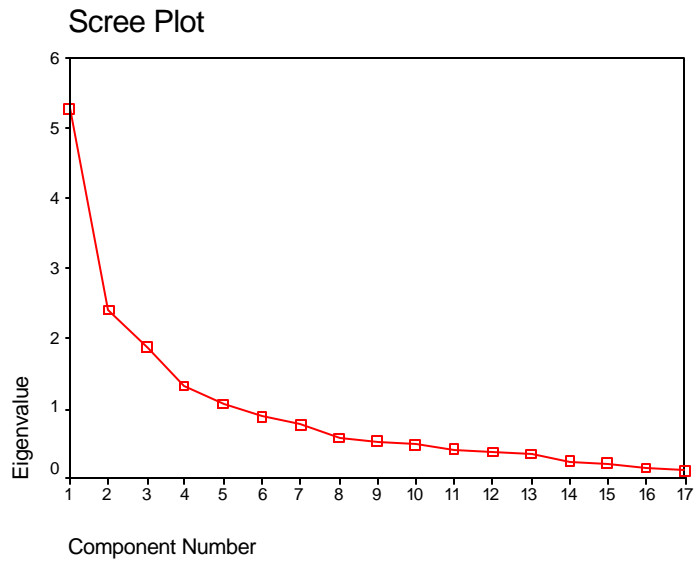


Figure 5.20: Scree plot for the summer dataset

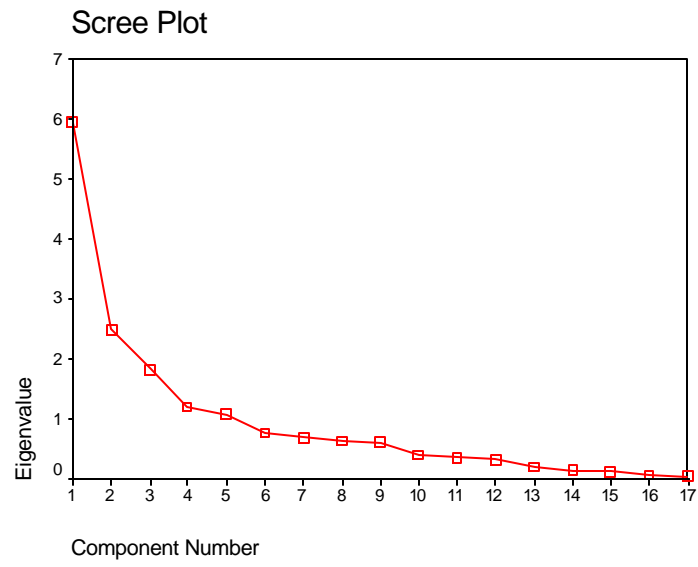


Figure 5.21: Scree plot for the winter dataset

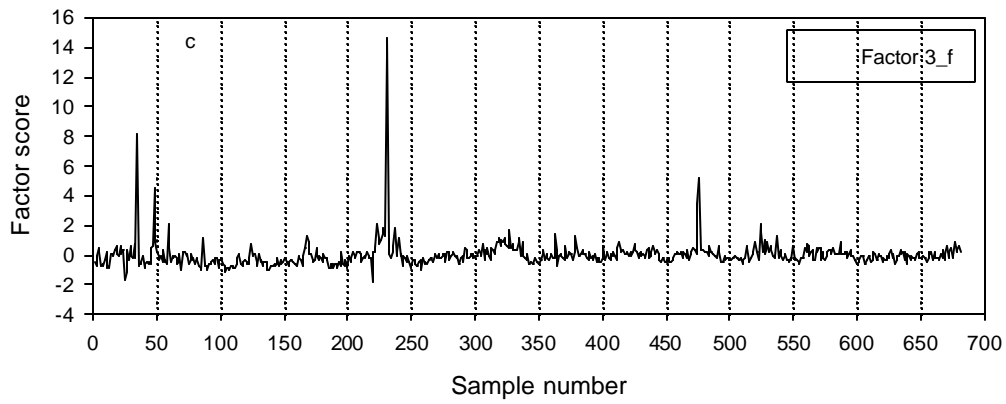
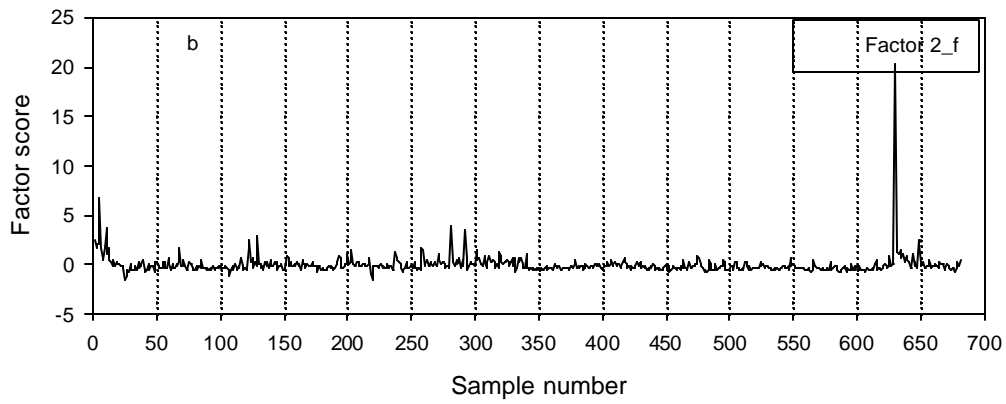
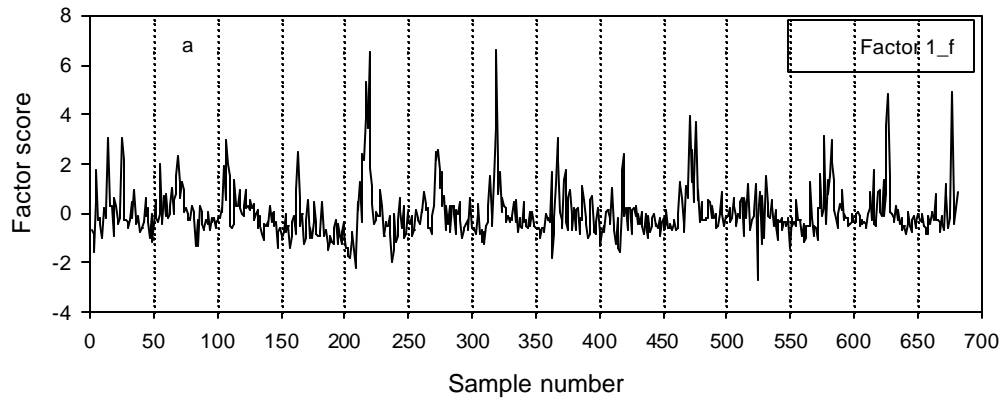


Figure 5.22: Factor score plots for factor 1, factor 2, and factor 3 of full dataset

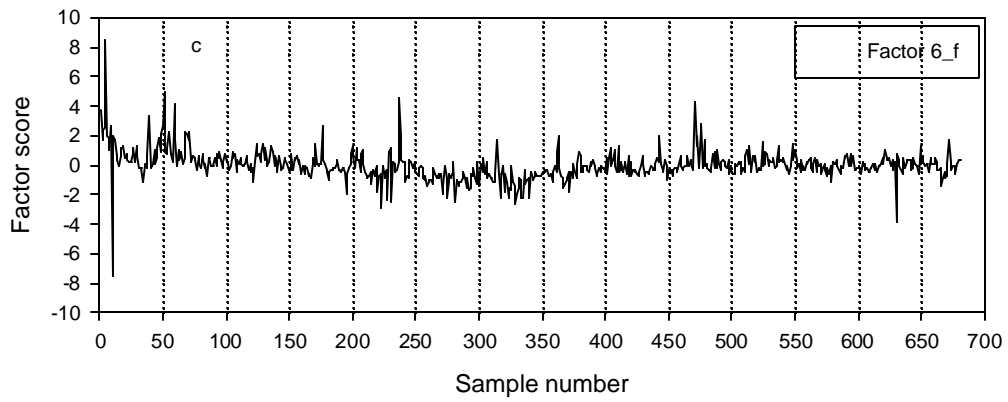
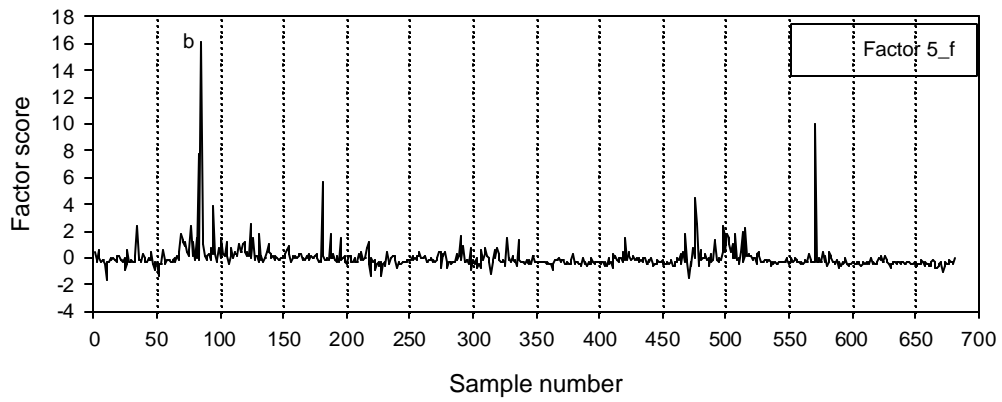
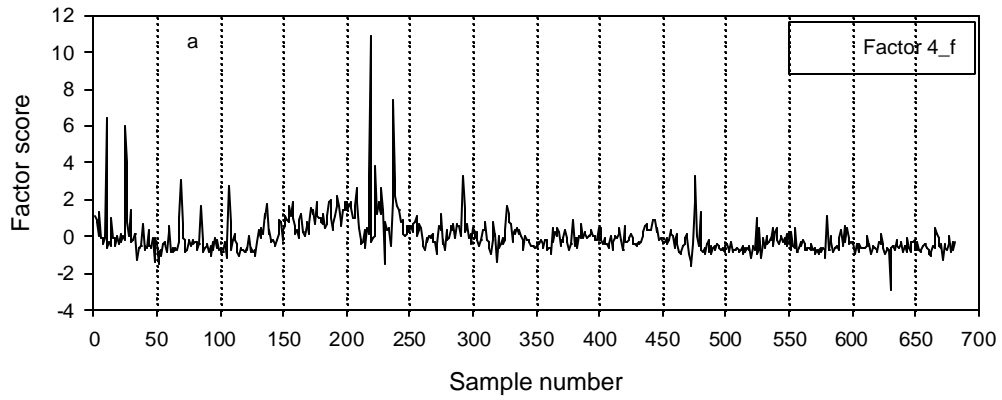


Figure 5.23: Factor score plots for factor 4, factor 5, and factor 6 of full dataset

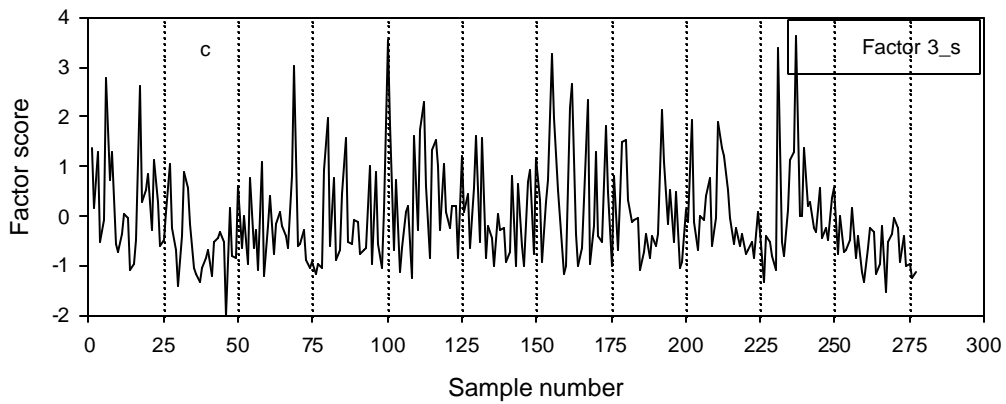
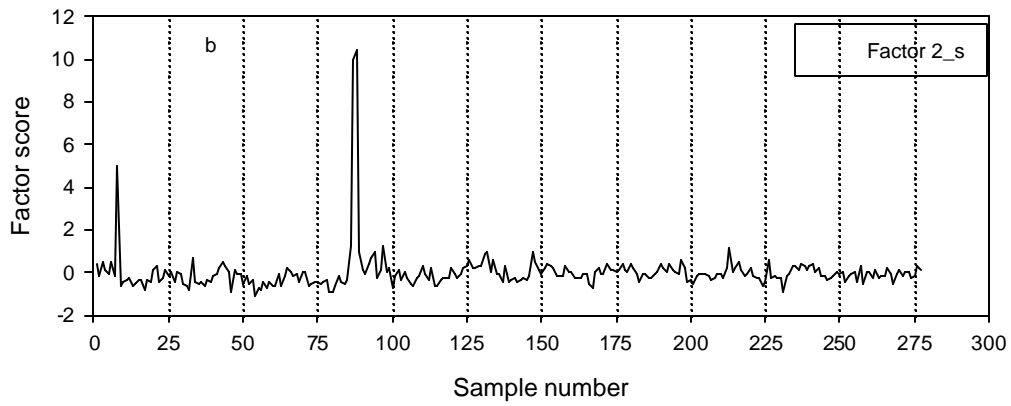
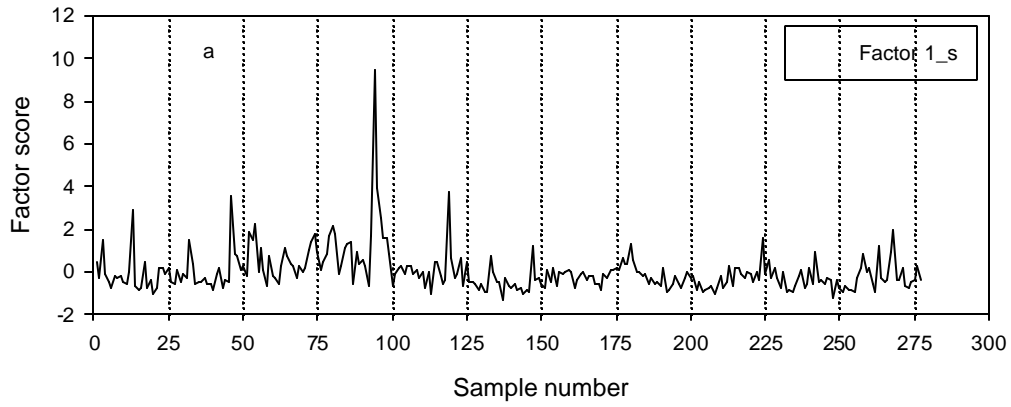


Figure 5.24: Factor score plots for factor 1, factor 2, and factor 3 of summer dataset

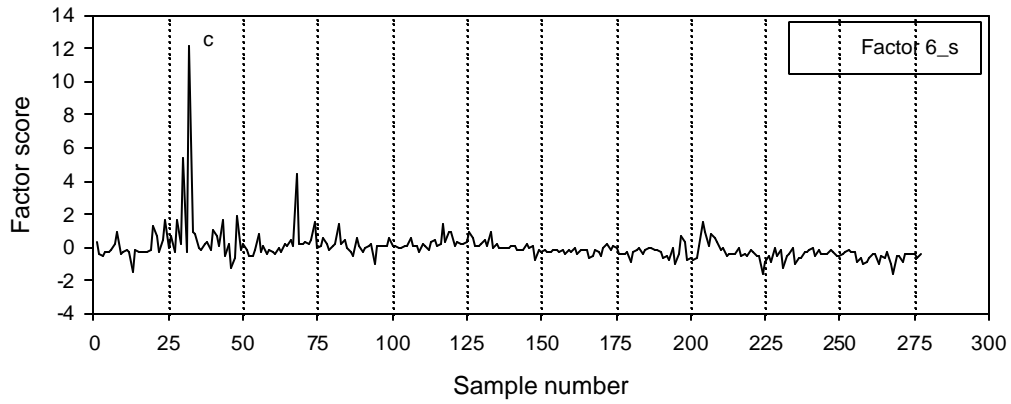
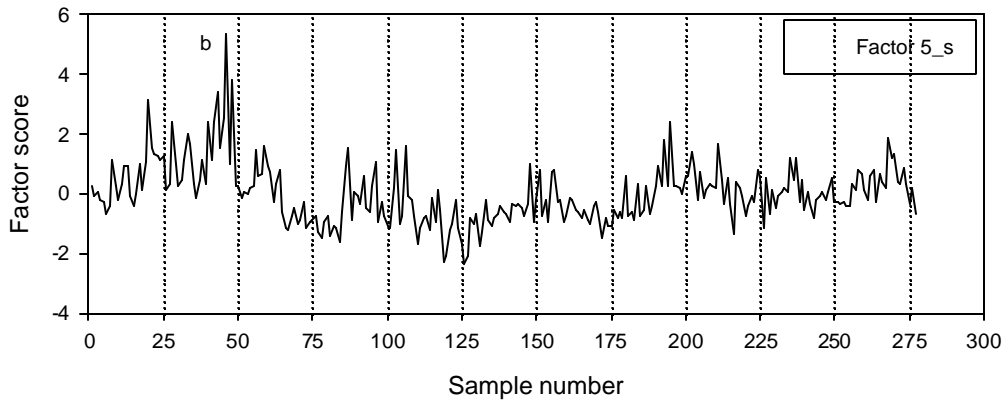
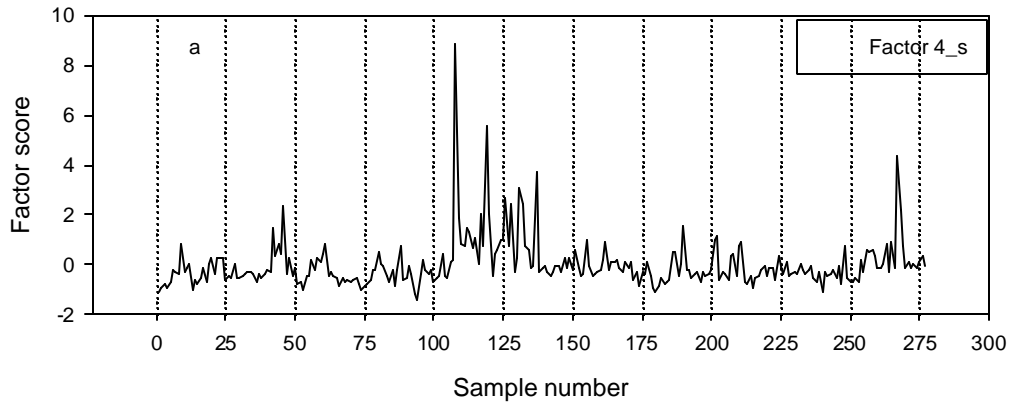


Figure 5.25: Factor score plots for factor 4, factor 5, and factor 6 of summer dataset

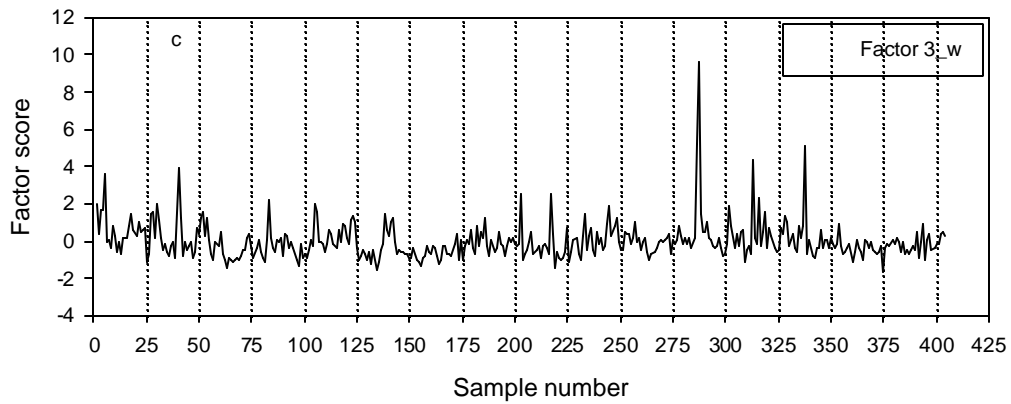
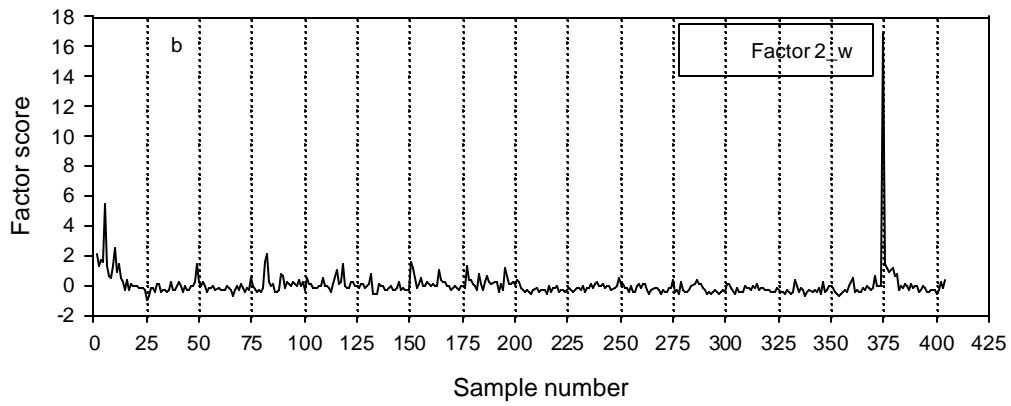
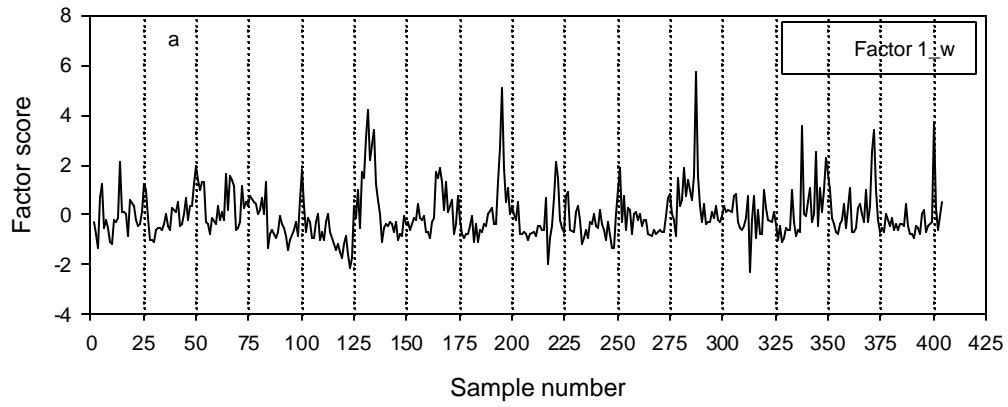


Figure 5.26: Factor score plots for factor 1, factor 2, and factor 3 of winter dataset

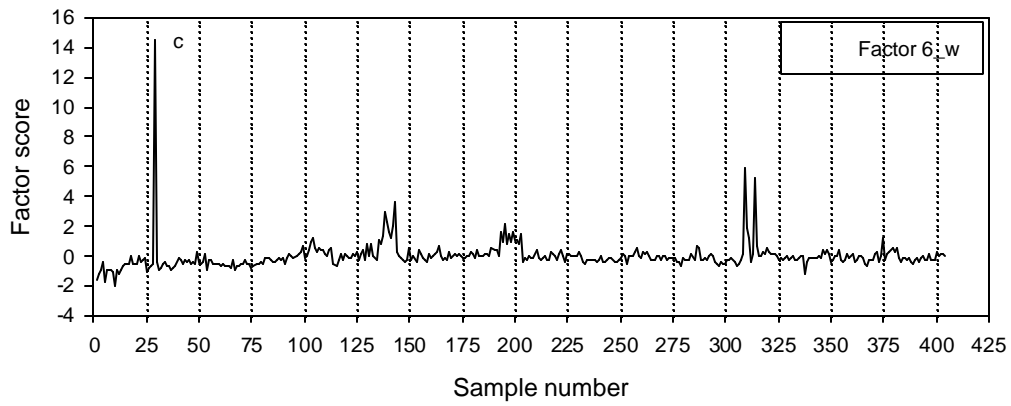
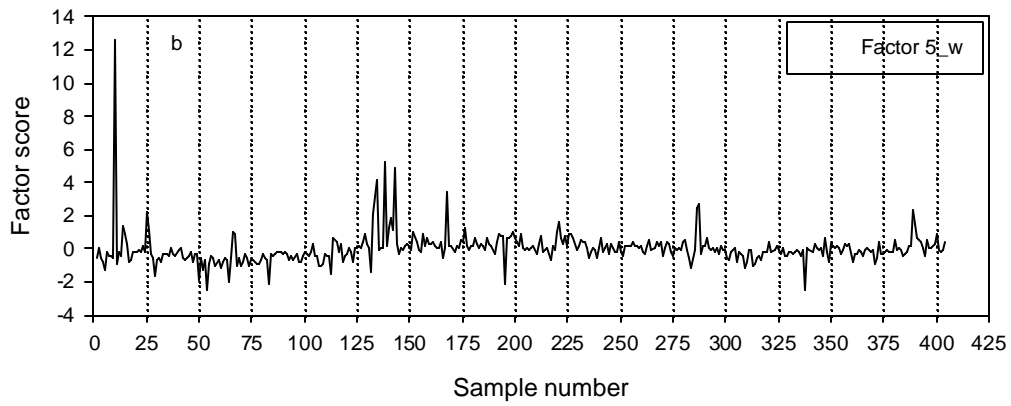
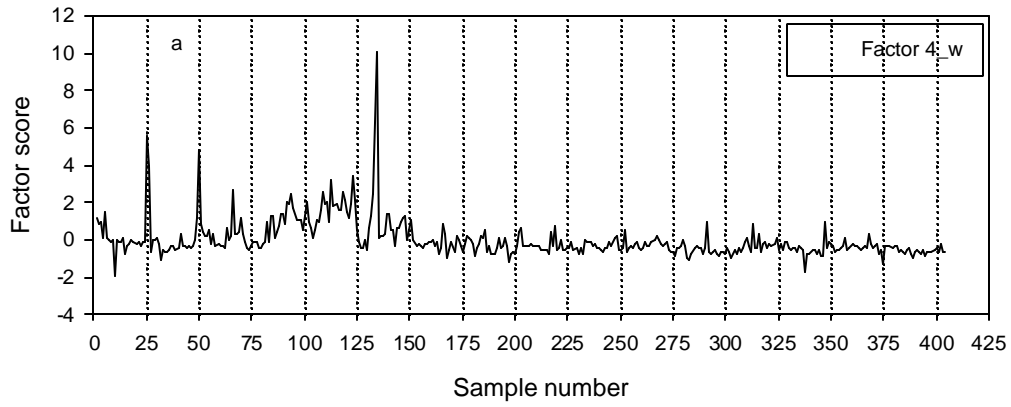


Figure 5.27: Factor score plots for factor 4, factor 5, and factor 6 of winter dataset

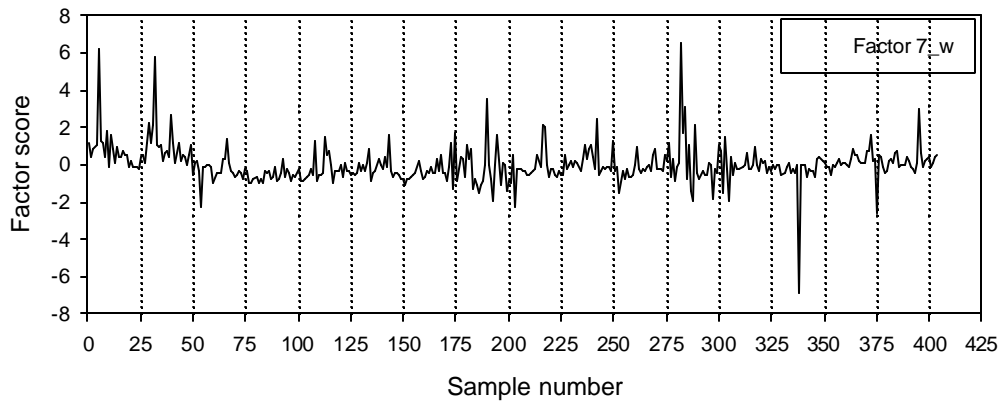


Figure 5.28: Factor score plots for factor 7 of winter dataset

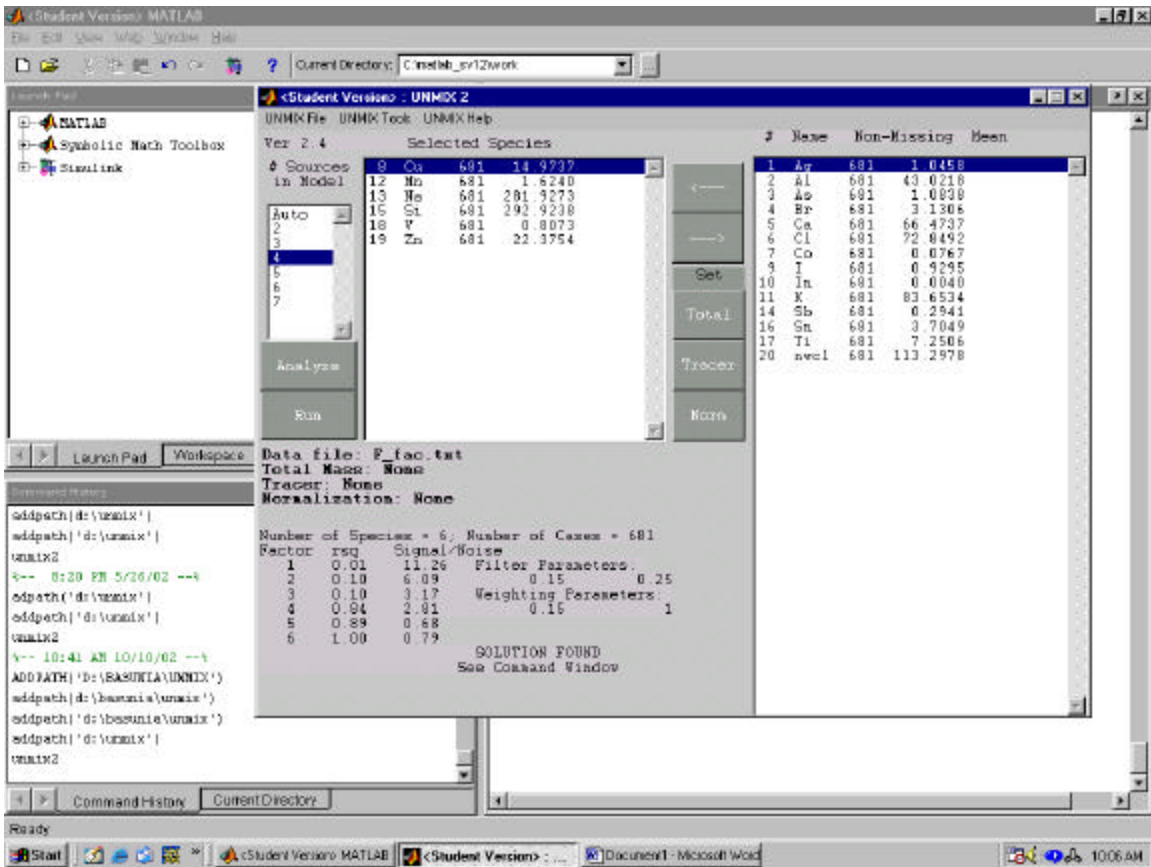
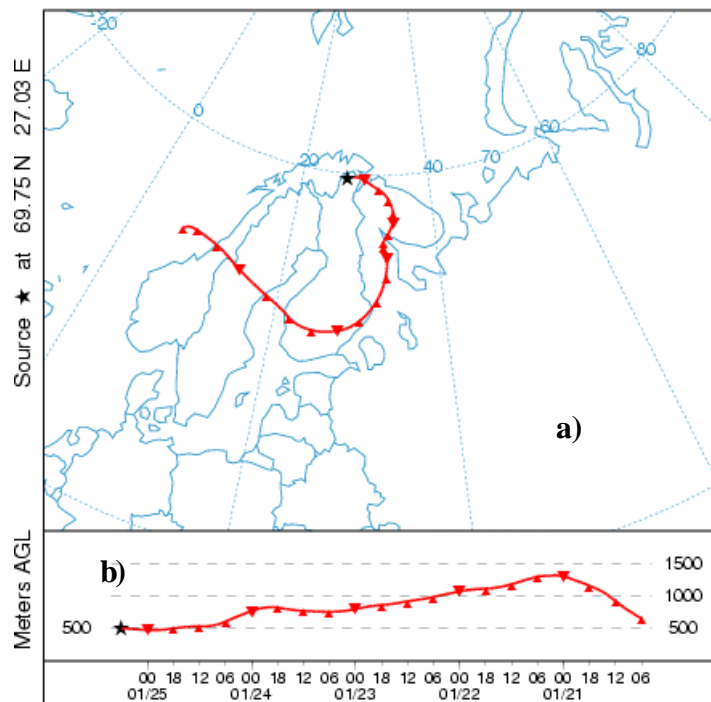


Figure 5.29: Unmix main interactive window run under MATLAB environment

NATIONAL OCEANIC ATMOSPHERIC ADMINISTRATION
Backward trajectory ending at 06 UTC 25 Jan 76
CDC1 Meteorological Data



**Figure 5.30: An air parcel back trajectory a) path in reference to earth's surface
b) vertical height from ground**

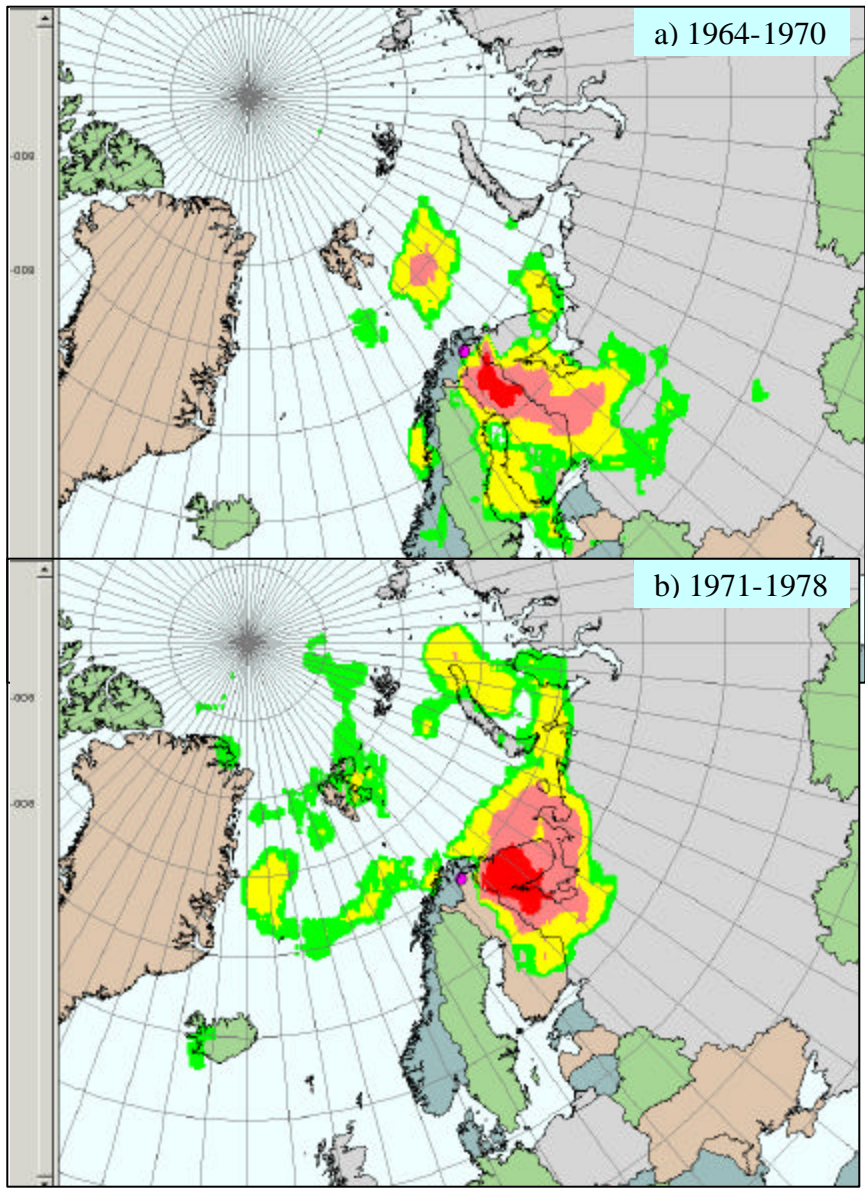


Figure 5.31: Silver RTA Incremental Probability Percent (IPP) plots, Smoothing Factor (SF) 441

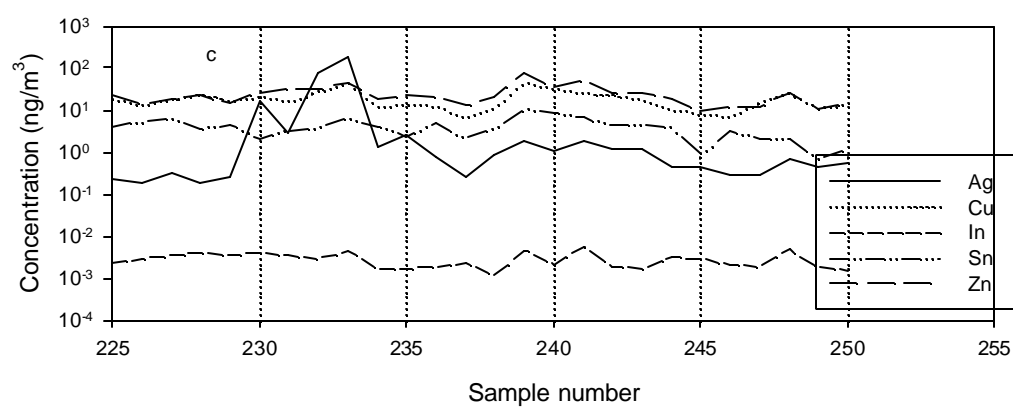
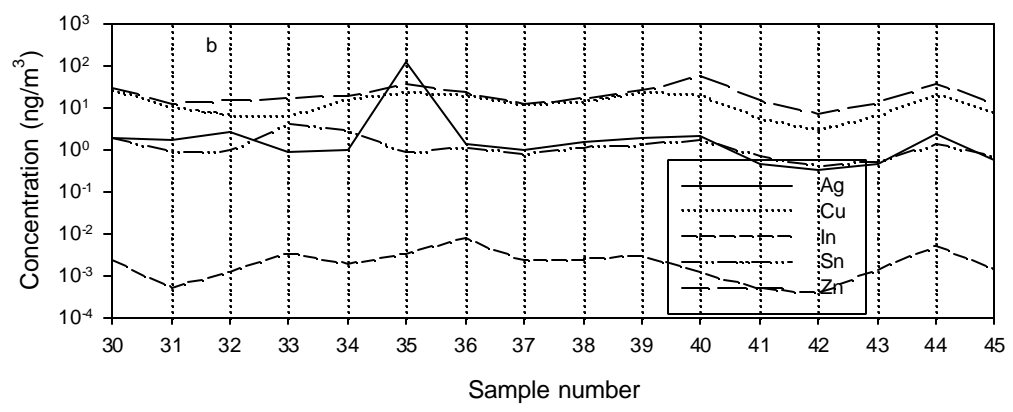
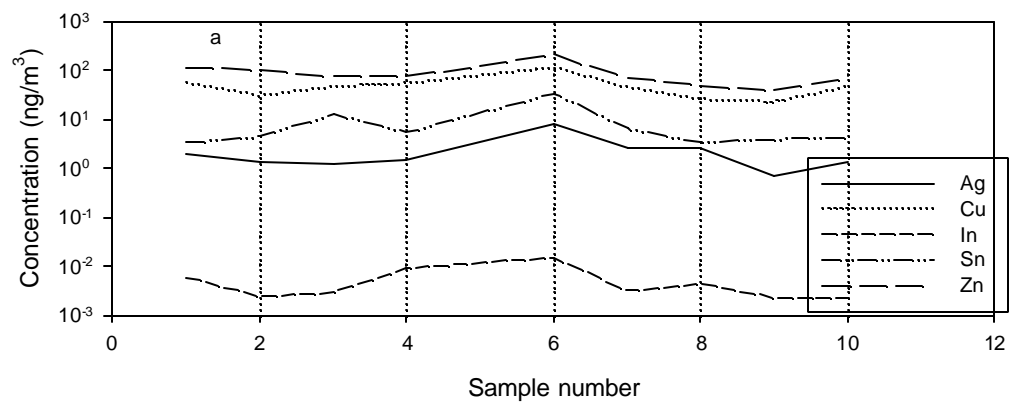


Figure 5.32: Multi-elemental line plots for Ag, Cu, In, Sn, and Zn

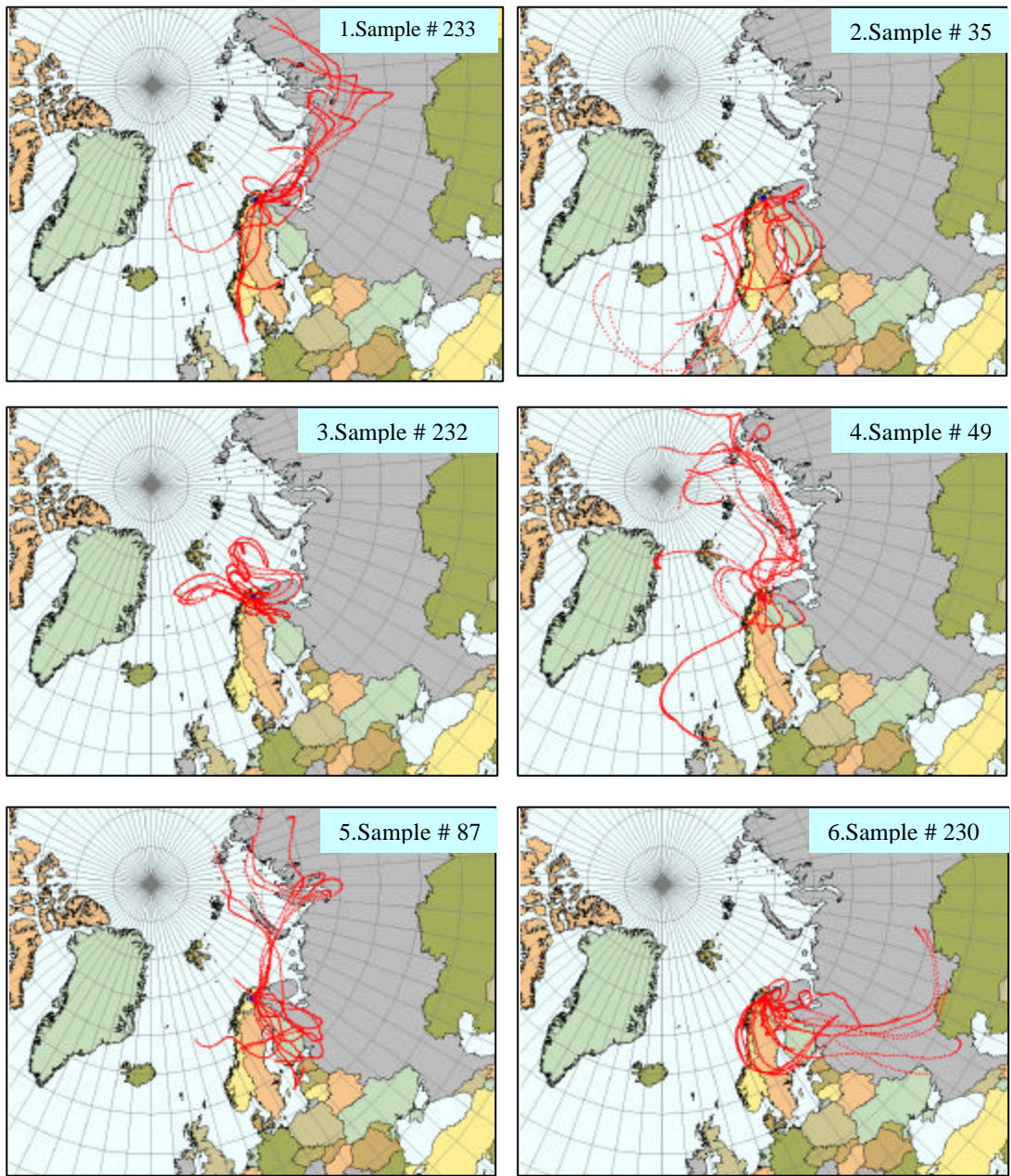


Figure 5.33: Back trajectory plots for the first six highest silver samples

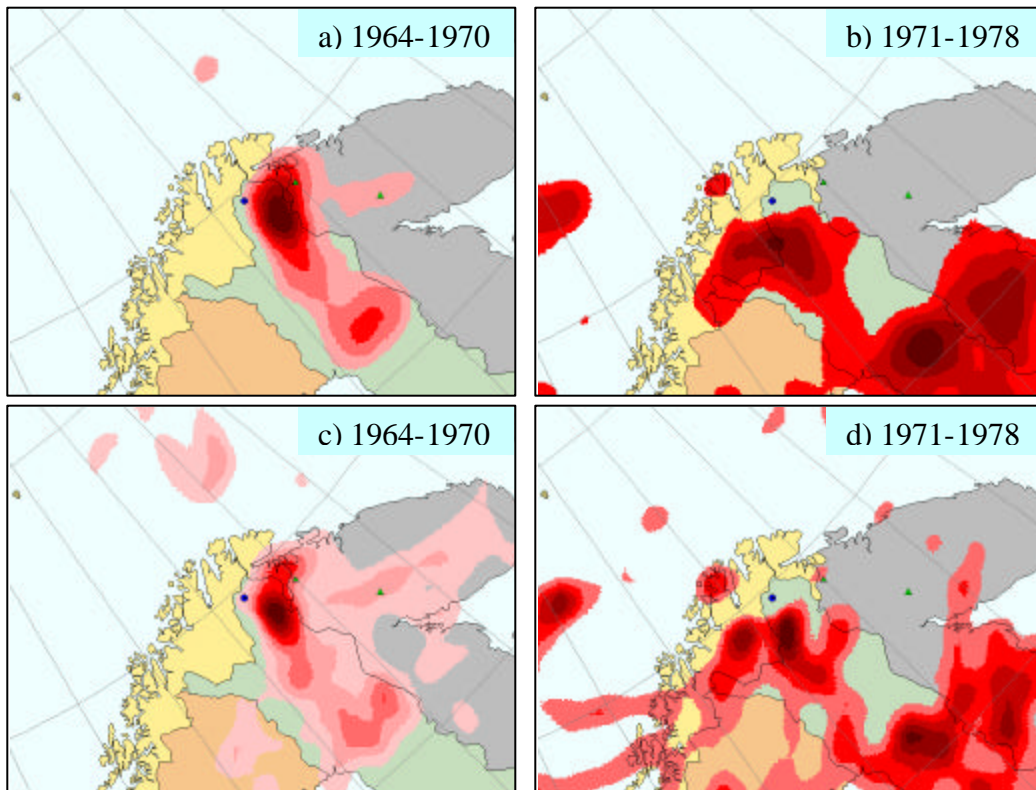


Figure 5.34: Silver RTA IPP plots, a) & b) SF 81, and c) & d) SF 25 (scales are relative)

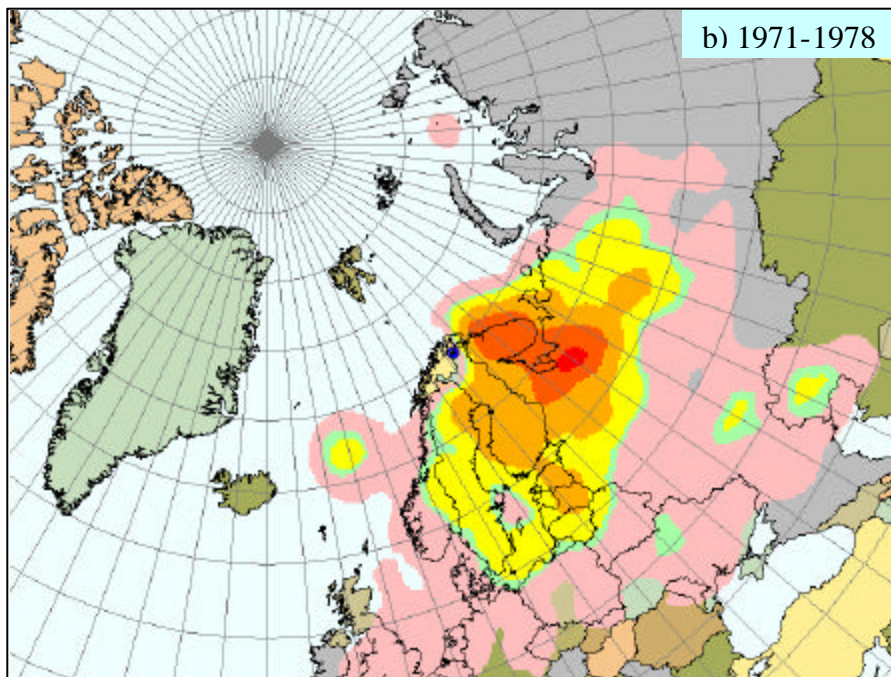
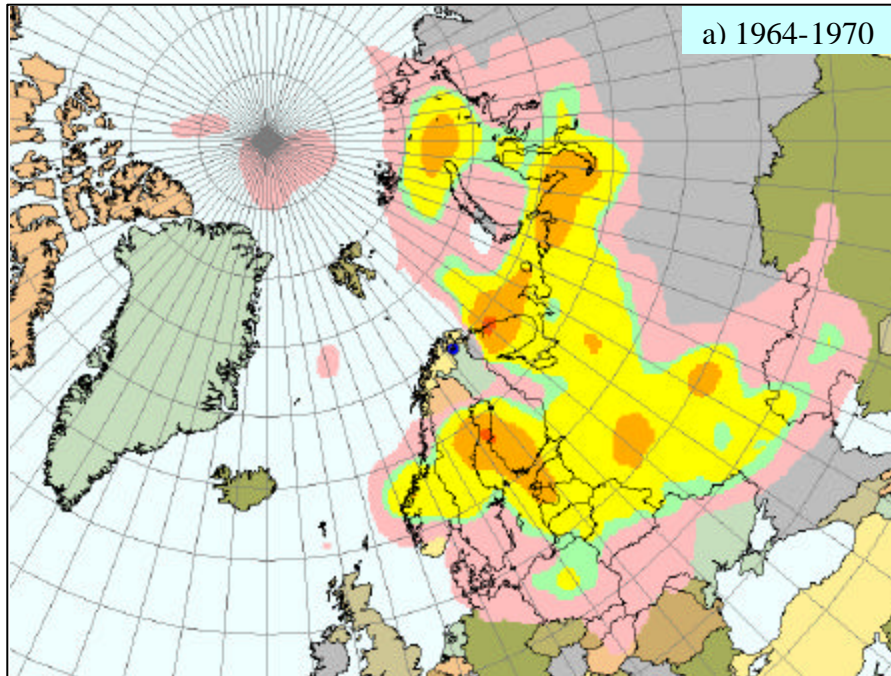
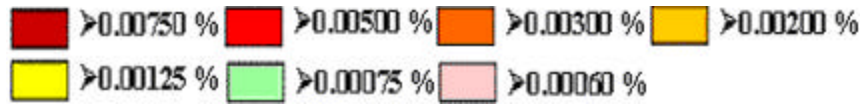


Figure 5.35: Arsenic RTA incremental probability plots, SF 81

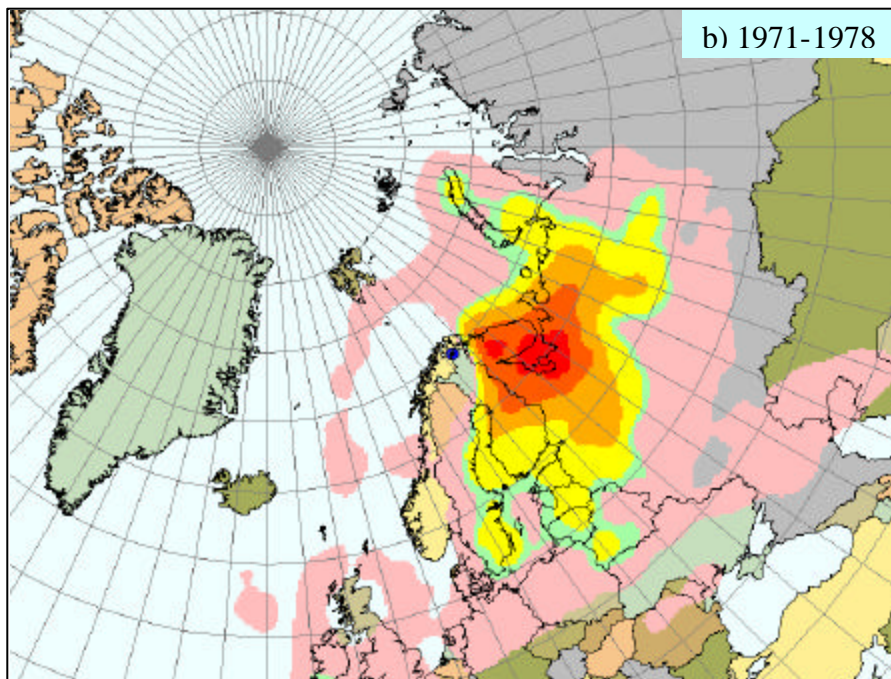
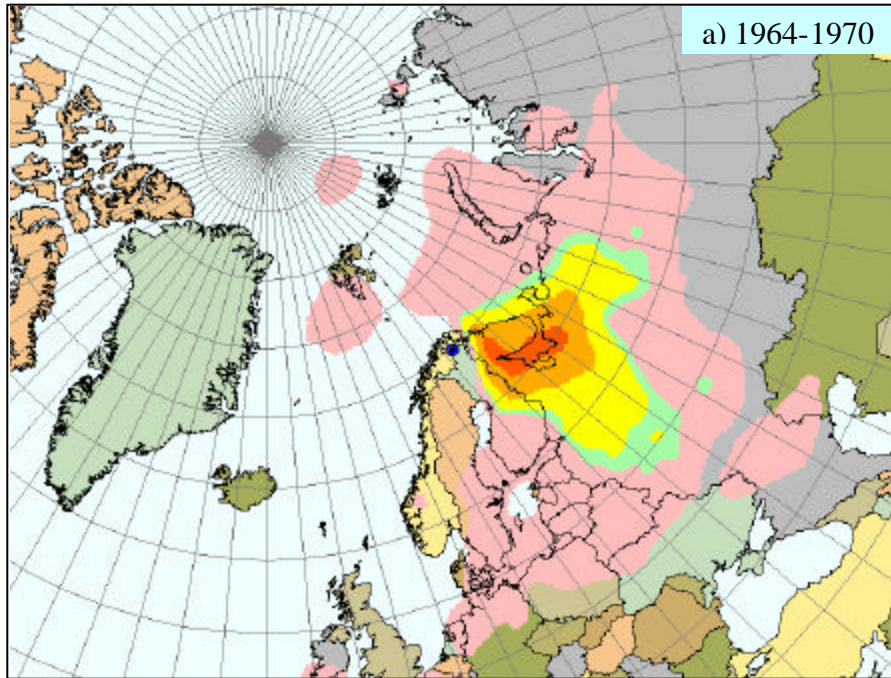
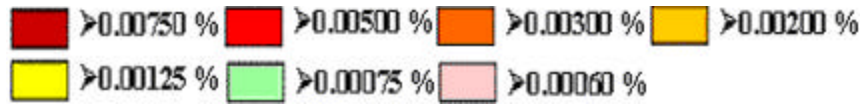


Figure 5.36: Cobalt RTA incremental probability plots, SF 81

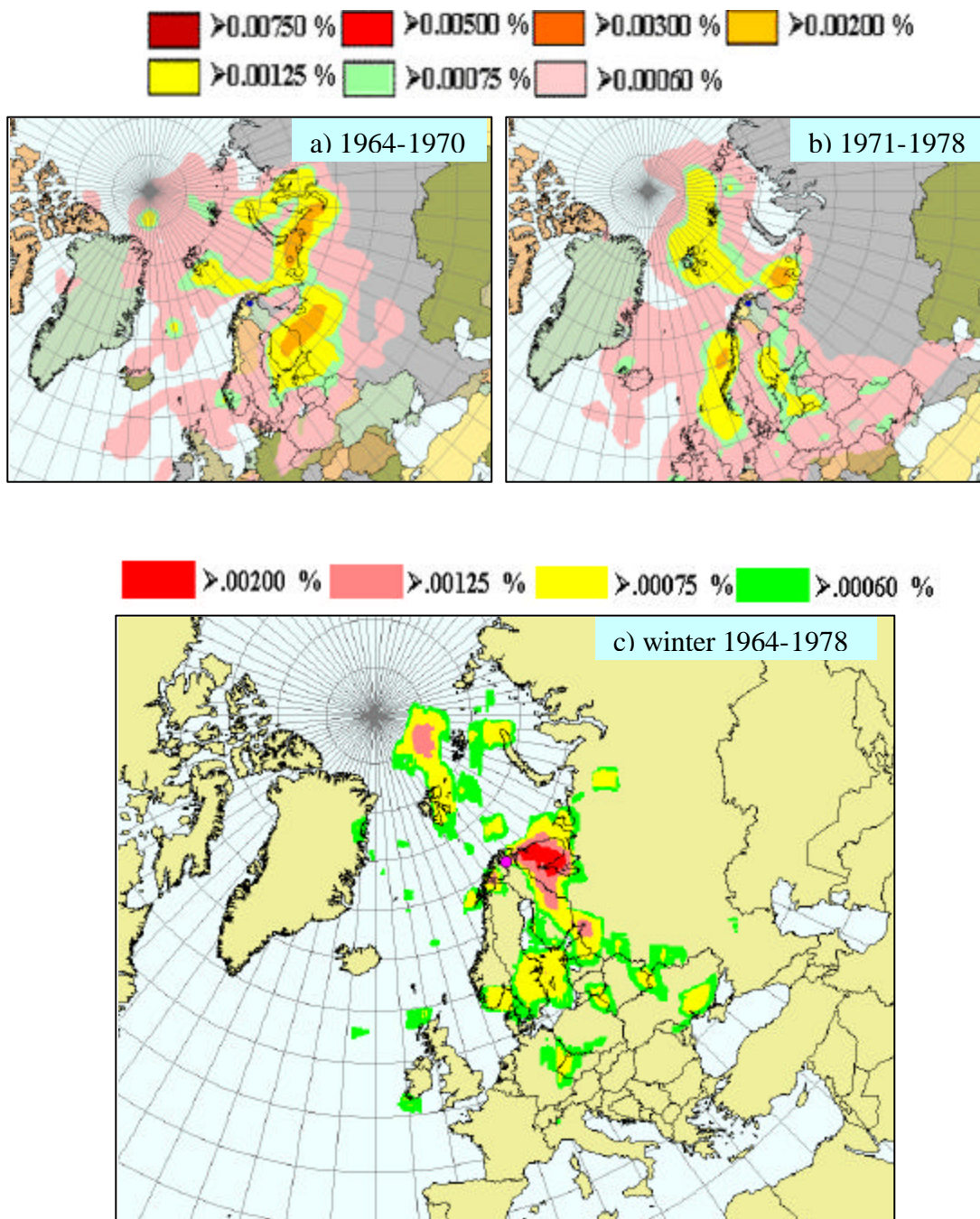


Figure 5.37: Copper RTA incremental probability plots; a) & b) SF 81, c) SF 441

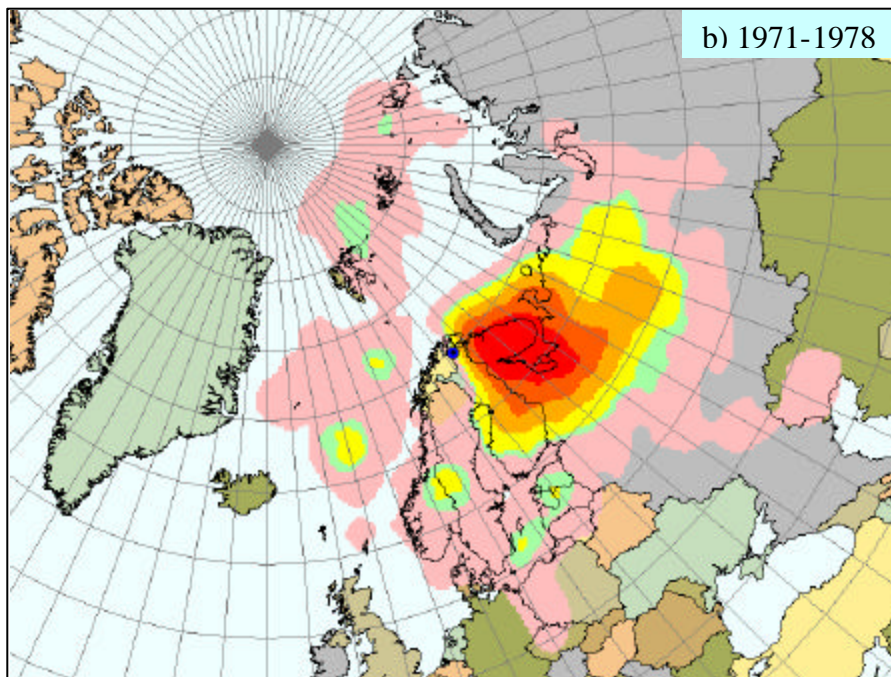
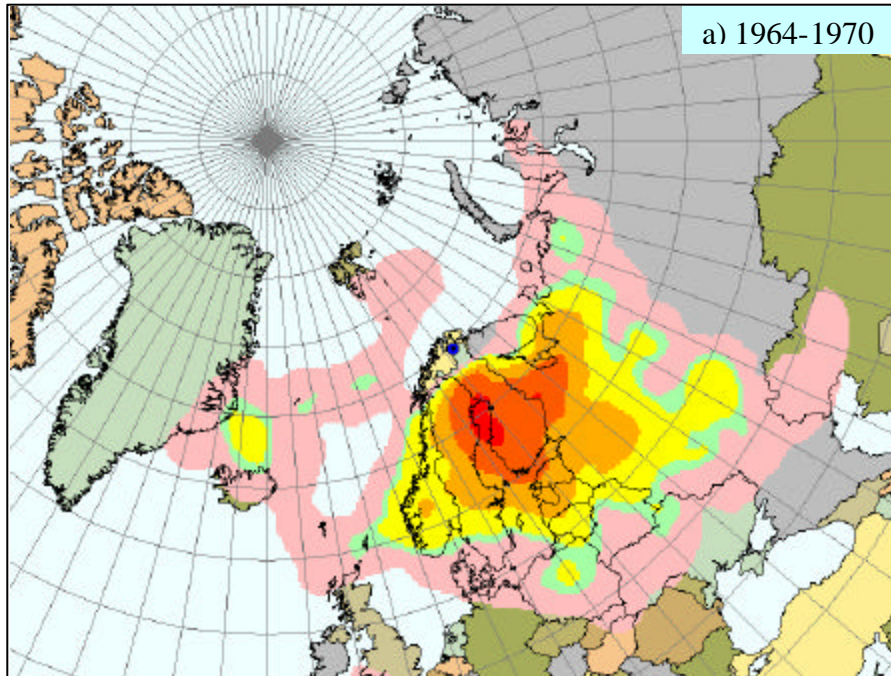
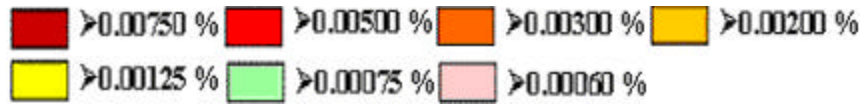


Figure 5.38: Indium RTA incremental probability plots, SF 81

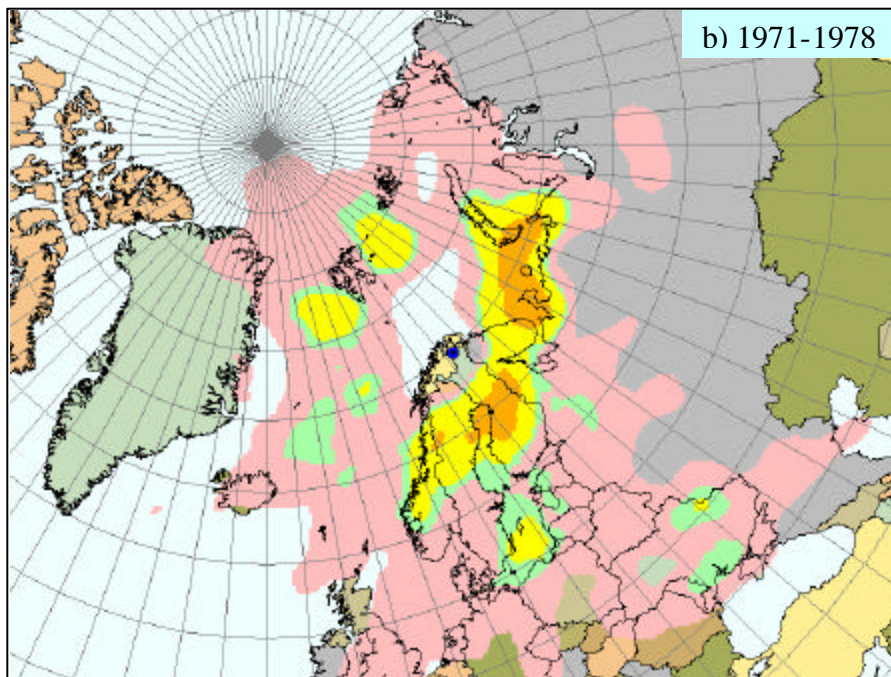
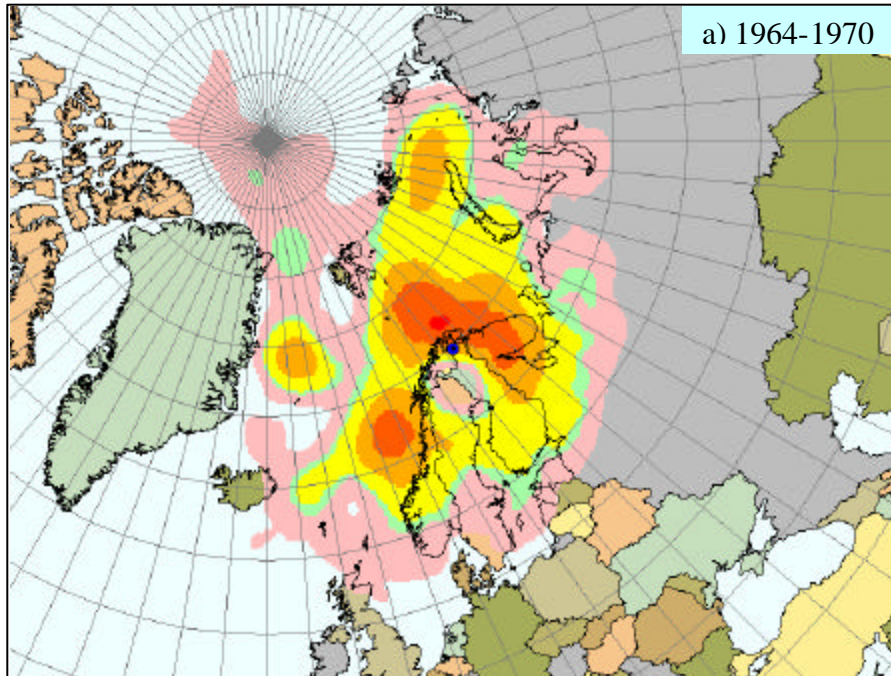
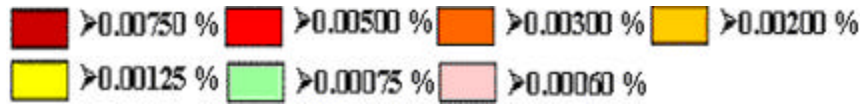


Figure 5.39: Antimony RTA incremental probability plots, SF 81

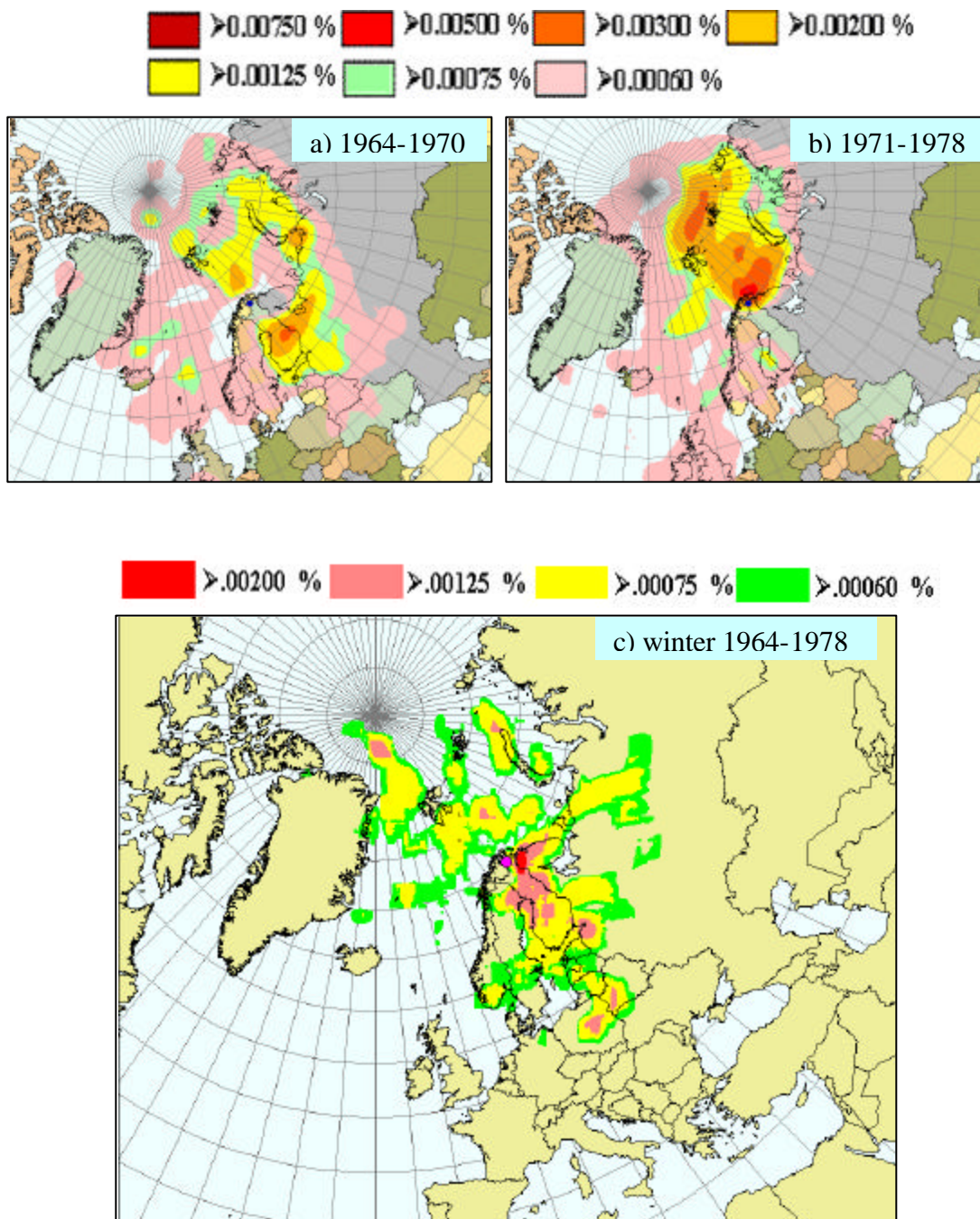


Figure 5.40: Tin RTA incremental probability plots; a) & b) SF 81, c) SF 441

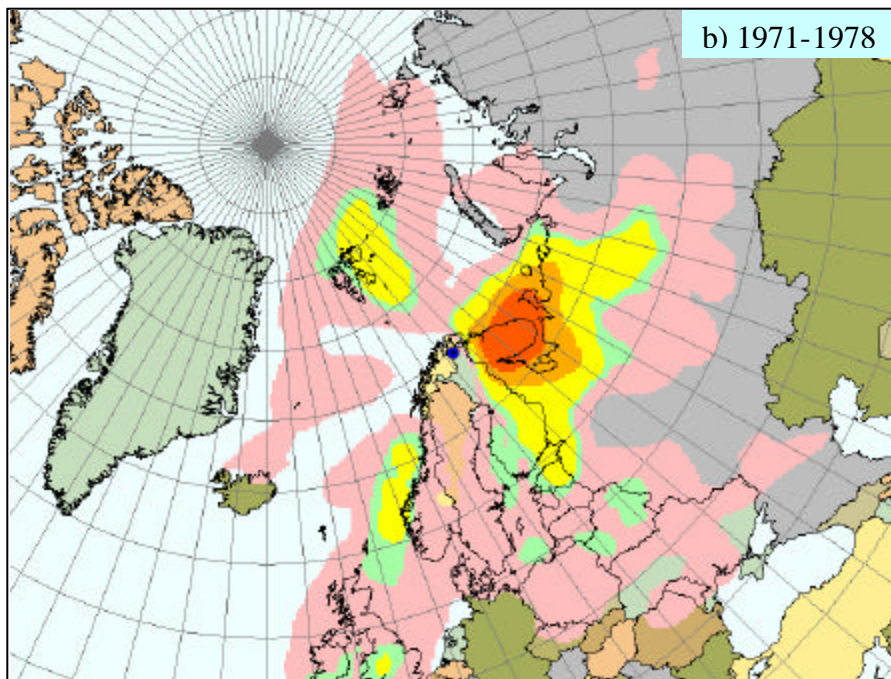
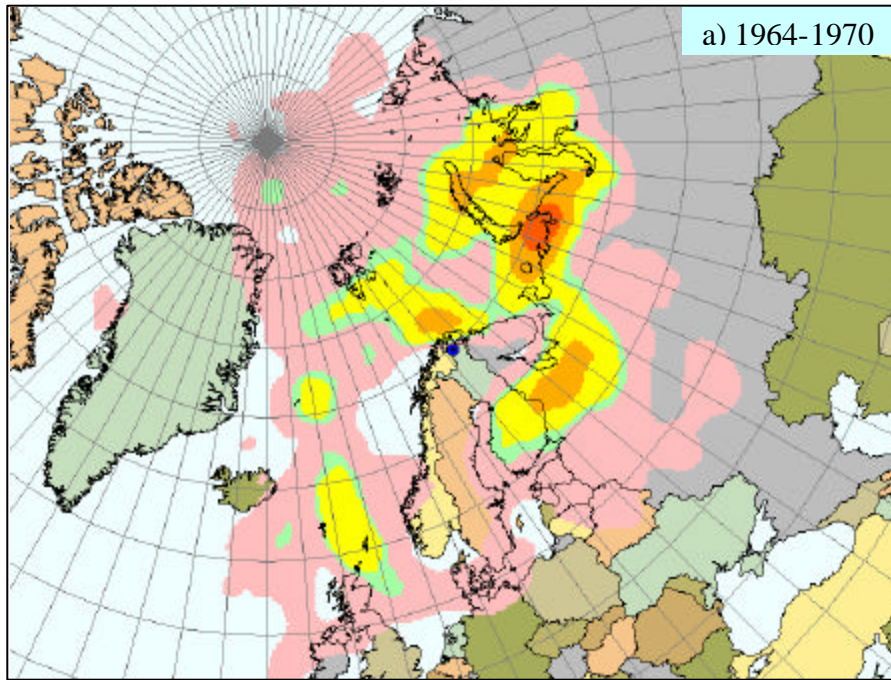
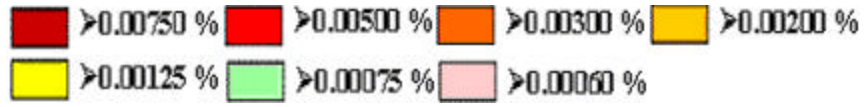


Figure 5.41: Zinc RTA incremental probability plots, SF 81

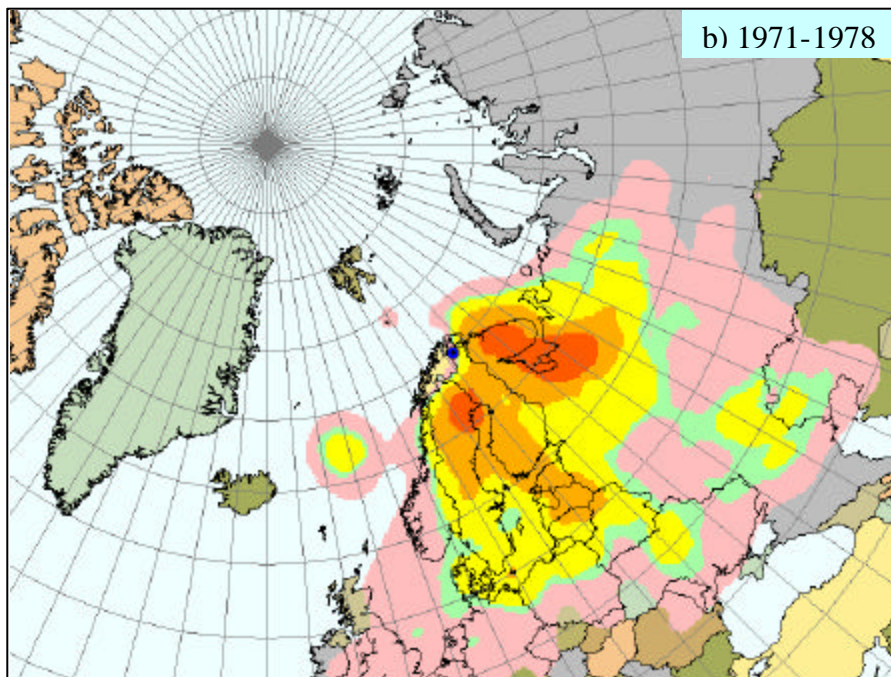
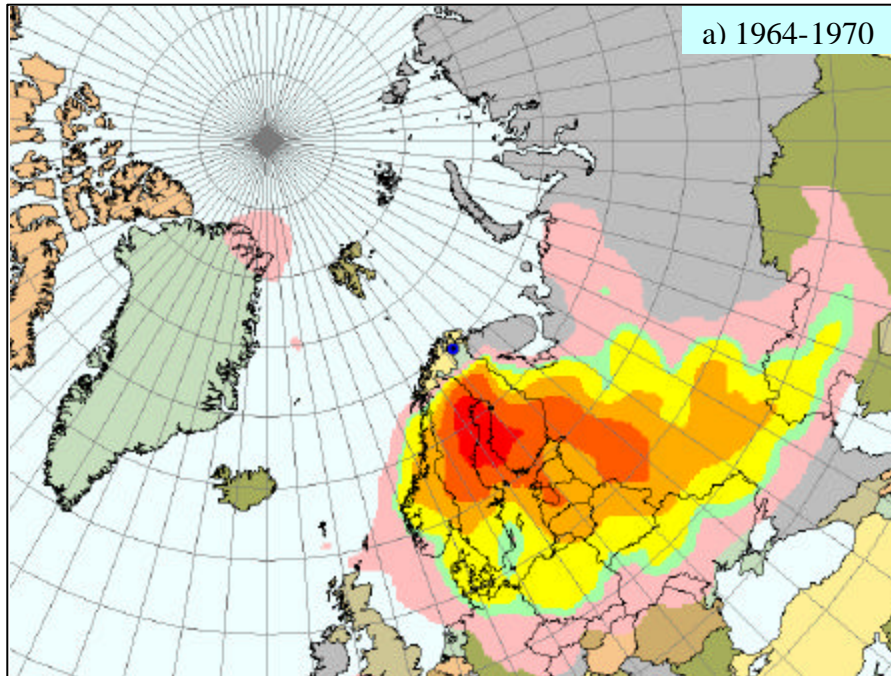
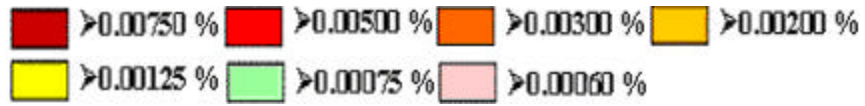


Figure 5.42: Manganese RTA incremental probability plots, SF 81

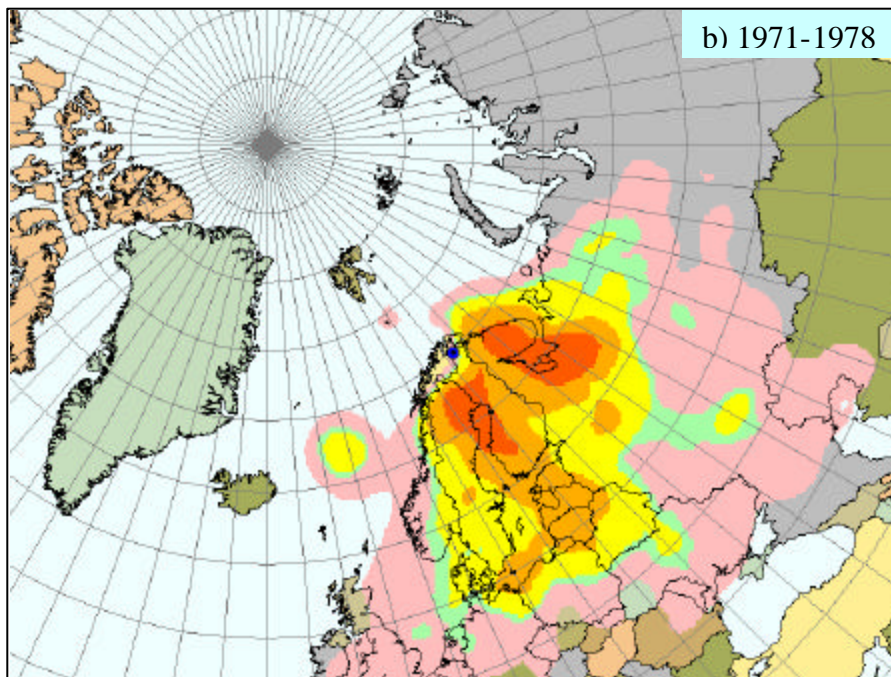
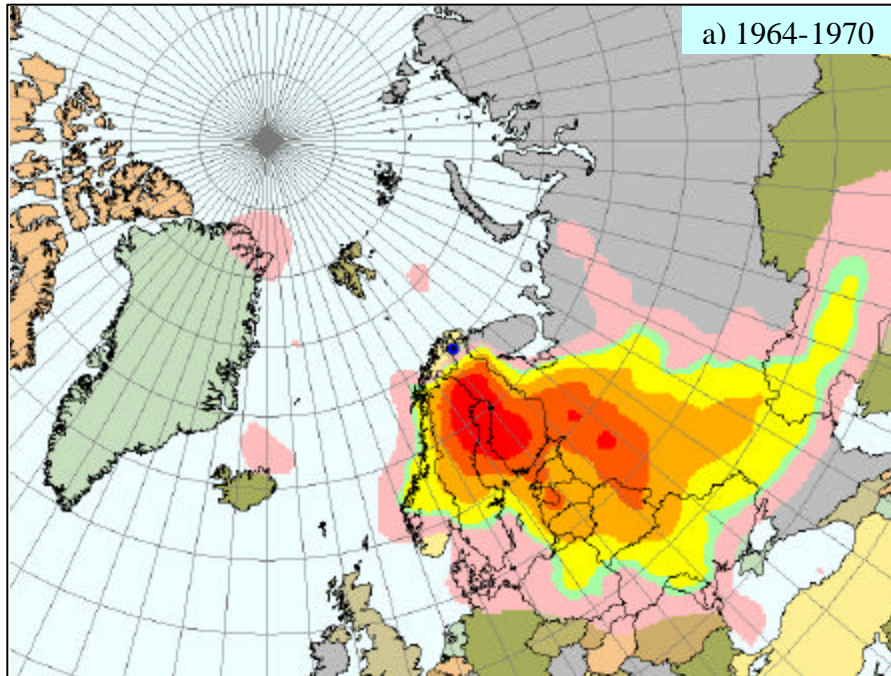
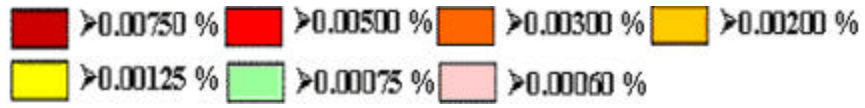


Figure 5.43: Vanadium RTA incremental probability plots, SF 81

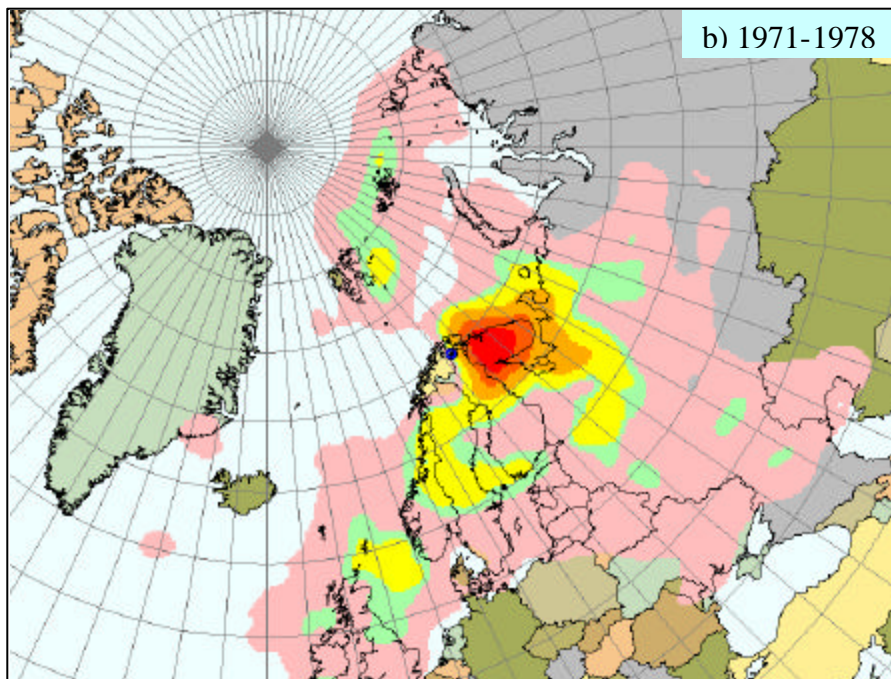
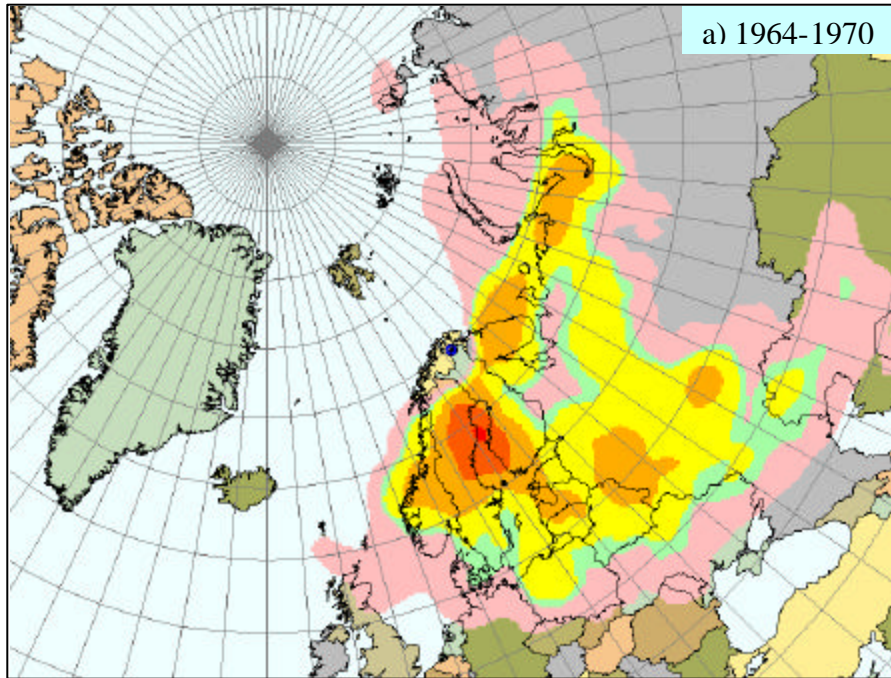
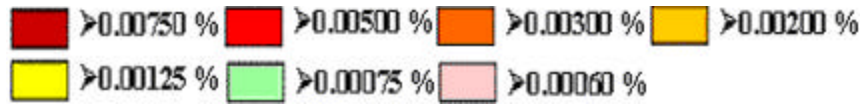


Figure 5.44: Aluminum RTA incremental probability plots, SF 81

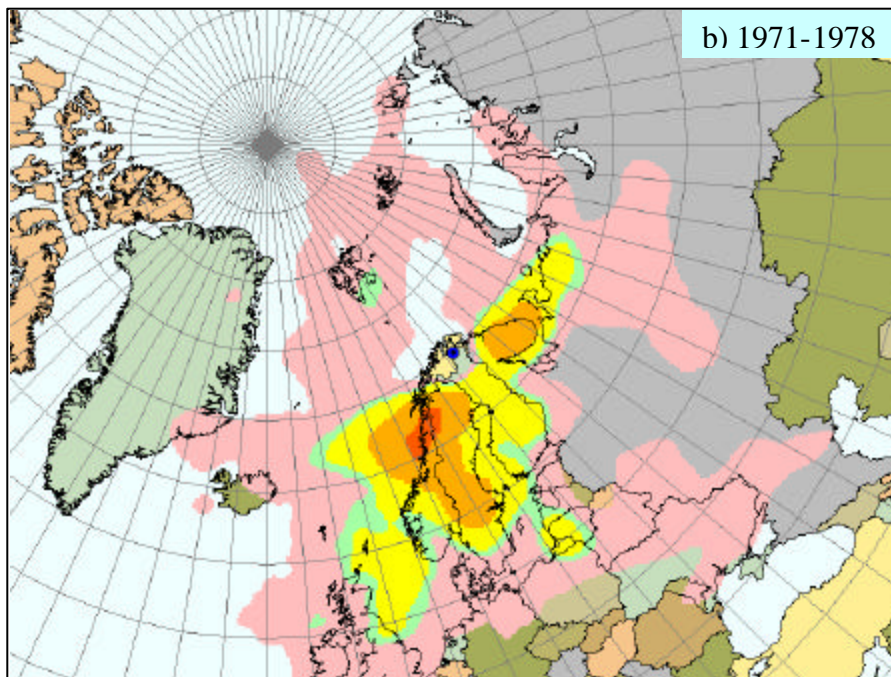
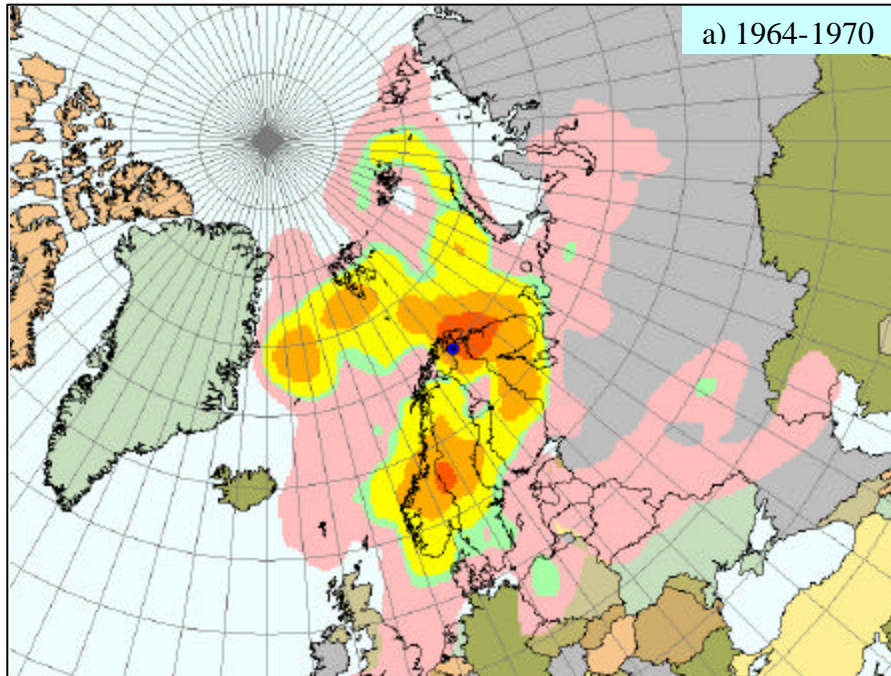
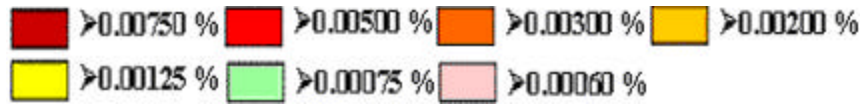


Figure 5.45: Silicon RTA incremental probability plots, SF 81

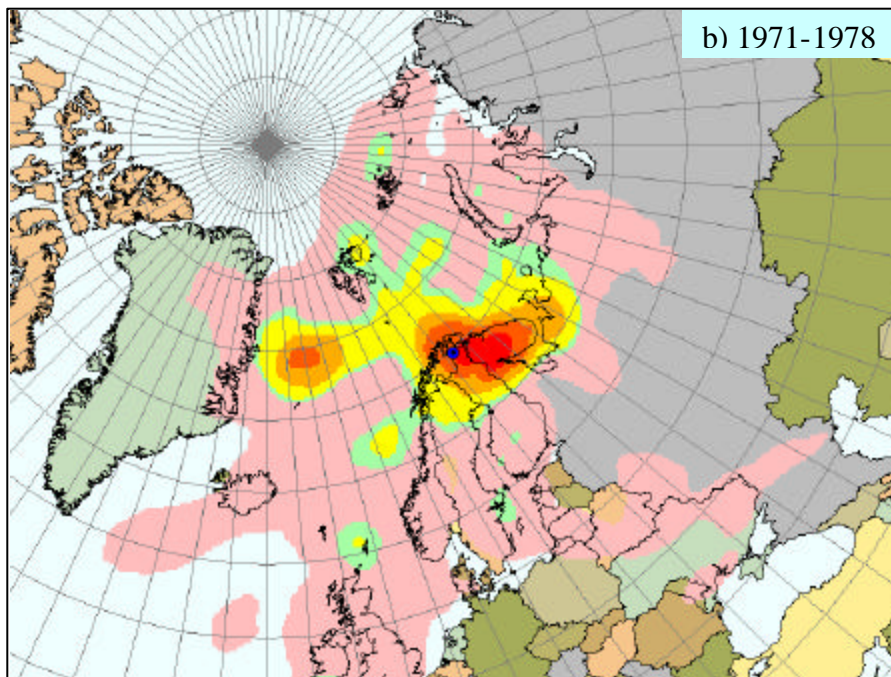
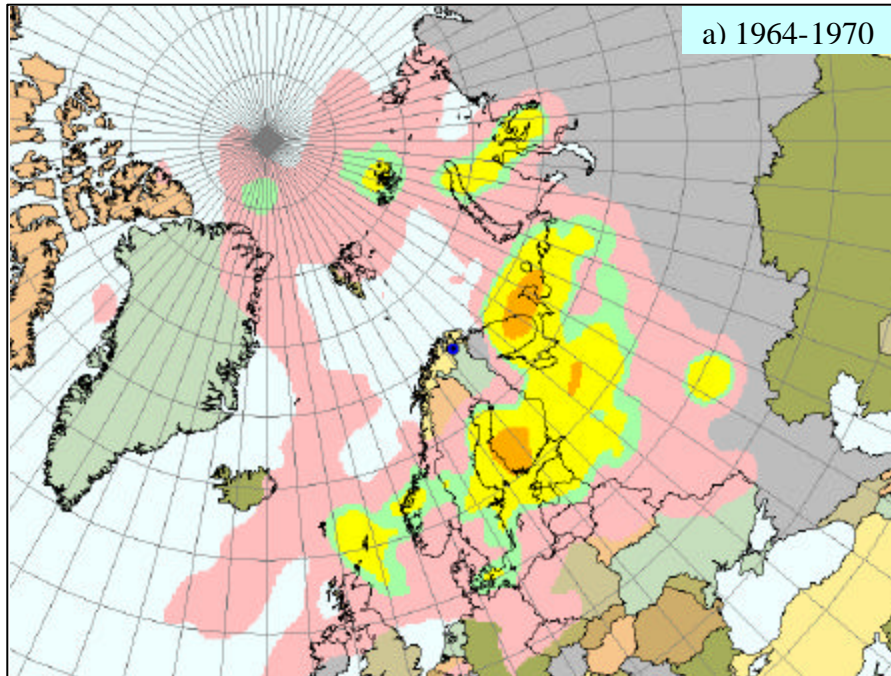
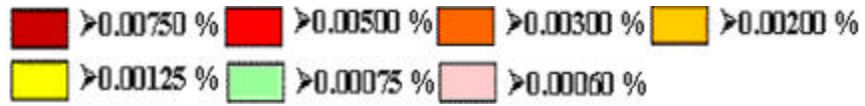


Figure 5.46: Calcium RTA incremental probability plots, SF 81

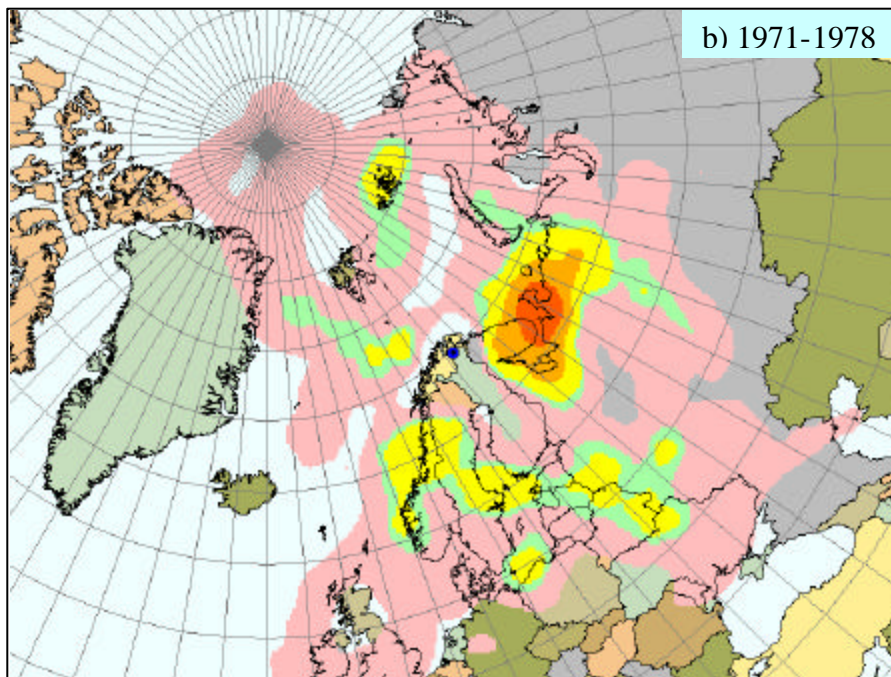
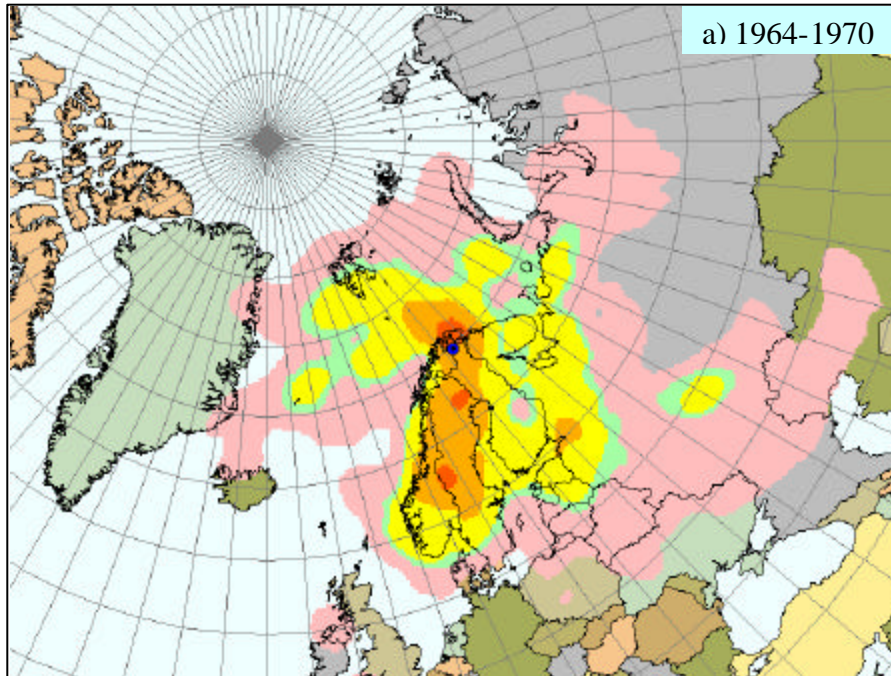
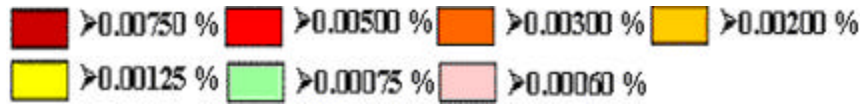


Figure 5.47: Titanium RTA incremental probability plots, SF 81

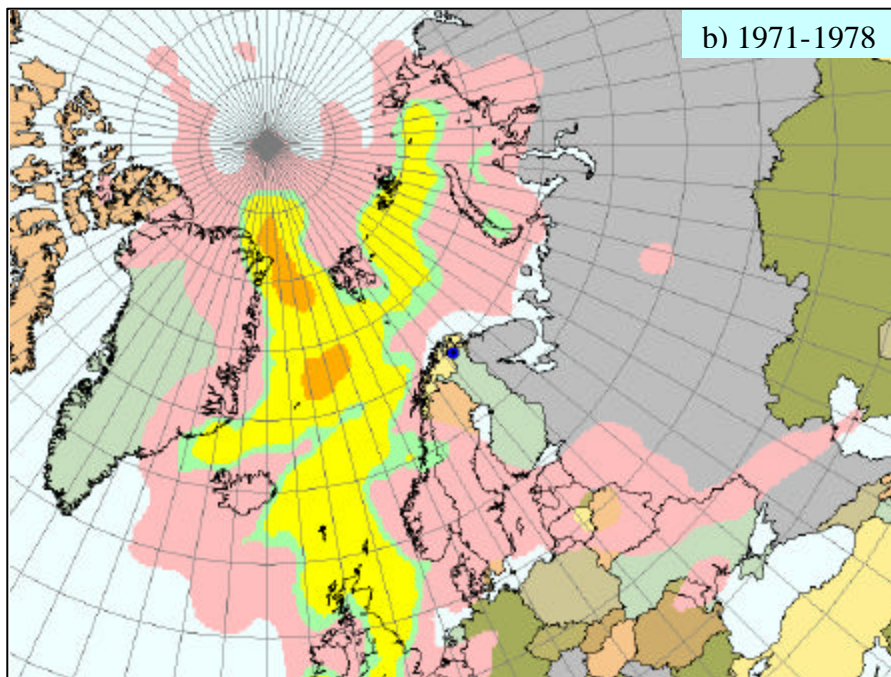
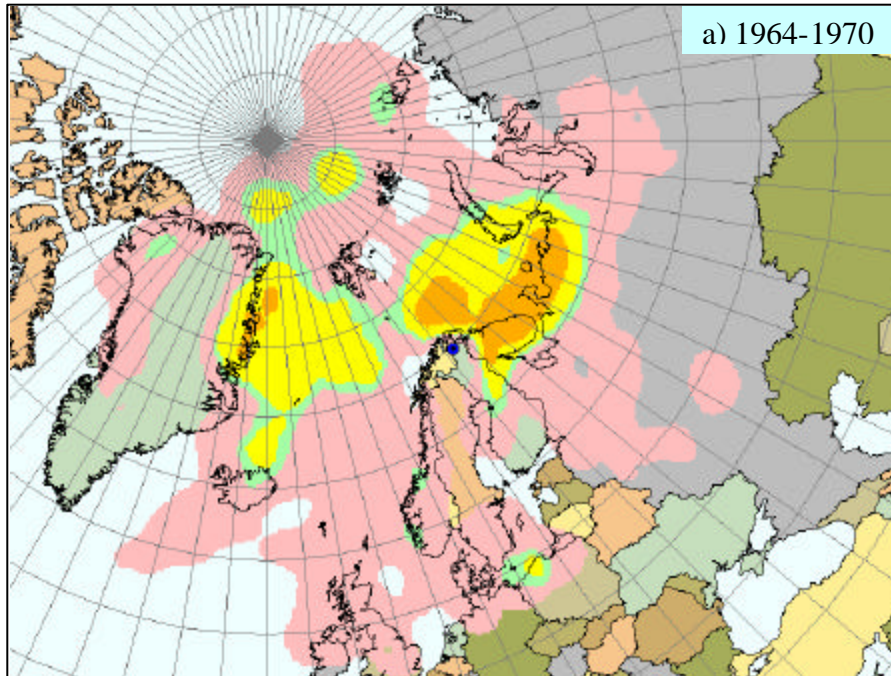
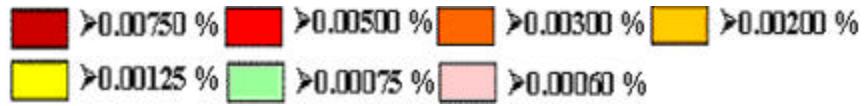


Figure 5.48: Sodium RTA incremental probability plots, SF 81

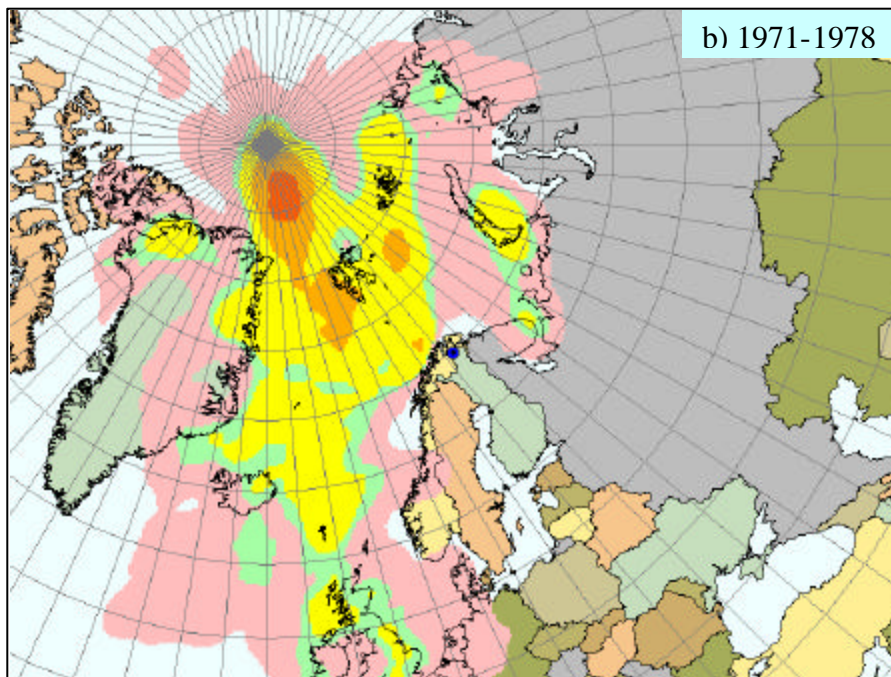
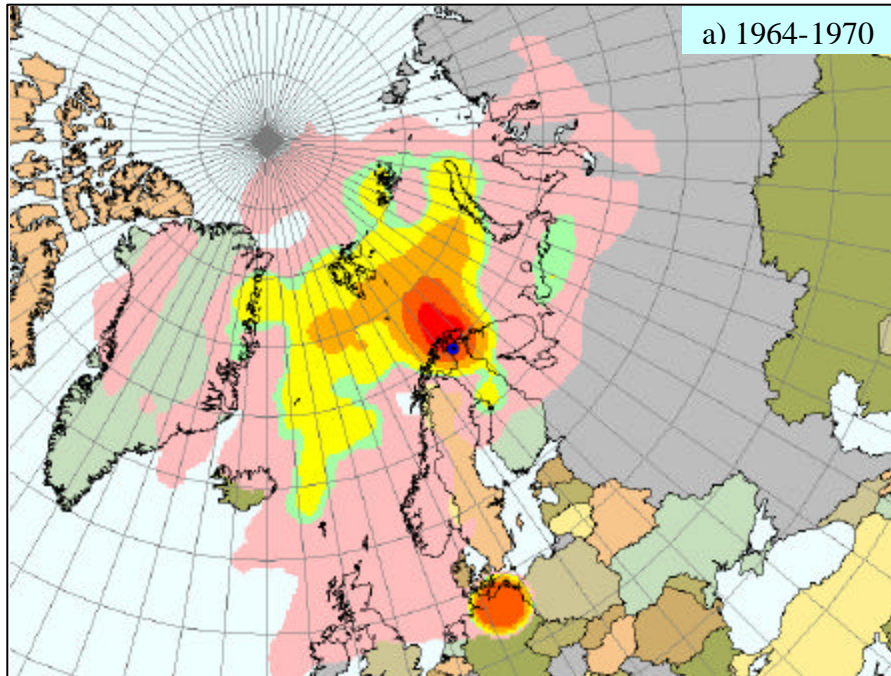
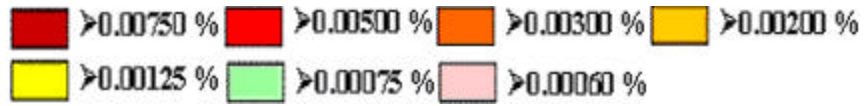


Figure 5.49: Chlorine RTA incremental probability plots, SF 81

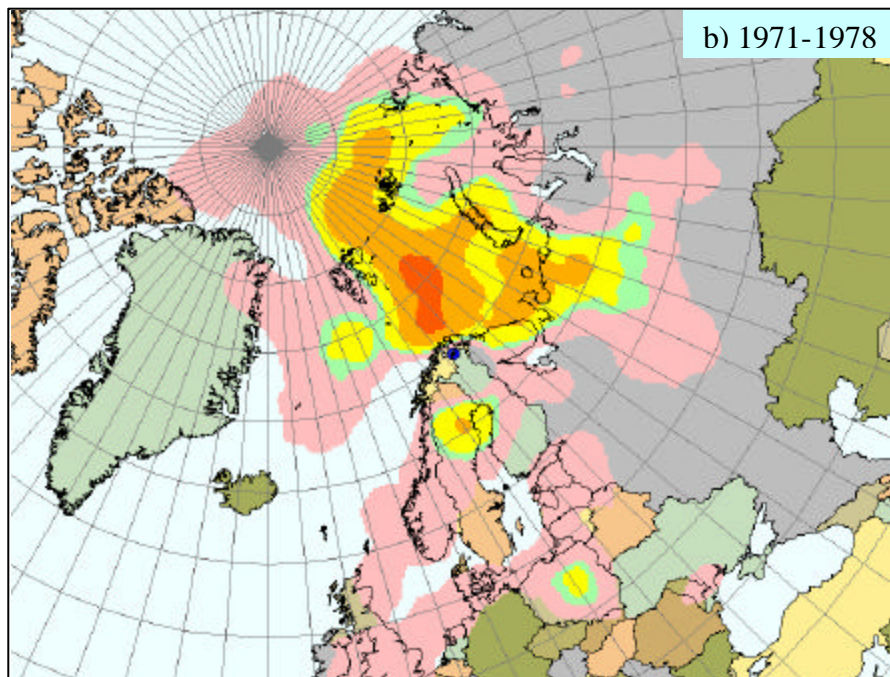
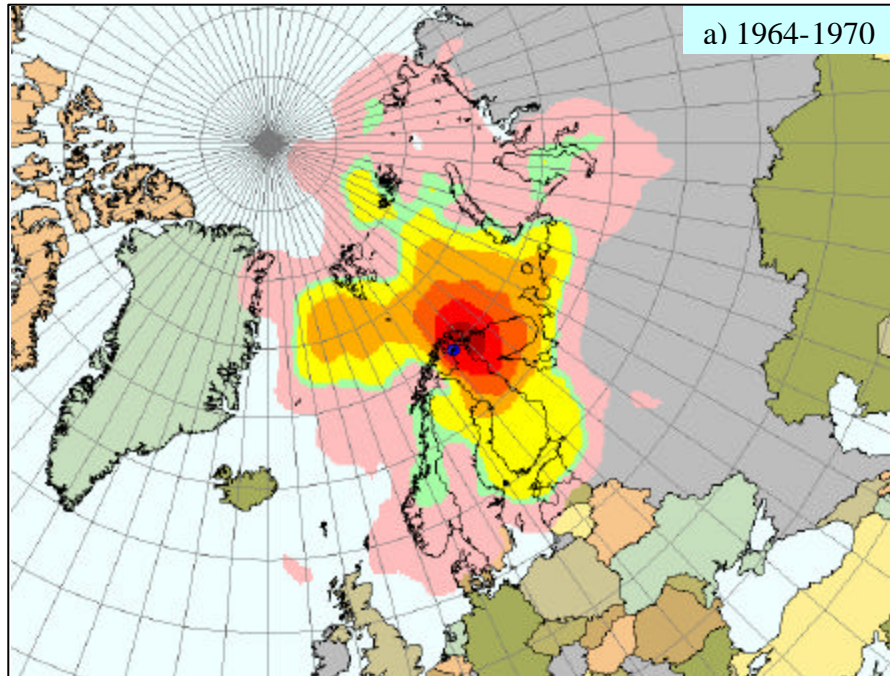
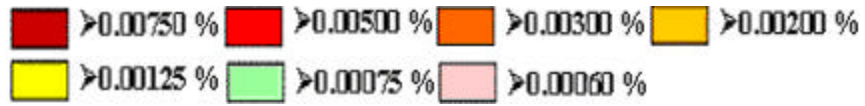


Figure 5.50: Bromine RTA incremental probability plots, SF 81

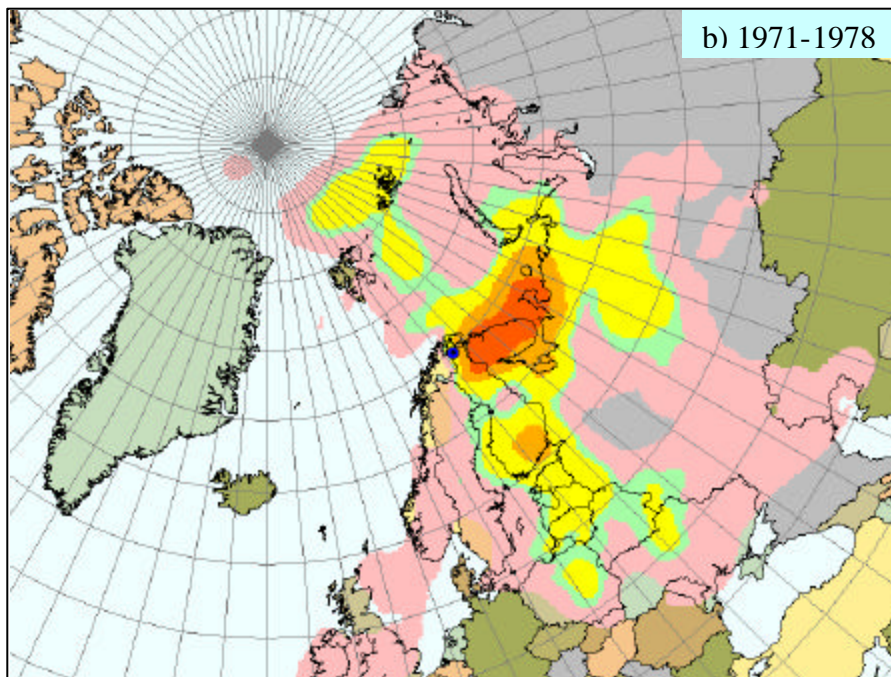
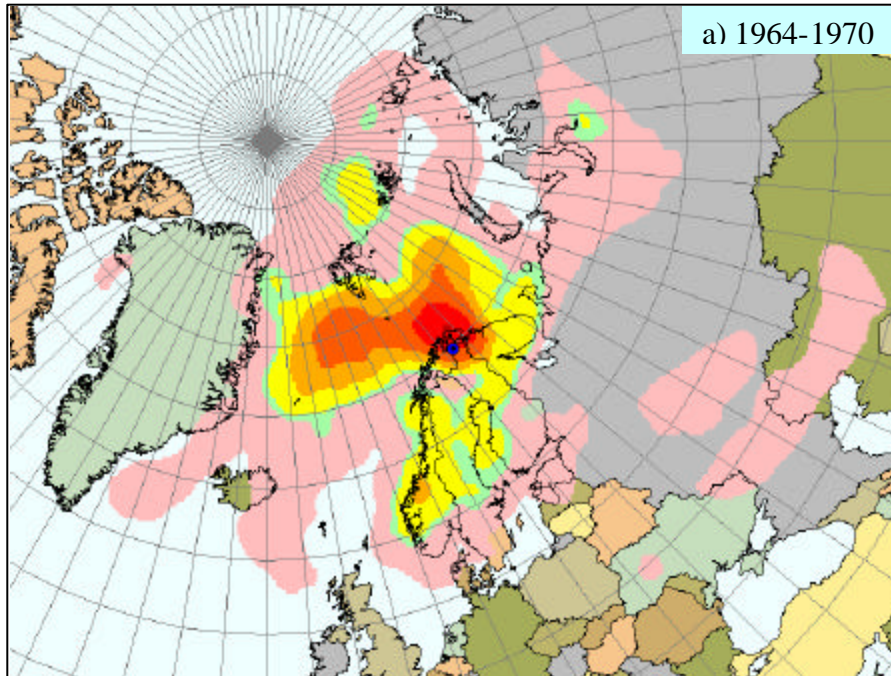
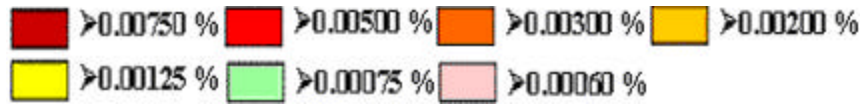


Figure 5.51: Iodine RTA incremental probability plots, SF 81

6. Impact of this Research

The impact of this research is three fold. First, it's contribution to the ongoing Arctic research. Second, the modeling experience obtained from this very large dataset could be used for future research and monitoring. Third, the development of new NAA methodologies for determining important industrial marker elements, like silver and cobalt, and the development of a new scheme for determining medium lived isotopes in a cost-effective way.

The aerosol trace elemental database, generated in this work, for the period of 1964-1978 at Kevo, northern Finland, is the oldest database in the Arctic region. This is also the longest continuous record for the sub Arctic Region. Earlier research at Alert, Canada; Alaska, USA; Spitsbergen, Norway, etc. indicated several sub Arctic locations as the major contributors for the Arctic pollutants [Rahn, 1981a, Maenhaut *et al.*, 1989, Pacyna *et al.*, 1989, Xie *et al.*, 1999]. The European sub Arctic is one of the highest pollution emission locations for the Arctic region. This research has resulted in an extensive and detailed database of trace elemental concentration levels and seasonal characteristics for this major source region. A comparison of elemental mean values of this work with other data indicated the influence of this particular location to the high Arctic pollution and is useful as an integral part of the Arctic research. The information generated in this work will also prove useful for the Arctic Monitoring and Assessment Program (AMAP), which was established in 1991 with responsibilities to monitor the levels and effects of anthropogenic pollutants in all compartments of the Arctic environment as a result of the Arctic Environmental Protection Strategy (AEPS) adopted by the governments of the eight Arctic rim countries.

This database can also be used to study the similarities and differences of the trace elemental concentration level among the reported literature data of this region for a three and a half decade period. Interestingly, the findings of the comparison were found to be consistent with the historical facts of human activities, geochemical behavior of the studied location, atmospheric characteristics, etc. For example, a low mean silver concentration period (1970-1978) of $\sim 0.1 \text{ ng/m}^3$ of this work matched well with the early 90's data by Vikrrula *et al.* (1999). An antimony anomaly in comparison to associated industrial components like arsenic, indium, copper, zinc, tin, etc., identified by the PCFA was consistent with the moss findings reported from the early 90's work by Reimann *et al.* (1998). Time series plot for aluminum of this work showed a lower magnitude and frequency of extreme values for aluminum concentration at Kevo, northern Finland, than that was found at Alert, Canada for the period of 1982-1992 [Zhang, 1996]. This observation probably indicated an additional source region for crustal component aluminum at Alert than that of at Kevo. Tin, an important smelter/industrial precursor element, is reported for the first time from this work in the Arctic region. This could be used as an additional signature element in Arctic research.

Elemental ratios are presented in a matrix form for full, summer, and winter periods to facilitate the use of much valuable trace elemental signatures in all pairs in the atmospheric research. It is also shown that a Cu/As ratio near the Monchegorsk smelters was about 50% times lower than that was calculated from this work. The use of all elements for elemental ratios facilitated this comparison. The earlier works mostly used the Mn/V ratio or As/Se, Sb/Se, V/Se, Zn/Se, Mn/Se, and In/Se as proposed by Rahn *et al.* (1981a, 1984). It can be mentioned here that one of the prime reasons for trace element determination in the aerosol is its use as a source signature. Almost all of the important chemical compounds, usually determined in aerosols, appear from the primary and secondary sources. A secondary source mainly refers to the production of the compound or species in the atmosphere through various complex chemical reactions. Thus, those chemical compounds might indicate the magnitude and variation of pollution levels for a specific receptor site, but of very little use as a source, regional, or local

signature. So, the use of trace elements as fingerprints is indispensable. Clearly, the more the elements in the system to use as signatures, the more powerful the resolution is. The study of aerosol elemental ratios is also very important to understanding the deposition pathways to the other compartments in the Arctic ecosystem, for example, in snow [Kelly *et al.*, 1995]

The receptor model PCFA revealed the trace elemental behavior in the Kevo atmosphere in conjunction with time series plots, box plots, scatter plots, and elemental ratios. As mentioned earlier, its findings for industrial components like antimony and arsenic at Kevo brings special attention for other research for these elements in this region. The findings of a deviated chlorine behavior from other sea source elements, like sodium, bromine, and iodine show the importance of in-depth study of this element in atmospheric aerosols. In atmospheric chemistry, chlorine has a particular role. Daniel *et al.* (1999) reported its role in ozone destruction and Kelly *et al.* (1995) reported a chlorine replacement mechanism by inorganic species in the same region of this work.

Unmix and Positive Matrix Factorization (PMF) are two recently developed methods categorized as advanced level receptor models. Recently, PMF was used on four aerosol datasets of Thailand consisting of only trace elements. Seventeen trace elements were used by PMF on all four datasets for a five/six source solution [Wanna *et al.*, 2000]. In this work, Unmix is used for the first time on a dataset consisting of only trace elements. As mentioned earlier, only six elements out of seventeen were used by Unmix for a four source statistically significant solution. The possible reasons were discussed. This exercise shows users to choose a model applicable for their particular interest.

RTA is a probability metric for identifying source locations. It clarified a few very striking facts for the studied period. In explaining the silver anomaly for the high and low periods (1964-1970 and 1971-1978), it resolved the smelters at Nikel, Zapoljarnij area to that at Mochegorsk area, which were within a distance of 200 km. This can be viewed as an unprecedented success for a source location model like RTA. Often in applying this kind of approach, the domain cell size suppresses the power of

such resolution. The resolution of these models also depends on the aerosol sampling duration, number of back trajectory ensembles, and the distribution characteristics of the element under study. Often a modeler seeks for an optimum number of back trajectory ensemble per sample to use in the model for identifying source locations for various sampling durations. Initially, it was thought that probably for a seven-day sampling period, consideration of only 14-back trajectory ensemble was not enough to identify silver smelters in such a close distance. However, it successfully showed the most probable smelting area of Norilsk ore was at Nikel, Zapoljarnij during the period of 1964-1970. The experience of the RTA model from this work can help in many ways. The model is developed more universally by creating the RTA grids over the European sub Arctic and Arctic region for future use. Also, present work showed that 14-back trajectory ensemble for weekly samples was quite successful. This means RTA models could be used to examine datasets for other applications like weekly precipitation, which have not been previously done due to the lack of confidence in its resolving power for a weekly sample. Also, the RTA plots presented in this work for zinc, indium, vanadium, and manganese showed different influencing locations in the Kevo atmosphere during the 1964-1970 and 1971-1978 periods, and it was consistent with the historical facts of the surrounding region at Kevo. This revealed the success and usefulness of this model for future use in the atmospheric research.

The development of cost effective methods and optimal uses of NAA is always important. Optimal NAA methods are developed in this work to determine two important industrial precursor elements, i.e. silver and cobalt, through two epithermal short irradiations. The advantages of a Compton suppression system and the choice of detector type for a cobalt measurement are presented. This will be useful for future analysis of this element. A cost effective way of determining medium lived isotopes like arsenic, antimony, zinc, bromine, potassium, tungsten, etc., are presented using the same ten-minute epithermal irradiation, that was used to determine short lived isotopes, like cobalt, iodine, indium, silicon, and tin. The NAA methodology for this new technique has been

presented in detailed and will be useful in the future for cost effective analysis of small or large sets of sample.

7. Conclusions and Recommendations

7.1 Conclusions

Lower atmospheric aerosols have been characterized for the period of 1964-1978 in the European sub Arctic region at Kevo, northern Finland. A total of 685 weekly samples were analyzed for Ag, Al, As, Br, Ca, Cl, Co, Cu, I, In, K, Mn, Na, Sb, Si, Sn, Ti, V, W, and Zn using neutron activation analysis. More than half of the measured elements were determined to very lower detection limit levels using epithermal NAA and Compton suppressed counting. A 10-minute epithermal irradiation was successfully used for the determination of short and medium lived isotopes like ^{82}Br , ^{76}As , ^{41}K , ^{122}Sb , $^{69\text{m}}\text{Zn}$, and ^{187}W . This approach was found to be cost effective.

Log normal distribution for almost half of the elements were found statistically significant. Assuming a log normal distribution of chlorine data, an approximate filter blank value was determined and subtracted from the total chlorine concentration levels. This approach of determining chlorine blank value reduced the below detection limit (BDL) data to 4.5% from 35%. Initially, 35% of the chlorine BDL data was resulted for considering the blank value determined from the new filters.

Study of time series concentration levels, box plots of the monthly subsets, and the descriptive statistics of seasonal dataset showed that seasonal weather had less influence in the lower atmospheric elemental concentration levels at Kevo. Two very distinct silver concentration level periods, high and low, were observed in the Kevo atmosphere during 1964-1970 and 1971-1978. A comparison of anthropogenic elemental concentration levels in the Kevo lower atmosphere were found in the same range or 2-8 fold higher than reported literature data of Russian and Canadian Arctic for winter and spring seasons. Elemental ratios calculated from geometric means were presented in a

matrix form to find a ratio in any pair for anthropogenic, crustal, and sea source elements. A summer Cu/As ratio of this work was about 50% higher than the recently reported ratio at Monchegorsk, Kola Peninsula, for these two elements. Ratios of Cl/Na and Br/Na were found about 6 fold lower and 2 times higher, respectively, than the ratios in the Seawater. Study of scatter plots did not show any well-correlated elemental pairs for this database and mostly appeared as a widely focused beam originating from the coordinate origin. Enrichment factors (EF) were calculated using both the local and global averages. Elements like In, Cu, Zn, As, Sb, Sn, and Ag were found highly enriched in the Kevo lower atmosphere. A comparison of EF values of this work with North Earth Archipelago (NEA), Russian high Arctic showed that most elemental EF values were comparable to the NEA values except Cu, which was about 3 times higher in the Kevo atmosphere than that of in the NEA. At Alert, Canada, a bromine EF value was about 14 times higher and antimony EF value was 3 times lower than that of Kevo.

Principal component factor analysis (PCFA) showed a strong smelting factor consisting of copper, zinc, indium, and tin. This factor was more important in the PCFA results for the winter dataset than that of the summer. A crustal factor was easily recognized in winter PCFA results, but in the summer result crustal components were mixed up with the anthropogenic components. Sea source components appeared in a single factor in the summer PCFA results but were found into several factors in pairs in winter PCFA results. Antimony always tended to be alone in a single factor. Manganese and vanadium mostly showed up with the anthropogenic components in a factor, however, in summer dataset these two were strongly correlated with aluminum and weakly to indium and cobalt.

An advanced atmospheric receptor model, Unmix, was used to identify sources and source composition in the Kevo atmosphere. In Unmix, only six out of seventeen elements were allowed to be included for a statistically significant solution. A total mass for aerosols in the filter was not recorded during sampling period, so source mass apportionments were not possible using PCFA or Unmix for this database.

Residence time analysis (RTA) was used for identifying the source location of all elements using air parcel back trajectory ensemble. Historical facts, data analysis, and extensive investigation of RTA plots showed that a high silver concentration period observed in the Kevo atmosphere during 1964-1970 most probably occurred due to the smelting of silver rich Norilsk ores at Nikel/Zapoljarnij smelters. Investigation of RTA plots for anthropogenic elements also indicated a distinctive emission pattern of emission location for most of the elements in two periods, 1964-1970 and 1971-1978. For most of the anthropogenic elements RTA incremental probabilities strongly indicated the elemental emission location to the Kola Peninsula region for 1971-1978 period. This probably indicated a higher magnitude of smelter's emission began in 1971 with the establishment of a stable northern sea route to transport Norilsk ore to Kola Peninsula for smelting.

7.2 Recommendations

Characterization of long-term aerosol samples for trace elemental concentration level at Kevo in the northern Finland, also known as European sub Arctic, is a unique database for this region. Future atmospheric monitoring and analysis should continue for identifying any changes in the atmospheric concentration level in this region. After 1991, there has been much discussion of installing emission-controlled devices in smelting industries at Kola Peninsula. Once installed, the concentration level can be measured and compared with this decade old database for any improvement.

In this work, a few very high silver concentration levels observed in the Kevo atmosphere indicated that probably in the vicinity of the smelters, the silver concentration levels in the ambient atmosphere was very high. Although, so far, there is no recommended ambient concentration level for many trace elements determined in this work, but it is very important and useful to have a general concentration level database in the vicinity of the smelters.

Based on the analysis and results of this database, it can be recommended that any episodic sampling campaign for a short period of time, especially during one or two winter months can produce a representative spatial database for this region. This kind of

spatial databases could be used to create regional subdivisions to use them in atmospheric research.

Major aerosol components like sulfur-bearing compounds, black carbon, and some other important elements like nickel, lead, cadmium, etc., which can be measured by other analytical methods, should be included in the model for an extensive analysis and mass apportionment to the sources.

Appendix

Section 1

Table A.1: Irradiation and counting data of standards and SRM for thermal irradiation

Standard & SRM	Concentration (ppm)	Weight (g)	Irradiation Time (sec)	Reactor Power (kW)	Decay Time (sec)	Counting height
Al	96700	1.12575	10	500	1021	B
Br	784	0.79655	10	500	3903	B
Ca	99000	0.84300	120	500	1220	B
Cl	776	0.79571	10	500	930	B
Cu	99900	0.85680	10	500	1972	B
I	822	0.79823	10	500	2335	B
Mn	53.8	0.80000	10	500	981	B
Na	503	0.79571	10	500	930	B
Ti	97300	0.87243	10	500	995	B
V	27.4	0.79604	10	500	628	B
1632 a		0.53166	10	500	1200	B
1632 b		0.76497	10	500	1110	B
1632 c		0.83251	10	500	1021	B
1572		0.42256	20	500	499	B

B = ~ 4.4 cm

Table A.2: Irradiation and counting data of standards and SRM for epithermal irradiation

Standard	Concentration (ppm)	Weight (g)	Irradiation time (sec)	Reactor power (kW)	Decay* time (sec)	Counting height
Ag	100	1.00100	10	500	95	A1
As	9.4	0.79875	120	500		A
Br	784.1	0.60300	120	500		A
Co	106.8	0.60016	300	500	1313	A
I	1000.0	0.59572	30	500	3555	A
In	5.3	0.78927	60	500	10120	A
K	104	0.76168	600	500		A
Sb	115.5	0.60430	120	500		A
Si	9350.0	0.52337	30	500	259	A
Sn	100.0	0.79556	120	500	1468	A
W	11.9	0.81120	180	500		A
Zn	200.2	0.80878	300	500		A
1572		0.43713	120	500		A
1632a		0.56605	60	500	1405	A
1632b		0.61886	180	500		A
1632c		0.83251	180	500		A
CH2		0.44453	5.6	500	21	D
KC-1		1.16176	10	500	726	D
NIST 2709		0.68095	10	500	1220	A
NIST 2709		0.69079	300	500		A

* For short-lived isotope measurement decay time is presented, not for medium-lived isotopes.

A = ~ 2.2 cm; A1 = ~ 2.8 cm; D = ~ 10.2 cm

Section 2

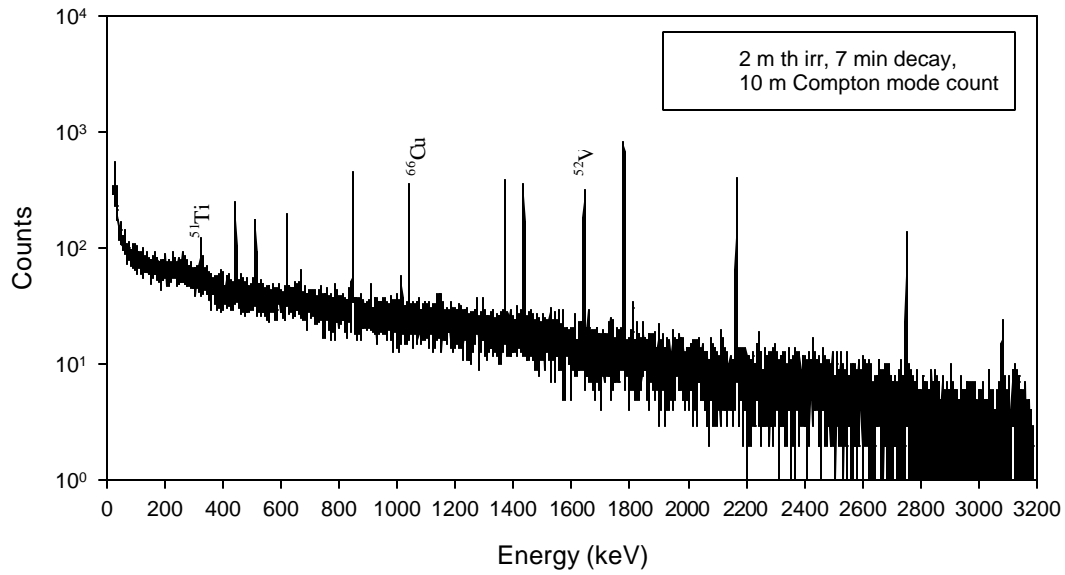


Figure A.1: A spectrum of pneumatic thermal irradiation Compton mode count

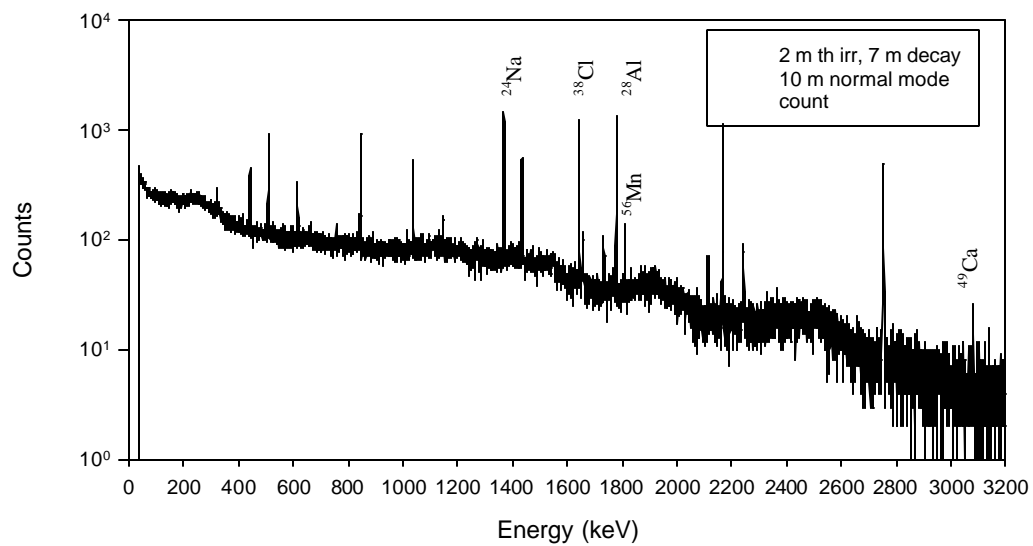


Figure A.2: A spectrum of pneumatic thermal irradiation normal mode count

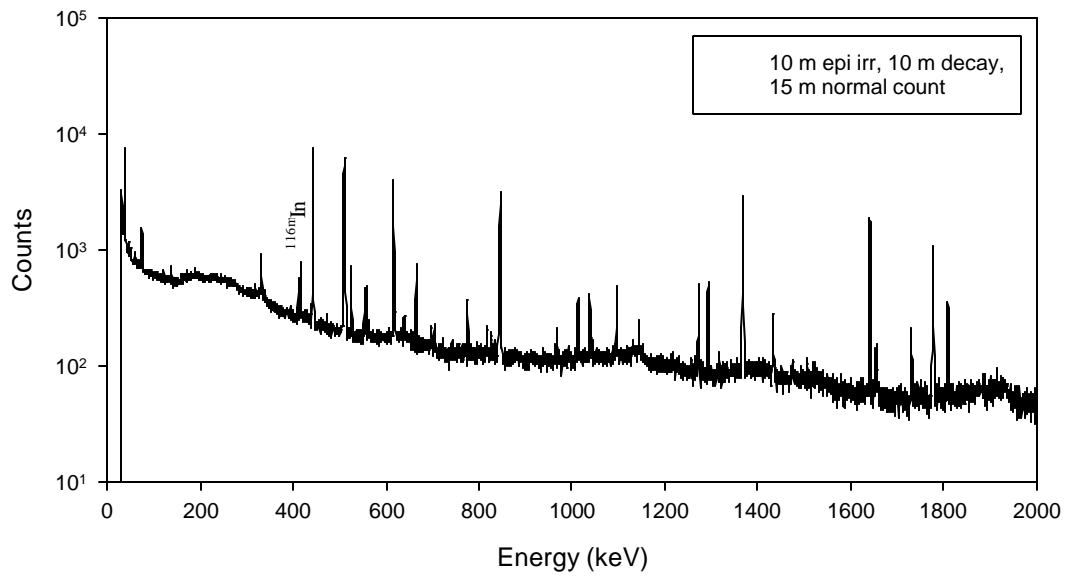


Figure A.3: A spectrum of pneumatic epithermal irradiation normal mode count

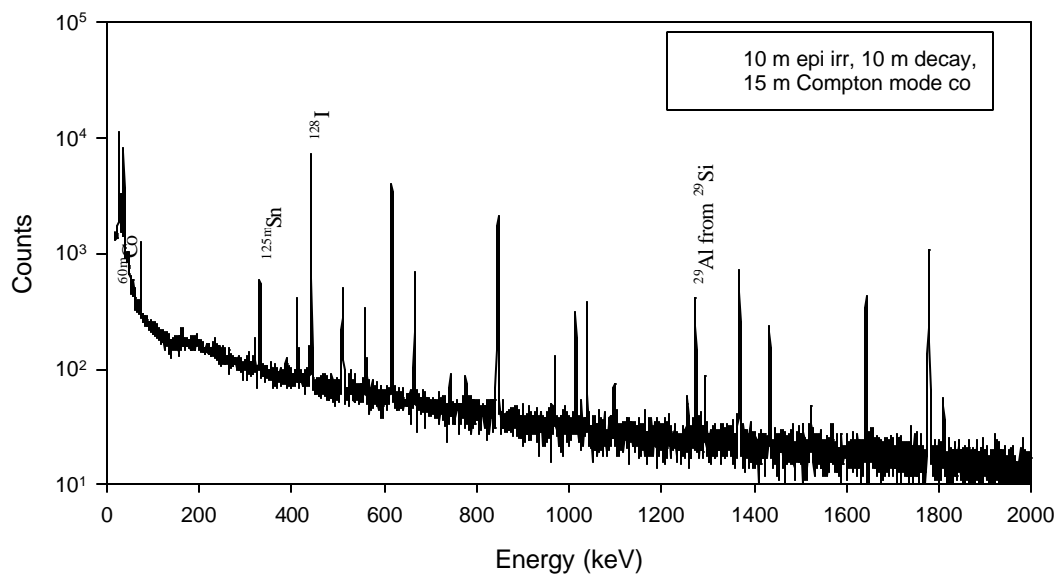


Figure A.4: A spectrum of pneumatic epithermal irradiation Compton mode count

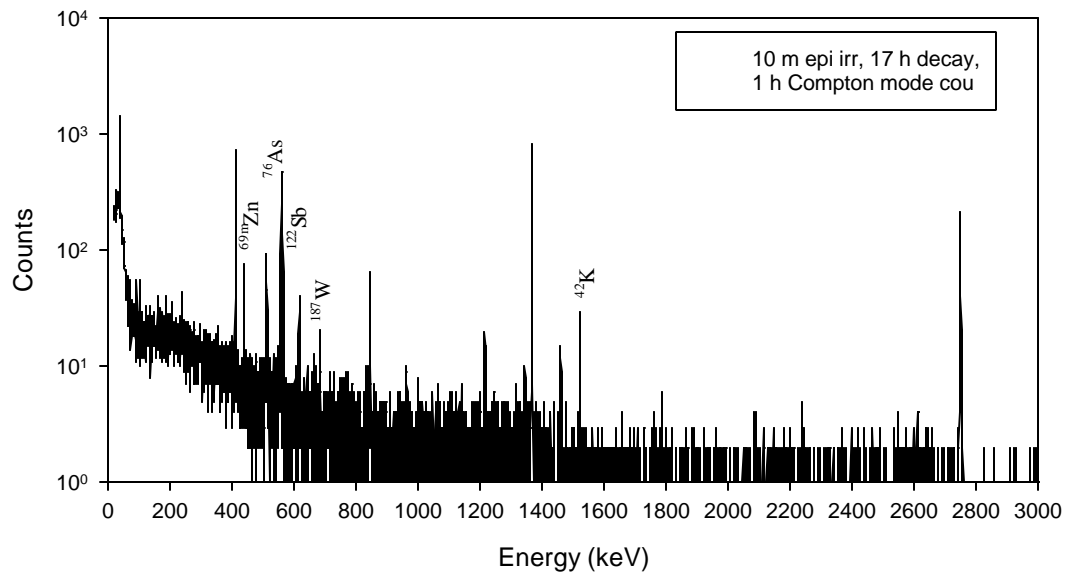


Figure A.5: A spectrum of pneumatic epithermal irradiation Compton mode count with a 17 h decay time

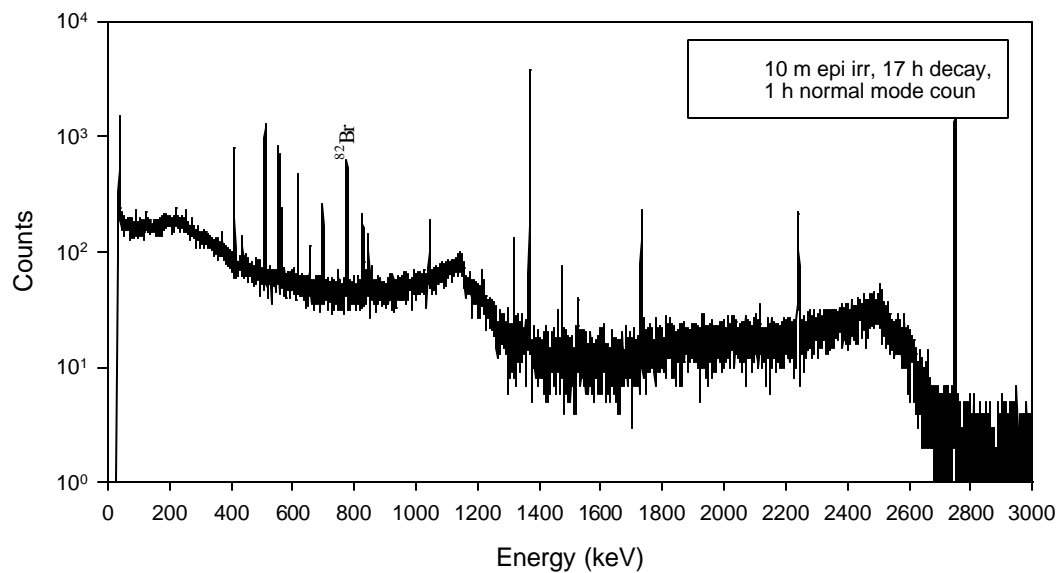


Figure A.6: A spectrum of pneumatic epithermal irradiation normal mode count with a 17 h decay time

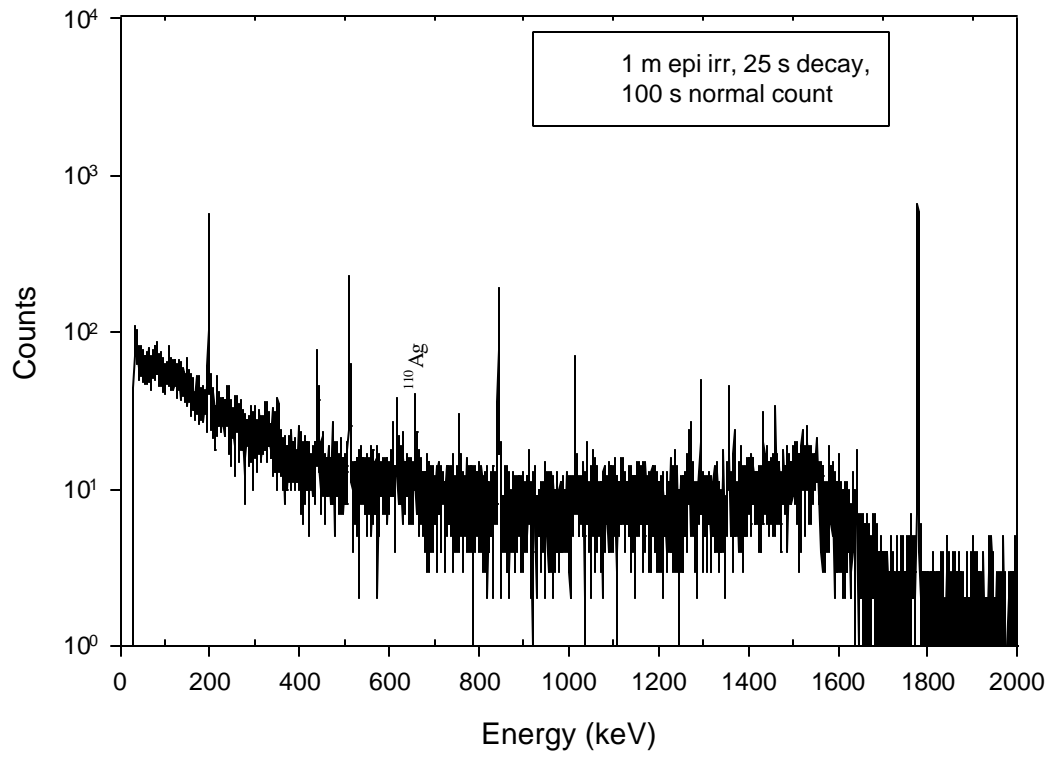


Figure A.7: A spectrum of one -minute epithermal irradiation and normal mode count

Section 3

Notations: n = Number of data points

x_i = Individual data point

s = Estimate of the standard deviation

Mean – A measure of central tendency of the data and calculated as the arithmetic average, i.e. the sum divided by the number of cases.

$$\bar{x} = \frac{\sum_{i=1}^n x_i}{n}$$

Median – A median is the value of the data point, which divides a distribution exactly in half. If there are even data points, the median is average value of the two middle data points.

Mode – In a set of values, a mode is the most frequently occurring value.

Standard deviation – A measure of dispersion of the data around the mean, calculated as

$$s = \left[\frac{\sum_{i=1}^n (x_i - \bar{x})^2}{(n-1)} \right]^{1/2}$$

Geometric mean – It is defined as

$$\bar{x}_g = \exp \left[\frac{\sum_{i=1}^n \ln x_i}{n} \right]$$

Geometric standard deviation – it is calculated as

$$s_g = \exp \left[\frac{\sum_{i=1}^n (\ln x_i - \bar{x}_g)^2}{(n-1)} \right]^{1/2}$$

Skewness - A measure of the asymmetry of a distribution. The normal distribution is symmetric, and has a skewness value of zero. A distribution with a significant positive skewness has a long right tail. A distribution with a significant negative skewness has a long left tail. The equation for skewness is defined as;

$$Skewness = \frac{n}{(n-1)(n-2)} \sum_{i=1}^n \left(\frac{x_i - \bar{x}}{s} \right)^3$$

Kurtosis - Kurtosis is based on the size of a distribution's tails. For a normal distribution, the value of the kurtosis statistic is 0. Positive kurtosis indicates that a longer tails than those in the normal distribution and negative kurtosis indicates a shorter tails. Kurtosis is defined as:

$$Kurtosis = \left\{ \frac{n(n-1)}{(n-1)(n-2)(n-3)} \sum_{i=1}^n \left(\frac{x_i - \bar{x}}{s} \right)^4 \right\} - \frac{3(n-1)^2}{(n-2)(n-3)}$$

Section 4

In RTA an air parcel back trajectory ensemble is used for identifying the elemental source locations around Kevo, Finland. An air parcel back trajectory can be computed using HYSPLIT model from NOAA web site, as mentioned earlier, is presented partly in Table A.3 for 120 hours. An air parcel's latitude and longitude locations, called endpoints, are available in the back trajectory output file. The calculation of residence time and incremental probability over a grid square is presented below.

Let us consider a section of the grid square domain as shown in Figure A.8.

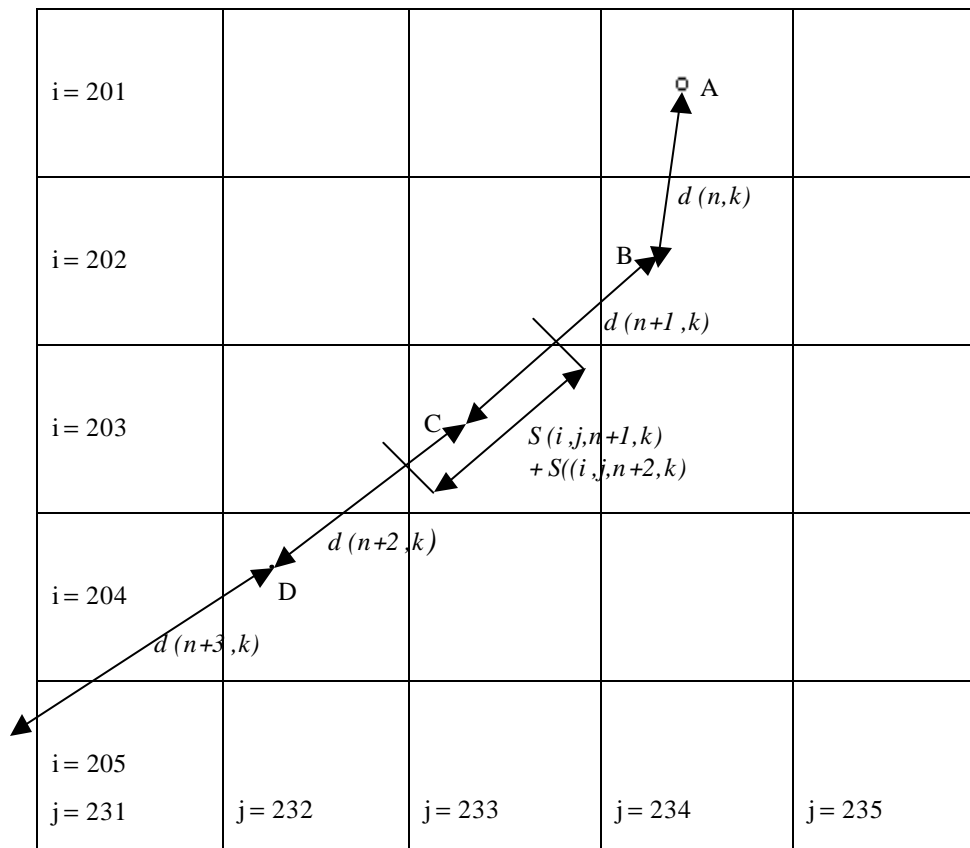


Figure A.8: Illustration of a trajectory residence time calculation

Suppose the receptor site is located at A and segments AB, BC, and CD are representing the distance of air parcel traveled per hour. Since the endpoints for the air

parcel are available every hour for a 120-hour period, each segment of the endpoint distance also equals to the speed of the air parcel per hour. The time of an air parcel spend over a grid square can be calculated from the distance of an air parcel over that grid square. Suppose we have the following:

$S_{(i,j,n,k)}$ = length of that portion of the n th segment of the k th trajectory which falls over the grid square (i,j)

$d_{(n,k)}$ = total length of the n th segment of the k th trajectory

$V_{(n,k)}$ = speed of the air parcel = $d_{(n,k)}/hour$ in the present case

$Tr_{(i,j,n,k)}$ = residence time over grid square (i,j) contributed by the n th segment of the k th trajectory

$TR_{(i,j)}$ = total residence time for all the trajectories over grid square (i,j)

$TR_{(i,j)}^h$ = total residence time for all the trajectories related to high subset samples over grid square (i,j)

$TR_{IP(i,j)}$ = incremental probability over grid square (i,j)

For example, let us consider the residence time calculation over the grid square (203,233). Referring to Figure A.8, suppose:

$$BC = d_{(n+1,k)} = 13 \text{ km}$$

and $CD = d_{(n+2,k)} = 12 \text{ km}$

and being able to calculate that portion of BC over grid square (203, 233) is say for instance 6 km in distance while the portion of CD over grid square (203, 233) is 4 km in distance, i.e.

$$S_{(203,233,n+1,k)} = 6 \text{ km}$$

$$S_{(203,233,n+2,k)} = 4 \text{ km}$$

The residence time over grid square (203, 233) due to the illustrated trajectory is given by:

$$\begin{aligned}
 TR_{(203,233)} &= \sum_{k=1}^1 \sum_{n=2}^3 S_{(203,233,n,k)} / V_{(n,k)} \\
 TR_{(203,233)} &= S_{(203,233,2,1)} / V_{(2,1)} + S_{(203,233,3,1)} / V_{(3,1)} \\
 TR_{(203,233)} &= 6/13 + 4/12 = 0.46 + 0.33 = 0.79 \text{ h}
 \end{aligned}$$

The difficult portion of this calculation lies in the fact that the output of the HYSPLIT model does not determine the values $S_{(i,j,n,k)}$ in the above nomenclature. RTA computer code performs all the above-mentioned computations.

Total ‘residence time’ for a particular grid square contributed by a set of trajectories can be computed by summing the individual ‘residence times’ contributed by each segment of all the trajectories in the set. Residence times is then converted to residence time probabilities so long as the total of all grid square residence times for that set of trajectories is large enough to allow for a truly representative sample over all the possible trajectory paths, i.e.

$$TR_{p(i,j)} = \left(\frac{TR_{(i,j)}}{\sum_{i=1}^l \sum_{j=1}^m TR_{(i,j)}} \right) \quad (1)$$

Similarly another residence time probability is calculated using all trajectories related to high concentration samples, so,

$$TR_{p(i,j)}^h = \left(\frac{TR_{(i,j)}^h}{\sum_{i=1}^l \sum_{j=1}^m TR_{(i,j)}^h} \right) \quad (2)$$

Finally, the incremental probability can be obtained for a grid square (i,j) by subtracting equation (1) from equation (2), i.e.

$$TR_{IP} \% = (TR_{p(i,j)}^h - TR_{p(i,j)}) \times 100 \quad (3)$$

Usually, these incremental probabilities for the grid squares are very small, so almost always a multiplication factor is used for producing a visible plot as presented in this work.

Table A.3: HYSPLIT output for an air parcel back trajectory for a 120-hour period

CDC1 68 12 1 0 0												
CDC1 68 11 1 0 0												
IBACKWARDOMEGA												
68 12 3 6 69.450 27.020 500.0												
1Pressure								Hour	Lat.	Long.	Height	
1	1	68	12	3	6	0	0	0.0	69.450	27.020	500.0	918.2
1	1	68	12	3	5	0	0	-1.0	69.819	26.489	511.8	918.7
1	1	68	12	3	4	0	0	-2.0	70.189	25.926	514.3	919.9
1	1	68	12	3	3	0	0	-3.0	70.556	25.350	513.8	923.1
1	1	68	12	3	2	0	0	-4.0	70.920	24.778	511.8	926.5
1	1	68	12	3	1	0	0	-5.0	71.281	24.218	503.2	929.9
1	1	68	12	3	0	0	0	-6.0	71.639	23.678	498.5	933.6
.....												
1	1	68	11	28	17	0	0	-109.0	77.234	41.686	94.0	1022.0
1	1	68	11	28	16	0	0	-110.0	77.002	41.715	100.0	1020.3
1	1	68	11	28	15	0	0	-111.0	76.772	41.807	105.4	1018.8
1	1	68	11	28	14	0	0	-112.0	76.545	41.954	110.2	1017.4
1	1	68	11	28	13	0	0	-113.0	76.322	42.151	114.1	1016.1
1	1	68	11	28	12	0	0	-114.0	76.106	42.393	117.3	1015.1
1	1	68	11	28	11	0	0	-115.0	75.899	42.673	119.2	1013.9
1	1	68	11	28	10	0	0	-116.0	75.695	42.978	120.8	1012.6
1	1	68	11	28	9	0	0	-117.0	75.497	43.306	122.1	1011.3
1	1	68	11	28	8	0	0	-118.0	75.306	43.658	123.0	1009.9
1	1	68	11	28	7	0	0	-119.0	75.123	44.031	123.6	1008.6
1	1	68	11	28	6	0	0	-120.0	74.950	44.426	123.8	1007.4

References

- Alpert D.J. and P.K. Hopke (1981) A determination of the sources of airborne particles collected during the regional air pollution study, *Atmospheric Environment*, Vol. 15, 675-687.
- Alpert D.J. and P.K. Hopke (1980) A quantitative determination of sources in the Boston urban aerosol, *Atmospheric Environment*, Vol. 14, 1137-1146.
- Anttila P., P. Paatero, U. Tapper, and O. Jarvinen (1995) Application of Positive Matrix Factorization to Source Apportionment: Results of a Study of Bulk Deposition Chemistry in Finland, *Atmospheric Environment*, Vol. 29, 1705-1718.
- Ashbaugh L.L., W.C. Malm, W.Z. Sadeh (1985) A residence time probability analysis of sulfur concentrations at Grand Canyon National Park, *Atmospheric Environment*, Vol. 19, 1263-1270.
- Ashbaugh L.L. (1983) A Statistical Trajectory Technique for Determining Air Pollution Source Regions, *Journal of Air Pollution Control Association*, Vol. 33, 1096-1098.
- Ayotte P., E. Dewailly, S. Bruneau, H. Careau, and A. Vezina (1995) Arctic air pollution and human health: what effects should be expected?, *The Science of the Total Environment*, Vol. 160/161, 529-537.
- Barrie L.A. (1993) Alert aerosol chemistry studies, in Alert Baseline Air Chemistry Report, Atmospheric Environment Service, Downsview, Canada.
- Barrie L.A., R.C. Bottenheim, R.C. Schnell, P.J. Crutzen, and R.A. Rasmussen (1988) Ozone destruction and photochemical reactions at polar sunrise in the lower Arctic atmosphere, *Nature*, Vol. 334, 138-141.
- Barrie L.A. and R.M. Hoff (1985) Five years of air chemistry observations in the Canadian Arctic, *Atmospheric Environment*, Vol. 19, 1995-2010.
- Barrie L.A., R.M. Hoff, and S.M. Daggupaty (1981) The influence of mid-latitude pollution sources on haze in the Canadian Arctic, *Atmospheric Environment*, Vol. 15, 1407-1419.
- Bartholomew D.J. (1987) *Latent Variable Models and Factor Analysis*, London: C. Griffin, New York, Oxford University Press.

- Baskaran M. and G.E. Shaw (2001) Residence time of arctic haze aerosols using the concentrations and activity ratios of ^{210}Po , ^{210}Pb and ^7Be , *Journal of Aerosol Science*, Vol. 32, 443-452.
- Bodhaine B. and E.G. Dutton (1993) A Long-Term Decrease in Arctic Haze at Barrow, Alaska, *Geophysical Research Letters*, Vol. 20, 947-950.
- Bowen H.J.M (1979) *Environmental Chemistry of the Elements*, Academic Press, New York.
- Cahill T.A. and R.A. Eldred (1984) Elemental Composition of Arctic Particulate Matter, *Geophysical Research Letters*, Vol. 11, 413-416, 1984.
- Chang S.N., P.K. Hopke, G.E. Gordon, and S.W. Rheingrover (1988) Target-Transformation Factor Analysis of airborne particulate samples selected by wind-trajectory analysis, *Aerosol Science and Technology*, Vol. 8, 63-80.
- Chekushin V.A., I.V. Bogytyrev, P. de Caritat, H. Niskavaara, and C. Reimann (1998) Annual atmospheric deposition of 16 elements in eight catchments of the central Barents region, *Science of the Total Environment*, Vol. 220, 95-114.
- Cheng M.D., P.K. Hopke, S. Landsberger, and L.A. Barrie (1991) Distribution characteristics of trace elements and ionic species of aerosol collected at Canadian High Arctic, *Atmospheric Environment*, Vol. 25A, 2903-2909.
- Cohen M.A. and P.B. Ryan (1989) Observation less than the analytical limit of detection: A new approach, *Air & Waste Management Association*, Vol. 39, 328-329.
- Currie L.A. (1968) Limits for qualitative detection and quantitative determination, *Analytical Chemistry*, Vol. 40, 568-593.
- Curry J.A. (1988) Arctic cloudiness in spring from satellite imagery: Some comments, *Journal of Climatology*, Vol. 8, 533-538.
- Daniel J.S., S. Solomon, R.W. Portmann, and R.R. Garcia (1999) Stratospheric ozone destruction: The importance of bromine relative to chlorine, *Journal of Geophysical Research*, Vol. 104, 23871-23880.
- Djupstrom M., J.M. Pacyna, J.W. Maenhaut, J.W. Winchester, and S.M. Li (1993) Contamination of Arctic Air at Three Sites During a Haze Event in Late Winter 1986, Vol. 27A, 2999-3010.
- Draxler R.R and G.D. Hess (1998) An overview of the HYSPLIT_4 modelling system for trajectories, dispersion and deposition, *Australian Meteorological Magazine*, Vol. 47, 295-308.
- Germanl M.S., I. Gokmen, A.C. Sigleo, G.S. Kowalczyk, I. Olmez, A.M. Small, D.L. Anderson, M.P. Falley, M.C. Gulovall, C.E. Choquette, E.A. Lepel, G.E. Gordon, and W.H. Zoller (1980) Concentration of elements in the National Bureau of Standards' Bituminous and Subbituminous Coal Standard Reference Materials, *Analytical Chemistry*, Vol. 52, 240-245.

- Heidam N.Z., P. Wahlin, and K. Kemp (1993) Arctic Aerosols in Greenland, *Atmospheric Environment*, Vol. 27A, 3029-3036.
- Heidam N.Z. (1984) The Component of the Arctic aerosol, *Atmospheric Environment*, Vol. 18, 329-343.
- Heidam N.Z. (1981) On the origin of the Arctic aerosol – a statistical approach, *Atmospheric Environment*, Vol. 15, 1421-1427.
- Heintzenberg J, H.C. Hansson, and H. Lannefors (1981) The chemical-composition of Arctic haze at Ny-Alesund, Spitsbergen, *Tellus*, Vol. 33, 162-171.
- Henry R.C., E.S. Park, and C.H. Spiegelman (1999) Comparing a new algorithm with the classic methods for estimating the number of factors, *Chemometrics and Intelligent Laboratory Systems*, Vol. 48, 91-97.
- Henry R.C. (1997) History and fundamentals of multivariate air quality receptor models, *Chemometrics and Intelligent Laboratory Systems*, Vol. 37, 37-42.
- Henry R.C., C.W. Lewis, and J.F Collins (1994) Vehicle-related hydrocarbon source compositions from ambient data: The GRACE/SAFER Method, *Environmental Science and Technology*, Vol. 28, 823-832.
- Henry R.C. and B.M. Kim (1990) Extension of self-modeling curve resolution to mixtures of more than three components, *Chemometrics and Intelligent Laboratory Systems*, Vol. 8, 205-216.
- Henry R.C. (1987) Current factor analysis receptor models are ill-posed, *Atmospheric Environment*, Vol. 8, 1815-1820.
- Hopke P.K., L.A. Barrie, S.M. Li, M.D. Cheng, C. Li, and Y. Xie (1995) Possible sources and preferred pathways for biogenic and non-sea-salt-sulfur for the high Arctic, *Journal of Geophysical Research*, Vol. 100, 16595-16603.
- Hopke P. K., N. Gao, and M.D. Cheng (1993) Combining chemical and meteorological data to infer source areas of airborne pollutants, *Chemometrics and Intelligent Laboratory Systems*, Vol. 19, 187-199.
- Hopke P.K. (1991) An introduction to receptor modeling, *Chemometrics and Intelligence Laboratory Systems*, Vol. 10, 21-43.
- Hopke P.K. (1988) Target Transformation Factor Analysis as an aerosol mass apportionment method: A review and sensitivity study, *Atmospheric Environment*, Vol. 22, pp 1777-1792.
- Hopke P.K. (1983) An introduction to multivariate analysis of environmental data, *Analytical Aspects of Environmental Chemistry*, Chapter 6, Edited by Dr. D. Natusch & Dr. P. Hopke, John Wiley & Sons, Inc.
- Horensma P. (1991) *The Soviet Arctic*, Routledge, London.

- Jaffe D., B. Cerundolo, J. Rickers, R. Stolzberg, and A. Baklanov (1995) Deposition of sulfate and heavy metals on the Kola Peninsula, *Science of the Total Environment*, Vol. 160/161, 127-134.
- Johnson R.A., and D.W. Wichern (1998) *Applied Multivariate Statistical Analysis*, 4th Edition, Prentice Hall, Upper Saddle River, New Jersey.
- Joranger E. and B. Ottar B. (1984) Air-Pollution Studies In The Norwegian Arctic, *Geophysical Research Letters*, Vol. 11, No. 5, 365-368.
- Kaiser H.F. (1958) The varimax criterion for analytic rotation in factor analysis, *Psychometrika*, Vol. 23, 187-200.
- Kelly J.A., D.A.Jaffe, and A.A. Baknalov (1995) Heavy metals on the Kola Peninsula: Aerosol size distribution, *Science of the Total Environment*, Vol. 160/161, 135-138.
- Kerminen V.M., Teinilä K, Hillamo R., and Pakkanen T. (1998) Substitution of chloride in sea-salt particles by inorganic and organic anions, *Journal of aerosol science*, Vol. 29, 929-942.
- Kim B.M. and R. Henry (2000) Application of the SAFER Model to Los Angeles PM10 data, *Atmospheric Environment*, Vol. 34, 1747-1759.
- Landsberger S., P. Zhang, D. Wu, and A. Chatt (1997) Analysis of the Arctic aerosol for a ten year period using various neutron activation analysis methods, *Journal of Radioanalytical and Nuclear chemistry*, Vol. 217, 11-15.
- Landsberger S., W.D. Cizek, and R.H. Campbell (1994) NADA93: An Automated, User friendly Program for Neutron Activation Data Analysis, *Journal of Radioanalytical and Nuclear Chemistry*, Vol. 180, 55-63.
- Landsberger S. V., G. Vermette, D. Stuenkel, P.K. Hopke, M.D. Cheng, and L.A. Barrie (1992) Elemental source signature of aerosols from the Canadian high Arctic, *Environmental Pollution*, Vol. 75, 181-187.
- Landsberger S., P.K. Hopke, and M.D. Cheng (1992a) Nanogram Determination of Indium Using Epithermal Neutrons and Its Application in Potential Source Contribution Function of Airborne Particulate Matter in the Arctic Aerosol, *Nuclear Science and Engineering*, Vol. 110, 79-83.
- Landsberger S., S.J. Vermette, and L.A. Barrie (1990) Multielemental Composition of the Arctic aerosol, *Journal of Geophysical Research*, Vol. 95, 3509-3515.
- Lowenthal D.L. and K.A. Rahn (1985) Regional sources of pollution aerosol at Barrow, Alaska during winter 1979-1980 as deduced from elemental tracer, *Atmospheric Environment*, Vol. 19, 2011-2024.
- Luzin G.P., M. Pretes, and V.V. Vasiliev (1994) The Kola Peninsula: Geography, History and Resources, *Arctic*, Vol. 47, 1-15.

- Maenhaut W., P. Cornille, J.M. Pacyna, and V. Vitols (1989) Trace element composition and origin of the atmospheric aerosol in the Norwegian Arctic, *Atmospheric Environment*, Vol. 23, 2551-2569.
- Malinowski E.R. 1991 *Factor Analysis in Chemistry*, 2nd Edition, JOHN WILEY & SONS, INC.
- Malm W.C., C.E. Jonson, and J.F. Bresch (1986) Application of principal component analysis for purposes of identifying source-receptor relations, *Receptor Methods for Source Apportionment*, Edited by T.G. Pace, APCA, 127-148.
- Mason B. (1966) *Principles of Geochemistry*, 3rd Edition, John Wiley & sons, Inc., New York.
- McConnell J.C., G.S. Henderson, L.A. Barrie, J. Bottenheim, H. Niki, C.H. Langford, and E.M.J. Templeton (1992) Photochemical bromine production implicated in Arctic boundary-layer ozone depletion, *Nature*, Vol. 355, 150-152.
- Michalowski B.A., J.S. Francisco, S. Li, L.A. Barrie, J.W. Bottenheim, and P.B. Shepson (2000) A computer model study of multiphase chemistry in the Arctic boundary layer during polar sunrise, *Journal of Geological Research*, Vol. 105, 15,131-15,145.
- Miller S.L., M.J. Anderson, E.P. Daly, and J.B. Milford (2002) Source apportionment of exposures to volatile organic compounds. I. Evaluation of receptor models using simulated exposure data, *Atmospheric Environment*, Vol. 36, 3629-3641.
- Mitchell M (1957) Visible range in the Polar Regions with particular reference to the Alaskan Arctic, *Journal of Atmospheric and Terrestrial Physics*, Special supplement, 195-211.
- Mughabghab S.F., M. Divadeenam, and N.E. Holden (1981) *Neutron Cross-Sections*, Vol. 1 and 2, Academy Press.
- Oltmans S.J., R.C. Schnell, P.J. Sheridan, R.E. Peterson, S.M. Li, J.W. Winchester, P.P. Tans, W.T. Sturges, J.D. Kahl, and L.A. Barrie (1989) Seasonal Surface Ozone and Filterable Bromine Relationship in the High Arctic, *Atmospheric Environment*, Vol. 23, 2431-2441.
- Pacyna J.M., V. Vitols, and J.E. Hanssen (1984) Size distributed composition of the Arctic aerosol at Ny-Alesund, Spitsbergen *Atmospheric Environment*, Vol. 18, 2447-2459.
- Paatero P., and U. Tapper (1993) Analysis of different modes of factor analysis as least squares fit problems, *Chemometrics and Intelligence Laboratory Systems*, Vol. 18, 183-194.
- Park E.S., R.C. Henry, and C.H. Spiegelman (2000) Estimating the number of factors to include in a high dimensional multivariate bilinear model, *Communications in Statistics: Simulation and Computation*, Vol. 29, 723-746.

- Petra M., G. Swift, and S. Landsberger (1990) Design of a Ge-NaI(Tl) Compton suppression spectrometer and its use in neutron activation analysis, *Nuclear Instrumentation and Methods in Physics Research*, Vol. 299, 85-87.
- Poirot R.L., P.R. Wishinski, P.K. Hopke, and A.V. Polissar (2001) Comparative application of multiple receptor methods to identify aerosol sources in Northern Vermont, *Environmental Science and Technology*, Vol. 35, 4622-4636.
- Poirot R.L., P.R. Wishinski (1986) Visibility, sulfate and air mass history associated with the summertime aerosol in northern Vermont, *Atmospheric Environment*, Vol. 20, 1457-1469.
- Polissar A.V., P.K. Hopke, P. Paatero, Y.J. Kaufmann, D.K. Hall, B.A. Bodhaine, E.G. Dutton, and J.M. Harris (1999) The aerosol at Barrow, Alaska: long-term trends and source locations, *Atmospheric Environment*, Vol. 33, 2441-2458.
- Polissar A.V., P.K. Hopke, W.C. Malm, and J.F. Sisler (1998) Atmospheric aerosol over Alaska 1. Spatial and seasonal variability, *Journal of Geophysical Research*, Vol. 103, 19,035-19,044.
- Qin Y., K. Oduyemi, and L.Y. Chan (2002) Comparative testing of PMF and CFA models, *Chemometrics and Intelligent Laboratory Systems*, Vol. 61, 75-87.
- Raatz W.E., and G. E. Shaw (1984) Long-range tropospheric transport of pollution aerosols into the Alaskan Arctic, *Journal of Climate and Applied Meteorology*, Vol. 23, 1052-1064.
- Rahn K.A. and D.H. Lowenthal (1984) Elemental tracers of distant regional pollution aerosols, *Science*, Vol. 223, 132-139.
- Rahn K.A., R.D. Borys, and G.E. Shaw (1981) Asian desert dust over Alaska: Anatomy of an Arctic haze episode, *Geological Society of America, Special paper*, Vol. 186, 37-70.
- Rahn K.A. (1981a) The Mn/V ratio as a tracer of large-scale sources of pollution aerosol for the Arctic, *Atmospheric Environment*, Vol. 15, 1457-1464.
- Rahn, K.A. (1976) *The Chemical Composition of the Atmospheric Aerosol*, Technical Report, Graduate School of Oceanography, University of Rhode Island.
- Rees W.G., and A.P. Kapitsa (1994) Industrial pollution in the Kol'skiy Poluostrov, Russia, *Polar Record*, Vol. 30, 181-188.
- Reimann C., M. Äyräs, V. Chekushin, I. Bogatyrev, R. Boyd, P. de Caritat, R. Dutter, T.E. Finne, J.H. Halleraker, ? . Jæger, G. Kashulina, O. Lehto, H. Nishkavara, V. Pavlov, M.L. Räsänen, T. Strand, and T. Volden (1998) *Environmental Geochemical Atlas of the Central Barents Region*, NGU-GTK-CKE special publication, Geological Survey of Norway, Trondheim, Norway.
- Reimann C., P.de Caritat, J.H. Halleraker, T.E. Finne, R. Boyd, ? . Jæger, T. Volden, G. Kashulina, I. Bogatyrev, V. Chekushin, V. Pavlov, M. Äyräs, M.L. Räsänen, and H.

- Nishkavara (1997) Regional Atmospheric Deposition Patterns of Ag, As, Bi, Cd, Hg, Mo, Sb and Tl in a 188,000 km² Area in the European Arctic as Displayed by Terrestrial Moss Samples – Long-Range Atmospheric Transportation vs. Local Impact, *Atmospheric Environment*, Vol. 31, 3887-3901.
- Reimann C., H. Niskavaara, P.de Caritat, T.E. Finne, M. Äyräs, and V. Chekusin (1996) Regional variation of snowpack chemistry in the vicinity of Nikel and Zapoljarnij, Russia, northern Finland and Norway, *Science of the Total Environment*, Vol. 182, 147-158.
- Rohlf J.F. and R.R. Sokal (1981) *Statistical Tables*, 2nd Edition, W.H. Freeman and Company, San Francisco.
- Sirois A. and L.A. Barrie (1999) Arctic lower tropospheric aerosol trends and composition at Alert, Canada: 1980-1995, *Journal of Geophysical Research*, Vol. 104, 11599-11618.
- Steinnes E., J.P. Rambæk, and J.E. Hanssen (1992) Large scale multi-element survey of atmospheric deposition using naturally growing moss as biomonitor, *Chemosphere*, Vol. 25, 735-752.
- Thurston G.D., and J.D. Spengler (1985) A quantitative assessment of source contributions to inhalable particulate matter pollution in metropolitan Boston, *Atmospheric Environment*, Vol. 19, 9-25.
- Vinogradova A.A. (2000) Anthropogenic pollutants in the Russian Arctic atmosphere: sources and sinks in spring and summer, *Atmospheric Environment*, Vol. 34, 5151-5160.
- Vinogradova A.A., and A.V. Polissar (1995) Elemental composition of the aerosol in the atmosphere of the Central Russian Arctic, *Atmospheric and Oceanic Physics*, Vol. 31, 248-257.
- Virkkula A., M. Aurela, R. Hillamo, T. Makela, T. Pakkanen, V. Kerminen, W. Maenhaut, F. Francois, and J. Cafmeyer (1999) Chemical composition of atmospheric aerosol in the European sub Arctic: Concentration of the Kola Peninsula smelter areas, central Europe, and the Arctic Ocean; *Journal of Geophysical Research*, Vol. 104, 23681-23696.
- Wanna C., P.K. Hopke, P. Paatero (2000) Investigation of sources of atmospheric aerosol at urban and suburban residential areas in Thailand by positive matrix factorization, *Atmospheric Environment*, Vol. 34, 3319-3329.
- Xie Y, P.K. Hopke, P. Paatero, L.A.Barrie, and S. Li (1999) Locations and preferred pathways of possible sources of Arctic aerosol, *Atmospheric Environment*, Vol. 33, 2229-2239.
- Zeng Y. and P.K. Hopke (1989) A study on the sources of acid precipitation in Ontario, Canada, *Atmospheric Environment*, Vol. 23, 1499-1509.

Zhang P. (1996) Relative composition of crustal and anthropogenic trace element constituents in Canadian Arctic aerosol from 1982-1992 as determined by neutron activation analysis, MS thesis, University of Illinois at Urbana-Champaign.

Vita

M. Shamsuzzoha Basunia was born in Rangpur, Bangladesh on June 15, 1963, the son of Abdur Rahman Basunia and Amina Khatun. He received the degree of Bachelor of Science in 1985 and the degree of Masters in Science in 1986 from Rajshahi University, Bangladesh. Both the degrees were in Physics. After completing his Masters he joined Bangladesh Atomic Energy Commission (BAEC) in May 1991 as a Scientific Officer. During the service years in BAEC, he completed several training courses on environmental pollution studies and nuclear analytical techniques in Germany, Austria, Thailand and USA. In August 1998, he entered the Graduate School at The University of Texas. He received his Masters of Science in Engineering in May 2000 from the University of Texas at Austin. In June 2000, he started study and research work for his Ph.D. degree at the same University.

Permanent Address: 185/1 J.N.C. Road
Rangpur 5402, BANGLADESH

This dissertation was typed by the author.